A STUDY OF TUNNEL STABILITY WITH SPECIAL REFERENCE TO THE EFFECT OF THE STRESS FIELD ENVIRONMENT

By

Hui Chen

BSc., MSc.

Thesis submitted to the University of Nottingham
for the Degree of Doctor of Philosophy

May 1992

This thesis is dedicated to my parents and my family

for their love, care and support.

A STUDY OF TUNNEL STABILITY WITH SPECIAL REFERENCE TO THE EFFECT OF THE STRESS FIELD ENVIRONMENT

by Hui Chen

SUMMARY

The thesis is a study of the stability, closure behaviour and rock fracture development associated with mine tunnels with particular reference to Coal Measures conditions. A detailed survey has been carried out of relevant theories and mathematical concepts which relate to tunnel stability and the effects of *in situ* stresses. Of special importance has been identifying appropriate mathematical theories which relate to the field of scholarship undertaken. The literature survey has found useful application especially in giving guidance on those areas needing further investigation. The author discusses mathematical theories in relation to the research undertaken.

The major area of investigation has been the effect of different *in situ* stress fields on various aspects of tunnel design and geometrical configuration. Attention has focussed on available research methods which allow ease of investigation of the parameters governing mine tunnel stability. After careful consideration, the author selected physical modelling using small scale sand plaster models of different mine tunnel and geological conditions. Much research effort has been directed at establishing the properties of such physical modelling materials, mathematical scaling aspects and the type of test rig for carrying out the investigations. Time was spent on establishing the accuracy and suitability of the research method employed.

A range of experiments were carried out whereby the horizontal and vertical components of the *in situ* stress field were varied. The tests were repeated using the common range of mine tunnel profiles which exist in UK coal mines, namely arch, circular, square and rectangular. The research enabled the fracture pattern to be

observed in association with the different tunnel profiles tested under the various stress field conditions employed. Closure of the model tunnels was observed in relation to the increasing stress field.

Discussion has focussed on how various combinations of horizontal to vertical components of *in situ* stress influence mine tunnel stability. The results are discussed in relation to the choice of support type. In particular, the merits of standing support types such as square sets, steel arches and concrete linings are discussed in relation to the results of the research.

The thesis draws attention to the practical application of the research method to investigate various mining situations as encountered in UK coalfields and in the Datong coalfield in North China, of which the author has particular experiences regarding rock mechanics and mine tunnel stability.

Affirmation

The work presented in this thesis is my own and has not been submitted to any institution for any degree before.

The following papers have been published based on the work of this thesis:

(1) Whittaker, B.N., Smith, S.F. and Chen, H. (1990) Fracture development around tunnels. Proc. Conf. "Tunnel 90", April, London.

(2) Chen, H. and Smith, S.F. (1991) An investigation into characteristics of physical modelling materials using the orthogonal design method. Department of Mining Engineering Magazine, Vol. No. XLIII.

(3) Whittaker, B.N., Smith, S.F., Sun, G. and Chen, H. (1992) Influence of in situ stress field on the stability of mine tunnels. A paper to be published at the Conference of EUROCK 92 in September, 1992.

ACKNOWLEDGEMENTS

CONTENTS

CHAPTER ONE

INTRODUCTION

CHAPTER TWO

REVIEW OF FACTORS INFLUENCING TUNNEL STABILITY

CHAPTER THREE

RESEARCH OBJECTIVES AND METHODS ADOPTED

CHAPTER FOUR
ANALYSIS OF STRESS AND DEFORMATION AROUND
MINE TUNNELS PRIOR TO ROCK FAILURE

CHAPTER FIVE

ANALYSIS OF TUNNEL STABILITY AND SUPPORT AFTER

OCCURRENCE OF ROCK FAILURE

CHAPTER SEVEN
ROCK FRACTURE AND STABILITY OF TUNNELS
IN STRATIFIED STRATA

XI

CHAPTER EIGHT

MINING INDUCED INFLUENCES ON TUNNEL STABILITY

CHAPTER NINE
GENERAL CONCLUSIONS AND RECOMMENDATIONS
FOR FURTHER RESEARCH

LIST OF FIGURES

LIST OF TABLES

LIST OF PLATES

CHAPTER ONE

INTRODUCTION

CHAPTER ONE

INTRODUCTION

1.1 Definition of Tunnels

In underground coal mines, various openings are driven after shafts have been sunk to a planned level. These openings stretch from the bottom of the shaft until designed working faces are formed and ready for coal winning. Different locations of these openings ..... have different names. Also, different regions and countries use different terms which define or describe the same kind of openings. For instance, in the United States, an opening directly connecting the bottom of the shaft is called a main entry or simply a main or mainway (Peng, 1986). In the United Kingdom, however, it is more often called a tunnel or a drift. Another example is that of the openings linking the ends of a longwall face. These are commonly called the head-entry and tail-entry in the USA and the maingate and tailgate or gateways in the UK.

As the coal industry in the World is becoming more and more modernised in aspects of coal winning technology and mining equipment used, the output of coal face is increasing and the underground development system of coal mines is tending to become more concentrated. In such case, terminologies used for describing the various underground openings are also tending to change, particularly in some countries which start to adopt and practice new mining techniques and equipment.

Terms used to describe the underground openings are also extensive, which can be found in thousands of references regarding coal mining and which sometimes also causes unnecessary inconvenience in communication among people from the different parts of the world. To avoid unnecessary confusion, the term "Tunnel" will mainly be used throughout the following text to indicate all underground openings at

1

level or near level position including those in rocks and in seams, if no specification is stated.

1.2 Functions of Tunnels in Coal Mines

Underground tunnels play vital roles in coal production of mines although the development of these tunnels usually does not yield an output of coal with few exceptions of those driving in seams. Generally, there are several functions the tunnels can and should perform. These functions are listed as follows:

(1) Tunnels provide access for men to enter and exit the working area. The tunnel should therefore allow the passage of transport facilities of man-riding. Man-riding cars and flat conveyor belts are the common means for carrying miners several miles inbye and outbye their working places. Footpaths are also provided alongside in some sections of the tunnel system.

(2) Tunnels provide access for various materials, such as various support elements, machines and their parts and spares, and various pipes and cables, etc, to be sent to the places where they are needed. Therefore, the daily maintenance of tunnels, the advance of headings and the production of faces can be normally carried out and on.

(3) Tunnels form a route for   transportation of raw coal and sometimes debris from the production faces and/or the panel bunkers outby to the bottom of shaft. Debris from the underground heading operations also needs to be disposed of through proper tunnels mainly by means of mine cars, hauled by a locomotive, or, at some places, haulage machines.

(4) Tunnels allow the movement of fresh air towards the working areas whilst the contaminated air is exhausted along the return tunnels or bleaders,   such that men can   breath   and the hazardous gases, released from coal seams, are diluted and dusts, caused at working places, are blown away. A ventilating

environment is thus created. The danger of explosion due to the ignition of accumulated gas or fine dust or both can be effectively prevented. An effective ventilation also removes the heat energy released from rocks surrounding tunnels and working faces, reducing the temperature of underground working places at depths and creating a decent working environment.

(5) Tunnels are utilised to lay the supply pipelines for compressed air and water. They also allow the layout of electric cables held along the tunnel wall.

All these functions are very important to keeping a coal mine running and are therefore required without exception by every type of mine in all coal producing countries. Where collapses, deformation or deterioration occur in tunnels, then disruption to some or even all of the above functions can occur. This can result in disruptions to the production of coal in terms of losses including creating hazards to men who work in or pass through the area. Machines working in such areas face the danger of being buried by the collapsed debris. Plate 1.2.1 shows a case of tunnel damage due to the severe deformation and failure of surrounding rock. In this situation, the tunnel can no longer be used to serve the functions required unless repair and ripping work, which is costly, is undertaken.

1.3 Requirements for the Design of Coal Mining Tunnels

In underground tunnel designs the mining engineer needs firstly to identify the functions which the tunnel under consideration is expected to perform. This is because different functions will require different considerations in the design. A tunnel for running locomotives would require the floor to have a favourable gradient and to experience much less deformation than in the case of a conveyor belt tunnel. A tunnel which merely serves as a return airway, can often disregard limited deformation of the tunnel if the air speed is still within the scope of allowance and that the resistance to air flow has not been unduly increased. It is of considerable importance, however, that bottle necks do not occur in such ventilation roadways in

3

Plate 1.2.1

Tunnel damage due to severe deformation and failure of

the surrounding rock in the heavy stress field environment.
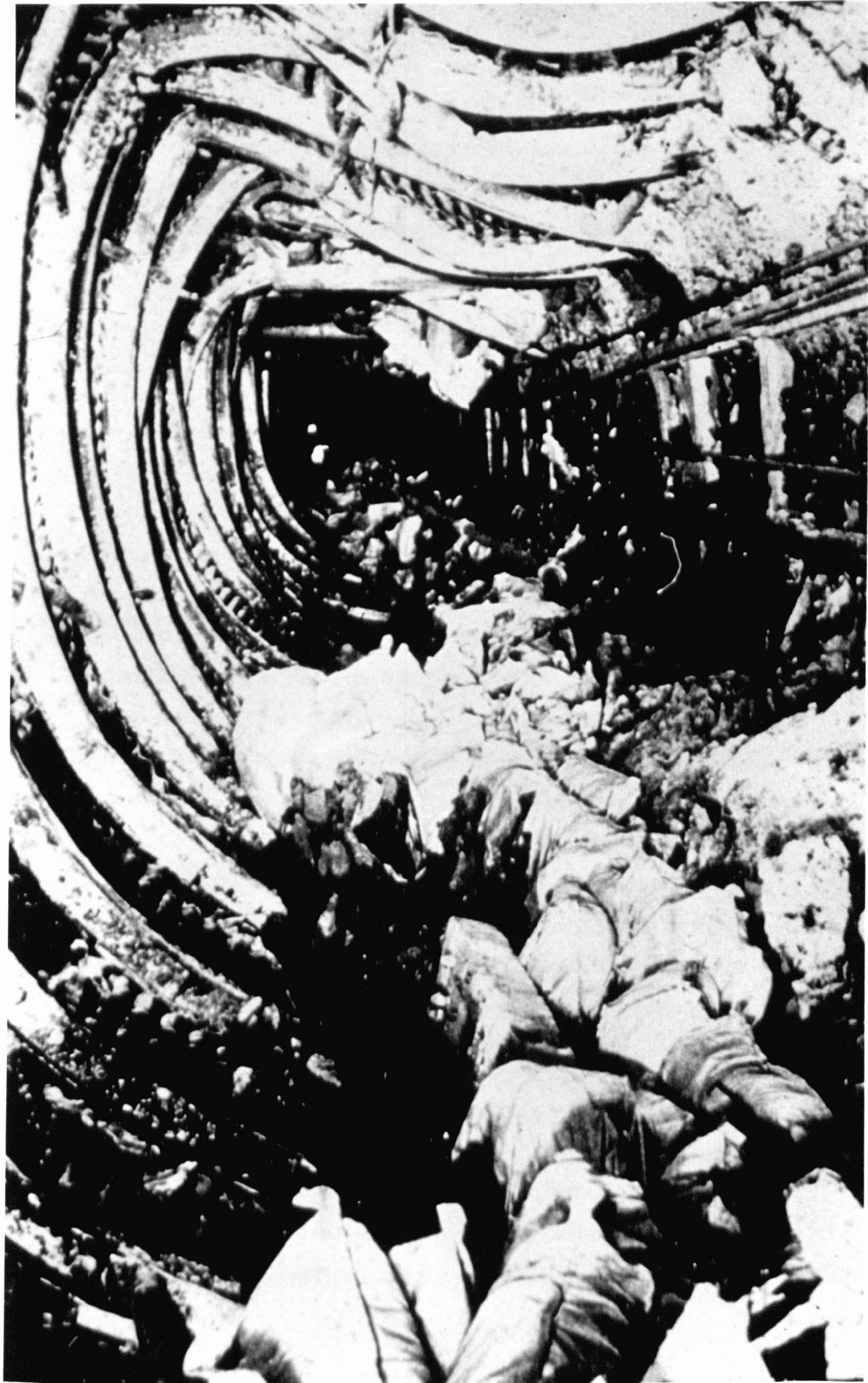
view of their highly restrictive nature. As a consequence, the choice of support to control deformation and ensure that the tunnel opening cross-sectional area is not excessively decreased is a very important factor in the overall design and planning.

Anyhow the mining engineer faced with the designing of all underground tunnels should always be concerned with the three aspects of safety, usability and economy.

In the safety aspect, the cross-section of the tunnel should meet the requirement by the functions which the tunnel will perform. The necessary clearance of the tunnel should be designed in accordance with the related design regulations. In practice, some extra clearance may be added to the necessary clearance provided that the deformations of the section, subject to the explicit effect of ground stresses, and the geological and/or mining operational disturbances occurred in the vicinity of it, are foreseen to be considerable. In China it is regulated in the Coal Mine Design Rules granted by the then Coal Industry Ministry that a minimum net clearance of not less than 75 centimetres must be provided for the footpath along one side of the tunnel when it is used for the coal or material transportation purpose. This is due to the consideration of the human body dimensions. Since the width of a human body is generally not exceeding 65 centimetres, this minimum net clearance would ensure the safety of men walking along the tunnel when a locomotive is passing by. To secure the safety of tunnels, various supports are used to protect the roof and walls of tunnels from severe failures and collapses, and reduce the deterioration of tunnels caused by various geological and operational influences.

A tunnel without safety protections cannot be said to be usable. Also a tunnel, though actually safe, may not be said to be usable either, if its cross-section or dimensions are below the lower limit required in the performance of some functions. A typical example is the conveyor belt tunnel for coal transportations, the cross-section of which is partly governed by the speed limits of air through it. The tunnel

may not be used to serve at the same time as a main return airway and a conveyor belt tunnel for coal transportation. Again, a tunnel with uneven or hump floor due to continuous floor deformations may not be used to serve the rail track transportation purpose.

Economic construction and maintenance of tunnels is a very important point that mine investors and mining engineers have to bear in mind and follow under the prerequisite of safety. Looking at the recent changes in the British Coal industry we can see that the changing economic environment has resulted in the progressive closure of a number of collieries due to low productivity and inefficiency and therefore loss of competition in the market. The effect has led the British mining industry to a situation that the size of mining and the workforce have been apparently reduced in the past few years. The challenge to the coal industry for a higher productivity and a better economic result, in order to compete with other cheap energy and the cheap imported coal, is facing the mining engineer. Looking forward towards the end of the century, coal mining in the UK can be expected to go deeper. Deeper seams will be won in existing coalfields and the average rate of increase of mining depth will be 100 metres per decade (Evans, 1981). Associated with this is the perennial British trouble of severe ground deformations around tunnel excavations. New developments will be very expensive. Some new main tunnels several kilometres in length are being planned and excavated, and they must be stable especially if they are to accommodate high speed transport. To respond to the challenge, more advanced and efficient equipment has been and needs to be further developed and introduced to the industry. In the tunnel development, more roadheaders have been used in operation. In 1987 a total of 67 medium duty roadheaders were in operation, whilst the number of this kind of machines has increased to 111 in 1990 (Cutts, 1991). This fact and others indicate that, in spite of the decline in the number of collieries within British Coal, the stage has been truly set

for the mining engineer to follow a higher economic target as well as to maintain and improve our safety standards.

In general, the three aspects of safety, usability and economy, as considered in the tunnel design and construction, interrelate. They should be borne in mind when introducing new technology and more advanced machinary in the tunnel excavation and construction.

1.4 Research General Objectives

It is the principal objective of the work described in this thesis, to investigate the role played by the stress field in influencing the deformation characteristics and general stability of mining tunnels.

In order to support the aims of the work, it has been necessary to review current knowledge of relevance to stress effects on mining tunnels. Various research publications, reports and theses have been reviewed in order to establish a clearer picture of the problem and to seek guidance on appropriate research methods.

A further important objective of the research has been to refine a physical modelling approach so that various parameters influencing stress effects on tunnels can be investigated. Physical modelling as a research tool has been meticulously researched and investigated to establish a procedure for the research method used in these studies.

The research has aimed at comparing the stability of different shapes of tunnels in various combinations of horizontal to vertical stresses acting on the tunnel.

The research has required high level photography in order to record the nature of fracture development. Consequently, this aspect needed to be taken into account in the early stages of research.

The nature of the deformation experienced by various tunnel geometries has needed to be carefully evaluated. It follows that one of the research objectives has been to identify the nature of tunnel deformation in relation to the stress field condition and to consider the role of supports applied in such tunnels.

CHAPTER TWO

REVIEW OF FACTORS INFLUENCING TUNNEL STABILITY

CHAPTER TWO

REVIEW OF FACTORS INFLUENCING TUNNEL STABILITY

Underground coal mining operations in the UK coalfields are virtually entirely confined to Carboniferous Coal Measures rock formations (Whittaker *et al.*, 1971) although, in other countries, the mining activities also take place in the Jurassic, Permian, Triassic and even Tertiary Periods of sedimentary rock formations (Martin, Doyle, *et al.*, 1986, Xu, 1987, Peng, 1986). The rock settings encountered in these coal fields are frequently those of sediments such as conglomerates, sandstones, limestones, clays and shales in addition to the coal itself.

They commonly exhibit typical sedimentary characteristics in their rock structures and their physical and mechanical properties. Moreover, each rock also has its own features different from those of the others due to variations in the early sedimentary circumstances and the later geological processes. The differences in the features of rocks make the rocks respond differently to the excavation formation and, thereafter, the stability of the tunnel. The fact that the ease of excavation in these rocks varies indicates the need for a proper choice of excavation method in a given strata circumstance since the approaches to excavation have a varied effect on the degree of disturbance and can result in damage or even destruction of the surrounding rocks. Obviously a review of the factors from both geological and operational points of view, which influence the stability of tunnels, is necessary before the extent of the problem can be properly appreciated and identified for study in detail. This is discussed later in the thesis.

2.1 The Influence of Lithological Factors on the Stability of Mine Tunnels

The lithology of rock refers to its mineralogy, texture and fabric. Lithology is a name or descriptive term. This description essentially refers to some approved classification system, e.g. limestone, conglomerate, sandstone, siltstone, mudstone, shale, etc. Sedimentary rocks as encountered in the Coal Measures are mostly derived from the past erosion of other rocks and the deposition of their fragments and particles, often on the sea bed or at the deltas of large rivers or in in-land seas or lakes. This is followed by consolidation. Sediments also include organic deposits of vegetable or material of animal origin.

The most common sediments are those in the clastic siliceous classification. They consist of fragments and grains derived from pre-existing rocks and minerals set in a finer grained matrix. The latter may have been deposited at the same time as, or formed subsequently to the deposition of the sediment. Subdivisions are made according to the size, shape, and nature of the component particles. Conglomerates, sandstones, siltstones, mudstones, shales and limestones are the general subclass commonly seen in underground conditions in coal mines.

Conglomerates consist of the rounded phenoclasts or pebbles with the interstices between pebbles being filled by finer grained material of similar composition and a natural cement, often consisting of quartz or calcite. The most typical conglomerates are ancient beach deposits.

Sandstones are composed predominantly of quartz fragments, which frequently constitute over 80 - 90% of the mineral grains in most British coal fields. The remainder are mainly rock fragments, micas and feldspars, together with a small percentage of heavy minerals of minor importance to the lithological classification although is sometimes useful as a means of correlation. In China, sandstones are further divided into coarse, medium and fine sandstones according to the size of the fragments.

Siltstones are common members of the Coal Measures in many countries. The grains of fragments in the siltstones are finer than those in the fine sandstones. They are constituted of the quartz and clay minerals. The content of clay minerals is usually higher than that in sandstones.

Mudstones and shales are extremely fine-grained, being chiefly composed of various clay minerals. Also present are small quantities of detrital material including micas, quartz grains and carbonaceous debris.

Fireclays are typically associated with coal seams, usually occurring below them as being called seatearths or underclays. Often occurring with them are dirt bands. Fireclays often grade vertically downwards and sometimes laterally into shales or mudstones and by an increase in quartz content into sandstones. Some fireclays have a smooth waxy feel due to their clay mineral content. This also results in their marked plasticity when wet, therefore creating problems of strata control in tunnel excavations such as floor heave or support penetration into the floor. Fireclays with low quartz contents are characteristically highly slickensided and non-laminated rocks which break easily along randomly arranged listric surfaces. The latter was probably formed by compacting during the dehydration of the strata but, in some cases, may result from induced stresses due to mining activities. These aspects relating to the nature of such sedimentary rocks are important in respect of floor behaviour in mining tunnels. Consequently, the nature of the sedimentary rocks can result in such tunnels becoming significantly influenced by relatively small changes in the stress field.

Limestones are rarely found within the vicinity of the British coal seams currently being extracted although they exist in the coal measures of other countries. In Northern China the water abundant Ocdacious limestone underlying some coal seams, threatens the safety of mining and tunnel excavations when the activities take place in areas where the interval between the sites and the limestone is very close or where there is an abundance of fissures and fractures linking the sites and the stratum.

All these sedimentary rocks can be thought to be composed of two components; the aggregate and the cement. The size of aggregates gives a lithological rank of rocks and partly determines the strength of the rock, whilst the characteristics of cement materials play a significant role in the mechanical behaviour of rocks. It is sometimes found in mining practice that tunnels in conglomerate appear more stable and require less support than those in sandstone although the uniaxial compressive strength of conglomerate is lower than that of sandstone (Chen, 1988 and 1989). This is considered to be due to the fact that the aggregate in conglomerate is much greater than those in sandstones. It is reported that in the Datong coalfield sandstones with clay cements were generally weaker in strength than those cemented by carbonate minerals, especially when they were immersed in water for a significant period of time (Niu and Gu, 1982). Clay cement material, when immersed in water, is liable to disintegrate, which results in a reduction of rock strength. The effect of water on the strength of carbonate cemented sandstone is not so evident.

Kaolin and illite are two main components in clay materials. They have the features of swelling and disintegration upon absorption of water. The swelling and disintegration of these minerals will lead to the development of microfissures in the rocks and accelerate their deterioration and, subsequently, the deterioration of tunnels. Since kaolin and illite are often found in shales, mudstones and fireclays, tunnels driven in these strata frequently suffer severe deformations especially floor lift and, in some cases, roof collapse problems if water is present.

Since rock strength is related to some extent to the size of the aggregate and the composition of the cement and the aggregate, then it follows that the value of a given mechanical property of any particular rock can be expected to fall within a certain range of values. Namely, the lithological description of a rock can indicate an approximate range of values of its mechanical properties and, thereafter, allow the

12

forecast to some extent of possible problems due to rock formations in a particular tunnel.

2.2 Effects of Geological Structures on Roadway Stability

The structure of strata may vary from a simple succession of nearly horizontal beds to a complex pattern of folding and faulting inclined at various angles. The strata may include deposits of a local occurrence and with variations in thickness, dip and strike.

2.2.1 Thickness, Dip and Strike of Strata in Relation to the Excavation Direction of the Roadway

The thickness of a stratum may vary greatly over the area along the line of the tunnel. Sometimes, a stratum disappears due to the effect of washout, as the development of a tunnel continues. The change in the strata around the tunnel may cause a change in tunnel stability. In the case of a combination of hard and soft rocks, some difficulties may arise in the choice of excavation method. With current practice, various roadheaders are applied to underground tunnel excavations. These machines can work effectively and efficiently in soft and weak ground conditions. The consumption of rock cutting picks is small in such ground conditions. However, if the hard and soft rocks are found to be combined and encountered in the tunnel heading, problems can sometimes become significant. On the one hand, the consumption of rock cutting picks will increase for cutting in hard rock. On the other hand, if a conventional blasting technique is adopted, the scope of damage to the weak part of the rock will be increased by the blasting effect, and therefore the stability of the tunnel may be affected.

The dip and its orientation relative to the excavation direction are of great importance in tunnel drivage through rock formations (Megaw and Bartlett, 1982). A level tunnel in the direction of the strike may be expected to remain in the same
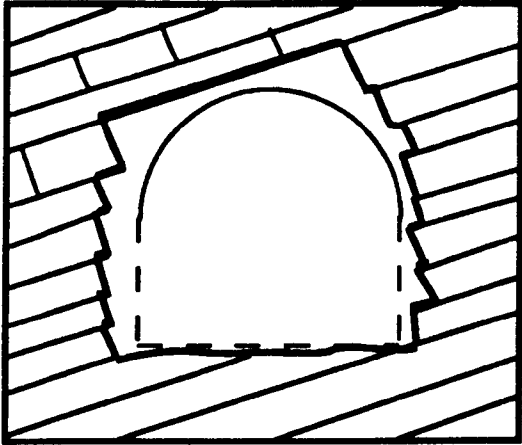
(a) Dip across tunnel
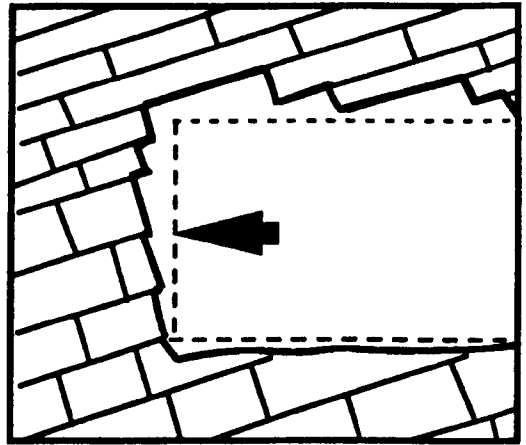
(b) Tunnel following in direction of dip
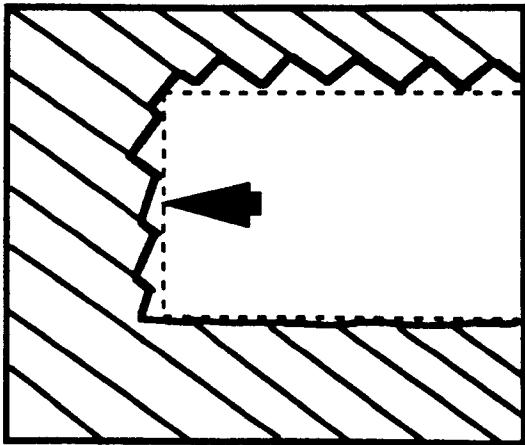
(c) Tunnel driven against direction of dip
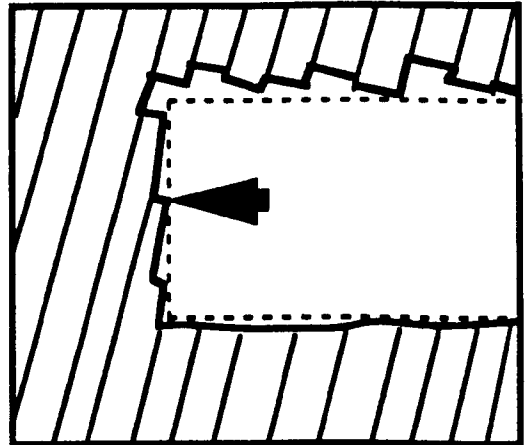
(d) Tunnel driven with near-vertical dip

Figure 2.2.1 Effects of the excavation direction on the stability of tunnels
in jointed rocks (after Megaw and Bartlett, 1982)

stratum, if it is thick enough. If the dip across the line of the tunnel (see Figure 2.2.1.a) is other than small, the roof will tend to break away on any weak bedding planes, and there is likely to be a weak side where rock slides into the excavation. If a tunnel runs level in the direction of the dip (Figure 2.2.1.b) it will progressively cut through higher beds of the succession with consequent changes of strength and behaviour; any weakness in shear on the bedding surfaces will result in weakness of the roof as support is cut away at the heading. Conversely, a tunnel driven against the direction of dip (Figure 2.2.1.c) will progress into lower beds and is less likely to be weak near the heading.

If the dip is nearly vertical the tunnel excavation would be very different according to whether the tunnel is driven along the strike or at right angles to it. If along the strike, the same layers and bedding surfaces persist, difficulties with support would arise with any weakness in shear or any water bearing stratum. Along the line of dip, however, (Figure 2.2.1.d) it will cut across the succession of beds at right angles; each bed is itself competent and can function as a transverse arch; a weak layer is only likely to require support while its thickness is penetrated.

2.2.2 Discontinuities

In the process of sedimentation and the movement of the Earth's crust, rocks in the Coal Measures have experienced various disturbances by ground stresses. Mountain building, regional tectonic movements, local volcanic activities, earthquakes, etc. have resulted in the geological discontinuities of the strata. Mining activities have shown that more difficult problems arise from a heading being located in the region suffering from significant geological disturbances. Most hazards and accidents regarding rock failure, breakage, falling and outbursts occur in relation to the strata possessing discontinuities and geological disturbances.

Geological discontinuities, according to the degree of disturbance, are classified into joints, beddings and laminations, faults and uncomformities.

2.2.2.1 Joints and Folds

Joints are rock fractures along which they have experienced no significant visible displacement. They occur systematically in two sets in Coal Measures. Each set of joints has a consistent strike and dip. The two sets of joints intercept commonly at a consistent angle although both are vertical or near vertical to the bedding surfaces.

Joint spacings in limestone and sandstone strata are usually metres apart while in shale and clay strata they tend to be closer. The spacing of joints plays an important role in tunnel stability. A well jointed stratum may fail and fall frequently and readily if a tunnel is driven in it. In such conditions, intensive sealing and/or backingfilling between standing supports, such as wire mesh and shotcrete, may therefore be needed in order to prevent surrounding jointed rocks from falling.

In sedimentary circumstances, major joints are chiefly formed by the effects of early regional tectonic movements, although few others may be formed due to the shrinkage of clays in argillaceous rock formations, or due to thermal effects by virtue of the magmatic intrusion during volcanic eruptions. Therefore the parameters of joint structures such as strike, dip and spacing may be related to the historic stress field. The latter may remain the same to date or result in the occurrence of residual effects which influence tunnel stability.

The dip and strike of joints is frequently influenced by folding effects. Wave-like fold structures may vary from slight folds with gentle strata dips to narrow and severe or well developed folds characterized by steeply dipping or even overturned beds. The scale of folds ranges from the order of centimetres to that of kilometres in amplitude.

Whittaker and Frith (1990) argue that severely distorted folds are frequently accompanied by plastic behaviour of rocks especially in the softer sedimentary rocks.

16

Relative sliding between layers also occurs in flexural folding in strongly stratified structures.

Due to folding and bending effects, tension joints are more likely to be well developed in the upper half of each stratum along the axis of anticlinal folds and, in contrast, they tend to be well generated in the lower half of each stratum in the axis of synclinal folds. Furthermore joints along the axis of folds are likely to spread downward in anticlinal structures and spread upward in synclinal structures. Hence tunnels driven along the axis of an anticlinal fold are more likely to experience frequent floor lift problems (Figure 2.2.2 a) whilst those excavated along the axis of synclinal folds have a higher probability of suffering roof falls (Figure 2.2.2 b).

2.2.2.2 Faults

Faults are rock fractures which have been dislocated by some source of ground stresses in the process of the earth crustal movements.

Faults may be simply classified into three types: normal, reverse and wrench faults although other classifications also exist. The occurrence of the three basic types of fault are attributed to the differences in orientations of the three principal stresses with respect to the earth's surface (Peng 1986, Anderson 1951). Figure 2.2.3 indicates the stress conditions that result in:

(a) a normal fault as the hanging wall is lowered or thrown down;

(b) a reverse fault as the hanging wall is raised or thrown up along the fault surface; and

(c) a wrench or strike - slip fault as the two parts of strata on both sides of the fault surface slip horizontally in opposite directions along the fault surface.

In the figure σ_1, σ_2, and σ_3 are the maximum, intermediate, and minimum principal stresses respectively.
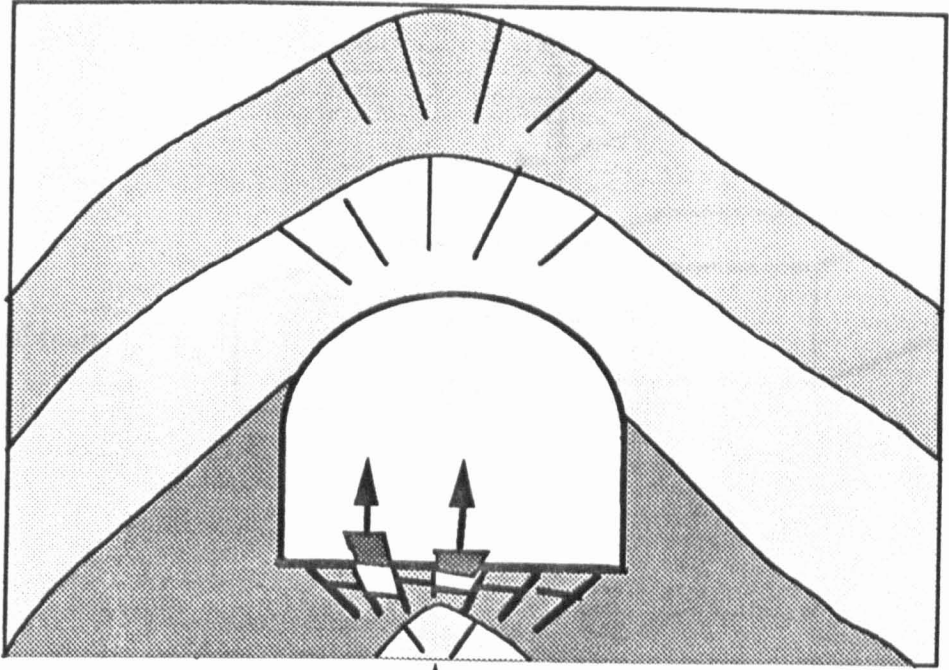
(a) Floor heave in association with the tunnel driven along an anticlinal fold
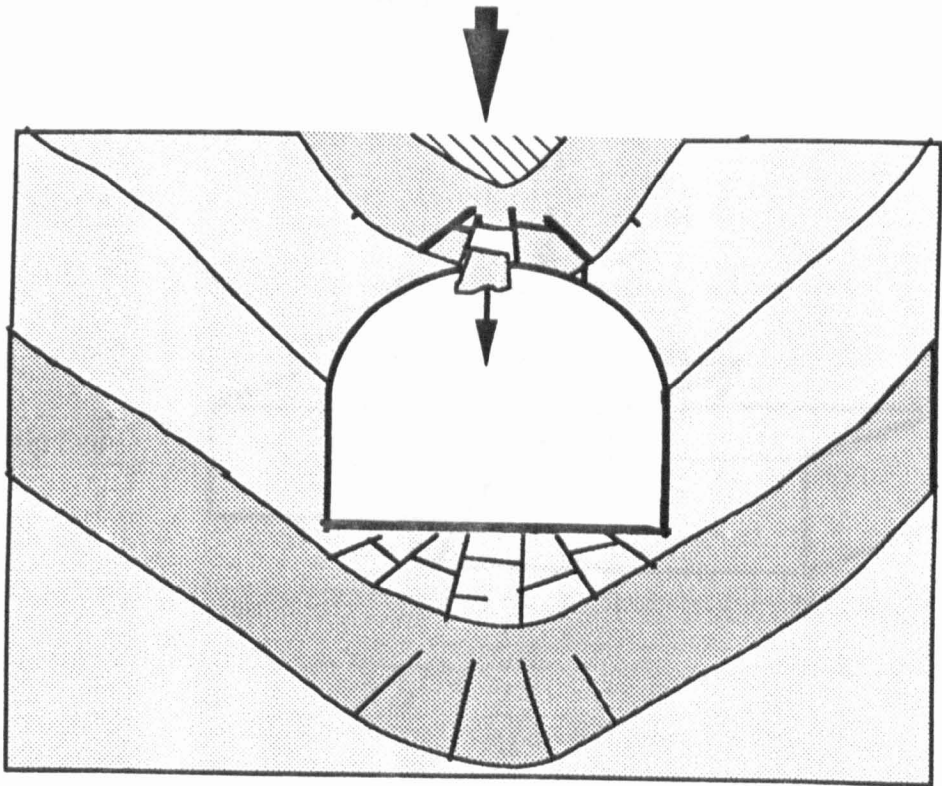
(b) Roof falling in association with the tunnel driven along a synclinal fold

Figure 2.2.2 Effects of fold features on tunnel stability

18

(a) Normal fault
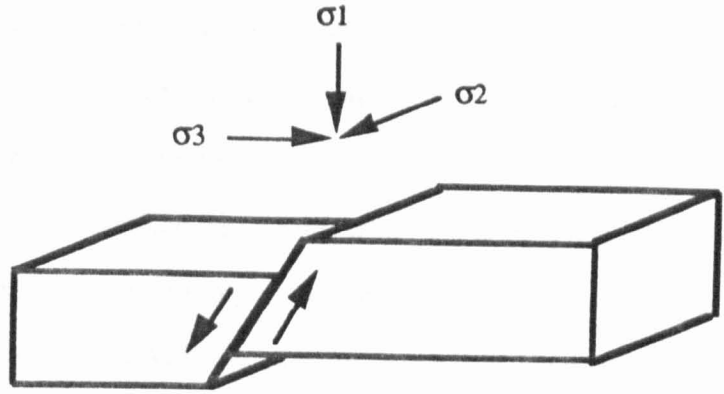
(b) Reverse fault
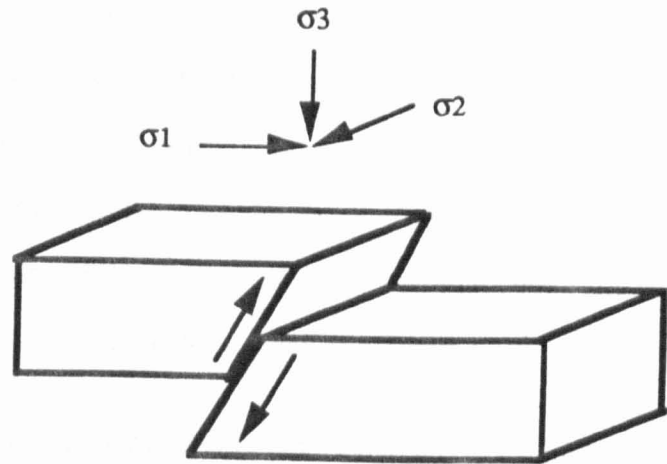
(c) Strike-slip fault
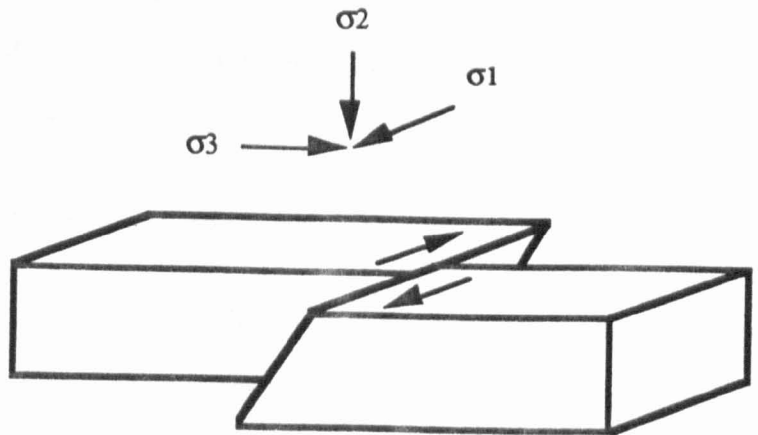
Figure 2.2.3 Three types of faults

Faults usually have adverse effects upon tunnel excavation and stability. In the case that the fault surface is filled with a large quantity of gouge or breccia materials, tunnel drivage through the fault may be exposed to the danger of water inrush conducted along the fault surface, especially when the fault is of tensile pattern and connected to an aquifer above the tunnel or occasionally to a mined-out area in an adjacent upper seam where a large volume of mine water has accumulated. Other problems which may be encountered in tunnel drivage in faulted areas are appreciable tunnel deformations, support failures and roof collapses. Shepherd and Fisher (1978) and Peng (1986) argue that normal dip slip faults do not appear to be associated with roof failures unless there are large offset, normal oblique and strike slip faults which are associated with severe roof failures and that the zones of influence are 1.2 to 3.0 metres on each side of the fault. Rutherford *et al.*, reported that roof falls in the faulted area are 20 times more likely than under normal conditions.

It can be seen from the abundance of mining practice in the world that a careful study and comprehensive understanding of faults with regard to their nature, elements, origination, and their effects on tunnel stability, are very important aspects to the mining tunnel designer.

2.2.2.3 Beddings and Laminations

Sedimentary strata are featured by bedding and lamination. Tunnels driven in such strata sometimes have to withstand the rock failure due to the splitting of rock. Williamson (1967) argues that, sedimentary rocks may be easily split along their bedding surfaces. As distinct from bedding, the possession of lamination does not always enable the rock to be split into thin individual units or laminae. To prove this point he lists some examples, indicating that shales are well laminated rock which, particularly when weathered, break along the lamination surfaces into often paper thin sheets, whereas the majority of fine sandstones though distinctly laminated often only separate along bedding surfaces.

It seems that the adhesive strength between the laminated and bedding surfaces plays an important role in keeping the strata competent. Generally the adhesive strength of bedding and lamination surfaces is weaker than the rock on the both sides of the bedding or lamination plane. Upon the application of the beam theory to the prediction of strata detachment problems, it may be found that shear failures are likely to occur along the beddings and laminations near the neutral plane of the beam when the detachment process is occurring.

Obviously, a careful study of the nature of the beddings and laminations may lead to some predictions being possible regarding the maximum span of an unsupported tunnel and the safe spacing of rock bolts or standing supports.

2.2.3 Ground Water

Ground water exists in the vast majority of collieries. It often brings trouble in coal mining operations and tunnel construction work. Hence the mining engineer needs to take it into consideration in tunnel designs.

Ground water in mines is present mainly in two forms, as stored in voids of some strata as aquifers and accumulated in abandent old mined-out areas. In some mines the quantities of ground water, expressed in tonnages, may be greater than the total coal output of the mines.

Main source of ground water is rainfall, which may migrate from the surface to the ground and become stored in aquifers. Intersections of aquifers with mine workings (mining or heading) will lead to discharges of the water from the strata which may result in a water inrush. Particularly large inflows of water in this way are sometimes encountered during the driving of cross-measures tunnels. As being penetrated by tunnels, some faults, especially tensile and fissured ones, may constitute ideal conduits for ground water to percolate along the fault surfaces into the tunnels.

Phenomenon of ground water affecting tunnel stability is mainly exhibited in two ways; rapid destruction of tunnels by virtue of a water inrush of large quantities, and gradual deterioration of the tunnel by means of long term percolation, with the latter being more common.

In the case of the water table of an aquifer at the place of a tunnel being higher than the level of the tunnel, water stored in the aquifer can inrush into the tunnel so long as a passage is formed between the stratum and the excavation. In such cases aquifers are not necessarily in immediate contact with seams when water problems occur. The occurrence of large roof falls over wide gate ends and crossings and extending upwards to the base of aquifer is considered to be possible for inrushes in some cases. Roof or floor breaks in association with longwall mining may extend through normally impervious argillaceous layers to the base of an overlying or underlying water bearing stratum and hence form considerable feeders. In Northern China, some water inrush accidents caused by the Ordovician Limestone aquifer underlying the Carboniferous and Permian Coal Measures give typical examples of rapid destruction of tunnels by ground water. In these accidents the water table of the Ordovician Limestone aquifer is much higher than the mining level. These water inrushes were initiated either by mining activities which disturbed and distructed the floor integrity by · inducing fissures and fractures in the floor, or by crosscutting of an excavation into a water conducting faulted zone.

Occurrences of swelling and squeezing of surrounding weak rocks of tunnels are, in many cases, due to the effect of water seepage. In such weak and soft rock conditions, comparatively high contents of dilatable minerals such as kaolin and ellite are found to be liable to cause tunnel deformations. A dominant feature of these minerals is their dilatancy upon absorption of water. Even in hard rock conditions, percolation of water over periods of time can also lead to rock failure and roof falls in tunnels. The author (1988) reported that in an investigation of an artificial water

injection into a very hard sandstone at a Datong Colliery for a longwall mining purpose, it was found that the quantity of water injected into the hard sandstone roof in front of the longwall faceline had a significant influence on tunnel or maingate stability. When the quantity of water was 400 cubic metres injected in each roof borehole, the maingate exhibited instability . . . near the face end as roof spallings to some extent were recorded. Therefore additional centre props had to be installed within 20 metres of the face line. When water was injected at a level of 300 cubic metres per borehole, roof instability problems in the maingate disappeared.

It should be noted that probability of seepage and inrush into new excavation sites by ground water (accumulated in mined-out areas) also requires special attention since such accidents may occur in many coal mines especially where the old mined-out areas are not clearly recorded and have been left over the currently mined. Also, the progressive closure of collieries in some coal fields, particularly in the UK, can result in the accumulation of ground water which, due to the interconnecting layouts of abandoned and operating mines, the over or under working of abandoned seams poses a serious threat of a dangerous situation arising from a sudden inrush of vast quantities of uncontrolled ground water, Lemon 1991.

2.2.4 Mechanical Properties of Rocks

The mechanical properties of rock are concerned with the response of rock to various applied loads of various sizes from laboratory samples to rock masses where tunnels are driven. The properties are usually considered to include modulus of elasticity, Poisson's ratio, various strength values, rheological behaviour and characteristics of homogeneity, isotropy and continuity.

There are three ways of defining the modulus of elasticity, i.e., secant modulus, tangent modules and initial tangent modulus. Table 2.2.1 shows some typical values of tangent moduli at the point of 50% of the uniaxial compressive strength.

23

Most values of Poisson's ratio for rocks lie between 0.15 and 0.35. Lower values are usually associated with the higher strength and higher modulus of rock, and vice versa.

Table 2.2.1 Typical mechanical properties of some coal measures rocks

Rock type	Uniaxial compressive strength (MPa)	Tensile strength (MPa)	Young's modulus (GPa)
Mudstone	35.0 - 50.0	4.0 - 5.0	3.1 - 6.0
Seatearth	21.0 - 37.0	2.2 - 4.8	3.8 - 5.0
Laminated siltstone	51.0 - 77.0	8.0 - 10.0	14.3 - 19.7
Massive siltstone	60.0 - 94.0	6.3 - 8.7	8.0 - 13.0
Fine-grained sandstone	85.0 - 156.0	17.5 - 25.0	18.3 - 31.4
Medium-grained sandstone	93.0 - 140.0	12.5 - 18.5	18.5 - 40.0
Coarse-grained sandstone	63.9 - 103.6	2.1 - 12.6	11.7 - 19.5
Conglomerate stone	59.0 - 82.4	2.1 - 11.0	14.5 - 17.7
Limestone	138.7 - 148.5	8.9 - 14.5	68 - 76

Tensile and uniaxial compressive strengths of rock are two of the most important parameters frequently used in rock engineering design . The calculation of safe tunnel span and support density needs to employ these strength values together with the use of an appropriate safety factor. Due to economic and convenience considerations, rock tensile strength and uniaxial compressive strength are usually determined by laboratory means which employs cylindrical samples, although the values from the laboratory are different from those of rock masses due to the presence of discontinuities in the latter. This explains the need for adopting an appropriate

safety factor in most design work. Table 2.2.1 also gives the values of tensile and compressive strengths of some rocks from coal formations.

Generally speaking, rock sample strength can reflect to some extent the strength of stratum together with the degree of jointing. Considering disturbance to strata after their formation, a subsequent geological disturbance would create more joints and fissures in weak rocks than in strong rocks. And a strata with more joints and fissures is weaker than that with less joints and fissures. That is why in the strata from which rock samples are weak in strength there are usually more joints and cracks, and vice versa.

Mudstones, shales, and fireclays may often exhibit rheological behaviour, that is, they possess properties that are time-dependent. A significant rheological phenomenon of which the mining engineer is mostly concerned with is the change in strata deformation time in a constant stress field, known as creep. In underground conditions, rock temperature and ground water have a pronounced effect on the creep destruction of a tunnel. Although the creep behaviour of rocks has long been recognised and studied and various creep models have been proposed, it still remains far from application to the satisfactory solution of engineering problems especially in respect of mine tunnel in coal mines.

The presence of beddings, laminations, faults and joints implies that rock strata within coal sequences are mostly anisotropic, discontinuous and even non-homogeneous. Taking these characteristics into account, it has long been recognised that the common assumptions of the theory of elasticity, that is , homogeneity, isotropy and continuity of material, may not be precisely applied to rock engineering. However, the rock characteristics of non-homogeneity, anisotropy and discontinuity cannot be accurately evaluated and so far there is difficulty in estimating them, although the advent of computer techniques has led to the possibility of solutions to many nonhomogeneous, anisotropic and discontinuous problems. Often, therefore,

there is no choice but to accept in design work that the assumptions of homogeneity, isotropy and continuity are valid to some extent and to use engineering judgement to assess the degree of departure of the behaviour of actual rock mass from that of the idealised material. For the large majority of problems this is likely to be the most useful approach even in the case of applying computer techniques to such problems.

2.2.5 Virgin Ground Stresses

Prior to the excavation of a tunnel, strata are in equilibrium and subjected to the effect of a virgin stress field. The virgin stress field consists, in general, of two components: one is due to gravity and the other due to regional tectonic movement resulting in horizontal stress components. Combinations of these stress influences may bring problems of various degrees to mining tunnels, such as floor lifting, support distortion and deformation, sidewall squeezing, roof falls, and even rockbursts in some severely disturbed rock zones. All these problems threaten man's safety and the efficiency of production, and therefore attract the attention of the mining engineer.

2.2.5.1 Virgin Ground Stresses due to Depth

In the gravity induced stress field, the vertical component of stress at a point in strata under consideration depends on the depth of cover above the point and the strata unit weight. If the overburden strata are constituted by n layers with each layer having a thickness of h_i and a unit weight $r_i (i=1, 2, \ldots, n)$, then the magnitude of vertical component of stress σ_z can be expressed as:

$$\sigma_z = \sum_{i=1}^{n} r_i . h_i \qquad (2.2.1)$$

where σ_z is vertical component of stress due to gravitational loading; and r_i and h_i are the unit weight and thickness of the i th stratum respectively.

A common assumption in the estimation of horizontal principal stress components for a gravity induced stress field is a condition of uniaxial vertical strain with complete lateral restraint. therefore the horizontal principal stress components σ_x, σ_y are given by the formula:

$$\sigma_x = \sigma_y = k\sigma_z \qquad (2.2.2)$$

where k is lateral stress factor.

In the elastic strata condition, derived from Hooke's law,

$$\sigma_x = \sigma_y = \frac{v}{1-v}\sigma_z ; \quad \text{or} \quad k = \frac{v}{1-v} \qquad (2.2.3)$$

where v is Poisson's ratio of the stratum under consideration.

Since Poisson's ratio of majority of strata lies in the range of 0.20 - 0.33 (Riggott, 1986), the lateral stress factor k is 0.25 - 0.50, i.e. the horizontal principal stress components in a gravitational stress field are smaller than the vertical one.

From equations 2.2.1, and 2.2.2 or 2.2.3 we know that the gravity induced stresses increase with depth. This result shows that under the effect of this kind of stress field a tunnel in the same stratum but at greater depth may suffer more pronounced instability problems.

The gravity induced stress field is an idealized assumption for the existence of the virgin ground stress field. This assumption is usually acceptable for and applicable to only those ground conditions where strata have experienced less tectonic disturbance in their formation process and subsequent development, and where there are very few geological structures such as severe faults and folds. For other ground conditions, however, numerous investigations have indicated that the horizontal principal stresses differ significantly from the value calculated by equation (2.2.3).

These facts reveal that the regional tectonic influence must be a source for this difference and should be considered in the estimation of horizontal principal stresses.

2.2.5.2 Virgin Ground Stresses Taking Tectonic Disturbance into Account

Tectonic activity may impose an extra force field on a stratum, forming a resultant ground stress field which could be greatly different from the gravity induced stress field. Brady and Brown (1985) point out stresses associated with this form of loading operate on a regional extent and may be correlated with such structural formations as faulting and folding in the domain. A significant tectonic movement may result in the occurrence of one substantial horizontal stress component. Hoek and Brown (1980) give a comprehensive collation of the results of the measurement of the virgin state of stress at many different locations (Figure 2.2.4). The figure shows that the action of tectonic disturbances is likely to result in a horizontal stress greater than the vertical one. It also reveals that it is very difficult or even impossible to accurately calculate the magnitude and direction of virgin ground stress by virtue of mechanical theory or by means of computer techniques.

Tectonic effects may cause a number of problems in respect of mining tunnel stability, in some areas, for instance, in severe faulted zones or along a folding axis. This is particularly a problem when the tectonic disturbances result in significant storage of elastic strain energy in strata. Excavation in such areas may result in the rapid release of the stored elastic strain energy and so initiate rockbursts. When a rockburst occurs, various quantities of rock, or coal for in-seam tunnel cases, may be ejected into tunnel excavations and thus result in destruction of the support system and the tunnel.

Obviously the protection of tunnels from rockburst damage requires identification of potential tectonic actions. Many field measurements and relevant

$$k = \frac{\text{AVERAGE HORIZONTAL STRESS} \quad \sigma_{h.av}}{\text{VERTICAL STRESS} \quad \sigma_z}$$
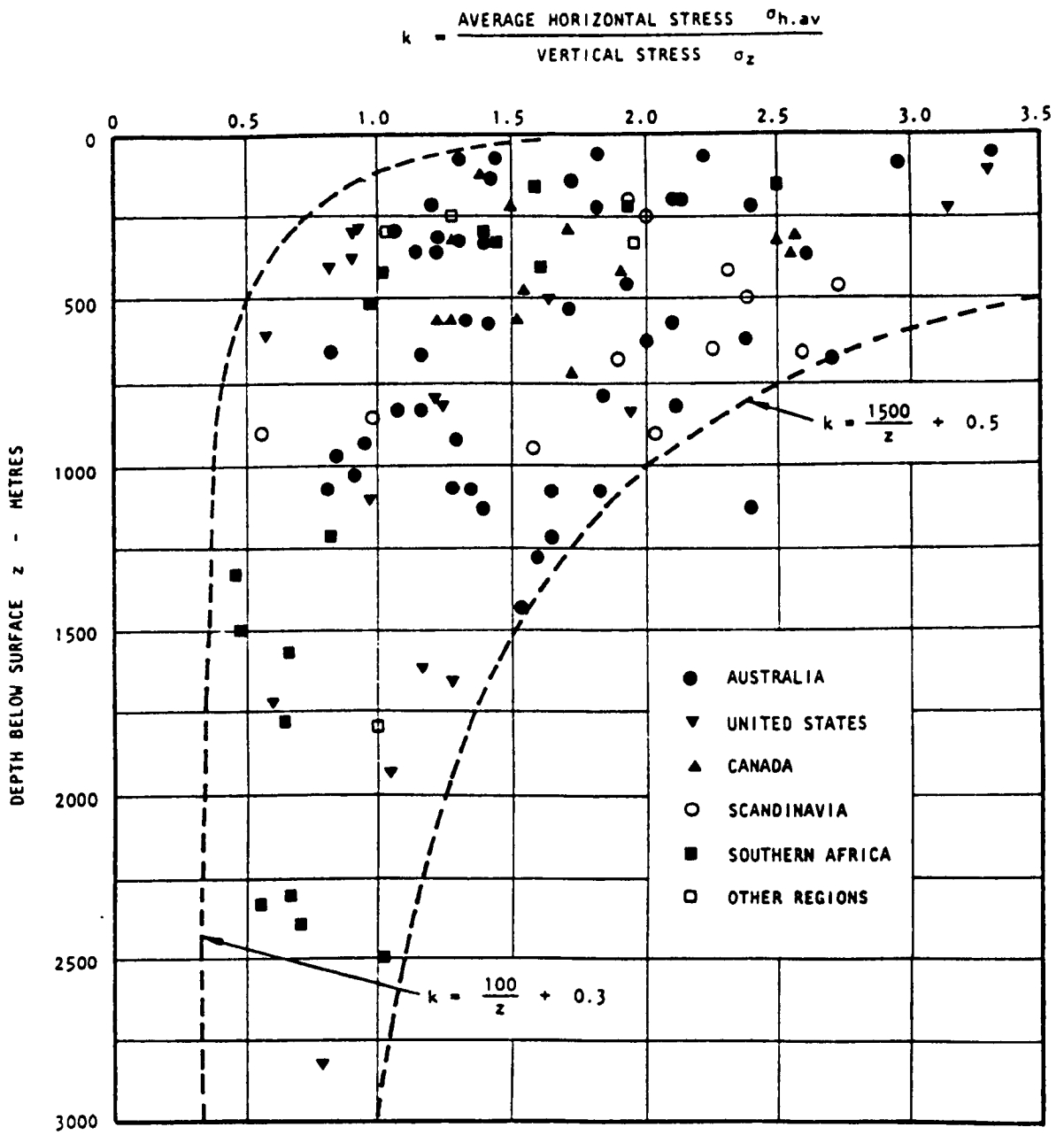
Figure 2.2.4 Results of measurements of the original stress field

(after Hoek and Brown, 1978)

research projects have therefore been carried out throughout the world in order to clarify understanding of such problems.

2.2.6 Classification of Rock Masses

Since strata in coal sequences can be referred to as assemblies of intack rock blocks together with interceptions of such geological discontinuities as joints, faults, beddings and laminations, engineering behaviour of these strata is affected by a group of parameters instead of any single one. According to their engineering behaviour, strata are usually divided into a number of groups, such as hard, medium and soft, or poor, fair, good, and excellent, etc. Within each group or class, strata should have the same or similar engineering behaviour and requirement for support. Obviously, a proper classification of strata can provide a basis for recognising the characteristics of each stratum within the same group. It would also make it possible to relate the experience of strata conditions at one site to the conditions and experience at other sites, and provide guide-lines for engineering design and facilitate communication among engineers and other relevant professionals.

A good scheme of strata classification is dependent on a proper selection of parameters or factors which have significant effects on tunnel stability. It is uneconomic and therefore unnecessary to include all influencing factors in strata classification. In the past few decades, therefore, many strata classification schemes have been proposed on the basis of different engineering considerations.

Terzaghi (1946) put forward the first rational method of classification by evaluating rock loads. The method is appropriate to the design of steel arch supports for tunnels. Cecil (1970) has pointed out that Terzaghi's classification was too general to permit an objective evaluation of rock quantity and that it provided no quantitative information on the properties of rock masses.

Lauffer (1958) recognised the importance of structural defects in rock masses and proposed a stand-up time classification in which rock masses are divided into several groups according to the stand-up time of any unsupported rock span after excavation. This classification indicates the effect of tunnel size on its stability and introduces the stand-up time and the span as relevant parameters for the determination of the type and intensity of tunnel support.. However this classification disregards some other factors such as shape of cross section and excavation method.

Deere (1967) *et al.*, introduced the concept of rock quality designation (RQD) index based on which rock masses are divided into five classes (Table 2.2.2).

Table 2.2.2 Rock classification based on the RQD method

RQD (%)	Rock quality
< 25	Very poor
25 - 50	Poor
50 - 75	Fair
75 - 90	Good
90 - 100	Excellent

The RQD is a modified core recovery percentage which incorporates only those pieces of core that are 100 mm or greater in length. In other word it is a ratio (in percentage) of those core pieces with length being 100 mm or greater to the total core run length. Based on rock mass quality defined by the RQD index, a number of relevant support schemes for various rock conditions have been proposed by a number of engineers (Merritt, 1972, Deere *et al.*, 1970, Cecil, 1970).

Obviously, the RQD is a simple and inexpensive index and it has been widely used in America and Europe. However it is still not sufficient to provide an adequate

description of a rock mass because it disregards joint orientation, tightness, and gouge material.

Wickham, Tiedemann, and Skinner (1972) proposed the rock structure rating (RSR) concept. The RSR concept considers two main categories of factors affecting strata engineering behaviour: geological and construction parameters. The geological parameters include rock type, joint pattern and spacing, joint orientation, faults and folds, rock material properties and weathering or alteration. The construction parameters include tunnel dimensions, driving orientation and excavation method. Some of these factors can be treated separately; others are considered collectively. In some cases these factors may be defined accurately while in others only a general approximation can be made (Wickham *et al.*, 1972, Bieniawski, 1989).

Bieniawski (1989) developed the Rock Mass Rating system during 1972 - 1973 for the rock mass classification purpose. This system employs six parameters: (1) uniaxial compressive strength of rock material; (2) rock quality designation (RQD); (3) spacing of discontinuities; (4) condition of discontinuities; (5) ground water conditions; and (6) orientation of discontinuities. The first five parameters are grouped into five ranges of values. According to the significance of each parameters to the overall classification, different weight values are assigned to each of the parameters (Table 2.2.3 a). The orientation of the discontinuities is also allocated five ratings and used for adjustment purpose (Table 2.2.3 b). An overall calculation of rating values of these parameters will then come to a final rating value ranging from 0 to 100 for the rock mass under consideration which indicates that rock masses with higher rating values will tend to behave more stably in tunnel construction. In the process of classification with this system, it can be seen that the assignment of rating values to each of the parameters and the division of the ranges of each of the parameters are very sensitive to the final rating value. They involve mostly subjective determinations and therefore require a lot of experience.

A. Classification parameters and their ratings

	Parameter		Ranges of values						
1	Strength of intact rock material	Point-load strength index (MPa)	>10	4 - 10	2 - 4	1 - 2	For this low range, uniaxial compressive test is preferred		
							5 - 25	1 - 5	<1
		Uniaxial compressive strength (MPa)	>250	100 - 250	50 - 100	25 - 50	5 - 25	1 - 5	0
		Rating	15	12	7	4	2	1	0
2	Drilling core quality RQD (%)		90 - 100	75 - 90	50 - 75	25 - 50	<25		
	Rating		20	17	13	8	3		
3	Spacing of discontinuities		> 2 m	0.6 - 2 m	200 - 600 mm	60 - 200 mm	<60 mm		
	Rating		20	15	10	8	5		
4	Condition of discontinuities		Very rough surfaces Not continuous No separation Unweathered wall rock	Slightly rough surfaces Separation < 1mm Slightly weathered walls	Slightly rough surfaces Separation < 1 mm Highly weathered walls	Slickensided surfaces or Gouge<5mm thick or Separation 1-5mm Continuous	Soft gouge> 5mm thick or Separation>5mm Continuous		
	Rating		30	25	20	10	0		
5	Ground water	Inflow per 10m tunnel length (L/min)	None	<10	10 - 25	25 - 125	>125		
		Ratio= Joint water Pressure / Major principal stress	0	<0.1	0.1 - 0.2	0.2 - 0.5	> 0.5		
		General conditions	Completely dry	Damp	Wet	Dripping	Flowing		
	Rating		15	10	7	4	0		

Table 2.2.3 (a) The rock mass rating system (after Bieniawski, 1989)

B. Rating adjustment for discontinuity orientations

Strike and dip orientation of discontinuities		Very favorable	Favorable	Fair	Unfavorable	Very unfavorable
Rating	Tunnels and mines	0	-2	-5	-10	-12
	Foundations	0	-2	-7	-15	-25
	Slopes	0	-5	-25	-50	-60

C. Rock mass classes determined from total ratings

Rating	100 - 81	80 - 61	60 - 41	40 - 21	<20
Class no.	I	II	III	IV	V
Description	Very good rock	good rock	Fair rock	poor rock	Very poor rock

D. Meaning of rock mass classes

Class no.	I	II	III	IV	V
Average standing-up time	20 yr for 15 m span	1 yr for 10m span	1 wk for 5m span	10 hr for 2.5m span	30 min for 1m span
Cohesion of the rock mass (kPa)	>400	300 - 400	200 - 300	100 - 200	<100
Friction angle of the rock mass (deg.)	>45	35 - 45	25 - 35	15 - 25	<15

Table 2.2.3 (b) The rock mass rating system (after Bieniawski, 1989) (Continued)

34

Barton, Lien, and Lunde (1974) proposed the Q-system of rock mass classification, based on an analysis of over 200 tunnel case histories. The Q-system uses six parameters: (1) RQD; (2) number of joint sets; (3) roughness of the most unfavourable joint or discontinuity; (4) degree of alteration or filling along the weaker joint; (5) water inflow; and (6) stress condition. These six parameters are incorporated and calculated to give the overall rock mass quality Q as follow:

$$Q = \frac{RQD}{J_n} * \frac{J_r}{J_a} * \frac{J_w}{SRF}$$ (2.2.4)

where RQD = rock quality designation; J_n = the number of joint sets; J_r = joint roughness number; J_a = joint alteration number; J_w = joint water reduction number; and SRF = stress reduction factor.

The rock mass quality Q can range from 0.001 to 1000 on a logarithmic rock mass quality scale with the higher value referring to better quality of rock.

The above classification schemes provide an assessment of the rational design of underground tunnels and the effective selection of excavation means and support methods.

There are other rock mass classification schemes which have been proposed in a number of countries for different and specified application purposes. A rock mass classification scheme for the identification of roof strata behaviour and the design of the coal face support pattern and density has been proposed in China coal industry, for example. Different from others, the scheme employs those parameters of the uniaxial compressive strength, joint spacing, thickness of roof layers, and the face advancing length when the first collapse of immediate roof occurs. And the immediate roof strata are grouped into four categories. Similarly main roofs are also classified into four kinds on the basis of the ratio of the immediate roof thickness to the extracted seam height, and the first weighting intensity of the main roof respectively (Niu and Chen 1986). Another rock mass classification scheme has also been

35

proposed in China for the design of mining tunnels and supports (Liu, *et al* 1989, Li *et al.*, 1990).

2.3 Effects of Operational Factors on Roadway Stability

The stability of mining tunnels is also influenced by a number of operational factors which are defined in this thesis as those resulting from man's activities underground. These factors include excavation method, mining induced stresses, pillar dimensions and support methods and timing, etc. A careful examination into these factors is helpful for a better understanding of tunnel stability and the problems likely to arise due to the occurrence of these factors. And relevant precautions aiming at avoidance or minimisation of these influences may thus be formed and put forward for engineering schemes.

2.3.1 Excavation Methods Influencing Rock Competence

Mining tunnel excavation approaches are classified into two main categories: drilling and blasting, and mechanical cutting.

In drilling and blasting operations, shotholes are first drilled at the heading face. Explosives are then charged in these space limited shotholes and initiated. On the initiation, a violent chemical reaction takes places, which results in the generation of high pressure gases and also an intense pressure wave.

The high pressure gases induce high stresses in the immediate vicinity of the shotholes. By exceeding the rock strengths the stresses break, shatter and crush the rock in a zone of a certain radius. Outside but next to this zone is another zone containing radial cracks which are formed by the tangential tensile stress component of the explosion. These cracks propagate radially as long as the tangential tensile stress at the crack tips exceeds the tensile strength of the rock.

During the outward propagation of the intensive pressure waves, some parts of the waves are reflected at   discontinuity surfaces of the rock mass, which may superimpose on the later-coming outward waves to result that vibrations caused by the explosion enhances at some points and weakens at other places. The consequence of this effect is that of the rock mass is broken into pieces.

It is, therefore, evident that blasting causes damage to the near shothole part of rock mass and generates more or less cracks of various degrees along the outline of remained rock mass. In other words when a tunnel profile is exposed by the means of drilling and blasting, there are more or less cracks generated in the vicinity of the tunnel, which is likely to give rise to the later instability problems, and thus requires intensive supports and sealing in order to prevent the cracked or fractured rock blocks from sliding, falling and spalling. Further more, tunnels excavated by drilling and blasting method usually exhibit less smooth surfaces around the profile in most cases. Standing supports used in these tunnels cannot easily contact the excavated profile and thereby undertake rock loadings equally along the whole configuration of the support. Consequently, more torsions and twists of supports are likely to occur along the support bearing surface.

The advent and application of roadheaders and tunnel boring machines (TBM) has greatly improved the tunnel excavation and stability by virtue of highly efficient cutting and much less disturbance to the surrounding rocks. Machine excavation method also makes the tunnel profile become smooth, which in turn provides ease to the effective erection of support. Supports working in such profile conditions will behave better in respect of stability. Accordingly, most major tunnel drivage projects in many countries consider the machine excavation method as a first choice unless the ground conditions such as the rock strengths exceed the capabilities of the machines and thereby rule out this preference.

It should be pointed out, however, that the damage to the surrounding rock mass by blasting can be relieved to a significant extent by careful design of the blasting pattern, the initiation sequence and the amount of explosive charged in each shothole, particularly those near the planned tunnel profile. The need for a smooth profile has led to the generation of a typical blasting technique known as the "smooth blasting technique". This technique has been widely used for many years in hard rock drivages in many countries. In many other rock conditions and economic circumstances (particularly in developing countries) perhaps drilling and blasting method is still the most feasible and practicable form of selection.

2.3.2 Mining Induced Stresses and Layout of Tunnels for a Longwall Panels

Many mining tunnels such as gateways in longwall mining districts, are close to the coal extraction sites. As a consequence the stability of these tunnels is often adversely influenced by the approach of coal winning operations since the winning of coal at the working face will inevitably cause a redistribution of rock stresses and induce strata abutment stresses to act on the tunnels within a certain range. A typical formation of strata abutment pressures in the case of simple or single panel is likely to be the one as shown in Figure 2.3.1 (Whittaker, 1974). As the face advances, immediate roof strata above the mined out area behind the face loses the previous support of solid coal and detaches from the overlying strata and irregularly caves in the goaf. The remaining roof strata (main roof and the other higher located strata) will bridge over the goaf to prevent further caving. The loads on this part of strata and overlying ones over the goaf are transferred through the bridge structure to the solid coal seam skirting the panel, forming the abutment pressures in front of the face line, and alongside both flanks of the panel. The strata pressure in the goaf gradually increases from the fully pressure relieved state immediately behind the

(a)
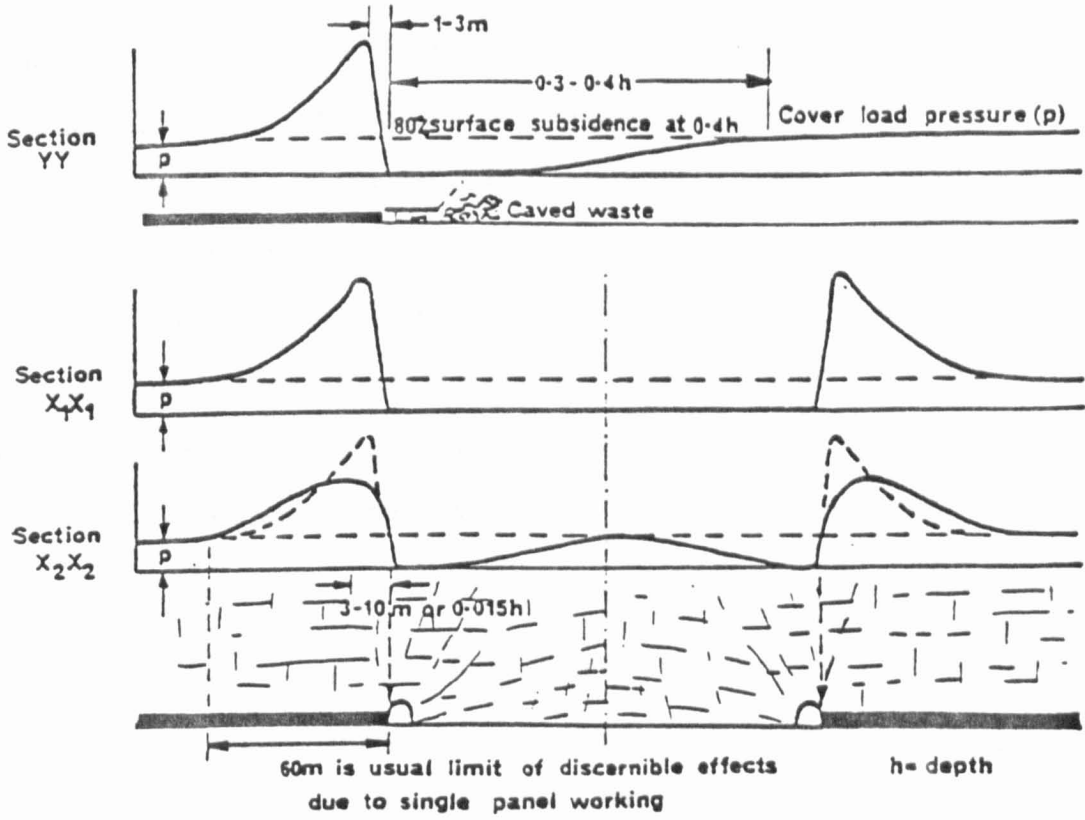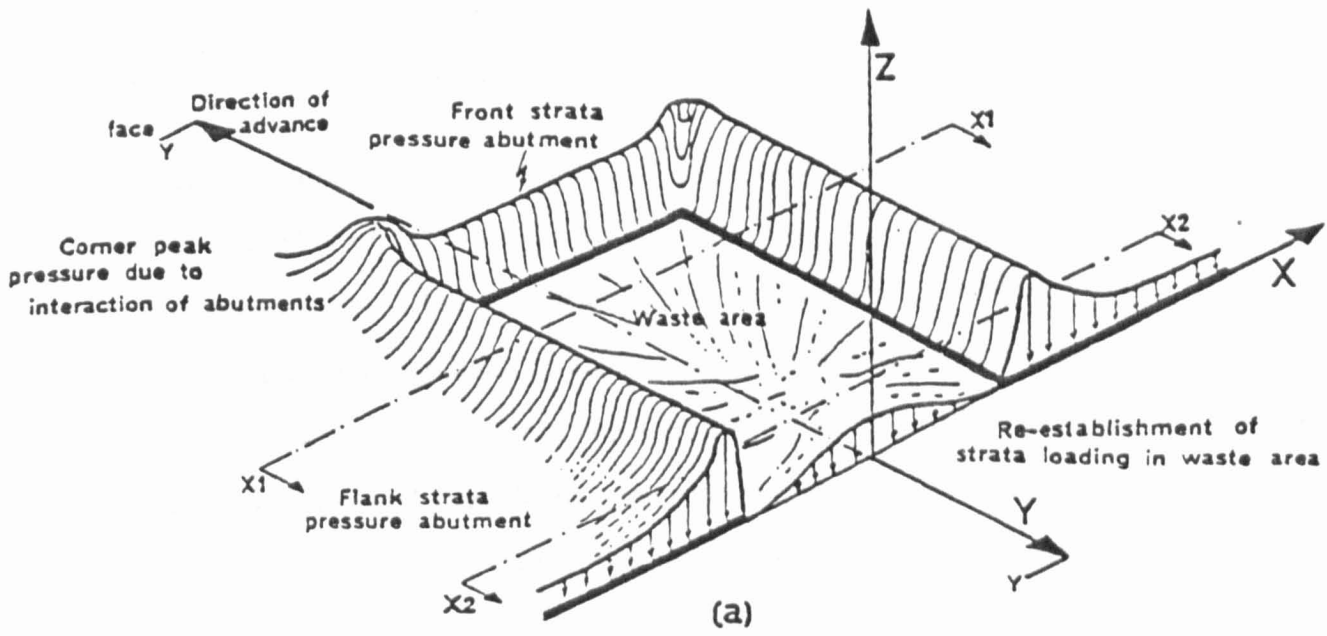
(b)

Figure 2.3.1 Abutment stress distribution around a working face

(after Whittaker, 1974).

longwall face supports to the retrieval of the original strata pressure some distance (100 -300 metres) behind the working face.

The redistribution of rock stresses around the longwall working area is governed by a number of factors such as the panel size, the winning height, the structural characteristics of the coal seam and adjacent strata, cavability of the immediate roof strata, mining depth or the state of virgin stresses of strata, type of support, with some factors being more effective on the tunnel stability than the others. In comparison to the original stress level, strata stresses are, in general, lower in the goaf and much higher in the solid coal at the edges of both rib sides and immediately in front of the faceline than the original pressure prior to mining. The front and side abutment pressures intersect at the corners of the panel and superimpose on each other to form zones liable to initiate roof instability problems. The pattern of the strata stress redistribution in the panel suggests that gate tunnels be located in the destressed zone in the goaf in order to gain   favourable stability. Otherwise, if they are positioned in the rib pillars or within the range of the appreciable abutment stress effect in front of the face line, the tunnels will be subjected to significant deformation problems, particularly in those sections of the tunnels within the zones near the positions of the peak abutment pressure which could be 2 - 6 fold of the original strata stress.

The panel layout systems are usually divided into two basic categories, i.e., those of the retreat mining and advance mining systems, with occasions of the combination of the two methods known as the Z pattern layout. In the USA (Peng, 1986), Poland, USSR and China the retreat mining method is prevailing whilst in most UK coal fields (Whittaker, 1972) the advance mining method is more widely employed.

In a retreat mining layout the gate roadways are predeveloped in full length before the coal extraction. On completion of a tunnel and the installation of face

equipment, the working face starts retreating the coal reserve of the panel blocked out by the gate tunnels. Accompanying the formation of a mined out area of sufficient width and length behind the face, immediate roof collapses in the goaf whilst the main roof bridges over the goaf and forms weighting at regular intervals as the length of the bridge structure increases to its limit state. The formation of the bridge structure causes the roof pressure to be concentrated in front of the face line, which further deforms the gate tunnels in the sections near both face ends since the gate roadways are always in front of the face line and thereafter under the action of the front abutment pressure. The gate stability problems arising in these sections could become so serious that the roof to floor convergence speed may reach 50 - 100 mm/day or even more. It has been encountered in practice in some coal mines in China that the gate tunnels with their original height of 2.2 - 2.4 metres converged to a height of around 1.2 metres as the retreating face approached.

The degree of the gate roadway convergence is usually related to the peak value and the range of the front abutment pressure. The peak value and the range of the front abutment pressure are, however, governed by the characteristics of both the seam and the roof strata. According to a finite element analysis (Chen, 1988), the range would become wider and the peak pressure would be higher if the main roof is stronger and well overhung in the goaf, see Figure 2.3.2.a. Improvement of the goaf filling by the caving of the immediate roof will reduce the length of the bridge structure of the main roof over the goaf and thus reduce the peak value and the range of the front abutment pressure (Figure 2.3.2.b). Softening of the coal seam in front of the face can lead to the position of the peak abutment pressure moving forward away from the face line (Figure 2.3.2.C). Based on these principles various measures can be taken in order to improve the peak magnitude and acting range of the abutment pressure, such as induced caving of hard roofs by either blasting or water injection for softening. Generally speaking, the capacity of longwall supports at present levels
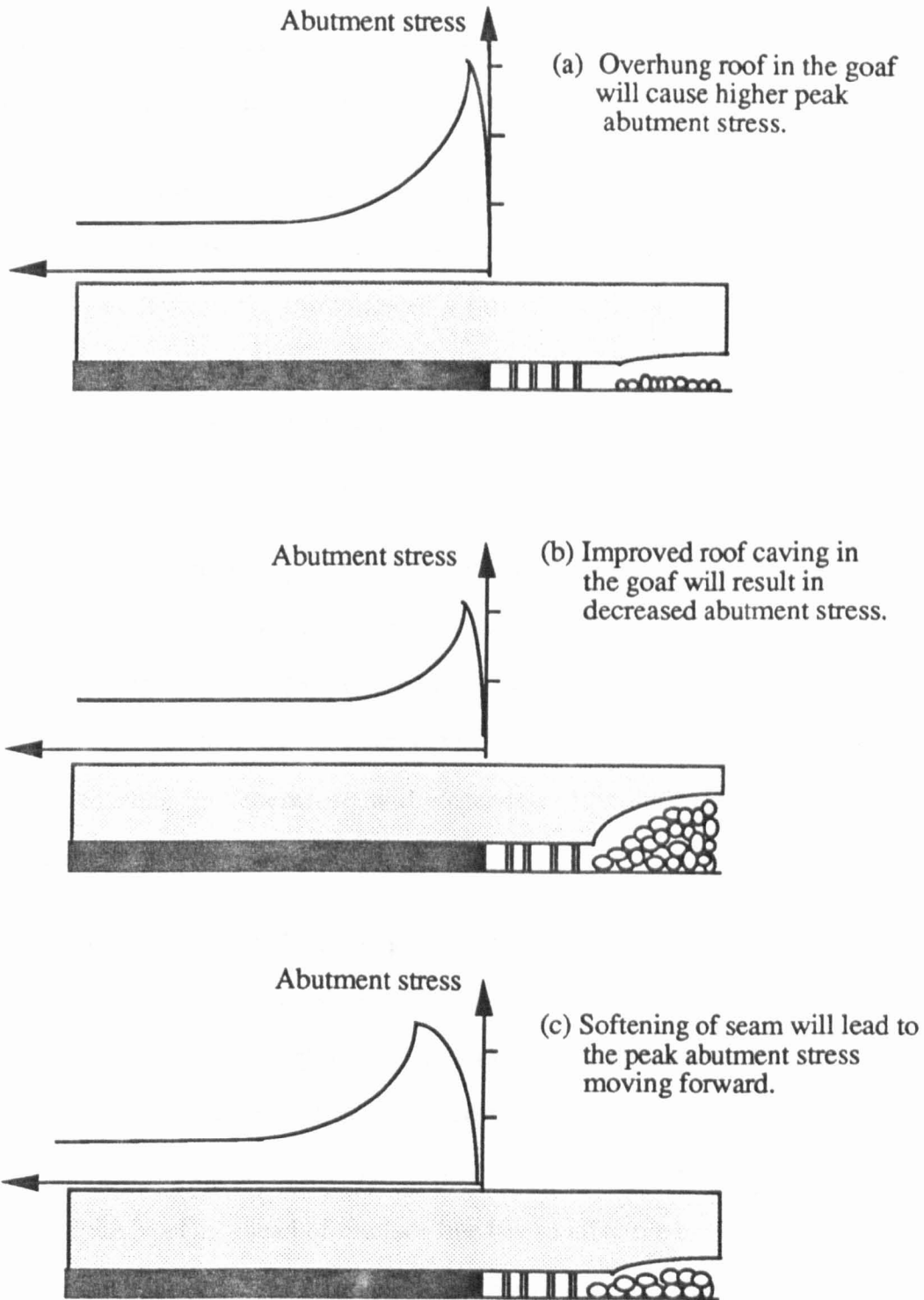
Figure 2.3.2 The abutment stress features are governed by the characteristics

of both the seam and the roof at the face.

has little effect on the peak position and the range of the front abutment pressure and therefore contributes little to the improvement of the gate tunnel stability.

In an advance mining layout, the gate tunnels are driven or formed with the advance of the working face and along the direction of mining, see Figure 2.3.3. In such mining layouts, the formation of a gate roadway plays a significant role on its ultimate stability. In mining practice three types of gate roadway layout are commonly encountered in the advance mining systems: conventional rip, face advanced heading and half heading (Figure 2.3.4).

In a conventional rip, the gate is formed along the flank solid coal behind the face line by means of packing along the goaf side (Figure 2.3.4.a). The ripped debris from widening to the full gate width can be disposed of in the adjacent packing side. The packing operation can be mechanized. The tunnel is formed and maintained in a destressed zone and therefore will experience less deformation and instability problems.

In an advanced heading, the gate is excavated several metres ahead of the face line (Figure 2.3.4.b). Obviously the heading is located in the front abutment pressure zone and is subjected to high levels of deformation and convergence rate. However, the convergence rate will decrease sharply as the face advances and the newly excavated part of tunnel is thus left behind the face line in the destressed zone. The length of the heading ahead of the face line has an effective bearing on the amount of deformation. UK experience (Szwilski and Whittaker, 1975) shows that the advanced heading with lengths under 20 metres ahead the face line will experience less deformation than those with lengths between 20 - 29 metres, although the maximum convergence rate always occurs near the face line and heading well ahead the face line will give an earlier detection and warning of the likely geological changes for the face operation. Some authors agree that only up to 3 m length of headings should be cut in advance of the face extraction in an advance mining system.

43
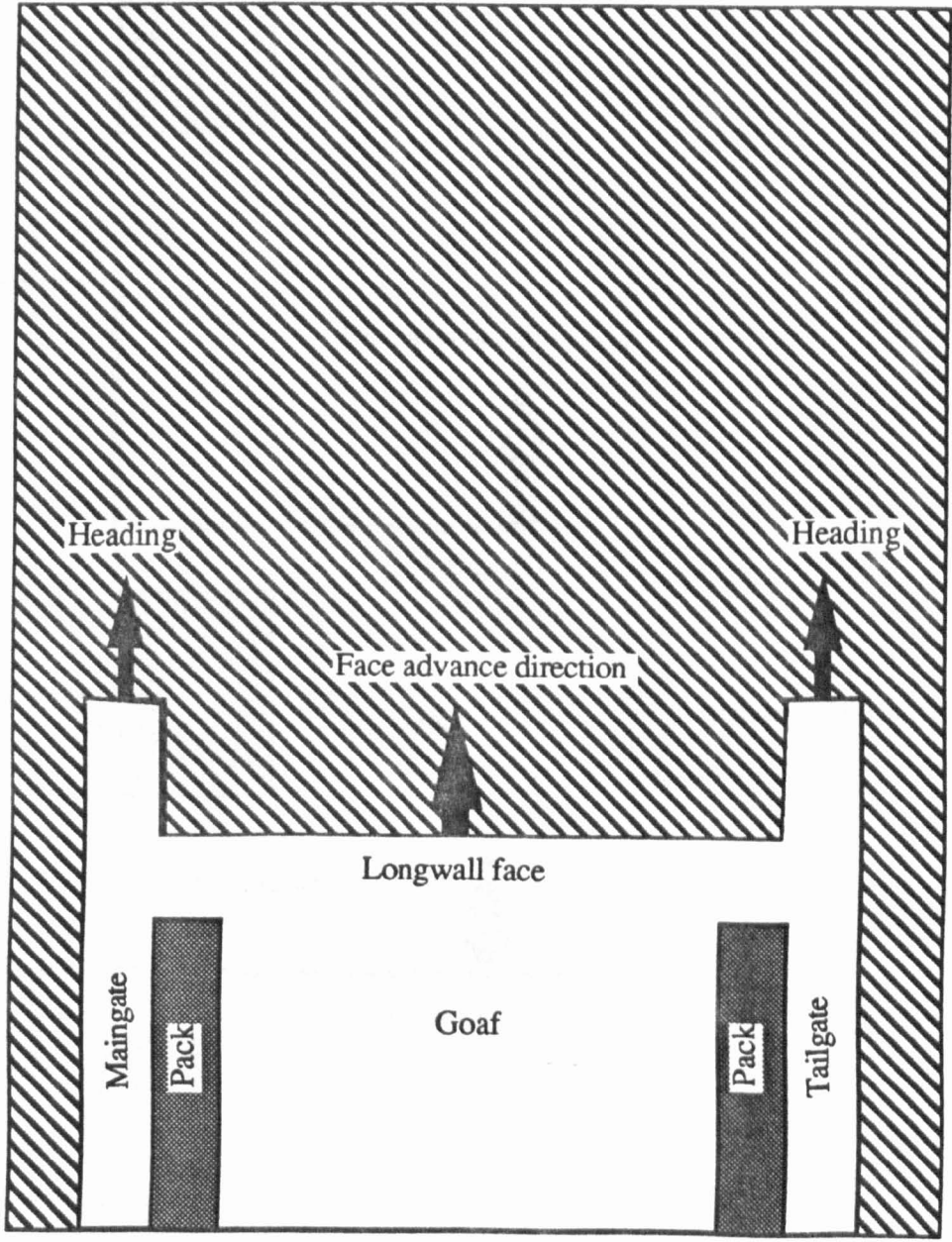
Figure 2.3.3 A typical longwall face layout for advance mining
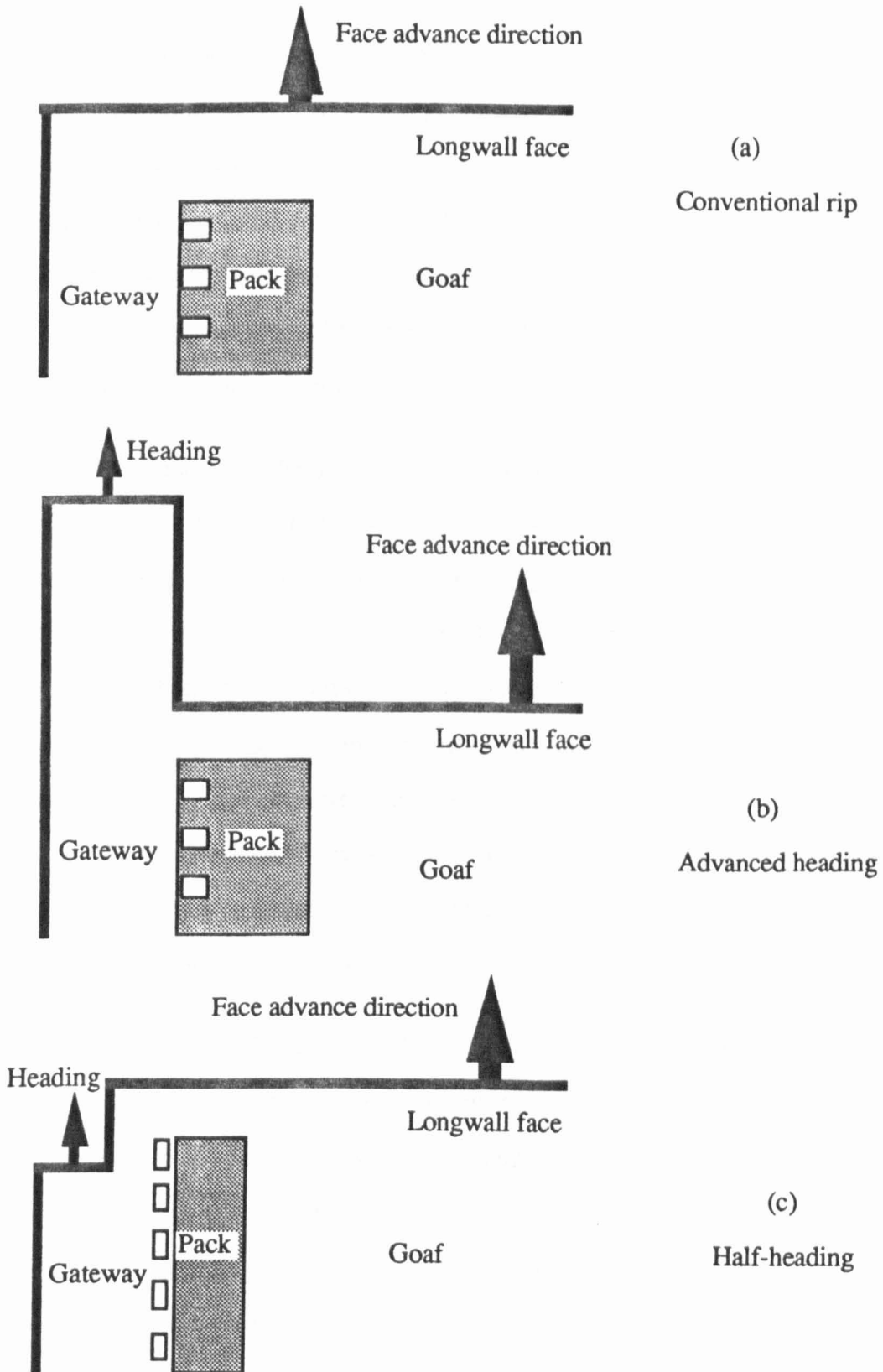
Figure 2.3.4 Three typical gateway formations for advance longwall mining

(after Whittaker, *et al* , 1985).

In a half face heading, the gate is formed behind the face line but displaced towards the solid with a part of the gate excavated along the edge of the solid coal (Figure 2.3.4.c). Such a gate has a high measure of inherent stability due to firstly being formed in relaxed ground behind the face line, secondly being located in more stable ground (displaced into the solid) which provides a protection of competent roof strata extending over most of the tunnel, and thirdly the pack is established and taking load before the tunnel is formed.

In comparison, the gates in the advance mining system are formed and maintained in the pressure relaxed zone and thus exhibit less deformation features than those in the retreat mining system. They also require a shorter maintenance period. However, the advance mining system is not widely employed in some countries such as the US and China due to a series of problems associated with the seam and ground conditions and spontaneous combustion initiated by the air flow leaking through poor packing structures into the goaf. In the advancing longwall system, the maintenance of packwalls and nearly perfect tunnels along the abandoned goaf is more costly in China. The face advance rate may also be limited by the tunnel formation and packing operation.

The preceding discussion on the stability of gate roadways is only limited to the influences due to strata pressure redistribution caused by the extraction of the present-mining panel. Such discussion would be enough if the panel is the first one in a virgin coal region without any sources of mining induced effects. For more common cases, however, consideration should be given to those involving the effects of abutment pressure due to the extraction of previous and adjacent panel(s). The interaction between two neighbouring panels often results in more rapid deformation of the tunnel existing in the zone of superimposition of the abutment pressures from the two panels. Usually a working panel is isolated from a worked panel by a barrier for the sake of ventilation and safety etc.. In practice, two kinds of barrier are available:

leaving a rib pillar or building an artificial packing wall along the goaf edge. Longwall mining layouts in European and Chinese coalfields mostly employ a continuous rib pillar between successive panels.

In the retreat mining system, if the tunnel (the maingate for instance) of the previously worked panel is not maintained to serve a subsequent panel, a new tunnel for the successive panel must be developed along the flank solid of the mined-out area by leaving a rib pillar to protect the newly developed tunnel from the effects owing to the transfer of overburden loads of the mined out area to the flank solid coal, see Figure 2.3.5.

When the successive panel is to be extracted by the advance mining method, a rib pillar is normally required to isolate the tailgate tunnel of the panel from the mined out area in order to avoid the tunnel being maintained in an uncompacted area where some ventilation difficulties together with intolerable convergence problems are mostly likely to occur.

2.3.3 Pillar Width

In the case of leaving a rib pillar to isolate the tailgate of the subsequent face from the mined out panel, the width of pillar has a significant effect on the stability of the tailgate tunnel. If the width of pillar tends to be too narrow, the tailgate becomes excavated and maintained in the zone of effect of high ribside abutment pressure due to the transfer of the overburden load which originally acted on the mined out area of the previous panel. The tailgate exposed in such an area is likely to suffer a series of problems in respect of stability, such as high rate of tunnel closure, speeding-up of tunnel deterioration, occurrence of localised roof caving, and even inducement of rock or coal bursts at depth. In the UK serious floor lift and side squeeze problems are more likely to be encountered in such circumstances. Experience within British Coal's mines has shown that significant tunnel closure may occur owing to side
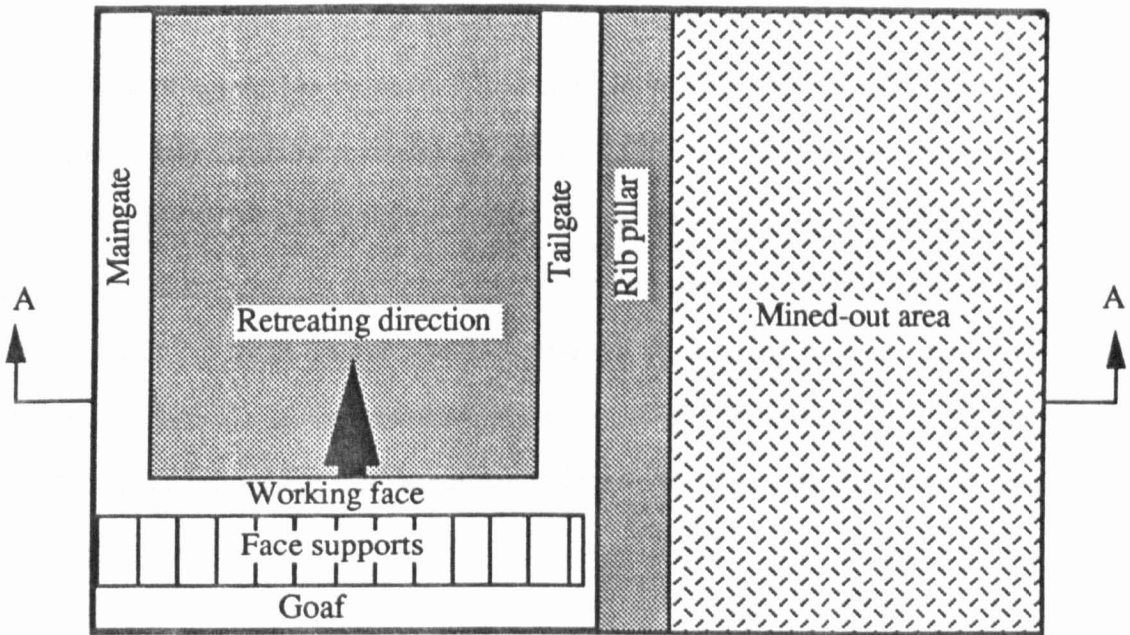
A - A
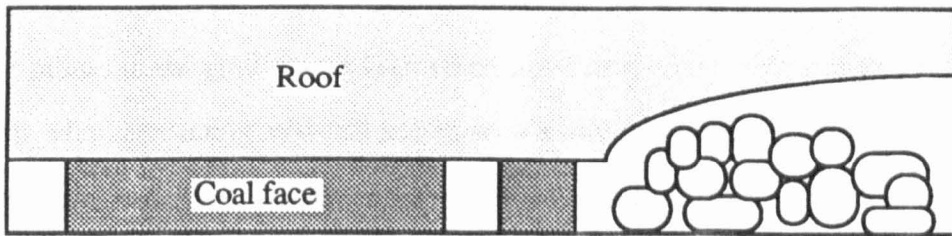
Figure 2.3.5 A typical retreat longwall face layout, illustrating a rib pillar
left to isolate the tailgate from the mined-out area.

failure of the rib pillar if the width of the pillar, x, is within 3 - 20 metres in advance mining cases at shallow depths (not greater than 500 - 600 metres below the surface).

However, unnecessary increases in pillar width will lead to an abandon of large quantities of workable resources and therefore decrease the seam recovery. In summary of the British experience, Whittaker (1972 and 1974) relates the pillar width to the mining depth,and points out that the satisfactory width of the protective rib pillar should be equal to one tenth of the mining depth in the UK coalfields where advance mining methods are practised and the mining depths are within 500 - 600 metres. In the case of conventional retreat mining Whittaker (1972) argues that a stable barrier pillar between two advance faces should not be less than 40 metres in width.

2.3.4 Effects of Remnant Pillars in Neighbouring Seams

Proper use of rib pillars to isolate adjacent faces can give tunnels a better protection and allow the two faces to be worked simultaneously. However, rib pillars exhibit disadvantages in that they are wasteful of reserves, particularly as mining depth increases. A more significant disadvantage of using rib pillars is that the remnant pillars in the goaf attract high strata pressures, which give rise to interaction problems when extracting adjacent seams with a thin interburden (less than 5 - 6 fold of the extraction height). Owing to a number of such problems, working conditions on the faces in the adjacent seams may   deteriorate. The immediate roof may become loosen ed and make supporting work very difficult. In the Datong Coalfield in China, where a number of seams with thin (15 - 25 metres) and hard interburden have been mined in the past few decades, mining layouts and roof control methods in the early days featured leaving coal pillars without paying sufficient attention to the likely effects of harmful abutment pressures and highly stressed zones on mining of subsequent seams. Therefore a number of instability accidents related to these remnant pillars have occurred with the most adverse ones being the sudden collapse

of roof over a large area with a record of 128,000 m^2 roof strata collapsing simultaneously. Face supports working in such circumstances also suffered major damage owing to intensive first and periodical weightings aggravated by upper remnant pillars and the hanging roof.

Positioning tunnels directly under or over remnant pillars in other adjacent seams promotes localised convergence and side crush, which may increase the cost several fold for the maintenance and repair of the latter tunnel . Niu (1981) gives a typical example, which occurred in China, that a rock tunnel placed 20 metres directly underneath a coal pillar (Figure 2.3.6.a) was seriously damaged resulting in an annual maintenance cost amounting to 400 RMB per metre. Under the same geological conditions, however, when the tunnel was run underneath the goaf area (Figure 2.3.6.b) the tunnel was stable and well maintained, and the annual maintenance cost was 20 RMB per metre, only 1/20 of the former one. According to the investigations into strata pressure distribution and rib pillar behaviour, Niu draws attention to the position of tunnel in relation to the abutment pressure zone, indicating that, in winning multiple seams, tunnels should be located under the goaf of the overlying coal seam. In Figure 2.3.7, the location of a tunnel in the lower seam as shown in (a) would behave more stably than the other two types of layout shown in (b) and (c) where the tunnel in (b) is subjected to stress concentration influence while the tunnel in (c) is on the fringe of a stress concentration zone.

In order to overcome the detrimental effects of remnant pillars, pillarless mining methods have been proposed and practised in many countries. In a pillarless mining layout the maingate tunnel of the first panel is re-used as a tailgate tunnel to serve the successive panel such that the rib pillars are eliminated. In order to shorten the period of maintenance and to avoid excessive convergence of the tunnel during the service for the second face, retreat mining method should be employed. Whittaker (1974) argues that using a tunnel twice by advancing the second face may result in closure up to 0.30 - 0.60 metre ahead of the face line owing to the effect of the front abutment

50
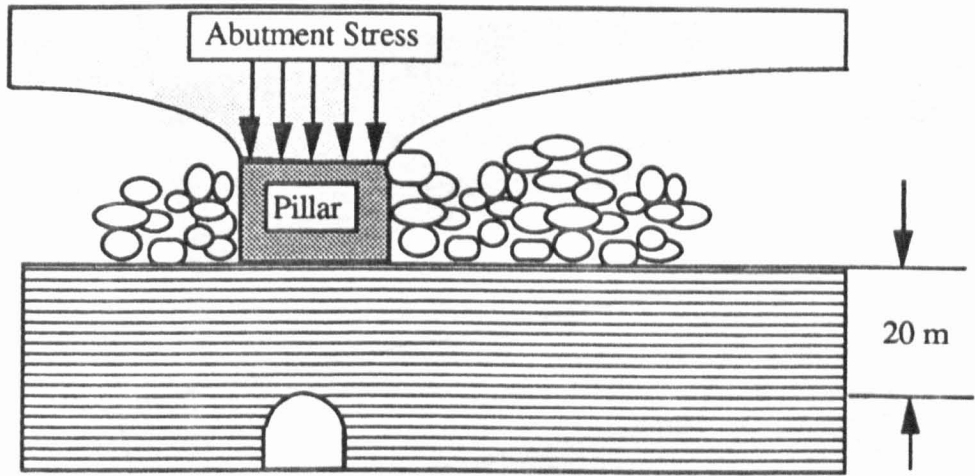
(a) A tunnel underneath a rib pillar was gradually damaged by the abutment stress
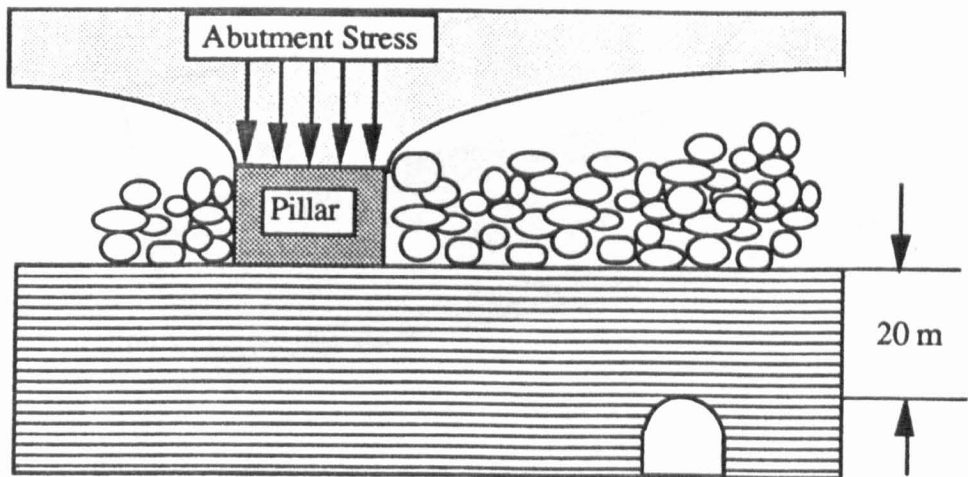
(b) A tunnel exhibited increased stability in a destressed zone underneath a goaf

Figure 2.3.6 Illustrating the relationship between the tunnel location,

abutment stress and tunnel stability (after Niu, 1981)

(a)
Tunnel in the
destressed zone
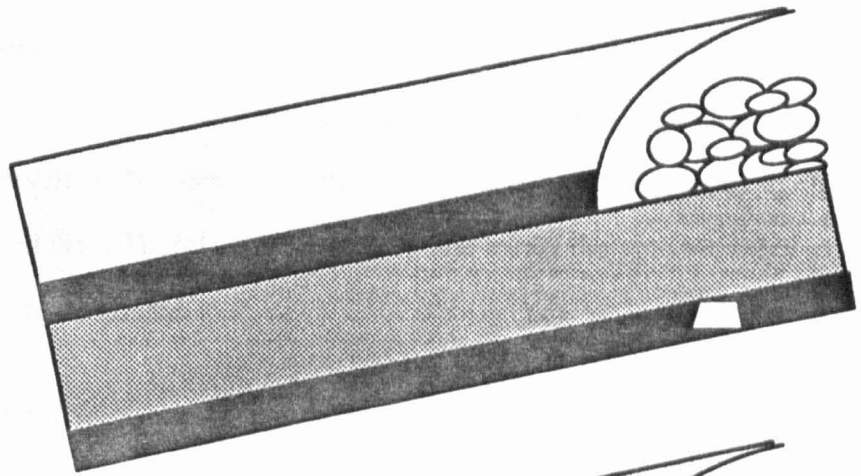
(b)
Tunnel in the
stress concertration
zone.
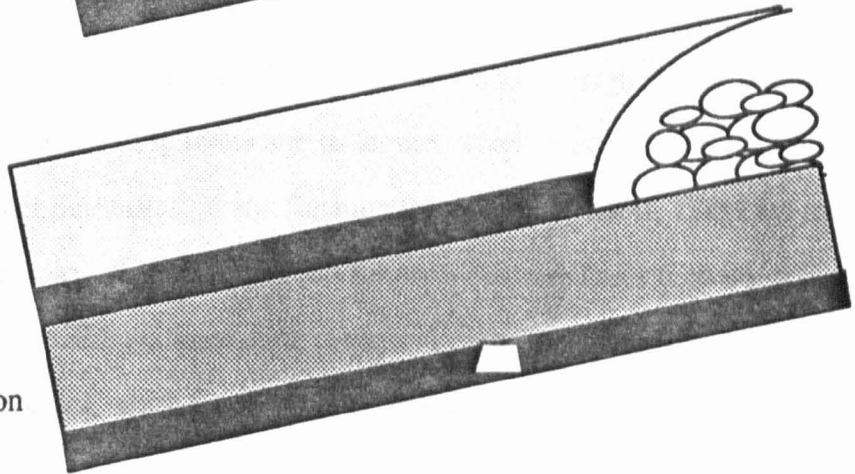
Ө
Tunnel at the fringe
of stress concentration
zone.
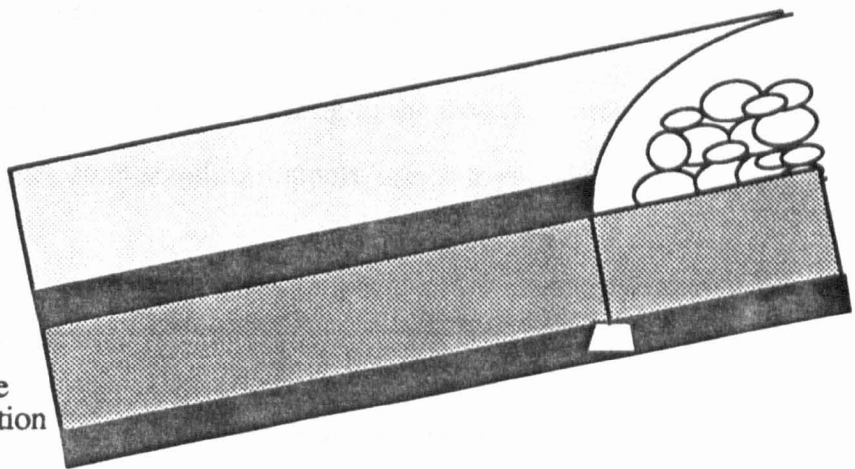
Figure 2.3.7 Illustrating the variation in the stability of tunnels in the lower seam

due to their locations in relation to the abutment stress caused by

mining of the upper seam, (after Niu, 1981).

pressure and the convergence behind the face is likely to be up to 50% of the extracted height during goaf settlement of the second face. A fracture zone existing over the solid ribside as a result of the first working may give rise to difficulties at the T junction of the second face. Therefore it is not practical to use the gate tunnel twice if the second face is to be advanced.

2.3.5 Support Method

Supports are commonly installed in mine tunnels to resist the deformation and further break up of surrounding rocks and to secure detached and loosen rock blocks or debris from further deterioration and flushing into the excavation. There are many kinds of supports employed in underground tunnels. The mechanical characteristics of these supports differ from each other and therefore their effects on tunnel stability and strata control, when they are used, are quite variable.

2.3.5.1 Support Categories and Applications

Supports may be classified, according to the material composition of support, such as timber support, steel standing support, concrete support, rock bolt, and stone or masonry support.

1. Timber Supports.

Timber supports used to be of the most important type in mine development in the UK until the end of World War II. At present timber is still used in a number of countries as a tunnel support material for panel developments that are usually short in service life ranging from several months to a couple of years. In some small or medium size collieries timber support sets are also encountered in some rock tunnels with a longer service life.

Timber when used as supports is easy to transport, cut, manipulate and place in the form of a mine support in underground circumstances in addition to the nature of

being light in weight. Breakage of timber almost occurs along the definite fibrous structures and gives visual and audible signs before , complete failure, the latter providing a warning to men at the site who may foresee a possible hazard of rock collapse.

However, timber is low in mechanical strength, its resistance to bending, tension, shear, compression and buckling are poor and dependent on its fibrous structure and natural defects occurring within the wood. Humidity and water content have a pronounced effect on the timber strength. Additionally, timber supports are easy to be attacked by microbiorganisms (bacteria and fungi) in the underground environment which is humid and warm.

Owing to these features, timber supports cannot work satisfactorily for a long time in heavy ground conditions where heavy repair work is required. They are however, effectively and successively used as temporary supports at heading sites and in dealing with partial or localised roof collapses, or when used to support those tunnels that are short in life time such as gate roadways. Timber supports in tunnels are mainly of trapezoidal type, consisting of two standing props and a roof bar.

2. Steel Supports.

The use of steel for underground supports may be traced back to the last century when the types of steel support were mainly of straight side and roof elements although arch types of varied sections with fish plate joints also came into use in the late nineteenth century, according to Spruth (1955). Since coal mining during that time took place at fairly shallow depths and the tunnels were much smaller in both cross section and length than today, the advantages of steel supports over other types of supports in term of strata control effects were not evident due to the considerably low tunnel pressures.

In the late 1920's yieldable and articulated supports were accepted to be more suitable in higher ground conditions and became more favoured than the rigid arches. The advent of the Toussaint-Heintzmann (or "TH" in short) arch in 1932 spread application of steel supports to various ground conditions and permitted an improvement in ground control. Further development of diverse steel supports has led to the current state that the steel supports have become a major type of tunnel support in European coal fields.

The basic characteristics of steel and steel support can be described as follow:

(i) Steel is homogeneous in material, free from natural defects;

(ii) Steel has greater Young's modulus and strength than other materials employed for underground support purposes, permitting it to give stronger resistance against deformation, buckling, and the like.

(iii) Steel can be manufactured in diverse forms of cross section to meet various requirements by ground structures and features.

(iv) Mechanical properties of steel are less influenced by the presence of underground environments.

(v) Most steel supports are reusable after proper repair and adjustment even though they may have been badly deformed or twisted.

(vi) Steel support is easy to install with mechanical facilities, particularly in the case of mechanised drivage.

(vii) Steel support can possess fairly high residual strengths after the rock load acting on it has reached the strength limit of the steel, so that the support can still perform to a satisfactory extent.

However, in many developing countries, the use of steel supports is restricted to a large extent due to the   steel price which is much higher than that of other materials.

Steel supports have several configurations and applications and these are listed below:

(i) Trapezoidal sets. These are used in those tunnels where flat roofs and effective spanning are present, such as in-seam gate roadways in seams of thick - medium thickness. Applications   are successful at shallow depths and in short life headings. The elements of a trapezoidal set include a girder and two legs of either rail or joist cross sections. Such elements are simple to transport and quick to install, which assists high speed developments.

(ii) Rigid arch sets. A rigid arch support consists of 2-5 pieces of rail or joist element connected by the use of fish plates and bolts. This kind of support, particularly of three pieces, has been proven by years of experience in the UK to be a very reliable system of support in heavy ground conditions and highly stressed situations. Various supports of this kind have been widespread and used with success in most UK mining tunnels, particularly in gate tunnels with likely significant deformation and high strata stresses where other support systems are likely to fail (Whittaker *et al.*, 1985).

In such support system, the fish plate connection constitutes the weakest element and often breaks when failure of the system occurs. Since such system allows relatively low roof-to-floor convergence, the increase in both the joist cross section and the connecting element size is often adopted as a main measure to increase the support strengths against bending, torsion, buckling of support caused by rock pressures.

(iii) Yieldable steel arch sets. These are usually of trough sections which are frequently called TH or U shaped section. A basic working principle of yieldable supports is one element of support sliding along inside the other, in which a frictional resistance is produced for supporting. The U shaped section offers a fairly large contact surface when one piece is sliding along the other, which forms a base for it to be adopted for yieldable supports.

In comparison with the H shaped section of most rigid supports the U shaped sections have higher resistance against lateral bending load due to its increase in the lateral section modulus while the longitudinal section modulus may retain the same.

Yieldable arch supports have been widely used in Germany. They are attracting more and more attention in both China and the UK. Such supports has been employed in China for main tunnel support where high ground stresses are encountered, but due to the high prices and shortage of steel supply, rarely used in gate tunnels of short life. In the UK the yieldable steel arch sets are finding their application in several tunnels mainly in Selby complex.

Generally speaking, yieldable supports are applicable to the tunnels where strata movement is mainly vertical and where weak rocks are encountered and a comparatively large magnitude of deformation requires a measure of yield of the supports without losing sufficient supporting capability. Whittaker et al., (1985) argue that high lateral movements of tunnels can disrupt the yielding mechanism and lead to early failure of support and that such kind of supports is difficult to incorporate a wide range of struts.

(iv) Circular steel support. This kind of support is also known as a closed type since other shaped supports such as horse shoe shaped are also included in this kind of supports.

Circular supports are used in heavy ground conditions where a hydrostatic stress field of significant magnitude and the like are present. The support system can take a form of either rigid or yieldable type. They have found favoured application with full face excavation (using TBM etc.) in most Coal Measures conditions, particularly in weak and soft ground conditions. This type of system is used in the long term tunnels rather than ..in short term ones such as gate tunnels. However, the circular profile of tunnels provides a comparatively low percentage of utilisation of the cross section and may give rise to difficulties in the excavation operation,especially when the full face excavation machine is not used. Of fundamental importance in such closed support designs is the need to assess the required degree of support resistance to obtain the desired level of stability.

3. Concrete Supports

Concrete support systems, used in coal mines, may be classified into three major types: segmental concrete standing set, monolithic concrete lining and shotcrete lining.

(i) Segmental concrete sets. These are often used in heavy ground conditions. They are a very strong form of support but are incapable of accepting appreciable yield before cracking due to the brittle nature of concrete. Therefore the application of them often requires incorporation of effective grouting or backfilling between segments and surrounding rock on prder to improve the flexibility of the support system and to reduce the possibility of point loading which may cause a rapid decrease in lining strength.

These supports are encountered mainly in long term tunnels such as major developments.

(ii) Monolithic concrete linings. Such linings involve constructing a 40 - 60 cm thick wall around the tunnel roof and sides, and sometimes, where the ground pressure is pronounced, the lining may need to cover the entire periphery.

Monolithic concrete linings are of a rigid type and allow very limited deformation although they can provide very high compressive strength. When the lining is not circular along the whole periphery, excessive lateral ground stresses and inward movements of side walls could make the support system break and fail in operation because of the brittle and low tensile resistance nature of concrete, though steel bars reinforcement and mesh can be incorporated in the linings during the construction of the system to enhance the tensile strength of the support. Therefore, this support system is mainly used to those ground conditions where less lateral stresses are likely to be encountered or where the surrounding rocks are fairly free from active or disturbing strata movements due to geology or mining activities after the support construction. For these reasons the system finds application in tunnels in shaft bottom areas that are usually protected by a considerably large shaft pillar.

(iii) Shotcrete linings. This lining employs cement and sand mixture pneumatically projected at high speed onto a tunnel surface through a hosepipe of the delivery device to form a layer of normally 2-7cm thickness thereby sealing the tunnel surface. There are two shotcrete processes: dry process and wet process. By the dry process, cement and sand are dry mixed and conveyed through the delivery hose to a nozzle where water is added. By the wet process, sand, cement and water are mixed before they enter the delivery hose.

Shotcrete lining is used as an immediate temporary support to prevent detachment of small slabs and deterioration of surrounding rocks shortly after the exposure of new tunnel periphery in most geological conditions including minor water flows. Due to the nature of less thickness, it improves the flexibility of concrete support. In particular, such a system can work more effectively in association with

rock bolting and mesh and even standing supports, which is known as the New Austrian Tunnelling Method (NATM).

4. Rock Bolts and Trusses

Rock bolts have been steadily increasingly used to reinforce and stabilize rocks surrounding tunnels world-wide in the last few decades. At present, there are four major types of rock bolts frequently employed in underground tunnels, (a) mechanically anchored rockbolts, (b) grouted rockbolts, (c) grouted cable bolts, and (d) friction anchored rockbolts. The mechanically anchored bolt consists of a solid steel bar or shank, an anchoring device at the top end of the bar, and a tensioning device at the lower end of the bar, whilst the rest three types of rockbolts all consist of a steel bar or a steel cable, a fast setting bonding medium (resin or cement) along the whole length of the steel bar or cable and a bearing plate and nut at the lower end of the bolt.

(i) Mechanically anchored rockbolts. There are three forms of anchoring device, slot and wedge, expansion shell, and resin grout. In the process of installation of a bolt, a bar is first anchored at the bottom of the borehole and then the tensioning device mainly of a plate and a nut is assembled at the lower end of the bar. By tightening the nut, a tensional stress is generated within the bar, which gives an early effect to the reinforcement of rock and offers a resistance against strata separation within the length of bolt. The mechanically anchored rockbolts make it possible to suspend the loose rock or weak layer at the lower part of strata near the roof line to the upper competent layers. The tensional stress in the rock bolt also produces a frictional resistance against slip on the interface between the thin strata, thus forming a single thick stratum and increasing the stability of bolted strata as a result that the flexure of the thick stratum becomes smaller than that of the thin one. Since the effectiveness of such rockbolts depends considerably on the anchor quality and the tensioning degree, the dimensions of the anchoring device should be carefully

60

considered and designed in conjunction with the diameter of both the steel bar and borehole, and the rock bolts should be tensioned because the frictional resistance resulting from the clamping action is solely due to the tension in the rock bolt. Additionally,the anchor point should be located at a competent horizon instead of a weak part of strata in the borehole so as to avoid the occurrence of failure of the anchored part of borehole wall and thereafter of the rockbolt anchoring device.

(ii) Grouted rockbolts. In the grouted rockbolt system, resin or cement are used as grouting agents to fill the void between the bolt and the borehole and therefore bond the full length of the bolt. Cement bonding is the early method of full column anchor bolting. Although this bonding medium can provide improved anchorage in weak strata, its shrinkage nature and the longer setting time required have limited its use as an immediate support in a number of tunnel developments. However this bonding method, due to its advantages of low cost and non-toxicity, is still used when the effects of setting time and shrinkage are acceptable within the life time of the tunnels.

The application of resin as a bonding material has promoted the importance of rock bolts as an effective support system. The use of resin materials can generate better anchorage over a wide range of strata types and require a much shorter setting time than that of cement, which indicates that the resin grouted rock bolt takes load much earlier and more effectively than the cement grouted rock bolt. However, the application of resin is still restrained in many countries particularly in developing countries due to the high cost. The current trend is to develop new and cheap formations of resin.

The fully grouted rock bolts usually provide a passive support in that they start taking up the load only at the time when the bonded strata begin to deform. As the bonding effect takes place along the full length of the bolt, the frictional resistance is the major function of the bolt for maintaining the integrity of the strata. Such a kind of

rock bolt has also shown other advantages, such as that the anchorage is independent of the strata type; the bolt is permanently effective throughout its full bonding length; the hole length is not critical because the bonding length can be adjusted depending on the strata type; they can resist both vertical and lateral movements; the grouting medium and the bolts seal wet holes and exclude air, thus reducing corrosion of the bolt assembly and weathering of the rock; damages to the bolt head, bearing plate or rock at the collar of the hole does not cause the grouted rock bolt to become ineffective; and the fully grouted bolts can absorb blast vibrations without bleeding-off of the bolt load.

(iii) Grouted cable bolts. This kind of bolt employs a flexible steel cable instead of a rebar or a thread bar, in conjunction with a bonding material (cement or resin) grouted along its full length. The grouted cable bolt provides both suspension and friction effects for stability of bolted rock around the tunnel. Such a bolt system can display very high load bearing capacity against tensional movements of rock along the longitudinal direction of the bolt, but comparatively low resistance to the shear action owing to the physical nature of the steel cable.

Since the cable can be installed to any length from a reel even in a limited tunnel space, any variation in bolt length which arises is not a problem. In China cable bolts are often made from the used cables replaced from underground haulage machines. In this case, the cost of cable bolts is very low and economic. However, the cable bolts used underground are not pretensioned, so that they usually offer no immediate load bearing capacity unless the grouting material has set and the bolted strata start to deform. For this reason the grouted cable bolts are primarily used as temporary supports with frequently being combined with other kinds of support.

(iv) Friction anchored rockbolts. For this type of bolt, a steel tube is employed to replace a steel bar in the preceding bolting system. The tube is expanded against the borehole wall when it has been installed in a borehole. A tight contact of the tube with

the hole wall creates a radial force against the borehole wall, thus resulting in the generation of a resistance along the full length of the bolt against the tendency of sliding of rock on the steel. There are two representing types of friction anchored rockbolts in use, one being the Split Set and the other the Swellex bolt system.

The anchoring mechanism of the split set rockbolts arises from frictional forces acting against a load which approaches the ultimate load bearing capacity of the bolt as the bolt is to slide. The bolt can then accommodate large displacements without failing.

A Swellex bolt system for rock reinforcement consists of a steel tubular bolt, an installation rod with chuck and a high pressure water pump. The steel tube is mechanically folded to an external diameter smaller than that of the borehole. The ends of the tube are reinforced with two short bushings sealed by welding. When installing a Swellex bolt, water is pumped at high pressure (30 bar for instance) into the tube through a connection at the lower bushing. This high pressure water causes the tube to swell in the borehole and to adapt its shape to the irregularities of the borehole (e.g. the existence of voids due to jointed pieces peeling off the wall), resulting in a tight contact with the borehole wall. As the swelling proceeds, the lower portion of the steel tube shortens, pulling the face plate firmly against the rock surface around the borehole collar and thus suspending the loose rock blocks at the lower part of the bolt. This indicates that the installation of the Swellex bolt produces immediate load bearing capacity which is virtually certain for each bolt, since the pump automatically stops at the preset inflation pressure.

Viewing the process of installation, it can be seen that the bolt anchorage is relatively insensitive to variations in the bolthole diameter over a range of a couple of centimetres; correct installation of the bolt does not rely on operator judgement and skill; the change in length of bolt is allowable on requirement and does not affect the

installation procedure; the bolt can tolerate shear movements across the bolt and thus is adapted to a variety of ground conditions including those containing joints.

From the above discussion, however, it can be seen that the need to tackle the corrosion problem arising from long term exposure to the damp and dusty air underground is undoubted, when friction anchored rockbolts are used for the permanent support system.

2.3.5.2 Interaction of Support and Surrounding Rock

There are two major functions that the tunnel support performs:

(a) to retain loosened surrounding rock in position so as to prevent it from falling inward into the excavation space;

(b) to restrain the strata movement to a minimum or acceptable level.

The first function of support is obvious and easy to be understood. However, the performance of the second function, namely to restrain the movement of strata around the tunnel, is a complicated process and is dependent on the rock support interaction which involves a large number of factors and therefore has attracted the attentions of many researchers, including Daeman (1977), Hoek and Brown (1980). These authors have outlined the basic principle of rock support interaction conceptually as follows:

Consider the section x-x in relation to a heading face of a tunnel in Figure 2.3.8, in which a full face driving method is employed together with the use of steel set supports and the *in situ* stress field is assumed to be hydrostatic with a magnitude of pressure p_0.

In step 1, the heading face has not yet reached the section x-x under consideration. The rock strata at the section is still in the original equilibrium because no disturbance has been generated in the rock at the section. The support pressure P_i
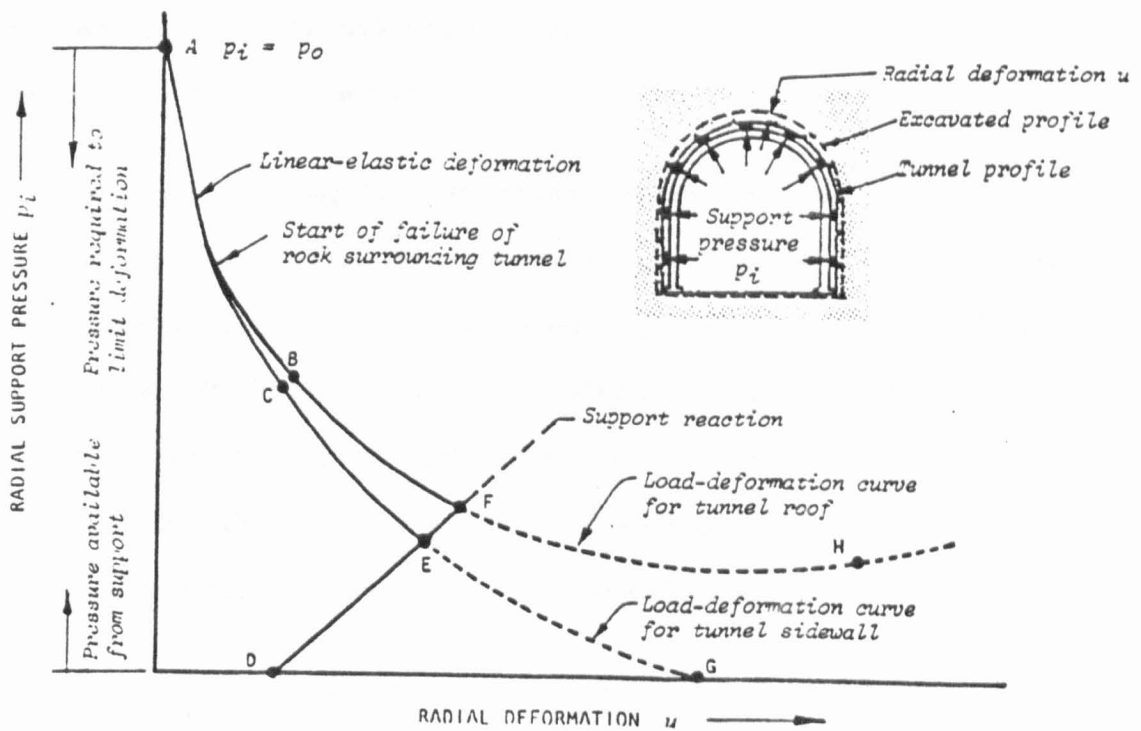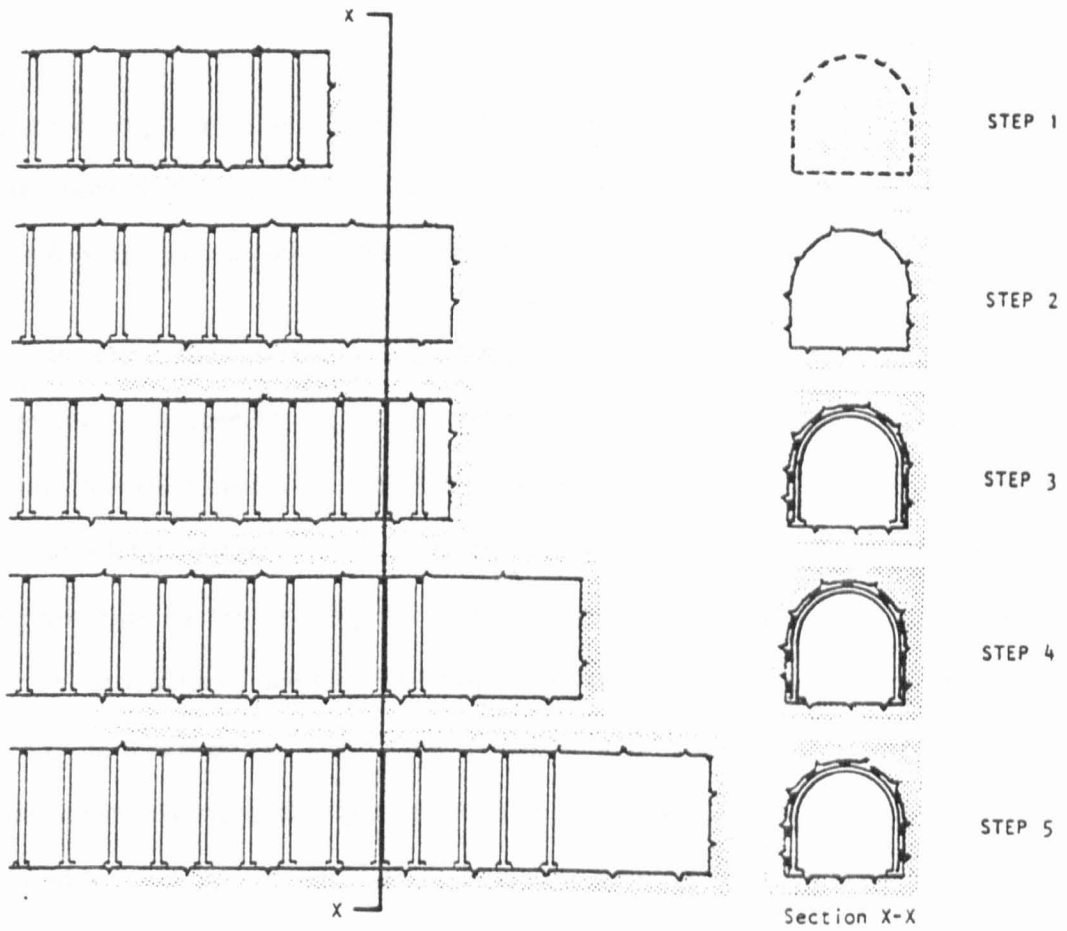
Figure 2.3.8 Interaction of the tunnel support and the surrounding rock

(after Hoek and Brown, 1978)

65

along the proposed tunnel profile is equal to the *in situ* stress P0, which is originated by the presence of the intact rock within the profile. This situation is presented by point A of the rock support interaction curves in Figure 2.3.8.

In step 2, the heading face has been advanced just beyond the section x-x, and the support pressure Pi, previously provided by the rock inside the tunnel at the section, has been removed. However, the surrounding rock at the section has not been completely released from strains because the radial deformation is still limited by the proximity of the heading face which provides a significant restraint. If this restraint provided by the face were not available, an internal support pressure Pi, given by points B and C in the graph in Figure 2.3.8 , would be required to limit the radial deformation u to the same value. Here, the support pressure Pi which would be required to limit the deformation of the roof is seen to be higher than that needed to limit the sidewall deformation because the weight of the zone of loosened rock above the tunnel roof must be added to the support pressure required to limit the stress induced displacement in the roof.

In step 3. the tunnel has been mucked out and steel sets have been installed close to the heading face. Since most supports undertake rock loads by the deformation of itself, the newly installed supports carry no load, as shown by point D on the graph in the Figure 2.3.8 due to the fact that the supports have not experienced the deformation caused by the further deformation of rock. Assuming that the rock strata do not exhibit time dependent deformation characteristics, the radial deformations of the tunnel section are still those defined by points B and C.

In step 4, the heading face has been advanced about 1.5 tunnel diameters beyond the section x-x and the restraint provided by the proximity of the face is now considerably reduced. This causes further deformation of the tunnel sidewalls and roof as indicated by the curves CEG and BFH in Figure 2.3.8. This inward radial deformation or convergence of the tunnel induces load on the support system which

would behave as a stiff spring. The support pressure Pi available from the blocked steel sets increases with radial deformation of the tunnel as indicated by the line DEF in the graph.

In step 5, the heading face has advanced so far beyond the section x-x that it no longer restrains the movement of strata at the section x-x. If no support had been installed, the radial deformations in the tunnel would increase along the dashed curves marked EG and FH in the graph. For the sidewalls, the pressure required to limit further deformation drops to zero at point G and, in this case, the sidewalls would be stable since there is no remaining driving force to induce further deformation. On the other hand, the support required to limit deformation of the roof drops to a minimum and then begins to increase again, due to the downward displacement of the zone of loosened rock in the roof, the dead weight of which would require additional support pressure. In the example illustrated, the roof would collapse if no support had been sufficiently installed in the tunnel.

Proper reaction of support to the surrounding deforming rock is very important for the performance of the second function of the support. In Figure 2.3.8, a support characteristic curve DEF intersects the deformation curves at point E for sidewalls and at point F for roof, illustrating that the support pressures required to limit further deformation of the sidewalls and the roof are exactly balanced by the support pressure available from the steel sets at the working points of E and F, such that the tunnel and the support system are in stable equilibrium.

From the above example, it can be seen that, for a given heading site, the rock deformation characteristic curve ABFH and ACEG are given and are unchanged. Therefore, whether or not the tunnel is stable would depend mainly on the support working curve marked in terms of the time lag between the exposure of the tunnel by excavation and the support setting, namely the position of point D, the working

characteristics of the support including the increasing rate of support resistance against deformation, the limit strength and the residual strength nature.

2.3.6 Size and Shape of Tunnels

The size of tunnel cross section has an effect on the tunnel stability. Particularly, in the Coal Measures strata, stratification is one of the evident features, which often leads to the application of beam theory. According to the beam theory, the magnitude of span of a beam or a layer of stratum effects the beam stability. In the case of a tunnel, the roof of a tunnel would sag more and approach towards an unstable condition, as the width of it increases.

The shape of tunnel influences the tunnel stability mainly in respect of stress redistribution around the excavation. On an assumption that ground stress fields at considerable depths or in soft strata conditions are featured hydrostatically, a circle shape of tunnel profile is usually recommended and employed. However, the application of circular tunnel profiles to the excavation at great depths or in soft ground conditions does not always show success, since the realities do not always agree with the theoretical assumption.

2.4 Concluding Remarks

Primary factors which have varied degrees of influence on tunnel stability have been outlined and reviewed in the present chapter. They are classified into two main categories, namely geological and operational. Some factors, such as rock formations and geological structures, are already constituted before the excavation and thus they are uncontrollable. Others should be controllable through man's activities in aspects of design and operations. The review of the effects of these factors would help find problems and guide the direction of further research in respect of tunnel design and the strata control aspect. In a tunnel design, the mining engineer should be aware of making use of those beneficial factors and avoiding traps and adverse influences

initiated from those harmful factors. In operations, he should make every effort to prevent the strata surrounding the tunnel from developing various destructions due to improper operations and to select and timely install the correct supports which are consistent with the requirements for effective ground control. Consequently, the strategy in the control of tunnel stability may be summarised as :

- properly select an appropriate strata location for the drivage of tunnels;

- carefully choose an excavating system and method, and train the relevant operators effectively;

- correctly appreciate and use effective support systems which should be able to provide a working characteristic consistent with the feature of strata movement;

- after installation of supports, ordinary maintenance of the tunnel should aim at the reduction or elimination of those factors possibly causing deformation and instability of the tunnel.

CHAPTER THREE

RESEARCH OBJECTIVES AND METHODS ADOPTED

CHAPTER THREE

RESEARCH OBJECTIVES AND METHODS ADOPTED

The discussions in the preceding chapter have shown that the stability of tunnels is governed by many factors. Wide variations of influences of these factors on tunnel stability have drawn the attention of mining engineers and attracted much research interest. As a result, many achievements in respect of both theory and practice of rock mechanics and strata control have been reported world-wide. Design and techniques of tunnel excavation have been duly advanced and improved. As one of the leading research institutions in the United Kingdom, the Department of Mining Engineering at the University of Nottingham have been continuously and actively involved in the investigation of the stability and design of mining tunnels and contributed to the needs of the UK coal industry. In the present chapter, work on the mining tunnel stability aspect, which has been carried out at the Department in the last decade, will be briefly reviewed before attention is given to identification of problems confronting the mining engineer in association with support design and control of tunnel stability. For the objectives proposed, relevant research methods available to serve the research purpose are carefully appraised and the decisions influencing selection of the methods employed are discussed.

3.1 Contemporary Research at the University of Nottingham

During the last decade, the Department of Mining Engineering at the University of Nottingham has launched a series of research programmes, aimed at the development of knowledge and techniques in the aspect of strata control for the design and stability of mining tunnels. In order to ensure the success of such systematic research programme, several methods have been used to conduct each individual project, including:

- long and short term underground observations and instrumentations;

70

- theoretical studies;

- laboratory tests including tests for rock sample properties and physical scale modelling;

- finite element modelling and other computer based methods.

The initiation of this systematic research work can be traced back to the contributions made by Miller (1981) who paid attention to the structural stability of mine tunnel supports. Whittaker (1983) directed his research interest towards showing an overall picture of the loading characteristics of strata on mine tunnel supports. His work was mainly based on the field investigations at both Gascoigne Wood and Cotgrave collieries.

Jukes (1983) focussed his studies on the characteristics of steel arch supports used in mining tunnels. He investigated in detail several kinds of scaled steel support models in terms of deformation and behaviour in response to various loading conditions, and then compared the laboratory results with the conclusions from relevant theory and underground instrumentations at Hucknall, Cotgrave and Bentinck collieries.

Riggott (1986) took part in the underground measurements at both Gascoigne Wood and Cotgrave collieries. He was mainly concerned with support stability investigated by means of measurements of rock deformation features at the sites of both collieries.

Fathollahzaden-Aghdam (1986) attempted to apply rock behaviour of nine kinds of samples under different loading circumstances to the description of instability problems of underground excavations. He proposed a division of three zones of rock behaviour from rock stress - strain curves obtained: pre-yield behaviour, yield behaviour and post - yield behaviour.

Carter (1986) studied the strength behaviour of monolithic pack support structures around longwall face ends. He carried out underground experiments aimed at comparisons of the convergence rates among various types of monolithic packs. He also initiated laboratory investigations on the effects of curing circumstances mainly of curing time and temperature, and pack constituents, on the strength of monolithic materials used for underground packing.

Kapusniak (1986) continued the work on tunnel closure prediction techniques using a personal computer system which was started by Bonsall (1985). He used an empirical equation which was summarized by Branch (1987) on the relation between maximum and minimum stresses of several kinds of rocks at the state of initial failure.

Frith (1988) went on with the computer based tunnel closure prediction technique by incorporating a modified failure criterion into the prediction. He applied the method to the sites at Gascoigne Wood Colliery .

Bonsall (1985) and Goshtasbi-Goharizi (1987) used physical modelling techniques to investigate the influence of local geology upon the stability of mining tunnels. The dimensions of the physical models the two authors used were 450 x 450 x75 mm. In testing, two kinds of stress field were employed,a hydrostatic field and a vertical stress being threefold the horizontal one.

Sutcliffe (1990) was mainly concerned with explanations and application of the results of underground instrumentations sited at Gascoigne Wood Colliery's major tunnels. A primary instrument he used was the multi-point extensometer.

Watson (1991) focussed his interest on the examination and appreciation of tunnel supports in terms of stability and failure mechanism of both rigid and yielding steel arch supports.

Thomas (1991) has recently devoted his research activity in the measurement of ground stresses associated with underground coal mining and tunnel heading at greater depths. He, from a geologist's point of view, carried out his research project in association with the British Coal Technical Headquarters at Bretby.

All of the authors mentioned above had contributed individually to a general project aimed at improving the control and stability of strata around mine tunnels. A collection and review of these individual findings and conclusions reflects the achievements made within the Department in the past few years and provides a solid path for the newcomers to continue the research, although some of conclusions, in particular those on the theoretical basis for the computer based tunnel closure prediction method are very questionable and should be re-examined as discussed later in this thesis.

3.2 Tunnel Stability Problems Facing the Coal Industry

Mining activities have posed various kinds of rock mechanics problems. In the process of a tunnel design, the stability of tunnel is always a focus of discussion. The assessment on tunnel stability needs first to take into account the required length of service life of the tunnel under consideration. According to the length of service life, tunnels may be classified in three categories, namely short term tunnels, medium term tunnels and long term tunnels.

Short term tunnels are those often encountered in association with longwall mining, namely the gateways. The length of service life of these tunnels may be as short as a couple months and up to 1 - 2 years. Such tunnels are usually subject to heavy loading effects due to the mining induced stress redistribution. As a consequence of short term service, these tunnels can tolerate tunnel closure of up to 30% of the original dimensions, generally without the need for repair.

Medium term tunnels refer to those with a service life span being between 2 - 10 years. Such tunnels are usually found to be accesses linking panels and pit major tunnels. Unlike short term gateways driven along seams, the medium term tunnels are often required to be designed and excavated in comparatively competent strata underneath or occasionally above coal seams. Such tunnels are likely to be subject to the mining induced stress effects. However, the influences that the tunnels can permit are less severe than those in gateway cases. Particularly, the deformations of the tunnels at the early stage of their service should be minimized.

Long term tunnels are those having life durations of several tens of years or even accompanying the operation of the whole mine to the end. Long term tunnels need to be located in more stable rock formations. Since they tolerate less instability disturbance, the tunnels require more intensive and effective support systems to be employed.

No matter which kind of tunnel is considered, the design of the tunnel must satisfy the requirements for the stability although the degree of stability and the duration of maintaining stability may vary from one case to another.

In modern coal mining operations there are two notable features :

(1) Excavation depth is increasing. In the British coal mining industry, the greatest depth has reached 1100 metres below the surface, with deeper excavations being considered. In China, coal mine tunnels have also been driven to depths of over 1000 metres below the surface. In Germany, the depth has reached 1400 metres. Gradual increases in mining depth would result in gradual increases in the ground stresess, at least in the vertical component of stress. This indicates that the rocks around the tunnels at greater depths would suffer greater loading effects. Consequently, more instability problems would be encountered. As another result of the increase in driving depth, the properties of the rocks may be subjected to changes.

74

The failure mode of the same kind of rock may also differ. Yielding zones around the tunnels at greater depths may develop into a wider scope and thus the tunnel closure may become more apparent. Rock mechanics problems which have been encountered so far in association with the increase in mining depth are rock bursts occurring mainly in brittle rock formations characterised by high mechanical strength, and floor heaves occurring largely in soft ground formations.

(2) Coal mining activities are moving towards more difficult ground conditions in terms of strata control. Having been won for a considerable time, the number of seams which are easy to be extracted are becoming less and less. Many remaining seams for the future will exhibit various difficulties in respect of ground control of excavations. For example, mining in small interval multiseams would pose a number of potential problems to the extraction and excavation in the remaining underlying seams, due to the fact that a large quantity of remnant pillars have been left in the mined-out areas in upper seams, which have attracted high roof pressures and given rise to stability problems in the undercut tunnels in the remaining seams. In particular, if the remnant coal pillars in upper seams have not been recorded in detail, tunnels for the underlying seams in the future are likely to be designed and driven in those adverse areas of stress concentration.

It seemed necessary at this stage to examine the rock mechanics problems occurring in association with tunnel stability and support design, before the research objectives of this thesis was identified. This has enabled the significance of the objectives to be highlighted.

If we carefully examine the most primary source of the above mentioned problems associated with tunnel stability, it is not difficult to find that the instability problems always arise from changes in the stress field. Excavation of a new tunnel removes the confinement on the surface of the profile and induces a stress concentration zone around the tunnel. The original equilibrium condition is thus

disturbed and destroyed The inequilibrium in the stress field triggers the deformation and closure of the tunnel , with the exceptions of those owing to the dilation nature of soft rocks. The mining induced instability problems can also be attributed to the effects of the change (increase in this case) in stress field.

If various detailed reasons which cause the change in stress field are overlooked in order to find the core of these problems, the investigation into tunnel stability problems may be reasonably simplified, and the research focus may thus be thrown onto the effects of the most basic factor, namely the change in stress field, on the tunnel stability. This consideration formed the major research objectives of this thesis.

3.3 Research Objectives

According to the above discussion, the research objectives of this thesis have been focussed on the following points:

(1) The concept of stress concentration in the vicinity of a tunnel due to the effect of stress field has been first studied prior to the occurrence of rock failure or yielding. Based on this study, the potential failure zones around the tunnel have been identified in relation to the stress field environment.

(2) The dimensional characteristics of the tunnel that copes well with the stress field condition in respect of tunnel stability has been studied. The relation between the tunnel dimensional feature and stability in the relevant stress field conditions has been developed, which is hoped to improve the current concept on tunnel design and construction.

(3) The currently prevailing prediction theories regarding the tunnel stability and the yielding radius have been studied and developed. The study aimed at correlating the available rock properties with the tunnel yielding radius and gathering them into a prediction theory on tunnel stability

76

(4) The influence of the stress field environment on the fracture development around the tunnel with various profiles has been intensively investigated. A detailed comparison on the fracture orientation and scope and the effect of the stress field features has been conducted, in order to give a clear picture regarding the effect of stress field on tunnel stability.

(5) The fracture and stability of tunnels in stratified rock conditions has been another study focus of this thesis. This has been hoped to outline the typical failure and deformation features of coal mining tunnels in association with sedimentary rocks. The study covered the effect of lamination thickness and the role that a standing rigid steel support plays. The failure and movement along the surfaces of beddings and laminations has been studied. The failure mode of the tunnel in the sedimentary rock formations has been studied in relation to the stress field features.

(6) Mining induced stress redistribution problems has been examined. The effect of the abutment stress on the stability of a tunnel closely underneath a working panel has also been studied. The stability of a typical rib pillar together with an in-seam tunnel has also been examined.

3.4 Research Methods Adopted

In order to realize the objectives listed above, particularly within the limited study duration of three years, the research methods and facilities were chosen to serve the research objectives are of particular importance. Obviously, there was a need for viewing all methods and facilities available and possible before the decision was made on which methods and facilities should be employed .

3.4.1 Review and Assessment of Research Methods

Looking into many literature sources and references on the aspect of tunnel design and stability, it is deemed that the methods used in rock mechanics researches

can be divided into four main categories, namely theoretical methods, laboratory tests, field instrumentations and observations, and computer based studies, although some investigators may divide the methods into three categories. All of these methods have their own advantages and disadvantages when they are adopted for research purposes.

3.4.1.1 Theoretical Methods

Theoretical methods consist of employing various mathematical tools to solve engineering problems. There are several kinds of mechanics theories which have been used to solve problems encountered in tunnel design and construction. These theories include rigid mechanics, material mechanics, structural mechanics, elastic mechanics, plastic mechanics, visco mechanics, and fracture mechanics.

In rigid mechanics, an object such as a rock block or a support component is seen as a rigid body.And the research interest is drawn to the analysis of the balance of the block under consideration when it is subject to several loadings, such that the unknown forces acting on the block are found through the solution of relevant equilibrium equations in terms of forces and moments. Obviously, such mechanics principles cannot answer all questions on deformations.

In material mechanics, the work is concentrated on the equilibrium and deformation of a single beam or bar. Such single beam theory has been frequently and widely used in early development of rock mechanics to explain the bending and failure of a tunnel roof , and the deformation and yield of a support girder, when the roof and the girder are simplified as a single beam subject to point loadings and/or distributed loadings from the surrounding rocks. In the analysis, the calculation of beam deformations such as flexure is based on an assumption that a constant neutral plane exists in the beam and it does not stretch nor shorten under loading conditions. A cross-cut plane of a beam prior loading is also assumed to be the same plane under loading conditions.

Structural mechanics was developed on the basis of material mechanics, the former being concerned with the equilibrium and deformation of a beam system. The beam system consists of a number of beams connected through joints. It has been spreadingly applied in civil engineering particularly in the structural design for bridges and buildings. It is rarely used in mining tunnel design except on the occasions of design of standing wooden supports or the steel girder and leg systems.

In elastic mechanics, analysis starts from finding the equilibrium conditions of an infinitesimal element. By referring to the boundary conditions, solved are a group of differential equations including equilibrium equations, constitutional equations and geometrical equations. The mechanics principles eliminates the assumptions as considered in material and structural mechanics. It has been widely used in the design of tunnels and support strengths. The application of this theory has made it possible to study the solution of problems regarding stress concentrations around underground tunnels of simple profiles, namely circular and elliptical, and the deformation characteristics of tunnels subject to various stress field conditions. However, the theory is limited to the materials that obey the linear constitutional law, which is an approximation of reality. A linear constitution of material is often assumed in such analysis of stresses and deformations in rocks.

In plastic mechanics, the ductile behaviour of material after reaching the material elastic limit is considered. Since the plastic behaviour of rocks varies from rock type to rock type, from rock sample to rock sample due to the uncertainty nature of rock formation and property, no model has been found to date to suit for describing the precise plastic behaviour of rocks in Coal Measures. However some models initially developed for describing the plastic characteristics of metals are employed in rock mechanics, with the model commonly used in the design of rock excavations being the idealised elasto-plastic model. Undoubtedly the consideration of plastic features of

material in the stress analysis for tunnel design has contributed to a further development in rock mechanics and shortened the distance between reality and theory.

Viscous mechanics considers the time dependent effect of loadings on the magnitude and direction of stress and strain. The development of the theory is far from perfect because of the existence of difficulties arising from solving the differential equations involving the time variable. Most models postulated for such problems are restricted to some combinations of the three elements of a spring, a pair of friction plates and the liquid container with a relief valves.

Fracture mechanics was initially developed on the basis of elasticity, when considering the conditions of stability and failure patterns of a crack (called the Griffith crack) which is referred to as an elliptical hole with the length of the shorter axis tending to become zero. This theory employs new strength indices instead of simple compression, tensile or shear strengths. Such theory is applicable with effectiveness so far only to the analysis of small cracks. The application of it is still limited within the scope of laboratory and far from engineering realities. The infant state of fracture mechanics as applied to rocks makes it difficult to solve rock engineering problems.

In reviewing the procedure of solutions of rock engineering problems by means of theoretical methods mentioned above, it can be seen that the theoretical analysis normally consists of resolving a problem into its simple elements, establishing solvable equations of the problems and then finding solutions to these equations by using proper but complicated mathematical tools. It is shown that the findings of theoretical solutions of these engineering problems would require the engineer to have sufficient knowledge of mathematics and mechanics. Owing to the nature of uncertainties of rock characteristics involved in tunnel design and the difficulties arising from finding a proper method to solve differential equations involving more than one variable, only rarely has an theoretical solution been found that fully fits the

problem geometry, rock behaviour laws and boundary conditions of a rock mechanics problem in prototype. However, the significance of the theoretical solution lies in that it establishes broader relations among relevant factors and thus helps distinguish between the factors of primary and secondary importance. The use and development of theoretical methods has played an important role in the development of rock mechanics and the design of tunnels and supports. Every solution to the simplified rock stability problems may present a contribution to the guide line for underground excavation design although the use of the solution is more qualitative rather than quantitative.

3.4.1.2 Laboratory Modellings

There are two physical modelling techniques frequently used in the laboratory for the study of tunnel stability and support problems, namely equivalent material modelling and photoelastic modelling.

The physical modelling using equivalent materials is based upon the theory of similarity. The most important and also the most difficult requirement for the model materials is that they should represent the rocks being modelled by the law of similarity. Materials often used for modelling are sand, plaster, cement, clay, power plant ash, mica, sawdust, and water, with occasional use of wax. The following mixtures are found in many literatures to have been used for the purpose of investigations into various tunnel stability problems:

- Sand, plaster and water;

- Sand, cement and water;

- Sand, clay and water;

- Sand, clay, plaster and water;

- Sand, plaster, mica and water;

- Sand, plaster, sawdust and water;

- Sand, wax, mica and water;

- Sand, power plant ash, plaster and water

The plaster cemented granular materials have been the most commonly used materials to model Coal Measures strata in the United Kingdom and Germany. This application largely arose from the simplicity of the preparation of model, cheapness of constituents and broad textural similarities, but reduced strengths and greater deformabilities, in relation to the prototype materials.

Sand-cement mixtures have been used for modelling. These materials are brittle and exhibit non-linear uniaxial stress- strain behaviour in compression. The ratio of compressive to tensile strength can vary between 6 to 16. The material is, however, not as convenient to cure as the sand-plaster mixes (Goshtasbi, 1987, Bonsall, 1985).

The materials cemented with oil or wax are, from a practical point of view, an ideal modelling material as they are inexpensive, easily fabricated and capable of giving measurable deformations at low loads. These materials have been extensively developed in the USSR, though elsewhere have been rarely used.

Photoelastic stress analysis is a powerful technique which is used to model many different engineering situations. The advantage of the photoelastic modelling is that the stress levels may be determined and the zones of stress concentration be found and visible. However, testing of the model is non destructive and therefore the use of the technique is feasible only within the elastic range of materials.

The technique of photoelastic stress analysis involves the making of a scale model in suitable transparent plastics or resin and placing the model in a beam of polarised light using an instrument called a polariscope. If loads are then applied to the model, an light interference pattern by means of fringes will be observed in the model. These fringes may give information on the magnitudes of the principal stresses and the maximum shear stress which are present in the model. It is then possible to relate these stresses by a simple formula to those existing around the mine tunnel and predict the tendency of failure likely to occur around tunnels. However,

problems may be encountered in simulating stratified structures with this technique, for example, the simulation of the interlayer contact and material properties for different layers is difficult.

Laboratory modelling has the advantages that it enables the study to be carried out one by one on the significance of each factor influencing the problem in question (e.g. stability). The study of a model may emphasize on the influence of one factor only each time, which will give a more clear picture of the importance of the factor. Also the physical modelling technique shows visible and intuitive results in terms of failures and their developments around tunnels. The advantage of this point cannot be found by the employment of other research methods. Further more, the modelling work costs much less and needs a shorter duration of working time.

3.4.1.3 Field Observations and Instrumentation

Field observation and instrumentation have long been accepted as a very important method for investigating the problems encountered in underground excavation.

Field observation by human eye is a cheap and easy access to localised problems and it provides the observer with the first hand information of the site. Accumulation of such empirical information will enrich him with the knowledge that can be used as a guide line to improve the design and construction of other structures with similar geological basis. In China this method is more favoured by the management staff of coal mines because those people have time and opportunity to observe every day the procedure and development of damage and failure of underground structures. Having collected specified information for several years a staff member may be qualified in the design and control of underground excavations. Therefore it is often found without any doubt that a production engineer at a coal mine may tackle a problems encountered in his mine better and quicker than a scientist from a research institution who is not very familiar with the local situation. Surely, it is also

83

found that the production engineer cannot tackle with success a problem encountered elsewhere rather than in his mine, unless identical conditions exist.

Instrumentation may be employed throughout the whole procedure of design, construction, and maintenance of an underground engineering structure, although the objective and focus of the instrumentation at various stages may vary.

At the design stage, instrumentation is needed in order to determine the information and relevant data required for the design of the excavation. Such information includes the strength of the *in situ* rock, the magnitude and direction of the *in situ* stresses, and the modulus of deformation of the rock mass.

At the construction stage, the purpose of instrumentation is to confirm the validity of the design and provide necessary evidence for the modification to the design. Additionally, monitoring of displacements plays an important role in providing information which may be used to assess the safety of the underground construction sites.

At the maintenance stage the instrumentation is directed towards the assessment of the stability of the excavations and the response of them to mining activities. Information from the instrumentation may serve the taking of decisions on the need for the replacement or supplement of supports.

Generally speaking, the data obtained from instrumentation are quantitative and comparable. Therefore they may be used as a reference for the future design of other excavations at other sites. These data can be input into a computer data base in order to serve a design programme for future design purposes. However, field observations and instrumentation require long durations of working time, and the precision of results is subject to the influence of many factors such as installation qualities and unforeseen geological disturbances at the site.

3.4.1.4 Computer Based Studies

As mentioned previously, the number of theoretical solutions of rock mechanics problems are limited owing to the nature of complexity of realistic problems encountered underground. Sometimes, the assumptions made in order to formulate a theoretical solution are so simplified that the solution does not at all agree with the reality or even oppose it. Thus some other technique is required aiming at elimination of the unreasonable assumptions so that realistic relations between factors of the problem are recovered and emphasised. This usually indicates that it is not attainable to solve the formulated differential equations by hand and pen methods and that a numerical method which involves the use of a suitable computer is needed.

The advent of computer techniques used to solve mining-related rock mechanics problems may be traced back to the 1960's when the computer technique was first introduced to the mining industry. During the last two decades significant developments in the application of computer techniques to the solution of rock mechanics problems have been made. Computers are now often used to carry out numerical calculations of rock mechanics problems. The most frequently used numerical methods as developed on the basis of computer techniques are the finite element method and the boundary element method.

The finite element method was developed to solve the model which simulates a prototype into a finite number of elements with finite dimensions, the process of which is usually called the formation of an finite element mesh. These elements are connected through a number of nodes usually at the corners of each element.

The equilibrium conditions of an individual element need to be first examined. Within an element, displacements of these nodes are related to the part of the element on an assumption of a given function called "a shape function". As soon as the displacements of all points within the element are determined, the components of strain of these points and thus the components of stress in the element can also be determined by using definitions and some theorems such as Hooke's constitutional

law in linear elastic cases. The solutions of all elements within the whole model are then collected and assembled to finally form a solution to the whole model.

Since the elements are connected at nodes, the interaction between two neighbouring elements is thus assumed to take place through the nodes, namely forces are transferred from one element to another only by the connecting nodes. Obviously, to determine the forces acting on these limited nodes is much easier than in order to determine loads distributed along the boundary of the element. This will make it possible to employ a computer to tackle the problems by use of a finite element programme.

The finite element method has been well developed for rock mechanics applications. It can now tackle nonlinear, nonelastic and multilayer problems. In order to calculate these problems, relevant failure criteria should be firstly assembled in the programme to be used. In the course of calculation, loads are firstly divided into a number of increments as desired and then applied to the finite element model. As every load increment is added to the model system, the computer carries out the process from element analysis, formation of every elemental stiffness matrix, assemble of a general stiffness matrix, to the solution of the general matrix equation, and then judges the failed elements by using the assembled failure criterion. Since the failure of an element will cause a change in the mechanical properties of the element and thus the stresses acting on the element will also change by transferring to neighbouring elements. The readjustment of stresses from the failed elements to neighbouring regions causes unbalance to the whole system. This means that the computer has to go through the whole procedure of processing again, namely from element analysis, formation of every elemental stiffness matrix, assemble of the general stiffness matrix, to the solution of the general matrix equation system and the judgement of occurrence of failed elements. Generally, the computer should repeat several times of such procedure for an increment of loads applied to the model system. Since the time required for each of such procedures is nearly equivalent to the

total time required for an elastic model calculation, the computation of a non-linear or non-elastic model would consume much more computing time and thus cost much more.

Errors arise in the procedure of calculation when the complicated situations in the scope of an element are represented by the motion of the relevant nodes through an assumed shape function which is simple and primary. The degree of an error is closely related to the size and shape of elements. When the element size is large and the shape is irregular, the error produced will tend to become evident. Although such error may be reduced to an acceptable level by increasing the number of elements and thus reducing the size of elements, dividing a model into elements of smaller sizes means increasing the total number of elements and nodes, which will lead to a need for a computer to provide a larger working space in memory and consume more extra time for computing the equilibrium of the increased nodes.

Generally speaking, the assembly of a finite element programme requires a computer to possess a large memory space. A personal computer is very difficult to carry out such task. Even if some PC computers can contain the programme, the time needed for computing an engineering problem could be tremendous. The author has experienced such case while he was working at the Central Coal Mining Research Institute in China. An elastic strata model which was divided into some 800 four-node elements was calculated by an IBM PC/AT and a frame computer separately. The time used for the computation with the frame computer was around one hour whilst over fifty hours were needed with the PC computer. Therefore, a fairly complicated finite element programme cannot be run in a personal computer. This restricts popularization of the technique as applied to engineering.

The boundary element method involves dividing a boundary of the problem such as a tunnel profile into a number of elements. The so-called boundary integral equations are proposed. By solving the boundary integral equations by means of a

computer and numerical methods, displacements, strains and stresses along the boundary elements are determined. And then the results from the boundary elements are used to estimate the values in the rest of the model.

With a boundary element programme, the problems of a model are solved by reducing one freedom of the problems. It thus seems that less space in computer memory and less time are needed for the calculation of the problem, compared with the finite element method for the same model. However, when the model involves a multilayer problem the formation of the boundary integral equation will become very complicated and the solution to these equations will require more computing time. In such cases. the speed of solution to the model may become slower than that by the finite element method.

3.4.2 Methods Employed in this Research Project

As stated above, there are a number of methods which can be used for the research purpose of this project. Each method has its own advantages and disadvantages. Before the making of decision on which methods should be used for this research, the author had to consider the time limit of his study duration of three years.

Although field instrumentation can give detailed and localised information on the factors influencing tunnel stability and allow the assessment on the localised tunnel stability situation, the work would require longer time to be spent on the installation of instruments and observation. Also the data from the instrumentation site would need to be inspected for there could be some errors in the collected data due to such reasons as imperfect installation, unforeseen geological structure and production interference. Therefore the field instrumentation method was not adopted for this research purpose.

In mining tunnel design, it is often possible to predict the performance of rock-support interaction by using some kind of theoretical model based upon proven physical principles. In order to develop a complicated theoretical model, much mathematical knowledge should be prepared before hand. The contribution of mathematics to rock mechanics and tunnel design is well noted. It may possibly be stated that rock mechanics cannot advance without continuous development in the theoretical aspect. Therefore, in this thesis, the author has attempted to use mathematics to develop a model for predicting the performance of a mining tunnel subjected to the effects of the stress field, and aimed at relating various geological and operational factors to the tunnel stability problems.

The theoretical models developed for engineering purposes have some common defects. For instance the models are usually based on some simplifications which may not explain the full procedure of the development of an engineering structure. In the case of tunnel design, theoretical models cannot explain the procedure of failure development around tunnels. These phenomena imply the need for other methods to be used in order to implement such defects. In this thesis, the physical modelling technique would be intensively used for further investigation purposes.

Physical modelling enables the assessment to be achieved of a large number of tunnel designs within a short time duration and avoids measurements in the actual mine tunnels which would be difficult and time consuming.

By using physical modelling, the performance of tunnels of various profiles in a homogeneous rock mass has been first examined in terms of stability, development of fracture and failures, and particularly in relation to the effect of the stress field.

After completion of the tests on the behaviour of the tunnels in homogeneous rock, the characteristics of stratification of Coal Measures have been simulated in later

models in order to study the effect of stratification on tunnel stability and its response to various ground pressures.

Further consideration has been given to the function of mine tunnel support in relation to the fracture development around a tunnel when subjected to the effect of two opposite stress fields.

CHAPTER FOUR

ANALYSIS OF STRESS AND DEFORMATION AROUND MINE TUNNELS PRIOR TO ROCK FAILURE

CHAPTER FOUR

ANALYSIS OF STRESS AND DEFORMATION AROUND MINE TUNNELS PRIOR TO ROCK FAILURE

4.1 Introduction

In the design of a new mining tunnel and the assessment for the stability of an existing tunnel, there is usually a need for theoretically estimating the stresses and deformations in the surrounding rocks and the ability of the tunnel to withstand the rock movements. The movements of the surrounding rocks also need to be predicted in relation to the visible rock failures, such as roof slabbing and falling, sidewall buckling and spalling, and floor lifting. One difficulty in the determination of the stresses in the underground rock mass around a tunnel is the uncertainty of the stress field which is generally formed by the weight of the overburden and probably the tectonic forces. Although the state of stress underground is often assumed to be due only to the weight of the overburden rock or simply in the state of hydrostatic stress as adopted by a number of investigators Frith (1988), and Wilson (1980), actual stress measurements and observations in existing tunnels indicate that estimates made on this basis may lead to a substantial error.

A lack of accurate information on the mechanical properties of the *in situ* rock mass presents another difficulty to the design and construction of tunnels. Although some knowledge may be obtained from a geological investigation of the area or by examining and testing exploratory drill cores, the rock and the geology in an area are so changeable that drill cores may not provide precise average data of the area.

The third difficulty arises in calculating the stress and deformation in the different parts of a tunnel. Firstly as the configuration of tunnel becomes more complex, it becomes more difficult to find a continuously smooth function to describe the geometry of the tunnel profile in order to determine the deformations of the tunnel.

Secondly, as the rock in Coal Measures becomes more variable, featured by the nature of stratification, and intersected by dikes, faults, or systems of joints, the complete rock structure around the tunnel becomes significantly too difficult to be treated mathematically in terms of the proper descriptive functions and the methods of solution other than the theory of continuity and homogeneity.

To overcome these obstacles, some approximations and assumptions for the rock properties and the stress field have been proposed and widely accepted. A number of formulae have thus been developed and deduced for the design and prediction of tunnel stability, as they have been summarized and listed by Frith (1988). Such design and prediction comprises an important part of rock mechanics although they are the result of simplification to some degree and often need to be modified as information from underground investigations and experience from practice become available.

The nature of variations in rock properties and geological features within Coal Measures implies that successful designs should not follow the same procedure. Nevertheless, all designs of mining tunnels and the prediction of the deformations require a theoretical basis on which different design formulae are deduced. When referring to many works on rock mechanics such as those by Obert and Duvall (1967) and Jaeger and Cook (1979), it would not be difficult to find that continuous solid mechanics has commonly been accepted as a foundation of rock mechanics, with the theory of elasticity being functioning as an important part of the foundation. The theories of plasticity, viscosity, and fracture mechanics have all been developed on the basis of the theory of elasticity. As a content of the rock mechanics research, the design of mining tunnels has always exhibited a need for the assistance of the elasticity theory in order to form a design theory. Therefore in this chapter the author first reviews the basic equations needed for solving elastic problems, and then further studies the features of stresses and deformations distributed around the tunnel, from

which he attempts to relate tunnel stability to a number of factors, in particular the stress field environment.

4.2 Basic Theory of Elasticity of Rock Mechanics

In order to apply the theory of elasticity to the analysis of stresses and deformations around mining tunnels, the assumptions of the elastic materials are also adopted for the rock mass under consideration, these being:

(1) Continuity. The rock mass is assumed to be continuous within a certain zone under consideration. This is based on such a logical deduction that, although the discontinuity nature of the rock mass has long been recognised owing to the existence of joints, cracks, igneous intrusions and faults, most joints and cracks in the surrounding rock of tunnel are closed and able to transmit stresses and deformations from one side of the crack or joint to another. Therefore, when neither faults nor igneous intrusions are present in the discussed rock zone and the joints and cracks are small in size by comparison with the tunnel dimensions, the zone is acceptably assumed to be continuous.

(2) Homogeneity. The rock mass is assumed to be homogeneous within a same layer. This is based on the view that the rock constitution in a layer is more or less the same and the visual voids with the size in the order of engineering excavations are very rarely found in Coal Measures strata, so that the assumption is applicable when there are no faults and igneous intrusions.

(3) Within a same layer the rock mass is assumed to be isotropic. Although in Coal Measures strata, the rock formations contain cracks and joints and exhibit a laminated structurre which causes the rocks to become anisotropic. We can still accept the assumption of isotropism when we take into account the feature of random distribution of cracks and joints in the rock mass and neglect the effects of lamination for the time being.

93

On the basis of such assumptions, the theory of elasticity can be applied to the analysis of stresses and deformations around mining tunnels before any rock failure takes place.

4.2.1 Definition of Stress, Displacement and Strain in Rock

The rock mass in underground conditions is usually subjected to compressive loading. Stresses in the rock around the mining tunnels are mainly compressive. In order to avoid too much use of the negative sign in the mathematical deduction and calculation, the definition of stress, strain and displacement in rock should follow the practice adopted in rock mechanics rather than that in the classic theory of elasticity.

Imagine a small cubic element cut from the interior of a rock mass under discussion. If the element is placed in a Cartesian coordinate system where the three mutually perpendicular edges of the element are oriented parallel with the coordinate axes, Figure 4.2.1, the intensity of force perpendicularly acting on a surface of the element is defined as the normal stress on the surface and the intensity of force tangentially acting on the surface is defined as the shear stress on the surface. If the element encloses a point in the centre, the state of stress at the point is defined, as the size of the element reduction to the point.

In a three dimensional Cartesian space, there are nine components of stress existing at a physical point in a rock mass, these being:

$$\begin{bmatrix} \sigma_x & \tau_{xy} & \tau_{xz} \\ \tau_{yx} & \sigma_y & \tau_{yz} \\ \tau_{zx} & \tau_{zy} & \sigma_z \end{bmatrix} \qquad (4.2.1)$$

They form a state of stress and should be called a tensor of stress instead of a vector as stated wrongly in a number of rock mechanics references. It may be worth mentioning here that the stress is a tensor of the second order whilst the vector is also a tensor but of the first order. The number of components of a tensor depends on the

94
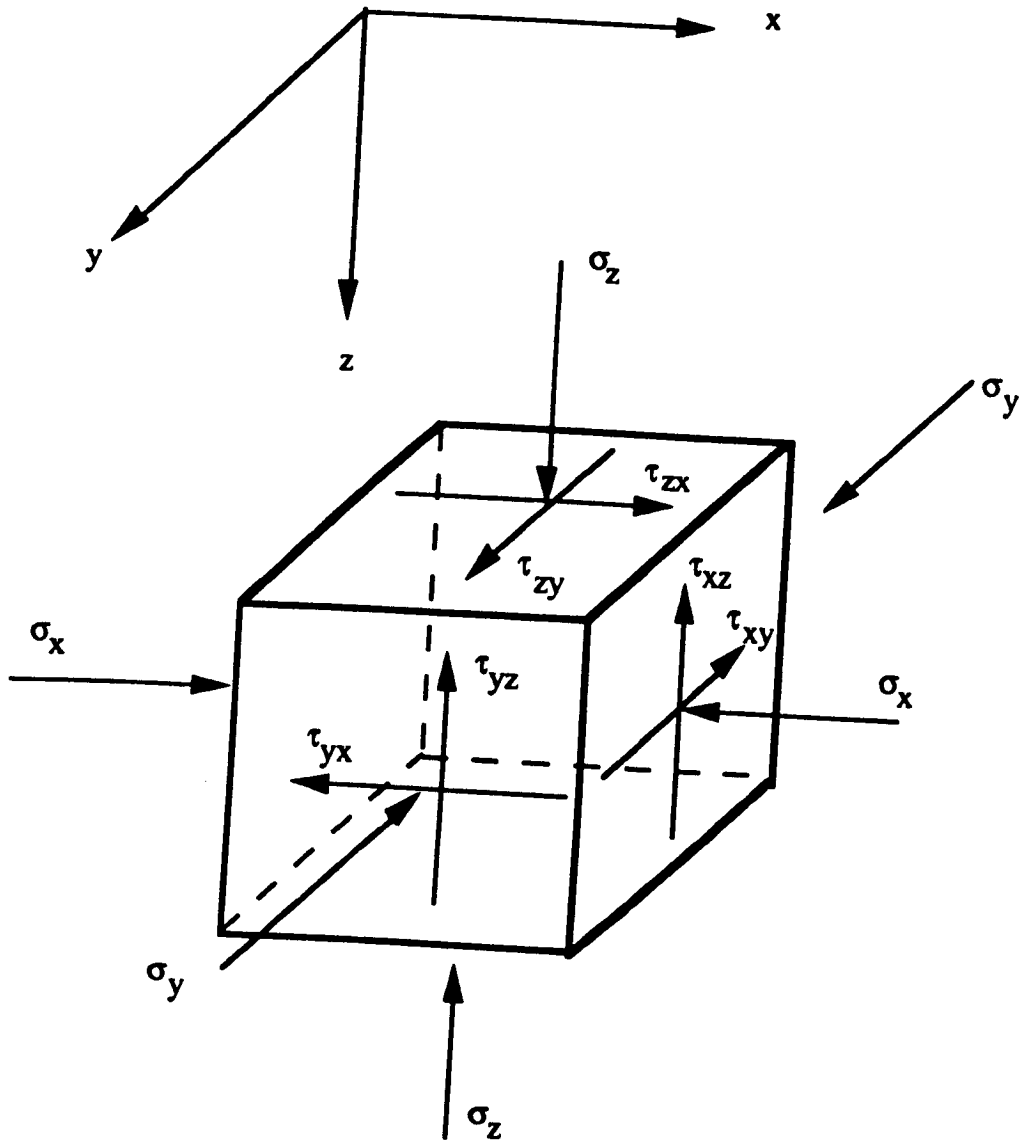
Figure 4.2.1 Definition of rock stress components in the Cartesian space.

degree of the tensor order. In a three dimensional system, the number of components of a tensor, N, is calculated as

$$N = 3^K \qquad\qquad (4.2.2)$$

where K is the degree of the tensor order. Therefore a tensor of the first order, i.e. a vector, at an arbitrary point has three components, whilst a tensor of the second order, like a stress tensor, has $3^2 = 9$ components. The tensor theory has constituted a branch of pure mathematics that has been developed in the last few decades. The laws of the tensor theory have been intensively applied in the study of modern theoretical mechanics. However, the application of the tensor theory to the analysis of stresses and deformations in rock around tunnels is still very rare. Since the application of the tensor theory to rock engineering designs will involve the use of very sophisticated mathematical knowledge which would exceed the scope of the thesis, the author has decided to avoid using the tensor theory in his thesis. Readers who are interested in this aspect of work are suggested to refer to the relevant mathematical works, notably by Green and Zerna (1954), Borisenko and Tarapov (1968), Chorlton (1976), and Bourne and Kendall (1977).

The rock stresses are mostly of compressive nature because the tensile loading conditions are rarely present underground. This situation is similar to that in soil mechanics but quite different from that in mechanical engineering and other branches of continuum solid mechanics. It is therefore necessary to introduce a convention of the sign for stresses, in order to facilitate the studies. In this thesis, the compressive stress is taken as positive whilst tensile stress as negative. When we take a right handed system of orthogonal coordinates and let the three mutually perpendicular edges of a small cubic element be parallel with the coordinate axes, the positive direction of shear stresses in Expression 4.2.1 are such defined that, on the face with its outward normal pointing to the positive direction of an axis (for example x-axis), a shear stress (for example τ_{xy}) is defined to be positive if it tends to cause the face to

96

slide towards the negative direction of another axis which is parallel with the face (i.e. y-axis), or to be negative if it tends to drag the face toward the positive direction of the (y -) axis. On the face with its outward normal pointing to the negative direction of an axis (x-axis), a shear stress (τ_{xy}) is reckoned to be positive if it tends to drag the face toward to positive direction of another axis parallel with the face (i.e. y-axis) and vice versa. The positive directions of all stress components for the small element are shown in Figure 4.2.1.

Upon loading, the particles in the rock mass will displace from their initial position to a final position so that a new equilibrium is achieved. In rock mechanics there are two fundamental concepts used to describe the rock deformation, i.e. displacement and strain. These two concepts are important in the design and stability of tunnels. The convention of sign for the displacement and strain also needs to be defined here.

In order that the displacements can show their response to the relevant stresses, namely positive displacements are corresponding to positive stresses, displacements are referred to as positive when they are in the negative direction of the coordinate axes. If u,v,w are the displacements of a particle initially at a point p(x,y,z), its final position at p'(x',y',z') after deformation will be

$$\left. \begin{array}{l} x' = x - u \\ y' = y - v \\ z' = z - w \end{array} \right\}$$

(4.2.3)

When the displacements (u,v,w) are constant for all particles in the rock mass under discussion, the rock mass is referred to as being in the state of translation of a rigid body, in which we have

$$\left. \begin{array}{l} x' = x - a \\ y' = y - b \\ z' = z - c \end{array} \right\}$$

(4.2.4)

where a,b,c are constants.

Another simple form of displacement is rotation as a rigid body about a fixed axis of reference. In two dimensions, suppose that ox and oy are the axes of reference and that the whole body including the particle p, is rotated through an angle ω so that p moves to p'. The particles of the body which lay along the axes ox and oy before rotation now lie in the directions ox' and oy'. The coordinates x' and y' of the point p' relative to the original axes ox and oy may be written from Figure 4.2.2 as:

$$\left.\begin{array}{l} x' = x\cos\omega - y\sin\omega \\ y' = x\sin\omega + y\cos\omega \end{array}\right\} \tag{4.2.5}$$

If ω is small these become

$$\left.\begin{array}{l} x' = x - y\omega \\ y' = x\omega + y \end{array}\right\} \tag{4.2.6}$$
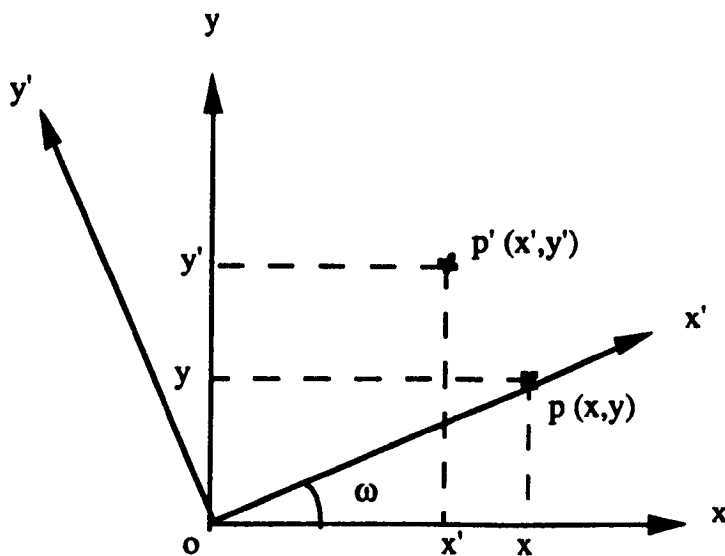
Figure 4.2.2 Coordinate transformation for rock rotation as a rigid body.

In three dimensions, for a small rotation about an axis defined by the direction cosines (l,m,n), the final position p'(x',y',z') of the point p(x,y,z) is expressed as follows (Thomson and Tait, 1962):

$$
\begin{aligned}
x' &= x + \omega(mz - ny) \\
y' &= y + \omega(nx - lz) \\
z' &= z + \omega(ly - mx)
\end{aligned}
\left.\right\} \qquad (4.2.7)
$$

In rock engineering, rock movements are rarely rigid. Instead, lots of deformable movements take place, such that the relative positions of the particles in rock mass are changed. The measurement between two arbitrary particles prior to the movement are no longer equal to that after deformation. The rock is therefore said to be strained.

The state of strain in rock can be described quantitatively. The convenient and thereafter the most commonly used quantities for the measurement of strain are the change of length of a line and the change of angle between two perpendicularly intersecting lines, the former being called elongation and the latter called the shear strain.

Assume that l is the distance between two points o and p in a rock mass in the unstrained state and l' is the corresponding distance between them after deformation, Figure 4.2.3. Then

$$
\varepsilon = \frac{(l - l')}{l} \qquad (4.2.8)
$$

is defined as the elongation corresponding to the point o in the direction of op. It is positive when a contraction results.

Assume that two perpendicular lines, op and oq, intercept at point o. When the rock mass including the lines is subject to loading, the point o moves to a position o',

(a)   (b)
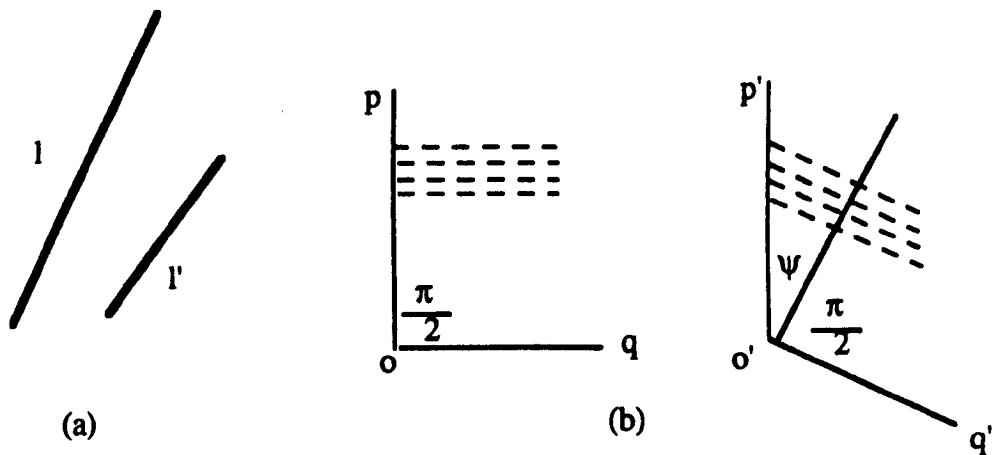
Figure 4.2.3 The definition of elongation and shear strain

(after Jaeger and Cook,1979).

and the angle poq becomes p'o'q'. If in the strained state, the angle p'o'q' is measured to be $\frac{\pi}{2} + \psi$, the quantity

$$\gamma = \tan \psi \qquad (4.2.9)$$

is defined as the shear strain for the point o along the directions of op and oq.

The sign of shear strain is defined as such: if the right angle consisting of two lines intercepting at point o becomes greater under the action of loads, the shear strain at the point along the directions of the two lines is positive, and vice versa. Obviously, such notation is in accordance with that for the stress and deformation.

4.2.2 Fundamental Equations for Solving Elastic Problems in Rock Engineering

In rock mechanics, stress, strain, and displacement are the three basic quantities. Solutions to the problems regarding the tunnel stability usually initiate from the analysis of stress, strain, and displacement. The analysis has deduced some fundamental equations in terms of stress, strain and displacement. These equations

100

constitute necessary and sufficient conditions to solve all rock mechanics problems, i.e. most part of the theory are deduced on the basis of such equations. Therefore they need to be reviewed before any further analysis is carried out.

Generally speaking, there are five major groups of fundamental equations necessitated for solving the rock mechanics problems, these including:

- Equilibrium equations;

- Geometrical equations;

- Constitutive equations;

- Compatibility equations; and

- Prescribed boundary conditions at the exterior surfaces of the body.

4.2.2.1 Equilibrium Equations

In rock mechanics, the equilibrium equations describe the relationship between the components of stress at an arbitrary point in a rock mass in equilibrium when it is subject to: (1) the action of forces and / or restriction of deformations on the boundary of the rock mass, and (2) the action of body forces such as gravity.

Consider the equilibrium conditions at a point p(x,y,z) in the rock mass under discussion. To do so, an infinitesimal rectangular parallellepiped element with centre at point p(x,y,z) is removed from the body and the stresses that existed before removal are restored (Figure 4.2.4). Let the faces of the parallellepiped element be parallel to the coordinate planes, x-y, y-z, and z-x in an oxyz orthogonal coordinate system. Denote X,Y,Z for the components of the body force at the point p along the three axes of reference, and the positive directions of the body force components are, in accordance with the previous convention, in the negative x-, y-, and z- directions. Assume the small side lengths are AA'=dx, AB=dy, and AD=dz, and the stresses are smooth and continuous functions of coordinates in the region occupied by the rock mass. For the small element in the body, the differences in stresses on opposite faces of the element can be expressed by increments of stress.
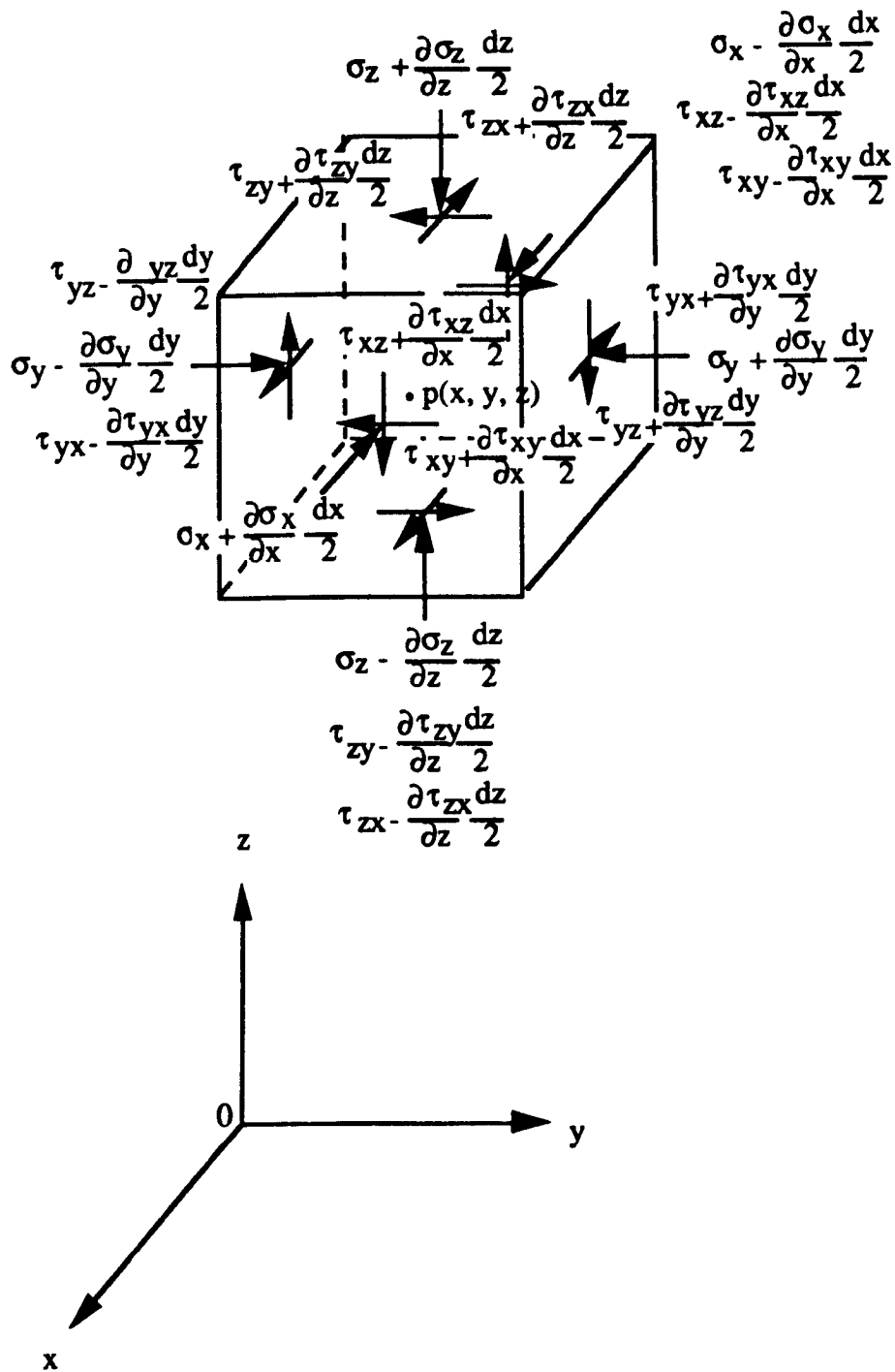
Figure 4.2.4 The equilibrium condition of an infinitesimal element at a point in rock

102

In order that the element can be in equilibrium, the following equilibrium conditions in terms of force components in the coordinate directions must be satisfied:

$$\Sigma F_x = 0; \ \Sigma F_y = 0; \ \Sigma F_z = 0 \qquad (4.2.10)$$

Summation of the forces in the x-direction gives

$$\Sigma F_x = -(\sigma_x - \frac{\partial \sigma_x}{\partial x} \frac{dx}{2})dydz + (\sigma_x + \frac{\partial \sigma_x}{\partial x} \frac{dx}{2})dydz - (\tau_{yx} - \frac{\partial \tau_{yx}}{\partial y} \frac{dy}{2})dxdz$$

$$+ (\tau_{yx} + \frac{\partial \tau_{yx}}{\partial y} \frac{dy}{2})dxdz - (\tau_{zx} - \frac{\partial \tau_{zx}}{\partial z} \frac{dz}{2})dxdy + (\tau_{zx} + \frac{\partial \tau_{zx}}{\partial z} \frac{dz}{2})dxdy + Xdxdydz$$

$$= 0 \qquad (4.2.11)$$

Similar summations for the forces in y- and z-directions can be written. Simplifying these equations and dividing by dxdydz yields:

$$\left. \begin{array}{l} \dfrac{\partial \sigma_x}{\partial x} + \dfrac{\partial \tau_{yx}}{\partial y} + \dfrac{\partial \tau_{zx}}{\partial z} + X = 0 \\[2mm] \dfrac{\partial \tau_{xy}}{\partial x} + \dfrac{\partial \sigma_y}{\partial y} + \dfrac{\partial \tau_{zy}}{\partial z} + Y = 0 \\[2mm] \dfrac{\partial \tau_{xz}}{\partial x} + \dfrac{\partial \tau_{yz}}{\partial y} + \dfrac{\partial \sigma_z}{\partial z} + Z = 0 \end{array} \right\} \qquad (4.2.12)$$

When the body is in equilibrium, the sums of moments about the axes through the point p(x,y,z) in the directions of x, y, and z must be zero, namely

$$\Sigma M_x = 0; \qquad \Sigma M_y = 0; \qquad \Sigma M_z = 0. \qquad (4.2.13)$$

In detail, we can write

$$\Sigma M_x = \frac{\tau_{yz}dxdydz}{2} + \frac{(\tau_{yz} + \frac{\partial \tau_{yz}}{\partial y}dy)dxdydz}{2} - \frac{\tau_{zy}dxdydz}{2} - \frac{(\tau_{zy} + \frac{\partial \tau_{zy}}{\partial z}dz)dxdydz}{2}$$

$$= 0$$

Therefore,

103

$$\tau_{yz} + (\tau_{yz} + \frac{\partial \tau_{yz}}{\partial y} dy) - \tau_{zy} - (\tau_{zy} + \frac{\partial \tau_{zy}}{\partial z} dz) = 0 \qquad (4.2.14)$$

As the element shrinks to the point p(x,y,z), dy and dz shrink to the limit of zero, and this produces:

$$\tau_{yz} = \tau_{zy}.$$

In the similar manner, the relations between the rest four shear stresses can be obtained. Putting these relations together yields

$$\left. \begin{array}{l} \tau_{xy} = \tau_{yx} \\ \tau_{yz} = \tau_{zy} \\ \tau_{zx} = \tau_{xz} \end{array} \right\} \qquad (4.2.15)$$

Equations 4.2.15 show that pairs of shear stresses are equal in magnitude and sign. Thus Equations 4.2.12 become

$$\left. \begin{array}{l} \dfrac{\partial \sigma_x}{\partial x} + \dfrac{\partial \tau_{xy}}{\partial y} + \dfrac{\partial \tau_{xz}}{\partial z} + X = 0 \\[2mm] \dfrac{\partial \tau_{xy}}{\partial x} + \dfrac{\partial \sigma_y}{\partial y} + \dfrac{\partial \tau_{yz}}{\partial z} + Y = 0 \\[2mm] \dfrac{\partial \tau_{xz}}{\partial x} + \dfrac{\partial \tau_{yz}}{\partial y} + \dfrac{\partial \sigma_z}{\partial z} + Z = 0 \end{array} \right\} \qquad (4.2.16)$$

Equations 4.2.16 indicate that the six components of stress that vary continuously throughout the body are related, and in the course of analysis they must satisfy these conditions.

4.2.2.2 Geometric Equations

Geometric equations describe the relations between strain and displacement. Under the assumption of linear elasticity, it is accepted that (1) the quantities ε and γ (see Equations 4.2.8 and 4.2.9) are so small compared to unity that their squares and products are negligible, and (2) in the neighbourhood of an arbitrary point p(x,y,z) in a rock mass, the strains are homogeneous, that is, changes in deformation with

position in the rock mass are linear over small areas within the body. As a result of these assumption, all straight lines in the neighbourhood of the point p(x, y, z) remain straight after straining and the parallel lines remain parallel, although their direction may change with strain. Also, the order of application of two deformations has no effect upon the final configuration of the body.

Consider one corner of a rectangular parallelepiped element removed from a strained body, which is projected onto the x-y plane, Figure 4.2.5. Let the coordinate axes coincide with the sides of the element before straining. After straining, point O has moved to point O', point A to A', and point B to B'. The displacement of a point will be represented by the three orthogonal components, u,v,and w parallel to the x,y, and z axes, respectively, in space. These displacement components are assumed to be continuous functions of the coordinates (x,y,z). Thus, if u is the displacement of point O in the x direction, the displacement of a neighbouring point A in x direction is $u + (\partial u / \partial x) \Delta x$. Higher derivatives and products are not required because of the two assumptions.

Therefore the length of the line segment O'A" is given by

$$O'A" = \Delta x + u - \frac{\partial u}{\partial x}\Delta x - u = \Delta x - \frac{\partial u}{\partial x}\Delta x \ ;$$

and the length of the line segment A'A" is

$$A'A" = v - \frac{\partial u}{\partial x}\Delta x - v = \frac{-\partial u}{\partial x}\Delta x$$

Thus the length of the line segment O'A' is given by

$$O'A' = \sqrt{(\Delta x - \frac{\partial u}{\partial x}\Delta x)^2 + (\frac{\partial v}{\partial x}\Delta x)^2} = \Delta x \sqrt{1 - 2\frac{\partial u}{\partial x} + (\frac{\partial u}{\partial x})^2 + (\frac{\partial v}{\partial x})^2}$$

Expanding the expression under the radical sign and neglecting second and higher order terms gives

$$O'A' = \Delta x (1 - \frac{\partial u}{\partial x})$$

105

By the definition, the strain

$$\varepsilon_x = \lim_{\Delta x \to 0} \frac{(O\,A\ -\ O'A')}{OA} = \lim_{\Delta x \to 0} \frac{\partial u \Delta x}{\partial x \Delta x} = \frac{\partial u}{\partial x} \qquad (4.2.17)$$

Since angles $\Delta\theta_1$ and $\Delta\theta_2$ are small as well as strains, by referring to Figure 4.2.5 the following equations can be written:

$$\tan \Delta\theta_1 = \Delta\theta_1 = \frac{|A'A''|}{|O'A''|} = \frac{|-(\partial v/\partial x)\Delta x|}{|\Delta x - (\partial u/\partial x)\Delta x|} \approx \frac{\partial v}{\partial x}$$

$$\tan \Delta\theta_2 = \Delta\theta_2 = \frac{|B'B''|}{|O'B''|} = \frac{|-(\partial u/\partial y)\Delta y|}{|\Delta y - (\partial v/\partial y)\Delta y|} \approx \frac{\partial u}{\partial y}$$

By the definition, the shear strain γ_{xy}, in the right angle AOB is $\Delta\theta_1 + \Delta\theta_2$; therefore

$$\gamma_{xy} = \frac{\partial u}{\partial y} + \frac{\partial v}{\partial x} \qquad (4.2.18)$$
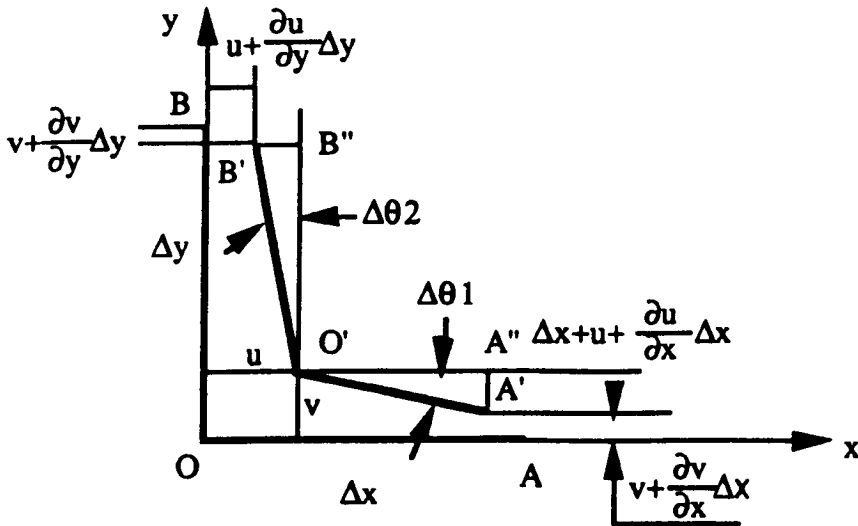
Figure 4.2.5 Geometric relationship for deformed rock

After a similar deduction for the yz and zx planes, the six components of strain can be related to the displacements by the following six equations

106

$$\left.\begin{array}{ll} \varepsilon_x = \dfrac{\partial u}{\partial x} & \gamma_{xy} = \dfrac{\partial u}{\partial y} + \dfrac{\partial v}{\partial x} \\[2ex] \varepsilon_y = \dfrac{\partial v}{\partial y} & \gamma_{yz} = \dfrac{\partial v}{\partial z} + \dfrac{\partial w}{\partial y} \\[2ex] \varepsilon_z = \dfrac{\partial w}{\partial y} & \gamma_{zx} = \dfrac{\partial w}{\partial x} + \dfrac{\partial u}{\partial z} \end{array}\right\} \qquad (4.2.19)$$

Equations 4.2.19 are called the geometric equations which relate the strain components to the displacement components. The three equations on the left are the components of normal strain and the three equations on the right are the components of shear strain in the cartesian directions. If u, v, and w are continuous functions of the space coordinates x,y, and z, of a body, the state of strain at a point in the body is then completely specified by Equations 4.2.19.

4.2.2.3 Compatibility Equations

Since there are three displacement components and six strain components, the six strain components in a body cannot be specified arbitrarily. In order to ensure that displacements induced by straining result in no separation between small elements in the rock mass there must exist some relations among the strain components. Such relations are called compatibility conditions. They can be derived as follows:

Taking second partial derivatives of ε_x and ε_y in Equations 4.2.19 with respect to y and x respectively, gives

$$\frac{\partial^2 \varepsilon_x}{\partial y^2} = \frac{\partial^3 u}{\partial y^2 \partial x} \qquad \text{and} \qquad \frac{\partial^2 \varepsilon_y}{\partial x^2} = \frac{\partial^3 v}{\partial x^2 \partial y}$$

Taking the partial derivatives of γ_{xy} with respect to x and y gives

$$\frac{\partial^2 \gamma_{xy}}{\partial x \partial y} = \frac{\partial^3 u}{\partial y^2 \partial x} + \frac{\partial^3 v}{\partial x^2 \partial y}$$

Comparing these three equations gives one of the compatibility equations as

$$\frac{\partial^2 \varepsilon_x}{\partial y^2} + \frac{\partial^2 \varepsilon_x}{\partial y^2} = \frac{\partial^2 \gamma_{xy}}{\partial x \partial y}$$

Taking the partial derivatives of γ_{yz}, γ_{zx} and γ_{xy} with respect to x,y, and z, respectively gives

$$\frac{\partial \gamma_{yz}}{\partial x} = \frac{\partial^2 v}{\partial x \partial z} + \frac{\partial^2 w}{\partial x \partial y}$$

$$\frac{\partial \gamma_{zx}}{\partial y} = \frac{\partial^2 w}{\partial y \partial x} + \frac{\partial^2 u}{\partial y \partial z}$$

$$\frac{\partial \gamma_{xy}}{\partial z} = \frac{\partial^2 u}{\partial z \partial y} + \frac{\partial^2 v}{\partial z \partial x}$$

Combining the last three equations as indicated below and taking partial derivatives with respect to x gives

$$\frac{\partial}{\partial x}\left(-\frac{\partial \gamma_{yz}}{\partial x} + \frac{\partial \gamma_{zx}}{\partial y} + \frac{\partial \gamma_{xy}}{\partial z}\right) = -\frac{\partial^3 v}{\partial x^2 \partial z} - \frac{\partial^3 w}{\partial x^2 \partial y} + \frac{\partial^3 w}{\partial y \partial x^2} + \frac{\partial^3 u}{\partial x \partial y \partial z} + \frac{\partial^3 u}{\partial x \partial z \partial y} + \frac{\partial^3 v}{\partial z \partial x^2}$$

Therefore a second compatibility equation is

$$\frac{\partial}{\partial x}\left(-\frac{\partial \gamma_{yz}}{\partial x} + \frac{\partial \gamma_{zx}}{\partial y} + \frac{\partial \gamma_{xy}}{\partial z}\right) = 2\frac{\partial^2 \varepsilon_x}{\partial y \partial z}$$

In a similar manner, four additional equations can be derived. By putting these equations together the following six compatibility equations are obtained:

$$\left.\begin{aligned}
\frac{\partial^2 \varepsilon_x}{\partial y^2} + \frac{\partial^2 \varepsilon_x}{\partial y^2} &= \frac{\partial^2 \gamma_{xy}}{\partial x \partial y} \\[6pt]
\frac{\partial^2 \varepsilon_x}{\partial y^2} + \frac{\partial^2 \varepsilon_x}{\partial y^2} &= \frac{\partial^2 \gamma_{xy}}{\partial x \partial y} \\[6pt]
\frac{\partial^2 \varepsilon_x}{\partial y^2} + \frac{\partial^2 \varepsilon_x}{\partial y^2} &= \frac{\partial^2 \gamma_{xy}}{\partial x \partial y} \\[6pt]
\frac{\partial}{\partial x}\left(-\frac{\partial \gamma_{yz}}{\partial x} + \frac{\partial \gamma_{zx}}{\partial y} + \frac{\partial \gamma_{xy}}{\partial z}\right) &= 2\frac{\partial^2 \varepsilon_x}{\partial y \partial z} \\[6pt]
\frac{\partial}{\partial x}\left(-\frac{\partial \gamma_{yz}}{\partial x} + \frac{\partial \gamma_{zx}}{\partial y} + \frac{\partial \gamma_{xy}}{\partial z}\right) &= 2\frac{\partial^2 \varepsilon_x}{\partial y \partial z} \\[6pt]
\frac{\partial}{\partial x}\left(-\frac{\partial \gamma_{yz}}{\partial x} + \frac{\partial \gamma_{zx}}{\partial y} + \frac{\partial \gamma_{xy}}{\partial z}\right) &= 2\frac{\partial^2 \varepsilon_x}{\partial y \partial z}
\end{aligned}\right\} \qquad (4.2.20)$$

These six compatibility equations must be satisfied if the six strain components are specified by Equations 4.2.19 and the displacement components u, v, and w are to be continuous functions of the space coordinates.

108

4.2.2.4 Constitutive Equations

Constitutive equations specify the relations between the components of stress and strain. These relations for linear elastic isotropic materials have been established by numerous experiments and are known as Hooke's law. The Hooke's law is expressed as follows :

$$
\left.
\begin{aligned}
\varepsilon_x &= \frac{1}{E}[\ \sigma_x - v(\sigma_y + \sigma_z)] \\[4pt]
\varepsilon_y &= \frac{1}{E}[\ \sigma_y - v(\sigma_z + \sigma_x)] \\[4pt]
\varepsilon_z &= \frac{1}{E}[\ \sigma_z - v(\sigma_x + \sigma_y)] \\[4pt]
\gamma_{xy} &= \frac{2(1+v)}{E}\tau_{xy} \\[4pt]
\gamma_{yz} &= \frac{2(1+v)}{E}\tau_{yz} \\[4pt]
\gamma_{zx} &= \frac{2(1+v)}{E}\tau_{zx}
\end{aligned}
\right\}
\qquad (4.2.21)
$$

where E is the modulus of elasticity, v is the Poisson's ratio.

4.2.2.5 Boundary Conditions

Boundary conditions of a deformed rock mass in equilibrium can take two forms, one being expressed in force and the other in displacement.

If the surface force components acting on a unit surface area of the rock are known to be F_x, F_y, F_z, the boundary conditions can be expressed as

$$
\left.
\begin{aligned}
l\sigma_x + m\tau_{yx} + n\tau_{zx} &= F_x \\
l\tau_{xy} + m\sigma_y + n\tau_{zy} &= F_y \\
l\tau_{xz} + m\tau_{yz} + n\sigma_z &= F_z
\end{aligned}
\right\}
\qquad (4.2.22)
$$

where l,m,n are the direction cosines of the outward normal of the surface at the point discussed, and σ_x, τ_{yx}, τ_{zx} , τ_{xy}, σ_y, τ_{zy}, τ_{xz}, τ_{yz}, and σ_z are the components of stress at the point.

4.2.3 Plane Strain Problems

Problems in the theory of elasticity as applied to rock mechanics are considerably simplified when the displacement of all points in a deformed rock mass are confined in planes normal to one direction. Such a state of deformation is known as a plane strain state. In the analysis of mining tunnel stability, it is frequently assumed that deformation of the tunnel takes place within the planes normal to the tunnel axis, such that the problems are simplified as the plane strain and the analytical solutions in respect of the distribution of stress and strain become less difficult.

If a plane strain state occurs in the x-y plane, all deformations takes place within the x-y plane and without any change along the z axis. The displacement components can be expressed as:

$$u = u\,(x, y); \quad v = v\,(x, y); \quad w = 0 \qquad (4.2.23)$$

Since u and v are the functions of the arguments x and y only, and w is equal to zero, the strain components are either the functions of x and y only or being equal to zero as expressed:

$$\left.\begin{aligned}
\varepsilon_x &= \frac{\partial u}{\partial x} = \varepsilon_x(x, y) \\
\varepsilon_y &= \frac{\partial u}{\partial y} = \varepsilon_y(x, y) \\
\gamma_{xy} &= \gamma_{yx} = \frac{\partial u}{\partial y} + \frac{\partial v}{\partial x} = \gamma_{xy}(x, y) = \gamma_{yx}(x, y) \\
\varepsilon_z &= \gamma_{xz} = \gamma_{yz} = \gamma_{zx} = \gamma_{zy} = 0
\end{aligned}\right\} \qquad (4.2.24)$$

From the Hooke's law (Equations 4.2.21), the followings are gained

$$\left.\begin{aligned}
\sigma_z &= v\,(\sigma_x + \sigma_y) \\
\varepsilon_x &= \frac{1}{E}\,[(1-v^2)\sigma_x - v(1+v)\sigma_y] \\
\varepsilon_y &= \frac{1}{E}\,[(1-v^2)\sigma_y - v(1+v)\sigma_x] \\
\gamma_{xy} &= \frac{2(1+v)}{E}\,\tau_{xy}
\end{aligned}\right\} \qquad (4.2.25)$$

110

Obviously, the stress components, σ_x, σ_y, σ_z, and τ_{xy}, are all the functions of x and y only.

The equilibrium equations is thus simplified as:

$$\left.\begin{array}{l} \dfrac{\partial\sigma_x}{\partial x} + \dfrac{\partial\tau_{xy}}{\partial y} + X = 0 \\[3mm] \dfrac{\partial\tau_{xy}}{\partial y} + \dfrac{\partial\sigma_y}{\partial y} + Y = 0 \end{array}\right\} \qquad (4.2.26)$$

The compatibility equations (4.2.20) are now automatically satisfied except:

$$\frac{\partial^2\varepsilon_x}{\partial y^2} + \frac{\partial^2\varepsilon_y}{\partial x^2} = \frac{\partial^2\tau_{xy}}{\partial x\partial y} \qquad (4.2.27)$$

Substitution of the second and the third of Equations 4.2.25 into Equation 4.2.27 gives

$$(1\text{-}v)(\frac{\partial^2\sigma_x}{\partial y^2} + \frac{\partial^2\sigma_y}{\partial x^2}) - v\,(\frac{\partial^2\sigma_y}{\partial y^2} + \frac{\partial^2\sigma_x}{\partial x^2}) = 2\frac{\partial^2\tau_{xy}}{\partial x\partial y} \qquad (4.2.28)$$

Differentiating the first equilibrium equation in Equations 4.2.26 with respect to x, and the second one with respect to y, and adding these results, yields:

$$2\frac{\partial^2\tau_{xy}}{\partial x\partial y} = -\frac{\partial^2\sigma_x}{\partial x^2} - \frac{\partial^2\sigma_y}{\partial y^2} - \frac{\partial X}{\partial x} - \frac{\partial Y}{\partial y}$$

Substitution of this equation into Equation 4.2.28 gives:

$$(\frac{\partial^2}{\partial x^2} + \frac{\partial^2}{\partial y^2})(\,\sigma_x + \sigma_y) = -(1\text{-}v)\,(\frac{\partial X}{\partial x} + \frac{\partial Y}{\partial y})$$

If the body force X and Y are constant or zero, the above equation becomes

$$(\frac{\partial^2}{\partial x^2} + \frac{\partial^2}{\partial y^2})(\,\sigma_x + \sigma_y) = 0 \qquad (4.2.29)$$

The Equations 4.2.26 and 4.2.29, together with the boundary conditions constitute the sufficient equations to obtain a solution to a plane strain problem since only three unknown stress components are involved in these three independent equations.

111

To solve these equations, some further method needs to be used, of which the Airy stress function is usually used when the body forces are constant or zero.

Assume the body forces are zero. Then the Airy stress function U is defined as:

$$\sigma_x = \frac{\partial^2 U}{\partial y^2}, \qquad \sigma_y = \frac{\partial^2 U}{\partial x^2}, \qquad \tau_{xy} = -\frac{\partial^2 U}{\partial x \partial y} \qquad (4.2.30)$$

Such definition of the Airy stress function makes the equilibrium equations 4.2.26 be automatically satisfied. Equation 4.2.29 becomes

$$\left(\frac{\partial^2}{\partial x^2} + \frac{\partial^2}{\partial y^2}\right)\left(\frac{\partial^2}{\partial x^2} + \frac{\partial^2}{\partial y^2}\right) U = \frac{\partial^4 U}{\partial x^4} + 2\frac{\partial^4 U}{\partial x^2 y^2} + \frac{\partial^4 U}{\partial y^4} = 0 \qquad (4.2.31)$$

or

$$\nabla^4 U = 0 \qquad (4.2.32)$$

This equation is called a biharmonic equation and the function U is called a biharmonic function. All solution of it will automatically satisfy both equilibrium and compatibility equations. Therefore any plane strain problem has now been deduced to finding a proper stress function which satisfies the equation 4.2.32 and the relevant boundary conditions of the problem.

4.2.4 Fundamental Equations for Plane Strain Problems in Polar Coordinates

In discussion of a plane strain problem involving a circular excavation, it may be easier to find the solution if the polar coordinate system is introduced.

Selecting a polar system as shown in Figure 4.2.5, the relations between the polar coordinates (r, θ) and the rectangular (x,y) are

$$\left. \begin{array}{l} x = r\cos\theta \\ y = r\sin\theta \end{array} \right\} \qquad (4.2.33)$$

By analysing the equilibrium conditions of a small element, the equilibrium equations along the radial and tangential directions can be obtained (Jaeger and Cook, 1979).

$$\left.\begin{array}{l} \dfrac{\partial \sigma_r}{\partial r} + \dfrac{\sigma_r - \sigma_\theta}{r} + \dfrac{1}{r}\dfrac{\partial \tau_{r\theta}}{\partial \theta} + f_r = 0 \\[4mm] \dfrac{1}{r}\dfrac{\partial \sigma_\theta}{\partial \theta} + \dfrac{\partial \tau_{r\theta}}{\partial r} + 2\dfrac{\tau_{r\theta}}{r} + f_\theta = 0 \end{array}\right\} \qquad (4.2.34)$$

where f_r, f_θ are the body force components in the radial and tangential directions; σ_r and σ_θ are the radial and tangential normal stress components; $\tau_{r\theta}$ is the shear stress component.

In the polar system, the geometric equations become

$$\left.\begin{array}{l} \varepsilon_r = \dfrac{\partial u}{\partial r} \\[4mm] \varepsilon_\theta = \dfrac{1}{r}\dfrac{\partial v}{\partial \theta} + \dfrac{u}{r} \\[4mm] \gamma_{r\theta} = \dfrac{1}{r}\dfrac{\partial u}{\partial \theta} + \dfrac{\partial v}{\partial r} - \dfrac{v}{r} \end{array}\right\} \qquad (4.2.35)$$

where ε_r and ε_θ are the normal strain components in the r and θ directions respectively; $\gamma_{r\theta}$ is the shear strain; u and v are the displacement components in r and θ directions.

The constitutive equations for the plane strain problems become

$$\left.\begin{array}{l} \varepsilon_r = \dfrac{1}{E}[(1-v^2)\sigma_r - v(1+v)\,\sigma_\theta] \\[4mm] \varepsilon_\theta = \dfrac{1}{E}[(1-v^2)\sigma_\theta - v(1+v)\,\sigma_r] \\[4mm] \gamma_{r\theta} = \dfrac{2(1+v)}{E}\tau_{r\theta} \end{array}\right\} \qquad (4.2.36)$$

According to the relationship between the Cartesian system and the polar system, the biharmonic equation in the polar coordinates can be derived from that in the Cartesian coordinates. This is because that:

$$r = \sqrt{x^2 + y^2} \quad ; \quad \arctan\frac{y}{x} = \theta$$

$$\frac{\partial r}{\partial x} = \frac{x}{\sqrt{x^2 + y^2}} = \cos\theta \quad ; \quad \frac{\partial r}{\partial y} = \frac{y}{\sqrt{x^2 + y^2}} = \sin\theta$$

113

$$\frac{\partial \theta}{\partial x} = \frac{\frac{-y}{x^2}}{1+(\frac{y}{x})^2} = \frac{-y}{x^2+y^2} = \frac{-\sin\theta}{r} \; ; \quad \frac{\partial \theta}{\partial y} = \frac{\frac{1}{x}}{1+(\frac{y}{x})^2} = \frac{x}{x^2+y^2} = \frac{\cos\theta}{r}$$

Therefore the following identities hold true:

$$\frac{\partial U}{dx} = \frac{\partial U}{\partial \theta}\frac{\partial \theta}{\partial x} + \frac{\partial U}{\partial r}\frac{\partial r}{\partial x} = -\frac{\partial U}{\partial \theta}\frac{\sin\theta}{r} + \frac{\partial U}{\partial r}\cos\theta \; ;$$

$$\frac{\partial U}{dy} = \frac{\partial U}{\partial \theta}\frac{\partial \theta}{\partial y} + \frac{\partial U}{\partial r}\frac{\partial r}{\partial y} = \frac{\partial U}{\partial \theta}\frac{\cos\theta}{r} + \frac{\partial U}{\partial r}\sin\theta \; ;$$

$$\frac{\partial^2 U}{\partial x^2} = \frac{\partial}{\partial \theta}(-\frac{\partial U}{\partial \theta}\frac{\sin\theta}{r} + \frac{\partial U}{\partial r}\cos\theta)\frac{\partial \theta}{\partial x} + \frac{\partial}{\partial r}(-\frac{\partial U}{\partial \theta}\frac{\sin\theta}{r} + \frac{\partial U}{\partial r}\cos\theta)\frac{\partial r}{\partial x}$$

$$= (-\frac{\partial^2 U}{\partial \theta^2}\frac{\sin\theta}{r} - \frac{\partial U}{\partial \theta}\frac{\cos\theta}{r} + \frac{\partial^2 U}{\partial r\partial \theta}\cos\theta - \frac{\partial U}{\partial r}\sin\theta)\frac{-\sin\theta}{r} +$$

$$+ (-\frac{\partial^2 U}{\partial r\partial \theta}\frac{\sin\theta}{r} + \frac{\partial U}{\partial \theta}\frac{\sin\theta}{r^2} + \frac{\partial^2 U}{\partial r^2}\cos\theta)\cos\theta$$

$$= \frac{\partial^2 U}{\partial \theta^2}\frac{\sin^2\theta}{r^2} + \frac{\partial U}{\partial \theta}\frac{\sin\theta\cos\theta}{r^2} - \frac{\partial^2 U}{\partial r\partial \theta}\frac{\sin\theta\cos\theta}{r} + \frac{\partial U}{\partial r}\frac{\sin^2\theta}{r} -$$

$$- \frac{\partial^2 U}{\partial r\partial \theta}\frac{\cos\theta\sin\theta}{r} + \frac{\partial U}{\partial \theta}\frac{\sin\theta\cos\theta}{r^2} + \frac{\partial^2 U}{\partial r^2}\cos^2\theta \; ; \qquad \text{(a)}$$

$$\frac{\partial^2 U}{\partial y^2} = \frac{\partial}{\partial \theta}(\frac{\partial U}{\partial \theta}\frac{\cos\theta}{r} + \frac{\partial U}{\partial r}\sin\theta)\frac{\partial \theta}{\partial y} + \frac{\partial}{\partial r}(\frac{\partial U}{\partial \theta}\frac{\cos\theta}{r} + \frac{\partial U}{\partial r}\sin\theta)\frac{\partial r}{\partial y}$$

$$= (\frac{\partial^2 U}{\partial \theta^2}\frac{\cos\theta}{r} - \frac{\partial U}{\partial \theta}\frac{\sin\theta}{r} + \frac{\partial^2 U}{\partial r\partial \theta}\sin\theta + \frac{\partial U}{\partial r}\cos\theta)\frac{\cos\theta}{r} +$$

$$+ (\frac{\partial^2 U}{\partial r\partial \theta}\frac{\cos\theta}{r} - \frac{\partial U}{\partial \theta}\frac{\cos\theta}{r^2} + \frac{\partial^2 U}{\partial r^2}\sin\theta)\sin\theta$$

$$= \frac{\partial^2 U}{\partial \theta^2}\frac{\cos^2\theta}{r^2} - \frac{\partial U}{\partial \theta}\frac{\sin\theta\cos\theta}{r^2} - \frac{\partial^2 U}{\partial r\partial \theta}\frac{\sin\theta\cos\theta}{r} + \frac{\partial U}{\partial r}\frac{\cos^2\theta}{r} +$$

$$+ \frac{\partial^2 U}{\partial r\partial \theta}\frac{\sin\theta\cos\theta}{r} - \frac{\partial U}{\partial \theta}\frac{\sin\theta\cos\theta}{r^2} + \frac{\partial^2 U}{\partial r^2}\sin^2\theta \qquad \text{(b)}$$

114

$$\frac{\partial^2 U}{\partial x \partial y} = \frac{\partial}{\partial y}(-\frac{\partial U}{\partial \theta}\frac{\sin\theta}{r} + \frac{\partial U}{\partial r}\cos\theta)$$

$$= \frac{\partial}{\partial\theta}(-\frac{\partial U}{\partial\theta}\frac{\sin\theta}{r} + \frac{\partial U}{\partial r}\cos\theta)\frac{\partial\theta}{\partial y} + \frac{\partial}{\partial r}(-\frac{\partial U}{\partial\theta}\frac{\sin\theta}{r} + \frac{\partial U}{\partial r}\cos\theta)\frac{\partial r}{\partial y}$$

$$= (-\frac{\partial^2 U}{\partial\theta^2}\frac{\sin\theta}{r} - \frac{\partial U}{\partial\theta}\frac{\cos\theta}{r} + \frac{\partial^2 U}{\partial r\partial\theta}\cos\theta - \frac{\partial U}{\partial r}\sin\theta)\frac{\cos\theta}{r} +$$

$$+ (-\frac{\partial^2 U}{\partial r\partial\theta}\frac{\sin\theta}{r} + \frac{\partial U}{\partial\theta}\frac{\sin\theta}{r^2} + \frac{\partial^2 U}{\partial r^2}\cos\theta)\sin\theta$$

$$= -\frac{\partial^2 U}{\partial\theta^2}\frac{\sin\theta\cos\theta}{r^2} - \frac{\partial U}{\partial\theta}\frac{\cos^2\theta}{r^2} + \frac{\partial^2 U}{\partial r\partial\theta}\frac{\cos^2\theta}{r} - \frac{\partial U}{\partial r}\frac{\sin\theta\cos\theta}{r} -$$

$$- \frac{\partial^2 U}{\partial r\partial\theta}\frac{\sin^2\theta}{r} + \frac{\partial U}{\partial\theta}\frac{\sin^2\theta}{r^2} + \frac{\partial^2 U}{\partial r^2}\sin\theta\cos\theta \qquad \text{(c)}$$

From (a) and (b) it is obtained that

$$\nabla^2 U = \frac{\partial^2 U}{\partial x^2} + \frac{\partial^2 U}{\partial y^2}$$

$$= \frac{\partial^2 U}{\partial\theta^2}\frac{1}{r^2} + \frac{\partial U}{\partial r}\frac{1}{r} + \frac{\partial^2 U}{\partial r^2}$$

$$= (\frac{\partial^2}{\partial\theta^2}\frac{1}{r^2} + \frac{\partial}{\partial r}\frac{1}{r} + \frac{\partial^2}{\partial r^2})U$$

$$\nabla^4 U = (\frac{\partial^2}{\partial\theta^2}\frac{1}{r^2} + \frac{\partial}{\partial r}\frac{1}{r} + \frac{\partial^2}{\partial r^2})(\frac{\partial^2}{\partial\theta^2}\frac{1}{r^2} + \frac{\partial}{\partial r}\frac{1}{r} + \frac{\partial^2}{\partial r^2})U \qquad (4.2.37)$$

Setting $\theta = 0$, the positive direction of x and y in the Cartesian system agrees accordingly with the positive direction of r and θ in the polar system. In this case the stress components in the Cartesian system, σ_x, σ_y, and τ_{xy} can be replaced directly by the stress components in polar system, namely by σ_r, σ_θ, and $\tau_{r\theta}$ correspondingly. And the stress components in the polar system can be easily expressed in terms of the stress function based on the above results (a), (b), and (c).

From the results (a), (b) and (c) it is found that

115

$$\left.\begin{aligned}
\sigma_\theta &= \sigma_y|_{\theta=0} = \frac{\partial^2 U}{\partial x^2}\bigg|_{\theta=0} = \frac{\partial^2 U}{\partial r^2} \\
\sigma_r &= \sigma_x|_{\theta=0} = \frac{\partial^2 U}{\partial y^2}\bigg|_{\theta=0} = \frac{1}{r^2}\frac{\partial^2 U}{\partial \theta^2} + \frac{\partial U}{\partial r}\frac{1}{r} \\
\tau_{r\theta} &= \tau_{xy}|_{\theta=0} = -\frac{\partial^2 U}{\partial x \partial y} = \frac{1}{r^2}\frac{\partial U}{\partial \theta} - \frac{1}{r}\frac{\partial^2 U}{\partial r \partial \theta} = -\frac{\partial}{\partial r}\left(\frac{1}{r}\frac{\partial U}{\partial \theta}\right)
\end{aligned}\right\} \quad (4.2.38)$$

Undoubtedly the stress components expressed by the stress function of Equations 4.2.38 will automatically satisfy the equilibrium equations 4.2.34 when the body forces are negligible or zero. Hence, the remaining problem in the polar system is to find a stress function U that satisfies the compatibility equation 4.2.37 and whose corresponding stress components, as given by Equations 4.2.38, satisfy the boundary conditions of the problem.

4.3 Stress and Displacement in Homogeneous Rock around a Single Circular Tunnel

In this section a theoretical analysis is given on the stresses and displacements around a circular tunnel driven in a homogeneous rock formation. The work aims at showing the effects of the stress field on the distribution of the stresses and displacements around the tunnel.

4.3.1 Stresses in the Rock Vicinity of a Single Circular Tunnel

Consider a circular tunnel of radius, a, located in a homogeneous and isotropic rock mass as shown in Figure 4.3.1. Let the origin of the coordinates be set at the centre of the tunnel with the horizontal direction being the x axis and the vertical direction the y axis. Assume that the tunnel support pressure is p_0, and that the applied horizontal and vertical stresses at a remote distance from the tunnel and have the magnitudes of p_h and p_v, respectively. At the remote distance from the excavation, the stresses in the rock are out of the influence range of the excavation and can be expressed in a polar coordinate system. They result from the effect by the applied p_h and p_v rather than the excavation induced stresses.

116
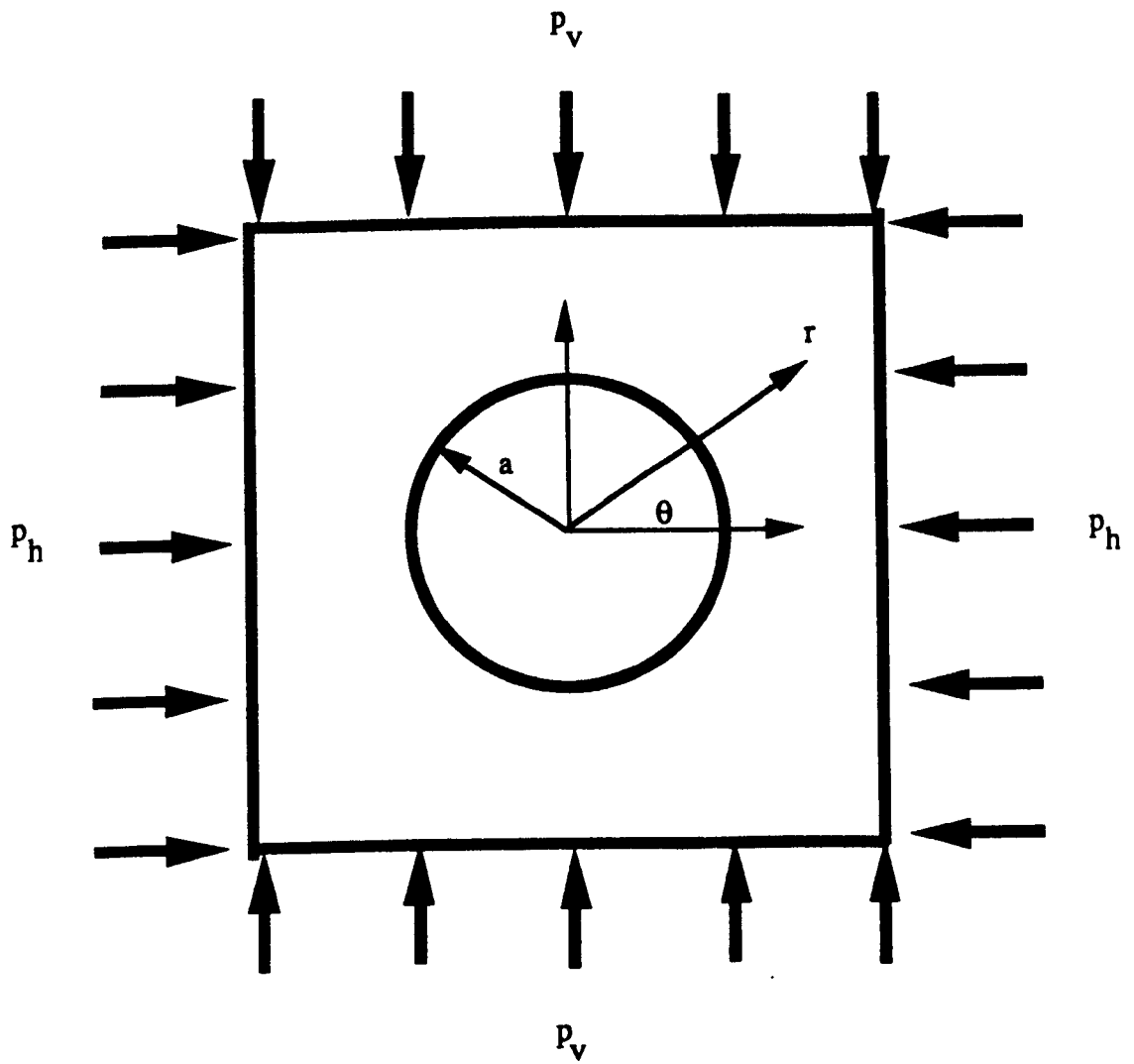
Figure 4.3.1 A circular tunnel located in a homogeneous and isotropic rock mass.

By isolating a small triangular element of unity thickness from the rock at a great distance from the tunnel, as illustrated in Figure 4.3.2. the expression of the polar stress components , σ_r and $\tau_{\theta r}$, are related to the applied stresses, p_h and p_v, as follows .

In the static state, the system of forces acting upon the element must be in balance in both horizontal and vertical directions, namely,

$$\left. \begin{array}{l} \Sigma f_{hi} = 0 \\ \Sigma f_{vi} = 0 \end{array} \right\}$$

or

$$\left. \begin{array}{l} p_h \, c \, \cos\theta + \tau_{r\theta} \, c \, \sin\theta - \sigma_r c \, \cos\theta = 0 \\ p_v \, c \, \sin\theta - \tau_{r\theta} \, c \, \cos\theta - \sigma_r c \, \sin\theta = 0 \end{array} \right\} \qquad (4.3.1)$$

where c is the hypotenuse of the triangle element;

θ is the angle of the normal r with respect to the x-axis;

σ_r and $\tau_{r\theta}$ are the polar stress components; and

p_h and p_v are the applied stresses acting on the element.
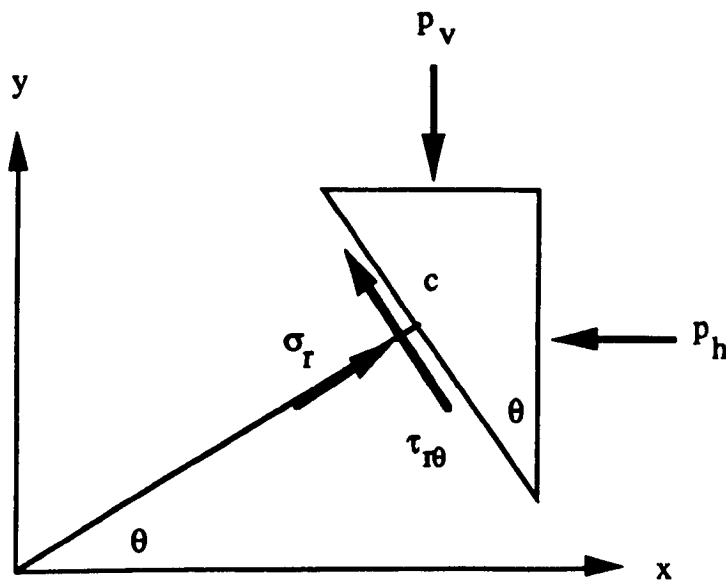
Figure 4.3.2 Relationship between the stress components in the rectangular system and the polar system.

Solving Equations 4.3.1 yields:

$$\left.\begin{array}{l} \tau_{r\theta} = -\dfrac{P_h - P_v}{2}\sin 2\theta \\[2mm] \sigma_r = \dfrac{P_h + P_v}{2} + \dfrac{P_h - P_v}{2}\cos 2\theta \end{array}\right\} \qquad (4.3.2)$$

Therefore, for a tunnel of radius a under the action of the stress field (p_h, p_v) and the support resistance of p_0, the boundary conditions are expressed as:

$$\left.\begin{array}{l} (\tau_{r\theta})_{r\to\infty} = -\dfrac{P_h - P_v}{2}\sin 2\theta \\[2mm] (\sigma_r)_{r\to\infty} = \dfrac{P_h + P_v}{2} + \dfrac{P_h - P_v}{2}\cos 2\theta \\[2mm] (\tau_{r\theta})_{r=a} = 0 \\[2mm] (\sigma_r)_{r=a} = p0 \end{array}\right\} \qquad (4.3.3)$$

In order to find the stress distribution around the tunnel, a stress function needs to be firstly considered. Here it is assumed that such a stress function has the form (Obert and Duvall, 1967):

$$U = A\log r + Br^2 + (Cr^2 + Dr^4 + Er^{-2} + F)\cos 2\theta \qquad (4.3.4)$$

Since $\left(\dfrac{\partial^2}{\partial\theta^2}\dfrac{1}{r^2} + \dfrac{\partial}{\partial r}\dfrac{1}{r} + \dfrac{\partial^2}{\partial r^2}\right)U$

$$= 4B + (12Dr^2 - 4Fr^{-2})\cos 2\theta$$

$$\nabla^4 U = \left(\dfrac{\partial^2}{\partial\theta^2}\dfrac{1}{r^2} + \dfrac{\partial}{\partial r}\dfrac{1}{r} + \dfrac{\partial^2}{\partial r^2}\right)\left(\dfrac{\partial^2}{\partial\theta^2}\dfrac{1}{r^2} + \dfrac{\partial}{\partial r}\dfrac{1}{r} + \dfrac{\partial^2}{\partial r^2}\right)U$$

$$= \dfrac{-4}{r^2}(12Dr^2 - 4Fr^{-2})\cos 2\theta + \dfrac{1}{r}(24Dr + 8Fr^{-3})\cos 2\theta + (24D - 24Fr^{-4})\cos 2\theta$$

$$= 0$$

Therefore, the expression 4.3.4 can be used as a stress function. If the stress components derived from this function satisfy the boundary conditions 4.3.3, the problem regarding the stress distribution around the tunnel as shown in Figure 4.3.1 is solved.

Corresponding to the stress function in Equation 4.3.4, the stress components are, according to Equations 4.2.38:

$$
\left.
\begin{aligned}
\sigma_\theta &= \frac{\partial^2 U}{\partial r^2} \\
&= -A\frac{1}{r^2} + 2B + (2C + 12Dr^2 + 6Er^{-4})\cos 2\theta \\
\sigma_r &= \frac{1}{r^2}\frac{\partial^2 U}{\partial \theta^2} + \frac{\partial U}{\partial r}\frac{1}{r} \\
&= A\frac{1}{r^2} + 2B + (-2C - 6Er^{-4} - 4Fr^{-2})\cos 2\theta \\
\tau_{r\theta} &= -\frac{\partial}{\partial r}(\frac{1}{r}\frac{\partial U}{\partial \theta}) \\
&= (2C + 6Dr^2 - 6Er^{-4} - 2Fr^{-2})\sin 2\theta
\end{aligned}
\right\} \qquad (4.3.5)
$$

Substitution of boundary conditions into Equations 4.3.5 yields:

$$
\left.
\begin{aligned}
&\text{When } r \to \infty
\begin{cases}
\tau_{r\theta} = (2C + 6Dr^2)\sin 2\theta = -\dfrac{P_h - P_v}{2}\sin 2\theta \\
\sigma_r = 2B - 2C\cos 2\theta = \dfrac{P_h + P_v}{2} + \dfrac{P_h - P_v}{2}\cos 2\theta
\end{cases} \\
&\text{When } r = a
\begin{cases}
\tau_{r\theta} = (2C + 6Da^2 - 6Ea^{-4} - 2Fa^{-2})\sin 2\theta = 0 \\
\sigma_r = Aa^{-2} + 2B + (-2C - 6Ea^{-4} - 4Fa^{-2})\cos 2\theta = p_0
\end{cases}
\end{aligned}
\right\}
$$

As the above equations must be true for all values of θ, and as the stress cannot become infinite as r approaches infinite distance ($r \to \infty$), the following equations must hold:

$$
\left.
\begin{aligned}
&D = 0 \\
&C = -\frac{P_h - P_v}{4} \\
&B = \frac{P_h + P_v}{4} \\
&Aa^{-2} + 2B = P_0 \\
&2C + 6Ea^{-4} + 4Fa^{-2} = 0 \\
&2C + 6Da^2 - 6Ea^{-4} - 2Fa^{-2} = 0
\end{aligned}
\right\}
$$

Solving this equation system gives:

$$A = (P_0 - \frac{P_h + P_v}{2}) a^2$$

$$B = \frac{P_h + P_v}{4}$$

$$C = - \frac{P_h - P_v}{4}$$

$$D = 0$$

$$E = - \frac{P_h - P_v}{4} a^4$$

$$F = \frac{P_h - P_v}{2} a^2$$

(4.3.6)

Substitution of these results into Equations 4.3.5 yields

$$\sigma_r = \frac{a^2}{r^2} P_0 + \frac{P_h + P_v}{2}(1 - \frac{a^2}{r^2}) + \frac{P_h - P_v}{2}(1 + 3\frac{a^4}{r^4} - 4\frac{a^2}{r^2})\cos2\theta$$

$$\sigma_\theta = - \frac{a^2}{r^2} P_0 + \frac{P_h + P_v}{2}(1 + \frac{a^2}{r^2}) - \frac{P_h - P_v}{2}(1 + 3\frac{a^4}{r^4})\cos2\theta$$

$$\tau_{r\theta} = - \frac{P_h - P_v}{2}(1 - 3\frac{a^4}{r^4} + 2\frac{a^2}{r^2})\sin2\theta$$

(4.3.7)

These solutions indicate that the composition of the stresses existing around the tunnel can be referred to as three parts. The first part is produced due to the existence of the support resistance, P_0. The second part is caused by the mean value of the applied stresses, $\frac{P_h + P_v}{2}$, which is sometimes called the hydrostatic stress. And the third part is the influence of the difference in the applied stresses, $\frac{P_h - P_v}{2}$. The magnitude of σ_r, σ_θ and $\tau_{r\theta}$ is proportional to the magnitude of P_0, $\frac{P_h + P_v}{2}$ and $\frac{P_h - P_v}{2}$. However, the effects of these three parts on the stress distribution around the tunnel vary as the location under consideration changes with the radius r. A further analysis as to how the change of stresses with the radius r, is caused by each of the three parts is needed for a better understanding of the rock - support interaction.

(1) The effect of the radial resistance of support, Po, on the stress distribution around a tunnel.

By setting the applied stresses equal to zero, for the time being, i.e. $p_h = p_v = 0$, Equations (4.3.7) become

$$
\left.\begin{aligned}
\sigma_{r1} &= \frac{a^2}{r^2} P_0 \\
\sigma_{\theta 1} &= -\frac{a^2}{r^2} P_0 \\
\tau_{r\theta 1} &= 0
\end{aligned}\right\}
\qquad (4.3.8)
$$

Where σ_{r1}, $\sigma_{\theta 1}$ and $\tau_{r\theta 1}$ are the stresses (the first part) induced by the support resistance, P_0.

Equations 4.3.8 indicate that both radial and tangential stresses in the vicinity of the tunnel decrease in magnitude very quickly as the radius, r, increases. Figure 4.3.3 shows this tendency of effect. When r = 2.5a namely at the locations of 1.5 times of tunnel radius outwards the tunnel wall, the magnitude of both σ_{r1} and $\sigma_{\theta 1}$ drops 84% of that at the tunnel wall. When r = 3a, the magnitude of both σ_{r1} and $\sigma_{\theta 1}$ drops to 1/9 of that at the tunnel wall.

This shows that the evident range of the effect of the support resistance on the stresses around the tunnel is limited to the near vicinity of the tunnel. Beyond the range at a distance approximately equal to the tunnel diameter, 2a, the effect of the tunnel support on the rock stresses is becoming weak and negligible. This is the active effect of the support on the tunnel stability, which is different from the passive response of the support to the dead weight caused by the failed materials in the stress relieved zone as is discussed in Chapters 6 and 7.

(2) The effect of the hydrostatic stress field, $\frac{P_h + P_v}{2}$, on the stress distribution around a tunnel.

Setting $p_h = p_v$ and Po $= 0$, the Equations(4.3.7) become

$$
\left.\begin{aligned}
\sigma_{r2} &= \frac{P_h + P_v}{2}\left(1 - \frac{a^2}{r^2}\right) \\
\sigma_{\theta 2} &= \frac{P_h + P_v}{2}\left(1 + \frac{a^2}{r^2}\right) \\
\tau_{r\theta 2} &= 0
\end{aligned}\right\}
\qquad (4.3.9)
$$
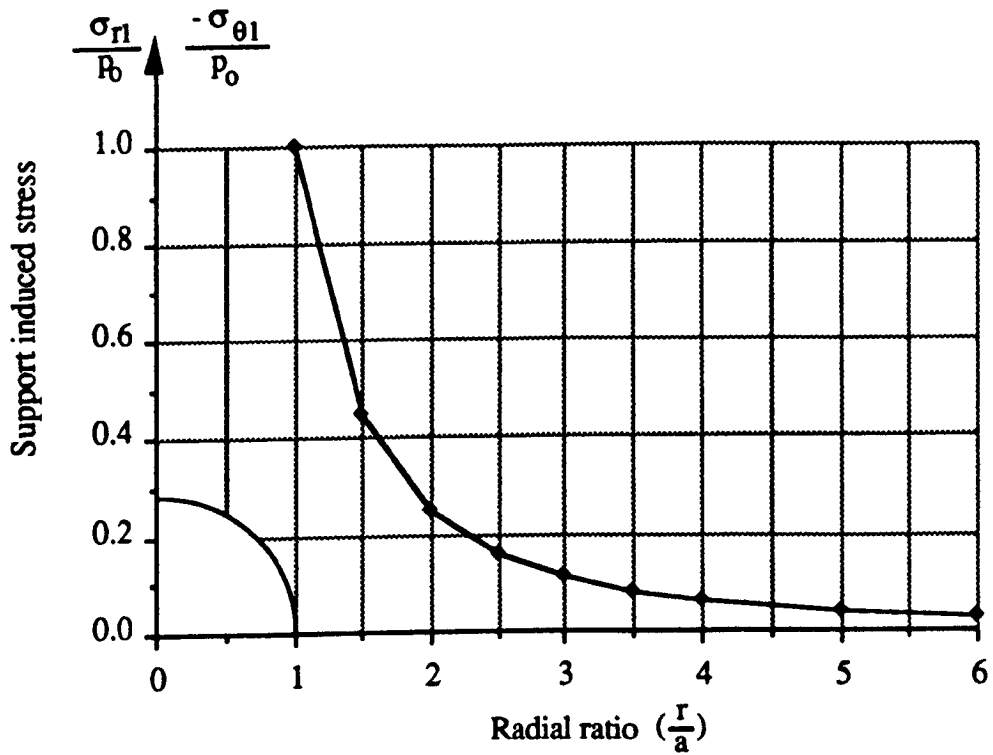
Figure 4.3.3 Illustrating the effective range of support on the rock stress distribution
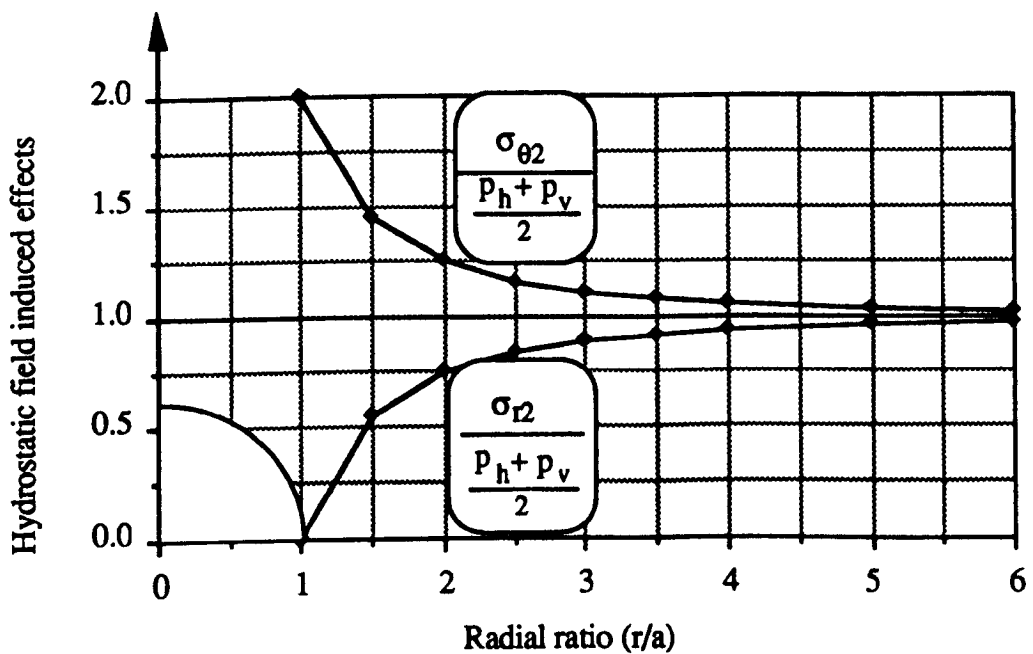
Figure 4.3.4 Effects of the hydrostatic stress field on the stress distribution

around the tunnel

where σ_{r2}, $\sigma_{\theta2}$ and $\tau_{r\theta2}$ are the stress components caused by the hydrostatic stress, $\frac{P_h+P_v}{2}$.

This is an analytical solution of the stress around a circular tunnel excavated in such ground conditions that a hydrostatic stress field is present and the surrounding rock has not undergone plastic failure. The changes of the stress magnitude of σ_{r2} and $\sigma_{\theta2}$ along the radius r are illustrated in Figure 4.3.4. It is apparent that, with the increase of r, the radial stress σ_{r2} increase from zero at the tunnel wall to the original applied stress of $\frac{P_h+P_v}{2}$ at the remote distance. The tangential stress $\sigma_{\theta2}$ decreases from the value of $2\frac{P_h+P_v}{2}$ at the tunnel wall to the original applied stress of $\frac{P_h+P_v}{2}$ at the remote distance. Obviously, the tangential and radial stresses become the principal stresses in this hydrostatic stress field environment.

Equations (4.3.9) have been used in the Department in the past few years as a basic assumption of a tunnel model for the purpose of the computerised prediction technique on tunnel stability (Frith, 1988).

(3) The effect of the difference of the applied stresses, $\frac{P_h-P_v}{2}$, on the stress distribution around the tunnel.

From Equations 4.3.7, it may be seen that the stress components induced by the existence of the difference in the applied stress components, (P_h-P_v), are of those:

$$\left.\begin{aligned}
\sigma_{r3} &= \frac{P_h-P_v}{2}(1+3\frac{a^4}{r^4} - 4\frac{a^2}{r^2})\cos2\theta \\
\sigma_{\theta3} &= -\frac{P_h-P_v}{2}(1+3\frac{a^4}{r^4})\cos2\theta \\
\tau_{r\theta3} &= -\frac{P_h-P_v}{2}(1-3\frac{a^4}{r^4} + 2\frac{a^2}{r^2})\sin2\theta
\end{aligned}\right\} \qquad (4.3.10)$$

where σ_{r3}, $\sigma_{\theta3}$ and $\tau_{r\theta3}$ are the stress components induced by (P_h-P_v).

Equations 4.3.10 show that the difference in the applied stress components (P_h-P_v) leads to the generation of the difference in stress distribution along the arbitrary

circumference. For instance, on a circumference of a given radius, the maximum and minimum magnitudes of σ_{r3} and $\sigma_{\theta3}$ will occur at the points where either the x or y axis intercepts it, whilst the shear stress $\tau_{r\theta3}$ at these points become zero. This indicates that only along the x and y axes, σ_{r3} and $\sigma_{\theta3}$ (and therefore σ_r and σ_θ in Equations 4.3.7) become the principal stresses. In elsewhere.σ_{r3} and $\sigma_{\theta3}$ are not the principal stresses.

For a given radius, however, $\tau_{r\theta3}$ becomes the maximum at the points where θ is equal to $\pm 45°$ from the x axis.

It is clear now that the stress components σ_{r3}, $\sigma_{\theta3}$ and $\tau_{r\theta3}$ are the main source that cause the difference in the distribution pattern of the stress components σ_r, σ_θ and $\tau_{r\theta}$ in Equations 4.3.7 along the tunnel circumference. Since the presence of σ_{r3}, $\sigma_{\theta3}$ and $\tau_{r\theta3}$ are due to the existence of a difference in the applied horizontal and vertical stresses in the undisturbed rock mass, it may be concluded that the difference in the applied stress components has a significant bearing on the stress distribution around a tunnel.

4.3.2 Effect of the Vertical to Horizontal Ground Pressure Ratio on Stress Distribution

Setting $P_o = 0$ in Equations 4.3.7, we have:

$$
\left.
\begin{aligned}
\sigma_r &= \frac{P_h + P_v}{2}(1 - \frac{a^2}{r^2}) + \frac{P_h - P_v}{2}(1 + 3\frac{a^4}{r^4} - 4\frac{a^2}{r^2})\cos2\theta \\
\sigma_\theta &= \frac{P_h + P_v}{2}(1 + \frac{a^2}{r^2}) - \frac{P_h - P_v}{2}(1 + 3\frac{a^4}{r^4})\cos2\theta \\
\tau_{r\theta} &= -\frac{P_h - P_v}{2}(1 - 3\frac{a^4}{r^4} + 2\frac{a^2}{r^2})\sin2\theta
\end{aligned}
\right\} \qquad (4.3.11)
$$

These equations indicate the stress distribution around the tunnel, immediately after the excavation but before the supports start taking load. Such a support situation may include two cases. One is that no support has been erected and the other is that,

125

although it has been installed, the support has not taken evident load from the ground movement.

In this case if the ratio of the applied horizontal to vertical stress is assumed to be a constant K, namely,

$$K = \frac{P_h}{P_v} \qquad (4.3.12)$$

then Equations 4.3.11 become

$$\left. \begin{aligned}
\sigma_r &= p_v\left[\frac{K+1}{2}(1-\frac{a^2}{r^2}) + \frac{K-1}{2}(1+3\frac{a^4}{r^4} - 4\frac{a^2}{r^2})\cos2\theta\right] \\
\sigma_\theta &= p_v\left[\frac{K+1}{2}(1+\frac{a^2}{r^2}) - \frac{K-1}{2}(1+3\frac{a^4}{r^4})\cos2\theta\right] \\
\tau_{r\theta} &= -p_v\frac{K-1}{2}(1-3\frac{a^4}{r^4} + 2\frac{a^2}{r^2})\sin2\theta
\end{aligned} \right\} \qquad (4.3.13)$$

It can be seen from Equations 4.3.13 that the stress components, σ_r, σ_θ and $\tau_{r\theta}$ are proportional to the applied vertical stress, p_v. Since the magnitude of p_v is largely dependent on the thickness of overburden strata, it can be derived that the stresses in the vicinity of the tunnel increase as the tunnel is driven at greater depths below the surface.

In order to study the effect of the applied horizontal to vertical stress ratio, K, on the stress distribution, a rearrangement of Equations 4.3.13 is needed.

Define: $\qquad K_r = \frac{\sigma_r}{p_v}, \qquad K_\theta = \frac{\sigma_\theta}{p_v} \quad$ and $\quad K_{r\theta} = \frac{\tau_{r\theta}}{p_v} \qquad (4.3.14)$

where K_r, K_θ, and $K_{r\theta}$ are termed the stress concentration factors of σ_r, σ_θ and $\tau_{r\theta}$ respectively, since they are explicit and are the results of comparison between the stress components and the applied vertical stress, p_v.

Applying these definitions to Equations 4.3.13 gives:

126

$$K_r = \frac{K+1}{2}(1- \frac{a^2}{r^2}) + \frac{K-1}{2}(1+3 \frac{a^4}{r^4} - 4 \frac{a^2}{r^2})\cos 2\theta$$

$$K_\theta = \frac{K+1}{2}(1+ \frac{a^2}{r^2}) - \frac{K-1}{2}(1+3 \frac{a^4}{r^4})\cos 2\theta$$

$$K_{r\theta} = - \frac{K-1}{2}(1-3 \frac{a^4}{r^4} + 2 \frac{a^2}{r^2})\sin 2\theta$$

(4.3.15)

Equations 4.3.15 show that the value of stress concentration factors varies with the relative position in the surrounding rock, which is governed by the applied stress ratio K. At every given point, K_r, K_θ, and $K_{r\theta}$ are linearly proportional to the value of K. In some regions this linear relation is positive whilst in others it is negative. Figures 4.3.5 (a) and (b) show the contours of K_r around one quadrant of the tunnel when the value of K is equal to 2 and 3 respectively. Figures 4.3.6 (a) and (b) show the contours of K_θ around one quadrant of the tunnel when the value of K is equal to 2 and 3 respectively. By rotating $\pi/2$, the contours of K_r and K_θ are obtained when the value of K is equal to 1/2 and 1/3 respectively.

4.3.3 Prediction of Shear Failure Tendency around a Tunnel

In underground rock engineering, the maximum shear stress in excess of rock strength is frequently referred to as a main source of ground failure. Indeed, shear failures are often seen in coal mine tunnels and coal faces. If the pattern of the maximum shear stress distribution can be identified before any failure takes place, proper measures may be proposed and taken in time, in order to enhance resistance to the zones where rocks are deteriorating or shear failures are due to occur. Effective support design also requires the knowledge of maximum shear stress distribution. All these indicate that a correct prediction of the maximum shear stress around a tunnel is also of paramount importance.

From Mohr circle theory, the value of the maximum shear stress at a given point is estimated as:
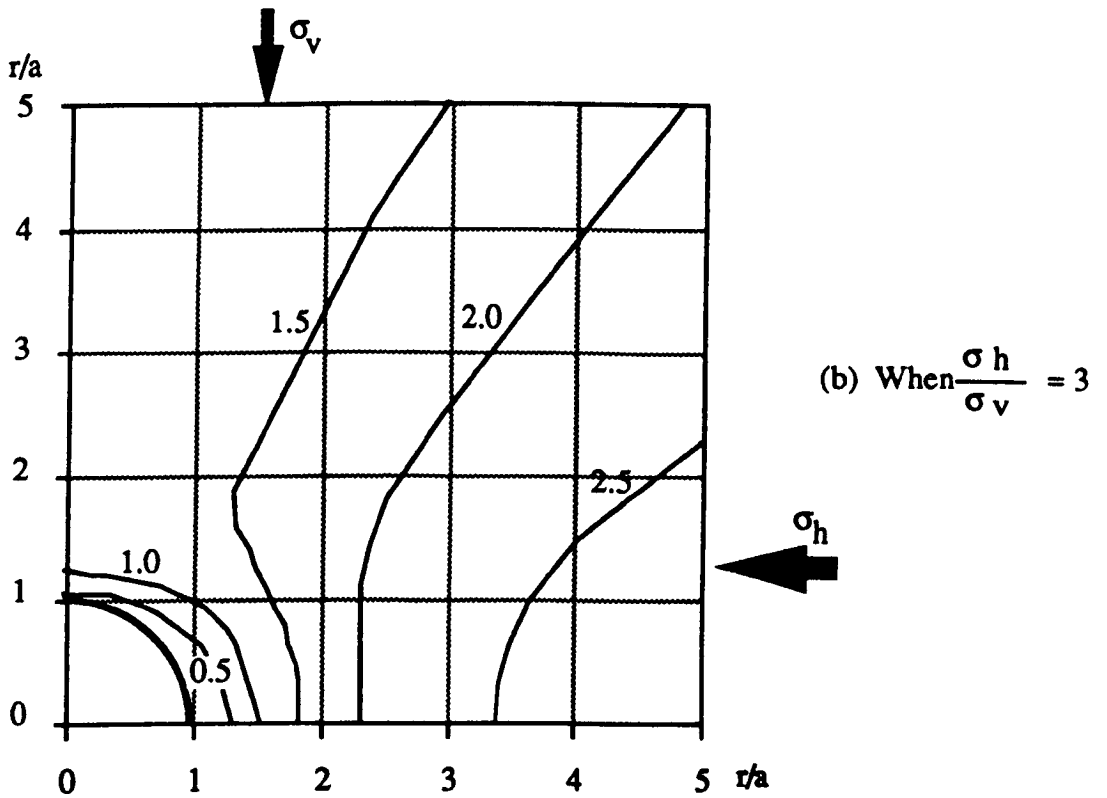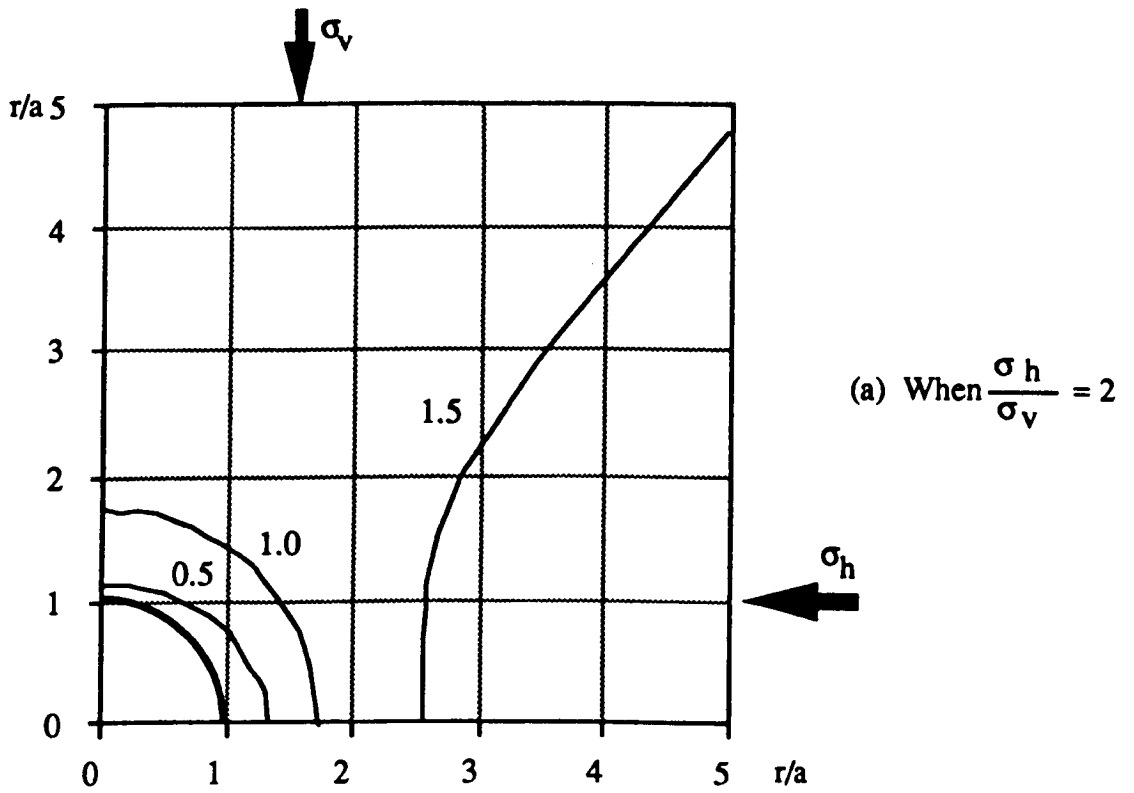
Figure 4.3.5 Contours of Kr around the tunnel

Figure 4.3.6 Contours of K_θ around the tunnel

(a) When $\dfrac{\sigma_h}{\sigma_v} = 2$

(b) When $\dfrac{\sigma_h}{\sigma_v} = 3$
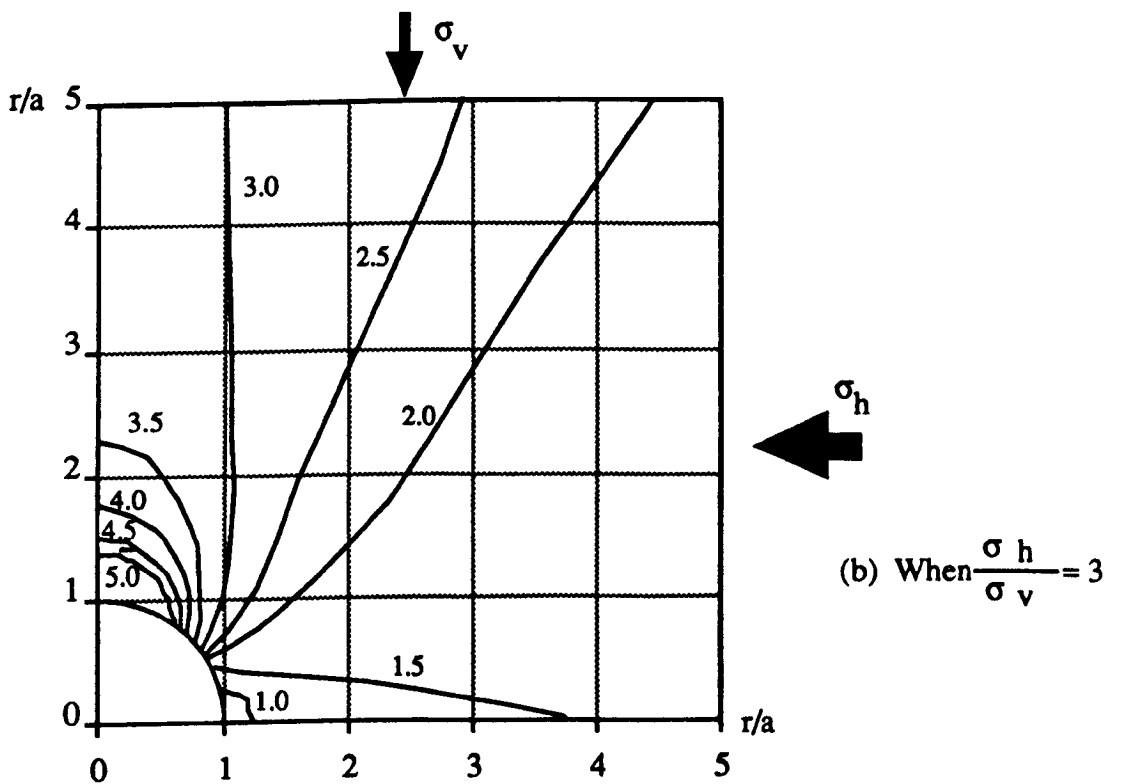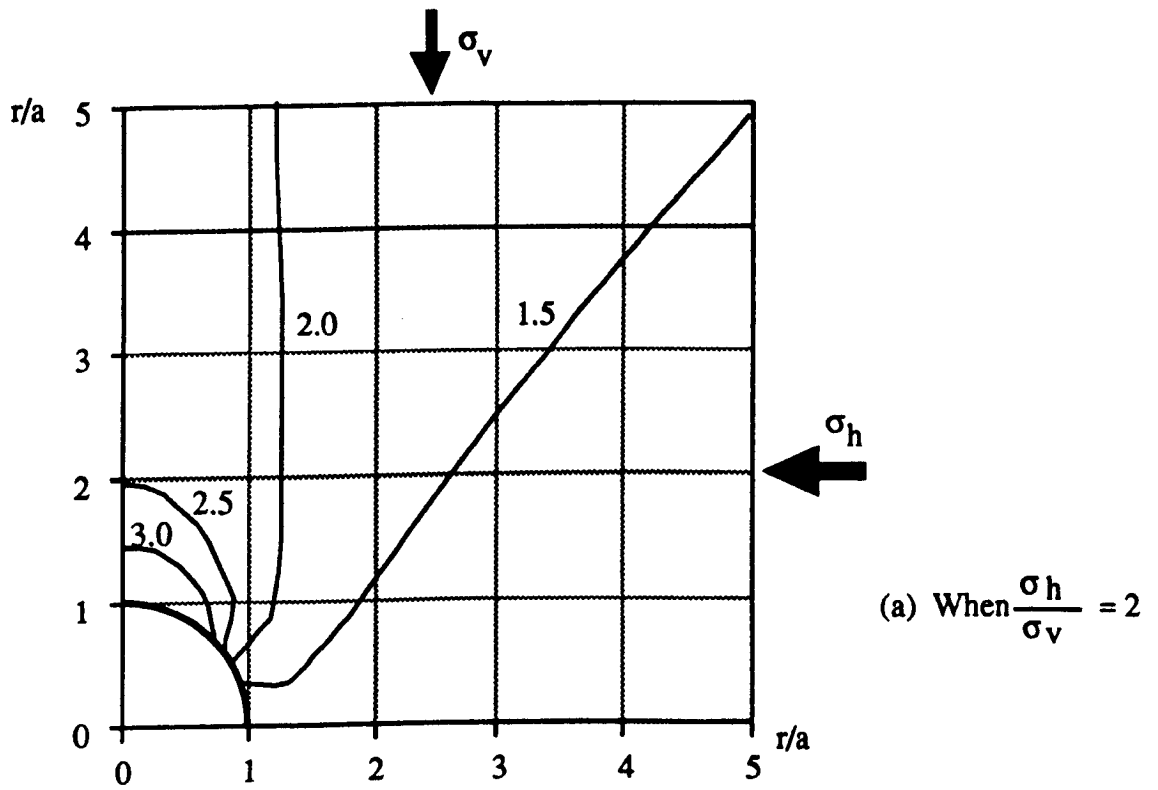
$$\tau_{max} = \sqrt{(\frac{\sigma_r - \sigma_\theta}{2})^2 + \tau_{r\theta}^2} \qquad (4.3.16)$$

where τ_{max} is the maximum shear stress, σ_r and σ_θ are the radial and tangential normal stresses and $\tau_{r\theta}$ is the radial or tangential shear stress.

Consider a circular tunnel without support, namely setting $P_o = 0$, stress distributions in relation to the applied stresses p_h and p_v have been obtained previously by Equations 4.3.11.

Using Equations 4.3.11 we have

$$\sigma_r - \sigma_\theta = - (p_h+p_v) \frac{a^2}{r^2} + (p_h-p_v) (1 - 2\frac{a^2}{r^2} + 3\frac{a^4}{r^4}) \cos2\theta \, ,$$

$$(\frac{\sigma_r - \sigma_\theta}{2})^2 = \frac{1}{4} [\frac{a^4}{r^4}(p_h+p_v)^2 - 2(p_h+p_v) \frac{a^2}{r^2} (p_h - p_v)(1 - 2\frac{a^2}{r^2} + 3\frac{a^4}{r^4})\cos2\theta +$$

$$+ (p_h-p_v)^2(1 - 2\frac{a^2}{r^2} + 3\frac{a^4}{r^4})^2 \cos^2 2\theta]$$

$$\tau_{r\theta}^2 = (\frac{p_h-p_v}{2})^2 (1-3\frac{a^4}{r^4} + 2\frac{a^2}{r^2})^2 \sin^2 2\theta$$

$$= (\frac{p_h-p_v}{2})^2 (1-3\frac{a^4}{r^4} + 2\frac{a^2}{r^2})^2 - (\frac{p_h-p_v}{2})^2 (1-3\frac{a^4}{r^4} + 2\frac{a^2}{r^2})^2 \cos^2 2\theta$$

Substitution of the above expressions into Equation 4.3.16 and carrying out simplification results in:

$$\tau_{max} = \{ (\frac{p_h+p_v}{2})^2 \frac{a^4}{r^4} - 2(\frac{p_h+p_v}{2})(\frac{p_h-p_v}{2}) \frac{a^2}{r^2} (1 - 2\frac{a^2}{r^2} + 3\frac{a^4}{r^4})\cos2\theta +$$

$$+ (\frac{p_h-p_v}{2})^2[1 - 2(2\frac{a^2}{r^2} - 3\frac{a^4}{r^4})\cos4\theta + (2\frac{a^2}{r^2} - 3\frac{a^4}{r^4})^2] \}^{1/2} \qquad (4.3.17)$$

We define

$$K_{\tau max} = \frac{\tau_{max}}{p_v} \qquad (4.3.18)$$

130

where $K_{\tau max}$ is termed as a maximum shear stress concentration factor.

The following is obtained by virtue of referring to Equations 4.3.12 and 4.3.17

$$K_{\tau max} = \left\{ \left(\frac{K+1}{2}\right)^2 \frac{a^4}{r^4} - 2\left(\frac{K^2-1}{4}\right)\frac{a^2}{r^2}\left(1 - 2\frac{a^2}{r^2} + 3\frac{a^4}{r^4}\right)\cos2\theta + \right.$$

$$\left. + \left(\frac{K-1}{2}\right)^2 \left[1 - 2\left(2\frac{a^2}{r^2} - 3\frac{a^4}{r^4}\right)\cos4\theta + \left(2\frac{a^2}{r^2} - 3\frac{a^4}{r^4}\right)^2\right] \right\}^{1/2} \qquad (4.3.19)$$

This shows that the value of the maximum shear stress concentration factor is closely related to the ratio of the applied horizontal to vertical stress, K. At points where $K_{\tau max}$ is highest, shear failures are most likely to be initiated.

Therefore the application of Equation 4.3.19 to tunnel design would help to identify critical areas where rocks need to be further supported.

Obviously, in hydrostatic fields, namely K = 1, contours of $K_{\tau max}$ become concentric circles and the value of $K_{\tau max}$ decreases with increasing radius, according to Equation 4.3.19. As the value of K varies away from 1 which means that the applied horizontal stress is no longer equal to the vertical, however, the contours of $K_{\tau max}$ change shape from the concentric circles. Figures 4.3.7 (a) and (b) show the contours of $K_{\tau max}$ when K is 2 and 3 respectively.

4.3.4 Displacement in Relation to the Excavation Diameter

Deformations of various patterns have more or less bearing on tunnel stability. Many rock failure phenomena, such as buckling, swelling and spalling of rocks are attributed to excessive displacements and deformations of surrounding rocks. Serious closure of a tunnel frequently requires the tunnel to be dinted, enlarged and repaired, which would cost extra time, labour and money. Therefore, prediction of tunnel closure becomes of another paramount importance in tunnel design. It is understood that the tunnel closure is referred to as the rock displacement at the tunnel periphery. A comprehensive understanding of the displacement field around the tunnel would
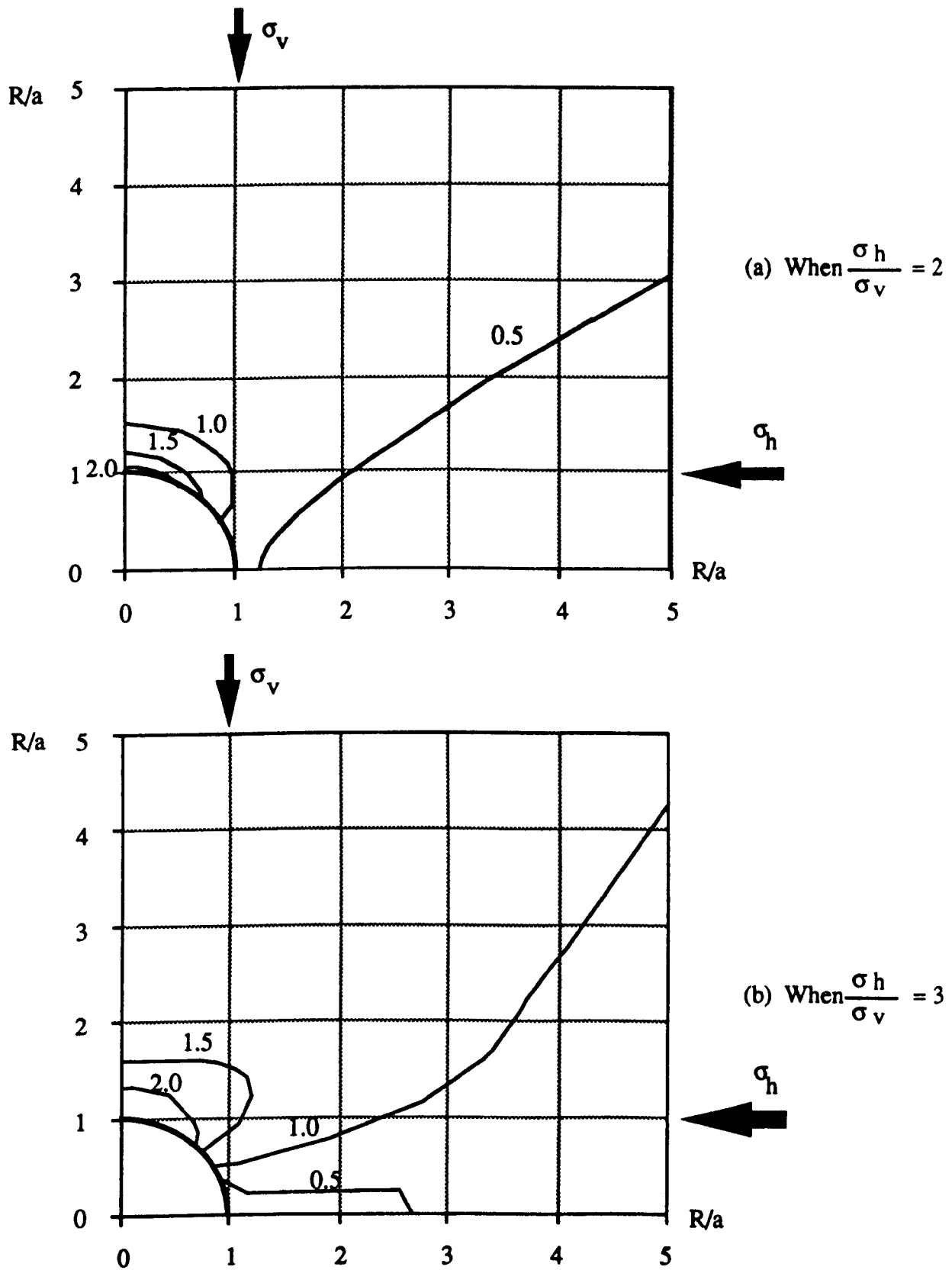
Figure 4.3.7 Contours of the maximum shear stress concentration factor around the tunnel

help predict the tunnel closure. In order to assess tunnel closure, it is preferable to have quantitative rather than qualitative information regarding the displacement field likely to be brought about in the rock mass by the excavation.

Because most rocks first exhibit elastic response to the tunnel drivage, in many cases, the theory of elasticity is used to evaluate the rock deformation and tunnel closure. Even though further more complicated behaviours like elasto-plastic, may be considered, these can be taken as modifications to the elastic behaviour. Hence the elastic solution can always be accepted as a first approximation.

In this chapter, only elastic displacements in rocks are considered. In order to calculate the displacements around the circular tunnel, geometric equations, constitutive equations and the solution of stress components in previous sections of this chapter need to be employed.

Substitution of Equations 4.2.35 of the geometric equations into the constitutive equations in Equations 4.2.36 yields

$$
\left.
\begin{array}{l}
\dfrac{\partial u}{\partial r} = \dfrac{1-v^2}{E}[\sigma_r - \dfrac{v}{1-v}\sigma_\theta] \\[3mm]
\dfrac{1}{r}\dfrac{\partial v}{\partial \theta} + \dfrac{u}{r} = \dfrac{1-v^2}{E}[\sigma_\theta - \dfrac{v}{1-v}\sigma_r] \\[3mm]
\dfrac{1}{r}\dfrac{\partial u}{\partial \theta} + \dfrac{\partial v}{\partial r} - \dfrac{v}{r} = \dfrac{2(1+v)}{E}\tau_{r\theta}
\end{array}
\right\}
\qquad (4.3.20)
$$

Tunnel closures take place under the combined loading effects of both applied stress field and support resistance. They exhibit the need for a whole mechanical system to achieve new equilibrium due to the excavation and support installation. Hence, calculation of the displacement field should take into account both applied stress field and support resistance.

In order to calculate the displacement in this case, we need to consider the relations among variables regarding displacement, strain, stress, and the constitutive

133

relationship as well. Firstly, input the solution of stress components expressed in Equations 4.3.7 into the first differential equation in Equations 4.3.20, which would yield:

$$\frac{\partial u}{\partial r} = \frac{1-v^2}{E}\left\{ \left[\frac{a^2}{r^2}P_0 + \frac{P_h+P_v}{2}\left(1-\frac{a^2}{r^2}\right) + \frac{P_h-P_v}{2}\left(1+3\frac{a^4}{r^4}-4\frac{a^2}{r^2}\right)\cos2\theta\right] - \frac{v}{1-v}\left[-\frac{a^2}{r^2}P_0 + \frac{P_h+P_v}{2}\left(1+\frac{a^2}{r^2}\right) - \frac{P_h-P_v}{2}\left(1+3\frac{a^4}{r^4}\right)\cos2\theta\right] \right\}$$

Integrating this differential equation with respect to the radius, r, yields

$$u = \frac{1-v^2}{E}\left\{ \left[-\frac{a^2}{r}P_0 + \frac{P_h+P_v}{2}\left(r+\frac{a^2}{r}\right) + \frac{P_h-P_v}{2}\left(r-\frac{a^4}{r^3}+4\frac{a^2}{r}\right)\cos2\theta\right] - \frac{v}{1-v}\left[\frac{a^2}{r}P_0 + \frac{P_h+P_v}{2}\left(r-\frac{a^2}{r}\right) - \frac{P_h-P_v}{2}\left(r-\frac{a^4}{r^3}\right)\cos2\theta\right] \right\} + f(\theta)$$

$$= \frac{1+v}{E}\left\{ (1-v)\left[-\frac{a^2}{r}P_0 + \frac{P_h+P_v}{2}\left(r+\frac{a^2}{r}\right) + \frac{P_h-P_v}{2}\left(r-\frac{a^4}{r^3}+4\frac{a^2}{r}\right)\cos2\theta\right] - v\left[\frac{a^2}{r}P_0 + \frac{P_h+P_v}{2}\left(r-\frac{a^2}{r}\right) - \frac{P_h-P_v}{2}\left(r-\frac{a^4}{r^3}\right)\cos2\theta\right] \right\} + f(\theta)$$

$$= \frac{1+v}{E}\left\{ \left[-\frac{a^2}{r}P_0 + \frac{P_h+P_v}{2}\left(r+\frac{a^2}{r}\right) + \frac{P_h-P_v}{2}\left(r-\frac{a^4}{r^3}+4\frac{a^2}{r}\right)\cos2\theta\right] - v\left[-\frac{a^2}{r}P_0 + \frac{P_h+P_v}{2}\left(r+\frac{a^2}{r}\right) + \frac{P_h-P_v}{2}\left(r-\frac{a^4}{r^3}+4\frac{a^2}{r}\right)\cos2\theta\right] - v\left[\frac{a^2}{r}P_0 + \frac{P_h+P_v}{2}\left(r-\frac{a^2}{r}\right) - \frac{P_h-P_v}{2}\left(r-\frac{a^4}{r^3}\right)\cos2\theta\right] \right\} + f(\theta)$$

So

$$u = \frac{1+v}{E}\left\{ \left[-\frac{a^2}{r}P_0 + \frac{P_h+P_v}{2}\left(r+\frac{a^2}{r}\right) + \frac{P_h-P_v}{2}\left(r-\frac{a^4}{r^3}+4\frac{a^2}{r}\right)\cos2\theta\right] \right.$$
$$\left. -2v\left[\frac{P_h+P_v}{2}r + 2\frac{P_h-P_v}{2}\frac{a^2}{r}\cos2\theta\right] \right\} + f(\theta) \qquad (4.3.21)$$

where $f(\theta)$ is a function of θ only.

Inputting the solutions of u of Equation 4.3.21 and σ_r and σ_θ of Equations 4.3.7 into the second equation of Equations 4.3.20 will yield:

$$\frac{\partial v}{\partial \theta} = \frac{1-v^2}{E}[r\ \sigma_\theta - \frac{\upsilon}{1-\upsilon}\ r\ \sigma_r] - u$$

$$= \frac{1-v^2}{E}\{[\ -\frac{a^2}{r}\ P_0 + \frac{P_h+P_v}{2}(r+\frac{a^2}{r}) - \frac{P_h-P_v}{2}\ (r+3\ \frac{a^4}{r^3})\cos2\theta] -$$

$$- \frac{v}{1-v}[\ \frac{a^2}{r}\ P_0 + \frac{P_h+P_v}{2}(r-\frac{a^2}{r}) + \frac{P_h-P_v}{2}\ (r+3\ \frac{a^4}{r^3} - 4\ \frac{a^2}{r})\cos2\theta]\} -$$

$$- \frac{1+v}{E}\{[-\ \frac{a^2}{r}\ P_0 + \frac{P_h+P_v}{2}\ (r+\frac{a^2}{r}) + \frac{P_h-P_v}{2}\ (r - \frac{a^4}{r^3} + 4\ \frac{a^2}{r})\cos2\theta]$$

$$- 2v[\ \frac{P_h+P_v}{2}\ r + 2\ \frac{P_h-P_v}{2}\ \frac{a^2}{r}\ \cos2\theta]\} - f(\theta)$$

$$= \frac{1+v}{E}\ \{(1-v)[\ -\frac{a^2}{r}\ P_0 + \frac{P_h+P_v}{2}\ (r+\frac{a^2}{r}) - \frac{P_h-P_v}{2}\ (r+3\ \frac{a^4}{r^3})\cos2\theta] -$$

$$- v[\ \frac{a^2}{r}\ P_0 + \frac{P_h+P_v}{2}(r-\frac{a^2}{r}) + \frac{P_h-P_v}{2}\ (r+3\ \frac{a^4}{r^3} - 4\ \frac{a^2}{r})\cos2\theta]\} -$$

$$- \frac{1+v}{E}\{[-\ \frac{a^2}{r}\ P_0 + \frac{P_h+P_v}{2}\ (r+\frac{a^2}{r}) + \frac{P_h-P_v}{2}\ (r - \frac{a^4}{r^3} + 4\ \frac{a^2}{r})\cos2\theta]$$

$$- 2v[\ \frac{P_h+P_v}{2}\ r + 2\ \frac{P_h-P_v}{2}\ \frac{a^2}{r}\ \cos2\theta]\} - f(\theta)$$

$$= \frac{1+v}{E}\ \{[\ -\frac{a^2}{r}\ P_0 + \frac{P_h+P_v}{2}\ (r+\frac{a^2}{r}) - \frac{P_h-P_v}{2}\ (r+3\ \frac{a^4}{r^3})\cos2\theta] -$$

$$- 2v[\frac{P_h+P_v}{2}\ r - 2\ \frac{P_h-P_v}{2}\ \frac{a^2}{r}\ \cos2\theta]\} -$$

$$- \frac{1+v}{E}\{[-\ \frac{a^2}{r}\ P_0 + \frac{P_h+P_v}{2}\ (r+\frac{a^2}{r}) + \frac{P_h-P_v}{2}\ (r - \frac{a^4}{r^3} + 4\ \frac{a^2}{r})\cos2\theta]$$

$$- 2v[\ \frac{P_h+P_v}{2}\ r + 2\ \frac{P_h-P_v}{2}\ \frac{a^2}{r}\ \cos2\theta]\} - f(\theta)$$

$$= \frac{1+v}{E}\ \{[\ -\frac{a^2}{r}\ P_0 + \frac{P_h+P_v}{2}\ (r+\frac{a^2}{r}) - \frac{P_h-P_v}{2}\ (r+3\ \frac{a^4}{r^3})\cos2\theta -$$

$$+ \frac{a^2}{r}\ P_0 - \frac{P_h+P_v}{2}\ (r+\frac{a^2}{r}) - \frac{P_h-P_v}{2}\ (r - \frac{a^4}{r^3} + 4\ \frac{a^2}{r})\cos2\theta] -$$

$$- 2v[\frac{P_h+P_v}{2}r - 2\ \frac{P_h-P_v}{2}\ \frac{a^2}{r}\ \cos2 - \frac{P_h+P_v}{2}\ r - 2\ \frac{P_h-P_v}{2}\ \frac{a^2}{r}\ \cos2\theta]\} - f(\theta)$$

135

$$= \frac{1+v}{E}[-2\frac{P_h \cdot P_v}{2}(r + \frac{a^4}{r^3} + 2\frac{a^2}{r})\cos2\theta + 8v\frac{P_h \cdot P_v}{2}\frac{a^2}{r}\cos2] - f(\theta)$$

So
$$\frac{\partial v}{\partial \theta} = -2\frac{1+v}{E}\frac{P_h \cdot P_v}{2}[(r + \frac{a^4}{r^3} + 2\frac{a^2}{r}) - 4v\frac{a^2}{r}]\cos2\theta - f(\theta) \qquad (4.3.22)$$

Integration of this differential equation with respect to the argument θ gives:

$$v = -\frac{1+v}{E}\frac{P_h \cdot P_v}{2}[(r + \frac{a^4}{r^3} + 2\frac{a^2}{r}) - 4v\frac{a^2}{r}]\sin2\theta - \int f(\theta)d\theta + g(r) \qquad (4.3.23)$$

where $g(r)$ is a function of the argument r only.

To determine the expression of integration constants, $f(\theta)$ and $g(r)$, the third equation of Equations 4.3.20 is to be employed.

From Equations 4.3.21 and 4.3.23 we have

$$\frac{1}{r}\frac{\partial u}{\partial \theta} = \frac{1+v}{E}[-2\frac{P_h \cdot P_v}{2}(1 - \frac{a^4}{r^4} + 4\frac{a^2}{r^2}) + 8v\frac{P_h \cdot P_v}{2}\frac{a^2}{r^2}]\sin2\theta + \frac{1}{r}\frac{df(\theta)}{d\theta}$$

$$= -\frac{1+v}{E}\frac{P_h \cdot P_v}{2}(2 - 2\frac{a^4}{r^4} + 8\frac{a^2}{r^2} - 8v\frac{a^2}{r^2})\sin2\theta + \frac{1}{r}\frac{df(\theta)}{d\theta} \qquad (4.3.24)$$

$$\frac{\partial v}{\partial r} = -\frac{1+v}{E}\frac{P_h \cdot P_v}{2}(1 - 3\frac{a^4}{r^4} - 2\frac{a^2}{r^2} + 4v\frac{a^2}{r^2})\sin2\theta + \frac{dg(r)}{dr} \qquad (4.3.25)$$

Substitution of Equations 4.3.23, 4.3.24, 4.3.25 and the solution of $\tau_{r\theta}$ of Equations 4.3.78 into the third equation of Equations 4.3.20 yields

$$-\frac{1+v}{E}\frac{P_h \cdot P_v}{2}(2 - 2\frac{a^4}{r^4} + 8\frac{a^2}{r^2} - 8v\frac{a^2}{r^2})\sin2\theta + \frac{1}{r}\frac{df(\theta)}{d\theta} +$$

$$+[-\frac{1+v}{E}\frac{P_h \cdot P_v}{2}(1 - 3\frac{a^4}{r^4} - 2\frac{a^2}{r^2} + 4v\frac{a^2}{r^2})\sin2\theta + \frac{dg(r)}{dr}] -$$

$$-[-\frac{1+v}{E}\frac{P_h \cdot P_v}{2}(1 + \frac{a^4}{r^4} + 2\frac{a^2}{r^2} - 4v\frac{a^2}{r^2})\sin2\theta - \frac{1}{r}\int f(\theta)d\theta + \frac{1}{r}g(r)]$$

$$= -\frac{P_h \cdot P_v}{2}\frac{2(1+v)}{E}(1 - 3\frac{a^4}{r^4} + 2\frac{a^2}{r^2})\sin2\theta$$

136

After some algebra and simplification, it is arrived that

$$\frac{1}{r}\frac{df(\theta)}{d\theta} + \frac{dg(r)}{dr} + \frac{1}{r}\int f(\theta)d\theta - \frac{1}{r}g(r) = 0$$

or

$$\frac{df(\theta)}{d\theta} + \int f(\theta)d\theta = -r\frac{dg(r)}{dr} + g(r) \qquad (4.3.26)$$

Obviously, the left hand side part of Equation 4.3.26 is a function of the variable θ instead of r, but the right hand side part is a function of the variable r only. Therefore, a necessary condition for Equation 4.3.26 to hold true is that both sides of the equation are equal to a constant which is assumed to be K_c, namely,

$$\left.\begin{array}{c} \dfrac{df(\theta)}{d\theta} + \displaystyle\int f(\theta)d\theta = K_c \\[3mm] -r\dfrac{dg(r)}{dr} + g(r) = K_c \end{array}\right\} \qquad (4.3.27)$$

Differentiating Equations 4.3.27 with respect to θ for the first and r for the second, it is, after some algebraic manipulation, the following is obtained

$$\left.\begin{array}{c} \dfrac{df^2(\theta)}{d\theta^2} + f(\theta) = 0 \\[3mm] \dfrac{dg^2(r)}{dr^2} = 0 \end{array}\right\} \qquad (4.3.28)$$

A general solution to the first of Equations 4.3.28 is of the form:

$$f(\theta) = e^{-\lambda\theta} \qquad (4.3.29)$$

where λ is a constant to be determined.

Substitution of this equation into the first equation of Equations 4.3.28 yields a so called characteristic equation:

$$\lambda^2 + 1 = 0$$

Solution to this characteristic equation is:

$$\lambda = \pm i$$

where i is an imaginary unit.

Therefore, the functions of $f(\theta) = e^{-\theta i}$ and $f(\theta) = e^{\theta i}$ are two particular solutions to the first of Equations 4.3.28. The general solution of the equation, according to the theory of ordinary linear differential equations, should be the sum of these two linearly independent functions with each multiplyed by a constant:

$$f(\theta) = c_1 e^{-\theta i} + c_2 e^{\theta i} = a_1 \cos\theta + a_2 \sin\theta \qquad (4.3.30)$$

where c_1, c_2, a_1 and a_2 are constants and $c_1 = \dfrac{a_1 + a_2 i}{2}$; $c_2 = \dfrac{a_1 - a_2 i}{2}$, and where the Euler formulae

$$e^{\theta i} = \cos\theta + i \sin\theta \qquad e^{-\theta i} = \cos\theta - i \sin\theta \qquad (4.3.31)$$

have been employed for transforming the exponential expressions into trigonometric expressions.

Twice integration of the second of Equations 4.3.28 gives the solution of $g(r)$ as:

$$g(r) = b_1 r + b_2 \qquad (4.3.32)$$

where b_2 indicates a rigid movement of the whole model and obviously for tunnelling related rock mechanics it is equal to zero.

Thus the solutions to the displacement components u and v by Equations 4.3.21 and 4.3.23 becomes :

$$
\left.
\begin{aligned}
u &= \frac{1+v}{E} \left\{ \left[-\frac{a^2}{r} P_0 + \frac{P_h + P_v}{2} (r + \frac{a^2}{r}) + \frac{P_h - P_v}{2}(r - \frac{a^4}{r^3} + 4\frac{a^2}{r})\cos2\theta \right] - \right. \\
&\quad \left. 2v[\frac{P_h + P_v}{2} r + 2\frac{P_h - P_v}{2}\frac{a^2}{r}\cos2\theta] \right\} + a_1\cos\theta + a_2\sin\theta \\
v &= -\frac{1+v}{E}\frac{P_h - P_v}{2}\left[(r + \frac{a^4}{r^3} + 2\frac{a^2}{r}) - 4v\frac{a^2}{r}\right]\sin2\theta - \\
&\quad - a_1\sin\theta + a_2\cos\theta + b_1 r
\end{aligned}
\right\} \qquad (4.3.33)
$$

To determine the constants incurred in the above equations, the symmetrical condition for the displacements, namely tangential displacement v = 0 when $\theta = 0$ or $\frac{\pi}{2}$, are used. Thus, from Equations 4.3.33,

$$v\big|_{\theta=0} = 0 = a_2 + b_1 r \quad \text{and} \quad v\big|_{\theta=\frac{\pi}{2}} = 0 = -a_1 + b_1 r$$

Hence, $\qquad\qquad\qquad a_1 = a_2 = b_1 = 0$

And the displacement components are given by

$$
\left.
\begin{aligned}
u &= \frac{1+v}{E}\left\{\left[-\frac{a^2}{r}P_0 + \frac{P_h+P_v}{2}\left(r+\frac{a^2}{r}\right) + \frac{P_h-P_v}{2}\left(r-\frac{a^4}{r^3}+4\frac{a^2}{r}\right)\cos2\theta\right]\right.\\
&\qquad\left.-2v\left[\frac{P_h+P_v}{2}r + 2\frac{P_h-P_v}{2}\frac{a^2}{r}\cos2\theta\right]\right\}\\
v &= -\frac{1+v}{E}\frac{P_h-P_v}{2}\left[\left(r+\frac{a^4}{r^3}+2\frac{a^2}{r}\right)-4v\frac{a^2}{r}\right]\sin2\theta
\end{aligned}
\right\} \qquad (4.3.34)
$$

Tunnel closure is a very important measurement in the assessment of tunnel stability. It is in fact the displacements of the tunnel periphery, which are obtained from Equations 4.3.34 by setting the parameter of radius, r, equal to the tunnel radius, a. That is:

$$
\left.
\begin{aligned}
u &= \frac{1+v}{E}a\left\{\left[-P_0+(p_h+p_v)+2(p_h-p_v)\cos2\theta\right]-2v\left(\frac{P_h+P_v}{2}+2\frac{P_h-P_v}{2}\cos2\theta\right)\right\}\\
v &= -2\frac{1-v^2}{E}(p_h-p_v)a\sin2\theta
\end{aligned}
\right\}
$$

or
$$
\left.
\begin{aligned}
u &= \frac{1+v}{E}a\left[-P_0+(p_h+p_v)(1-v)+2(1-v)(p_h-p_v)\cos2\theta\right]\\
v &= -2\frac{1-v^2}{E}(p_h-p_v)a\sin2\theta
\end{aligned}
\right\} \qquad (4.3.35)
$$

This theoretical tunnel closure by Equations 4.3.35 consists of two parts. One is termed historical deformation which has taken place prior to tunnel excavation. This is considered to be the effects of geological processes over long history. The other is caused by the excavation. Only this part of deformation can be observed underground. Mining engineers are mainly concerned about this part. If the components of the first part deformation, namely the historical one, are assumed to be u_0 and v_0, then the observed deformation or the real tunnel closure will be:

$$u = \frac{1+v}{E} a \left[-P_0 + (p_h + p_v)(1-v) + 2(1-v)(p_h - p_v)\cos 2\theta\right] - u_0$$
$$v = -2 \frac{1-v^2}{E}(p_h - p_v) a \sin 2\theta - v_0$$

(4.3.36)

These solutions show that observed tunnel closure in this case is proportional to the tunnel radius, a. This would indicate that the excavation size has a direct and evident effect on tunnel deformation and stability. The larger the excavation size is, the greater the tunnel closure would be. Underground phenomena have also proved this point. For instance, larger tunnels are less stable. This is partly due to the fact that larger tunnels are subject to greater closure deformation and problems regarding tunnel stability are often initiated by excessive tunnel closure. At the place where rocks around a tunnel collapse, the tunnel diameter measurements may have, in many cases, reduced dramatically prior to rock collapse. .

Occurrence of heavy rock pressures often causes inevitable tunnel deformation. In such cases, reducing the tunnel diameter properly is sometimes an effective measure for improving tunnel stability. However, if the reduction of tunnel excavating sizes is aimless or beyond a limit, such a measure may not achieve the desired results. In particular, when the measurements of tunnels after deformation, such as tunnel width, height and cross section area, cannot satisfy the requirements as stated earlier in Chapter One, dinting and repairing of the tunnels would be required. This kind of work is costly. This problem may be illustrated by rearranging Equation 4.3.35. In fact, if the ratio of tunnel closure u to the tunnel diameter a is referred to as the tunnel closure rate, according to Equations 4.3.35 this rate can then be obtained as:

$$\frac{u}{a} = \frac{1+v}{E}\left[-P_0 + (p_h + p_v)(1-v) + 2(1-v)(p_h - p_v)\cos 2\theta\right] + \frac{u_0}{a}$$

(4.3.37)

This shows that the tunnel closure rate for a given geological setting is totally governed by the applied stress field and the support resistance as well. Greater

applied stresses would result in greater tunnel closure rates. Increasing support resistance without exceeding support capability could reduce the tunnel closure rate.

Equation 4.3.37a also shows that the percentage of the residual to original excavation dimensions can be accounted as

$$100 \times (1 - \frac{u}{a}) \%$$ (4.3.37a)

In tunnel design, therefore, if the value of $\frac{u}{a}$ is found by means of underground instrumentation, the designed dimensions of a tunnel section for similar geological settings may be found according to the production required tunnel dimension. For instance, if the value of $\frac{u}{a_1}$ is found by monitoring tunnels in similar geological settings, and the production required tunnel dimension is a_2, then the designed tunnel dimension, a, should be

$$a = \frac{a_2}{(1 - \frac{u}{a_1})}$$ (4.3.38)

This indicates that results of measuring tunnel closure in an existing tunnel will benefit future design of new tunnels in similar geological conditions. Tunnel design in this way may avoid a need to measure the original stress field. Instrumentation for tunnel closure rate is comparatively simple and easy. The formula 4.3.38 has a simple form of expression. It provides a different way for tunnel design. It may therefore be concluded that the formula 4.3.38 is significant when applied in tunnel design.

4.4 Analysis of Tunnel Stability Taking the Height to Width Ratio into Account

Tunnels usually have profiles *other than* circular. Analysis of stress distribution and deformation features of tunnels with these profiles requires employment of even more sophisticated mathematical theory. Most difficulty in such

analysis arises in finding a proper continuous function which can describe the tunnel profiles. In elastic theory, complex variable theory is probably an effective measure used to investigate elastic plane problems regarding stress, strain and deformation, when excavations of various tunnels are involved.

The complex variable method tackles the problems by virtue of the conformal mapping technique by which a complicated tunnel profile in a physical plane will be mapped conformally as a unity circle in another plane (known as a mapping plane). Solutions of the original problem will be found by solving the related equations for the unity circular profile in the mapping plane and converting the solutions back to the expressions in the original physical plane. In this section, this method will be used.

4.4.1 Expression of Fundamental Equations by Complex Functions

It has been shown in the second section of this Chapter that, if body forces are constant, there exists a biharmonic stress function U with respect to position coordinates (Equation 4.2.32).

Assume that
$$\nabla^2 U = P(x,y) \tag{4.4.1}$$

Then $P(x,y)$ is a harmonic function, namely $\nabla^2 P = 0$.

If a function $Q(x,y)$ is the conjugate function of $P(x,y)$, according to the complex variable theory, the function

$$P(x,y) + i\, Q(x,y) = f(z) \tag{4.4.2}$$

must be analytic for complex variable z where $z = x + i\, y$.

Definition of another complex function $\phi_1(z)$ is given by

$$\phi_1(z) = \frac{1}{4} \int f(z) dz = p + i\, q \tag{4.4.3}$$

According to a analytic theorem (Kreyszig, 1979), $\phi_1(z)$ is also analytic, and p and q are harmonic functions and conjugate to each other, namely,

$$\nabla^2 p = 0, \quad \nabla^2 q = 0 \qquad (4.4.4)$$

Differentiating Equation 4.4.3 with respect to x gives

$$\phi_1'(z) = \frac{1}{4} f(z) = \frac{\partial p}{\partial x} + i \frac{\partial q}{\partial x} \qquad (4.4.5)$$

Substitution of Equation 4.4.2 into this produces

$$\frac{1}{4}(P + i Q) = \frac{\partial p}{\partial x} + i \frac{\partial q}{\partial x} \qquad (4.4.6)$$

The real parts on both sides are equalizing, given by

$$\frac{1}{4} P = \frac{\partial p}{\partial x} \qquad (4.4.7)$$

Since $\phi_1(z)$ is analytic, according to the Cauchy-Riemann equations (Kreyszig, 1979), the following identity holds true:

$$\frac{\partial p}{\partial x} = \frac{\partial q}{\partial y} = \frac{1}{4} P \qquad (4.4.8)$$

Take another real function p_1 which is defined as:

$$p_1 = U - px - qy \qquad (4.4.9)$$

Differentiation of p_1 with respect to x and y respectively produces

$$\frac{\partial p_1}{\partial x} = \frac{\partial U}{\partial x} - p - x \frac{\partial p}{\partial x} - y \frac{\partial q}{\partial x}$$

$$\frac{\partial p_1}{\partial y} = \frac{\partial U}{\partial y} - x \frac{\partial p}{\partial y} - q - y \frac{\partial q}{\partial y}$$

$$\frac{\partial^2 p_1}{\partial x^2} = \frac{\partial^2 U}{\partial x^2} - 2 \frac{\partial p}{\partial x} - x \frac{\partial p^2}{\partial x^2} - y \frac{\partial^2 q}{\partial x^2}$$

$$\frac{\partial^2 p_1}{\partial y^2} = \frac{\partial^2 U}{\partial y^2} - x \frac{\partial^2 p}{\partial y^2} - 2 \frac{\partial q}{\partial y} - y \frac{\partial^2 q}{\partial y^2}$$

Therefore the Laplace's operation for p_1 is obtained by

$$\nabla^2 p_1 = \frac{\partial^2 p_1}{\partial x^2} + \frac{\partial^2 p_1}{\partial y^2} = \nabla^2 U - x \nabla^2 p - 2(\frac{\partial p}{\partial x} + \frac{\partial q}{\partial y}) - y \nabla^2 q$$

$$= P - 0 - 2(\frac{1}{4} P + \frac{1}{4} P) - 0$$

$$= 0$$

Thus p_1 is also a harmonic function.

If q_1 is defined as the conjugate function of p_1, then the complex function

$$\theta_1(z) = p_1 + i\, q_1 \qquad (4.4.10)$$

is also analytic.

From Equation 4.4.9 it is now recognised that the stress function U may be expressed by three harmonic functions p_1, p and q, namely

$$U = p_1 + xp + yq$$

Since p_1, p and q are the real or imaginary parts of the analytic functions, $\phi_1(z)$ and $\theta_1(z)$ (see Equations 4.4.3 and 4.4.10), these analytic functions can be used to express the stress function U, i.e.

$$U = p_1 + xp + yq = \text{Re}\,[\,\bar{z}\,\phi_1(z) + \theta_1(z)] \qquad (4.4.11)$$

where Re means the real part of the term in the following pair of brackets, $\bar{z}$ is the conjugate complex variable of z.

Let $\overline{\phi_1(z)}$ and $\overline{\theta_1(z)}$ be the conjugate functions of $\phi_1(z)$ and $\theta_1(z)$ respectively. Equation 4.4.11 then becomes

$$U = \frac{1}{2}\,[\,\bar{z}\,\phi_1(z) + z\,\overline{\phi_1(z)} + \theta_1(z) + \overline{\theta_1(z)}\,] \qquad (4.4.12)$$

This indicates that, if the expression of the analytic functions $\phi_1(z)$ and $\theta_1(z)$ can be found, the stress function and therefore the stress components are also found. In fact, differentiation of Equation 4.4.12 with respect to x and y respectively produces

$$\frac{\partial U}{\partial x} = \frac{1}{2}\,[\phi_1(z) + \bar{z}\,\phi_1{}'(z) + \overline{\phi_1(z)} + z\,\overline{\phi_1{}'(z)} + \theta_1{}'(z) + \overline{\theta_1{}'(z)}\,]$$

$$\frac{\partial U}{\partial y} = \frac{i}{2}\,[-\phi_1(z) + \bar{z}\,\phi_1{}'(z) + \overline{\phi_1(z)} - z\,\overline{\phi_1{}'(z)} + \theta_1{}'(z) - \overline{\theta_1{}'(z)}\,] \qquad (4.4.13)$$

Combination of these two expressions in complex form yields

144

$$\frac{\partial U}{\partial x} + i\frac{\partial U}{\partial y} = \phi_1(z) + z\,\overline{\phi_1'(z)} + \overline{\theta_1'(z)} \qquad (4.4.14)$$

Differentiation of Equation 4.4.14 with respect to x gives

$$\frac{\partial^2 U}{\partial x^2} + i\frac{\partial^2 U}{\partial x \partial y} = \phi_1'(z) + \overline{\phi_1'(z)} + z\,\overline{\phi_1''(z)} + \overline{\theta_1''(z)} \qquad (4.4.15)$$

Differentiation of Equation 4.4.14 with respect to y and then multiplication by imaginary unit i gives

$$i\frac{\partial^2 U}{\partial x \partial y} - \frac{\partial^2 U}{\partial y^2} = -\phi_1'(z) - \overline{\phi_1'(z)} + z\,\overline{\phi_1''(z)} + \overline{\theta_1''(z)} \qquad (4.4.16)$$

Subtraction of Equation 4.4.16 from Equation 4.4.15 gives

$$\frac{\partial^2 U}{\partial x^2} + \frac{\partial^2 U}{\partial y^2} = 2[\,\phi_1'(z) + \overline{\phi_1'(z)}\,] = 4\,\mathrm{Re}\,\phi_1'(z) \qquad (4.4.17)$$

Referring to Equation 4.2.30, it is found that

$$\sigma_y + \sigma_x = 4\,\mathrm{Re}\,\phi_1'(z) \qquad (4.4.18)$$

Addition of Equations 4.4.15 and 4.4.16 gives

$$\frac{\partial^2 U}{\partial x^2} - \frac{\partial^2 U}{\partial y^2} + 2i\frac{\partial^2 U}{\partial x \partial y} = 2[\,z\,\overline{\phi_1''(z)} + \overline{\theta_1''(z)}\,]$$

Taking the conjugate function of both sides of this equation produces

$$\frac{\partial^2 U}{\partial x^2} - \frac{\partial^2 U}{\partial y^2} - 2i\frac{\partial^2 U}{\partial x \partial y} = 2[\,\overline{z}\,\phi_1''(z) + \theta_1''(z)] \qquad (4.4.19)$$

Referring to Equations 4.2.30, it is found that

$$\sigma_y - \sigma_x + 2i\,\tau_{xy} = 2[\,\overline{z}\,\phi_1''(z) + \theta_1''(z)] \qquad (4.4.20)$$

Hence, if the analytic functions $\phi_1(z)$ and $\theta_1(z)$ are known, separation of the real and imaginary parts of Equation 4.4.20 will give $(\sigma_y - \sigma_x)$ and τ_{xy}. By using the expression of $(\sigma_y - \sigma_x)$ and Equation 4.4.18, σ_x and σ_y can be found respectively. Thus Equations 4.4.18 and 4.4.20 determine the stress components by means of two analytic functions.

Displacements can also be expressed in complex functions. From the geometric equations 4.2.24 and the constitutive equations 4.2.25, it can be shown that

$$\left. \begin{array}{l} \dfrac{\partial u}{\partial x} = \dfrac{1-v^2}{E} [\sigma_x - \dfrac{v}{1-v}\sigma_y] \\[2mm] \dfrac{\partial v}{\partial y} = \dfrac{1-v^2}{E} [\sigma_y - \dfrac{v}{1-v}\sigma_x] \\[2mm] \dfrac{\partial u}{\partial y} + \dfrac{\partial v}{\partial x} = \dfrac{2(1+v)}{E}\tau_{xy} \end{array} \right\} \qquad (4.4.21)$$

In the first of Equations 4.4.21, replacing σ_x and σ_y with $\dfrac{\partial^2 U}{\partial y^2}$ and $\dfrac{\partial^2 U}{\partial x^2}$ respectively and then using Equation 4.4.1 produces

$$\dfrac{\partial u}{\partial x} = \dfrac{1-v^2}{E}[\dfrac{\partial^2 U}{\partial y^2} - \dfrac{v}{1-v}\dfrac{\partial^2 U}{\partial x^2}] = \dfrac{1-v^2}{E}[(P-\dfrac{\partial^2 U}{\partial x^2}) - \dfrac{v}{1-v}\dfrac{\partial^2 U}{\partial x^2}] = \dfrac{1-v^2}{E}[P - \dfrac{1}{1-v}\dfrac{\partial^2 U}{\partial x^2}]$$

or

$$\dfrac{E}{1+v}\dfrac{\partial u}{\partial x} = P(1-v) - \dfrac{\partial^2 U}{\partial x^2}$$

Combining Equation 4.4.8 into this gives

$$\dfrac{E}{1+v}\dfrac{\partial u}{\partial x} = 4(1-v)\dfrac{\partial p}{\partial x} - \dfrac{\partial^2 U}{\partial x^2}$$

Integrating it with respect to x yields

$$\dfrac{E}{1+v} u = 4(1-v) p - \dfrac{\partial U}{\partial x} + f_1(y) \qquad (4.4.22)$$

where $f_1(y)$ is an arbitrary function of y.

Similarly it can be obtained that

$$\dfrac{E}{1+v} v = 4(1-v) q - \dfrac{\partial U}{\partial y} + f_2(x) \qquad (4.4.23)$$

where $f_2(x)$ is an arbitrary function of x.

146

Substituting Equations 4.4.22 and 4.4.23 into the third of Equations 4.4.21, using the Cauchy - Riemann equations to relate p and q by $\frac{\partial p}{\partial y} = -\frac{\partial q}{\partial x}$, and inputting $\tau_{xy} = -\frac{\partial^2 U}{\partial x \partial y}$ will give

$$\frac{df_1(y)}{dy} + \frac{df_2(x)}{dx} = 0$$

The solution to this equation is

$$f_1(y) = u_0 - \omega y \quad f_2(x) = v_0 + \omega x$$

Obviously, $f_1(y)$ and $f_2(x)$ represent rigid body displacements (see Equations 4.2.4 and 4.2.5) that have no contribution to deformation and strain. Therefore they can be discarded. Thus Equations 4.4.22 and 4.4.23 for displacement components become

$$\frac{E}{1+v} u = 4 (1-v) p - \frac{\partial U}{\partial x}$$

$$\frac{E}{1+v} v = 4 (1-v) q - \frac{\partial U}{\partial y}$$

Combination of these two equations in complex form gives

$$\frac{E}{1+v} (u + i v) = 4 (1-v)(p + i q) - (\frac{\partial U}{\partial x} + i \frac{\partial U}{\partial y})$$

Substitution of Equations 4.4.3 and 4.4.13 into this equation yields

$$\frac{E}{1+v} (u + i v) = (3 - 4v) \phi_1(z) - z \overline{\phi_1'(z)} - \overline{\theta_1'(z)} \qquad (4.4.24)$$

Boundary conditions can also be expressed in complex functions. Based on Equations 4.2.22 the boundary conditions for plane strain problems are expressed as

$$\left. \begin{array}{l} F_x = \sigma_x \cos \alpha + \tau_{xy} \sin \alpha \\ F_y = \sigma_y \sin \alpha + \tau_{xy} \cos \alpha \end{array} \right\} \qquad (4.4.25)$$

where α is the angle between the right-hand normal N and the x axis, see Figure 4.4.1.
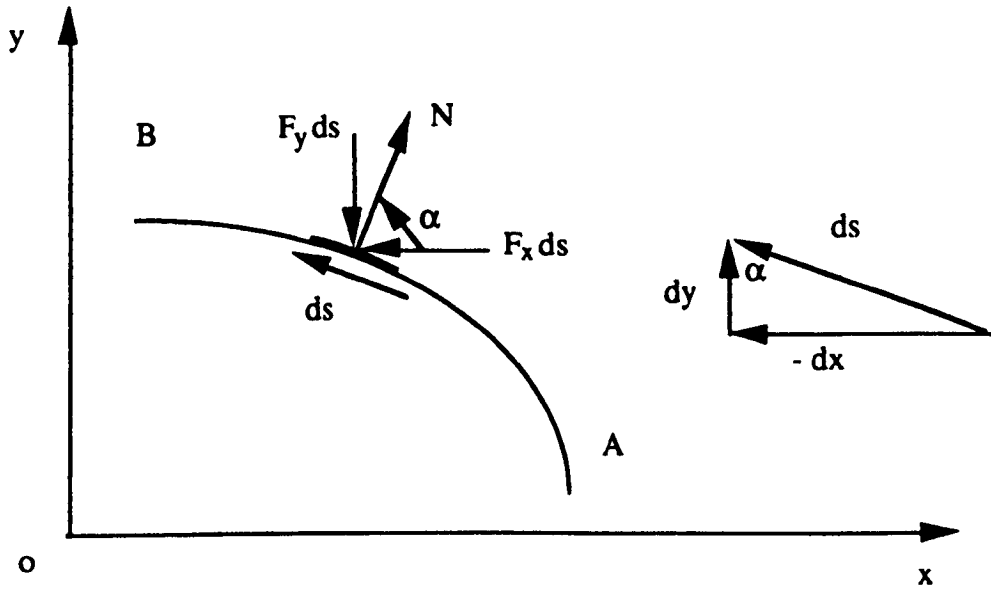
Figure 4.4.1 The incremental relationship between the arc and the coordinates

As the arc ds traverses in the direction AB, x decreases and thus dx will be a negative value and following relations hold

$$\cos \alpha = \frac{dy}{ds} \qquad \sin \alpha = - \frac{dx}{ds} \qquad (4.4.26)$$

Inserting these, together with Equations 4.2.30 into Equations 4.4.25 yields

$$\left. \begin{array}{l} F_x = \dfrac{\partial^2 U}{\partial y^2} \dfrac{dy}{ds} + \dfrac{\partial^2 U}{\partial x \partial y} \dfrac{dx}{ds} = \dfrac{\partial}{\partial y}(\dfrac{\partial U}{\partial y}) \dfrac{dy}{ds} + \dfrac{\partial}{\partial x}(\dfrac{\partial U}{\partial y}) \dfrac{dx}{ds} = \dfrac{d}{ds}(\dfrac{\partial U}{\partial y}) \\[4mm] F_y = - \dfrac{\partial^2 U}{\partial x^2} \dfrac{dx}{ds} - \dfrac{\partial^2 U}{\partial x \partial y} \dfrac{dy}{ds} = - \dfrac{d}{ds}(\dfrac{\partial U}{\partial x}) \end{array} \right\} \qquad (4.4.27)$$

The components of the resultant force on the arc AB are therefore of those given by

$$\left. \begin{array}{l} \overline{X} = \displaystyle\int_a^b F_x ds = \dfrac{\partial U}{\partial y} \Big|_A^B \\[4mm] \overline{Y} = \displaystyle\int_a^b F_y ds = - \dfrac{\partial U}{\partial x} \Big|_A^B \end{array} \right\} \qquad (4.4.28)$$

These may be written in complex form

$$\overline{X} + i\,\overline{Y} = \left[\frac{\partial U}{\partial y} - i\frac{\partial U}{\partial x}\right]_A^B \qquad (4.4.29)$$

Inputing Equation 4.4.14 times (-i) in the above equation produces

$$\overline{X} + i\,\overline{Y} = -i\left[\phi_1(z) + z\,\overline{\phi_1'(z)} + \overline{\theta_1'(z)}\right]_A^B \qquad (4.4.30)$$

4.4.2 Conformal Mapping, Stress and Strain in Curvilinear Coordinates

It has been shown mathematically that a mapping from a region in the z plane to a region in the ζ plane through $z = f(\zeta)$ is conformal if $f(\zeta)$ is analytic and $f'(\zeta) \neq 0$ (Kreyszig, 1979). By conformal mapping an analytic function of complex variable z will be transformed to another analytic function of variable ζ. The real and imaginary parts of this last function also satisfy the Laplace Equation, namely they are all harmonic. In solid mechanics, the conformal mapping theory has been employed to solve plane problems (Timoshenko and Goodier, 1951, Muskhelishvili, 1948, Savin 1951,Greenspan 1944, Ling, 1948, England 1971).

Assume that in the ζ plane, the real curvilinear axis is ξ and the imaginary curvilinear axis is η, then $\zeta = \xi + i\,\eta$.

Although stress components σ_x, σ_y, and τ_{xy} can be expressed in terms of ξ and η by applying $z = f(\zeta)$ to Equations 4.4.19 and 4.4.20, it is convenient to specify the stress as:

σ_ξ representing the normal stress on a curve ξ = constant;

σ_η representing the normal stress on a curve η = constant;

$\tau_{\xi\eta}$ representing the shear stress on both curves.

These components are indicated in Figure 4.4.2.a. A static analysis of a very small triangular prism (see Figure 4.4.2.b) gives:
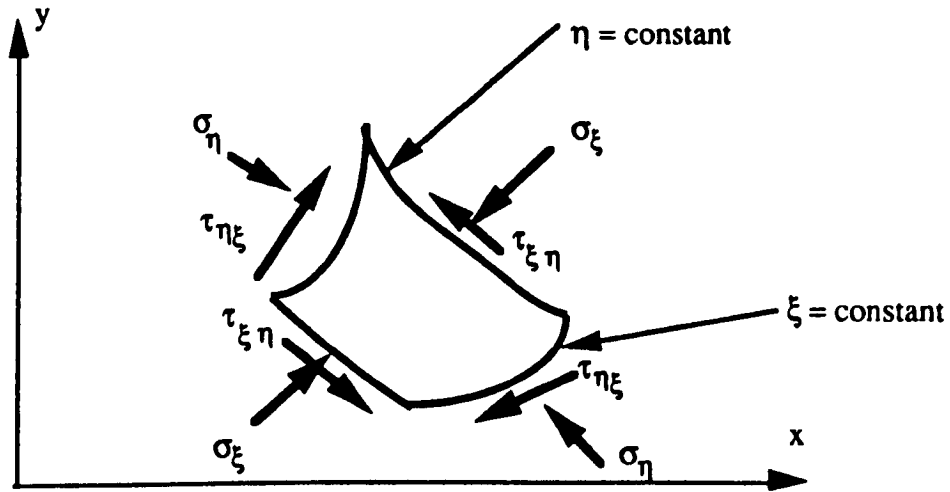
(a) Stress components in curvilinear coordinates
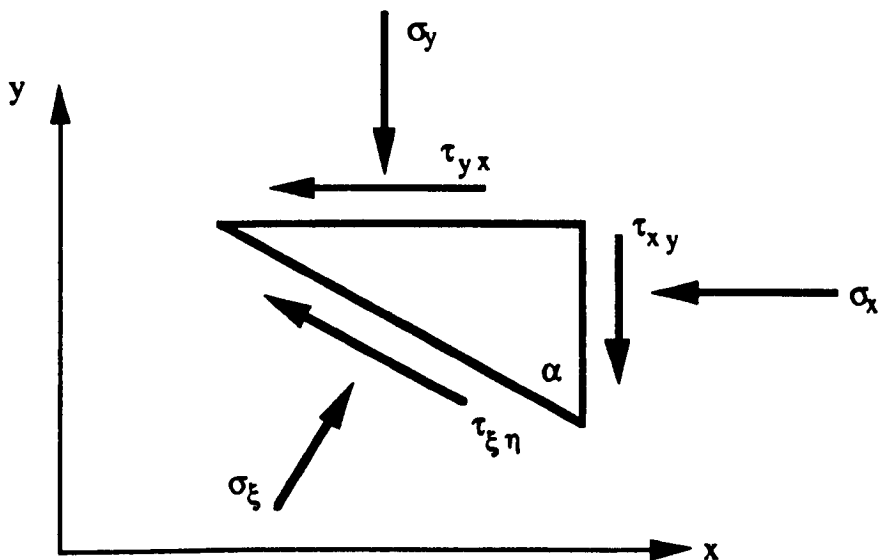
(b) Relationship between the stress components in the cartesian and
the curvilinear systems

Figure 4.4.2 Conformal mapping of the stress components to the

curvilinear coordinates.

$$\sigma_\xi = \frac{1}{2}(\sigma_x + \sigma_y) + \frac{1}{2}(\sigma_x - \sigma_y)\cos 2\alpha + \tau_{xy}\sin 2\alpha$$

$$\tau_{\xi\eta} = -\frac{1}{2}(\sigma_x - \sigma_y)\sin 2\alpha + \tau_{xy}\cos 2\alpha$$

Similarly, replacing α by $\frac{\pi}{2} + \alpha$ in the above first equation gives

$$\sigma_\eta = \frac{1}{2}(\sigma_x + \sigma_y) - \frac{1}{2}(\sigma_x - \sigma_y)\cos 2\alpha - \tau_{xy}\sin 2\alpha$$

From these relations, the following relations are easily found:

$$\left.\begin{array}{l} \sigma_\xi + \sigma_\eta = \sigma_x + \sigma_y \\ \sigma_\eta - \sigma_\xi + 2i\tau_{\xi\eta} = e^{2i\alpha}(\sigma_y - \sigma_x + 2i\tau_{xy}) \end{array}\right\} \qquad (4.4.31)$$

The factor $e^{2i\alpha}$ for curvilinear coordinates defined by the $z = f(\zeta)$ can be found if we set (Timoshenko and Goodier, 1951):

$$f'(\zeta) = J\,e^{i\alpha} \qquad (4.4.32)$$

where J and α are real.

Thus $\qquad f'(\overline{\zeta})) = J\,e^{-i\alpha} \quad$ and $\quad e^{2i\alpha} = \dfrac{f'(\zeta)}{\overline{f'(\zeta)}} \qquad (4.4.33)$

The displacement components in curvilinear coordinates are specified by u_ξ along ξ-decreasing direction and u_η along η-deceasing direction. If u and v are the Cartesian components of the displacement, it is obtainable by projecting the displacement vector or u and v onto the ξ and η axis that

$$u_\xi = u\cos\alpha + v\sin\alpha, \qquad u_\eta = v\cos\alpha - u\sin\alpha \qquad (4.4.34)$$

This may be illustrated by Figure 4.4.3. Therefore, the following identity holds

$$u_\xi + i\,u_\eta = e^{-i\alpha}(u + i\,v) \qquad (4.4.35)$$

Combination of Equations 4.4.18, 4.4.20, 4.4.24, 4.4.31, and 4.4.35 yields
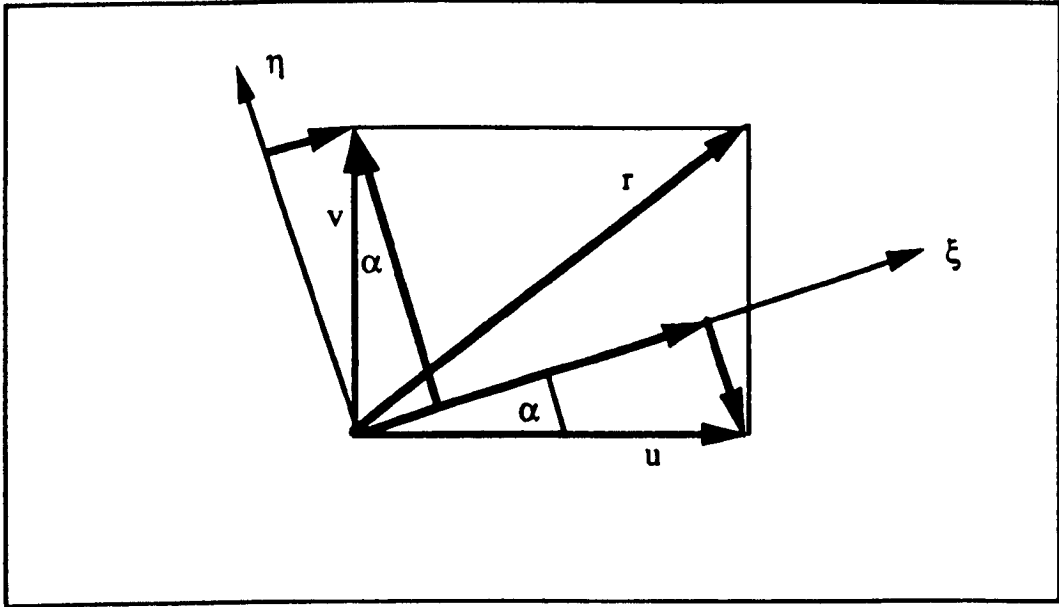
Figure 4.4.3 Relationship between the displacement components in the cartesian coordinates and the curvilinear coordinates.

$$
\left.
\begin{aligned}
&\sigma_\xi + \sigma_\eta = 4\ \mathrm{Re}\ \phi_1{}'(z) \\
&\sigma_\eta - \sigma_\xi + 2i\tau_{\xi\eta} = 2e^{2i\alpha}[\ \overline{z}\ \phi_1{}''(z) + \theta_1{}''(z)] \\
&u_\xi + i\ u_\eta = \frac{1+\upsilon}{E}\ e^{-i\alpha}[(3 - 4\upsilon)\ \phi_1(z) - z\ \overline{\phi_1{}'(z)}\ - \overline{\theta_1{}'(z)}\ ]
\end{aligned}
\right\}
\qquad (4.4.36)
$$

4.4.3 Stress Analysis of an Elliptical Tunnel

Figure 4.4.4 shows an elliptical tunnel excavated in a homogeneous and isotropic rock mass. The applied horizontal and vertical stress at a remote distance from the tunnel is p_x and p_y respectively. The difference of the tunnel profile from the circular makes the mathematical method presented in previous section unable to be directly applied in the present problem. Instead, a complex method is therefore used.

Upon the consideration of the elliptical tunnel profile, an elliptical coordinate system is chosen for the problem. A mapping function is defined as

$$
z = c\ \mathrm{ch}\zeta \qquad (4.4.37)
$$
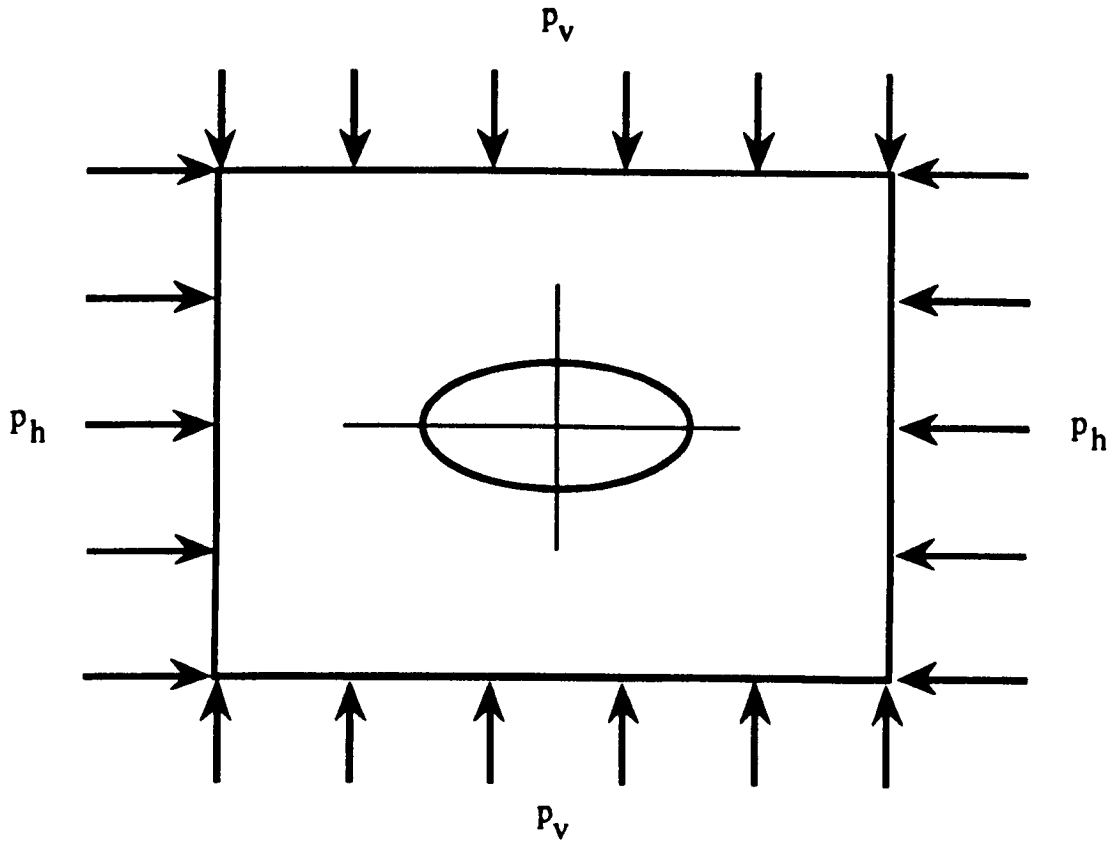
Figure 4.4.4 An elliptical tunnel model.
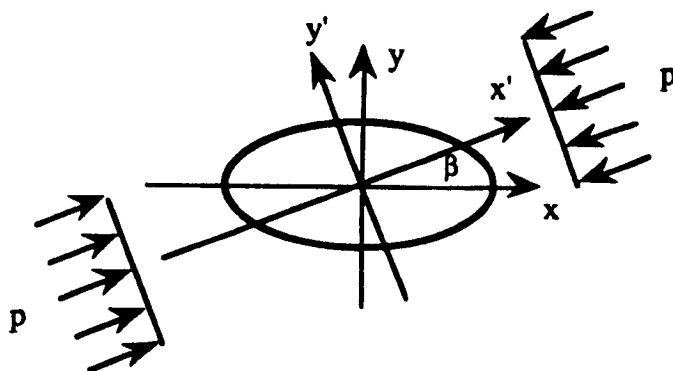
Figure 4.4.5 An elliptical tunnel under a uniaxial loading effect.

153

Substitution of $z = x + iy$ and $\zeta = \xi + i\eta$ into the mapping function gives

$$x + iy = c \, ch(\xi + i\eta) = c \, ch \, \xi \, cos\eta + i \, c \, sh \, \xi \, sin\eta \qquad (4.4.38)$$

Equalizing both the real and the imaginary parts on both sides of the equation gives

$$x = c \, ch \, \xi \, cos\eta \qquad y = c \, sh \, \xi \, sin\eta \qquad (4.4.39)$$

Given $\xi = \xi_0$, Equations 4.4.39 represent the parametric equations for an ellipse, as this may be shown by eliminating η to form the equation:

$$\frac{x^2}{(c \, ch\xi_0)^2} + \frac{y^2}{(c \, sh\xi_0)^2} = 1 \qquad (4.4.40)$$

If the semiaxes of an elliptic tunnel are given as a along the x-axis and b along y-axis, c and ξ_0 can be found from

$$a = c \, ch \, \xi_0 \qquad b = c \, sh \, \xi_0 \qquad (4.4.41)$$

and the foci of the elliptical tunnel are at $x = \pm c$ since $a^2 - b^2 = c^2$.

It can be checked that a point on any one ellipse goes once around the ellipse in z plane as η goes from 0 to 2π. In this respect η resembles the angle θ of polar coordinates and the fact that $\xi = \xi_0$ may be seen as a circle in the ζ plane. Therefore, by the mapping function Equation 4.4.37 an elliptical tunnel in the z plane is transformed to a circle in the ζ plane.

Since the stress and displacement at a given point of rock around the tunnel are single-valued, the expression of the stress and displacement should be a periodic function of η with period 2π, such that they will have the same values for $\eta = 2\pi$ as they have for $\eta = 0$. Functions

$$sh \, nz = sh \, n\xi \, cos \, n\eta + i \, ch \, n\xi \, sin \, n\eta$$

$$ch \, nz = ch \, n\xi \, cos \, n\eta + i \, sh \, n\xi \, sin \, n\eta \qquad (n = integer)$$

and $c^2\zeta$ satisfy this requirement.

Before the solution to the problem shown in Figure 4.4.4 is found, one simple case should be first considered, that is an elliptical tunnel under the effect of an applied uniaxial stress p in a direction at an angle β to the x axis, see Figure 4.4.5.

If the solution to this problem is found, the stress and displacement around the elliptical tunnel influenced by any state of uniform stress specified by the principal stresses at infinity in any orientation can be found. An application of the superposition principle to bi-directional loading problems would lead to the solution of stresses and displacements.

Let ox' and oy' be Cartesian axes obtained by rotating ox through the angle b so as to bring it parallel to the direction of the applied stress, p. Then by Equation 4.4.31,

$$\left. \begin{array}{l} \sigma_{x'} + \sigma_{y'} = \sigma_x + \sigma_y \\ \sigma_{y'} - \sigma_{x'} + 2i\tau_{x'y'} = e^{2i\beta}(\sigma_y - \sigma_x + 2i\tau_{xy}) \end{array} \right\} \qquad (4.4.41)$$

Since at infinity $\sigma_{x'} = p$, $\sigma_{y'} = \tau_{x'y'} = 0$, it is obtainable that

$$\sigma_x + \sigma_y = p \qquad\qquad \sigma_y - \sigma_x + 2i\tau_{xy} = -p\,e^{-2i\beta} \qquad \text{at infinity.}$$

From Equations 4.4.18 and 4.4.20, it attains that

$$\left. \begin{array}{l} 4\,\text{Re}\,\phi_1'(z) = p \\ 2[\,\overline{z}\,\phi_1''(z) + \theta_1''(z)] = -p\,e^{-2i\beta} \end{array} \right\} \quad \text{at infinity} \qquad (4.4.42)$$

At the periphery of the tunnel, namely $\xi = \xi_0$,

$$\sigma_\xi = \tau_{\xi\eta} = 0 \qquad\qquad\qquad (4.4.43)$$

Consider $\phi_1(z)$ and $\theta_1(z)$ having the forms (Muskhelishvili, 1948, Timoshenko and Goodier, 1951):

$$4\phi_1(z) = Ac \, ch\zeta + Bc \, sh\zeta$$
$$4\theta_1(z) = C \, c^2\zeta + Dc^2 \, ch2\zeta + E \, c^2 \, sh2\zeta \qquad (4.4.44)$$

where A, B, C, D and E are constants to be determined, of which A and C are real and the rest are complex having the form:

$$B = B_1 + i \, B_2$$
$$D = D_1 + i \, D_2 \qquad (4.4.45)$$
$$E = E_1 + i \, E_2$$

Hence,
$$4\phi'_1(z) = [Ac \, sh\zeta + Bc \, ch\zeta] \frac{1}{\frac{dz}{d\zeta}}$$

$$= [Ac \, sh\zeta + Bc \, ch\zeta] \frac{1}{c \, sh\zeta} \qquad \text{(since } z = c \, ch\zeta\text{)}$$

$$= A + B \frac{ch\zeta}{sh\zeta}$$

$$4\phi''_1(z) = B \frac{sh^2\zeta - ch^2\zeta}{sh^2\zeta} \frac{1}{c \, sh\zeta}$$

$$= B \frac{-1}{c \, sh^3\zeta}$$

At infinity, $z \to \infty$, $\zeta \to \infty$ such that

$$4\phi'_1(z) = A + B_1 + i \, B_2.$$

Using the boundary conditions at infinity as shown in Equations 4.4.42 gives

$$4 \, Re \, \phi_1'(z) = A + B_1 = p \qquad (4.4.46)$$

Similarly, from the second of Equations 4.4.44, it can be obtained that

$$4\theta_1'(z) = (C \, c^2 + 2Dc^2 \, sh2\zeta + 2E \, c^2 \, ch2\zeta) \frac{1}{\frac{dz}{d\zeta}}$$

$$= (C + 2D \, sh2\zeta + 2E \, ch2\zeta) \frac{c}{sh\zeta}$$

$$4\theta_1''(z) = (4D\ ch2\zeta + 4E\ sh2\zeta)\frac{1}{sh^2\zeta} - (C + 2D\ sh2\zeta + 2E\ ch2\zeta)\frac{c\ ch\zeta}{sh^2\zeta}\frac{d\zeta}{dz}$$

$$= (4D\ ch2\zeta + 4E\ sh2\zeta)\frac{1}{sh^2\zeta} - (C + 2D\ sh2\zeta + 2E\ ch2\zeta)\frac{ch\zeta}{sh^3\zeta}$$

From these relations, it can be found that

$$2[\ \bar{z}\ \phi_1''(z) + \theta_1''(z)]\ |_{|z|\to\infty}$$

$$= \frac{1}{2}[c\ ch\ \bar{\zeta}\ B\frac{-1}{c\ sh^3\zeta} + (4Dch2\zeta + 4Esh2\zeta)\frac{1}{sh^2\zeta} - (C+2Dsh2\zeta+2Ech2\zeta)\frac{ch\zeta}{sh^3\zeta}]|_{\zeta\to\infty}$$

$$= \frac{1}{2}[\ 8D + 8E - 4D - 4E]$$

$$= 2D + 2E$$

$$= -p\ e^{-2i\beta} \tag{4.4.47}$$

Combination of the first and the second of Equations 4.4.36 by eliminating σ_η yields

$$2\ (\sigma_\xi - i\tau_{\xi\eta}) = 4\ Re\ \phi_1'(z) - 2e^{2i\beta}[\ \bar{z}\ \phi_1''(z) + \theta_1''(z)]$$

Using Equation 4.4.33 and the expressions of $\phi_1'(z)$, $\phi_1''(z)$ and $\theta_1''(z)$ as developed above, it can be found that

$$4\ (\sigma_\xi - i\tau_{\xi\eta})$$

$$= [4\ \phi_1'(z) + 4\ \overline{\phi_1'(z)}\ ] - \frac{\overline{f'(\zeta)}}{f'(\zeta)}[\ 4\ \bar{z}\ \phi_1''(z) + 4\ \theta_1''(z)]$$

$$= (A + B\frac{ch\zeta}{sh\zeta} + A + \bar{B}\ \frac{ch\ \bar{\zeta}}{sh\ \bar{\zeta}}) -$$

$$- \frac{sh\zeta}{sh\ \bar{\zeta}}\ [-B\frac{ch\ \bar{\zeta}}{sh^3\zeta} + (4Dch2\zeta + 4Esh2\zeta)\frac{1}{sh^2\zeta} - (C+2Dsh2\zeta+2Ech2\zeta)\frac{ch\zeta}{sh^3\zeta}]$$

$$= \frac{1}{sh\,\bar{\zeta}}[(2A+B\frac{ch\zeta}{sh\zeta})sh\,\bar{\zeta} + \bar{B}\,ch\,\bar{\zeta} + B\frac{ch\,\bar{\zeta}}{sh^2\zeta} - 4D\frac{ch^2\zeta+sh^2\zeta}{sh\zeta} - 8Ech\zeta +$$

$$+ (C+4Dsh\zeta ch\zeta+2Ech^2\zeta+2Esh^2\zeta)\frac{ch\zeta}{sh^2\zeta}]$$

$$= \frac{1}{sh\,\bar{\zeta}}[(2A+B\frac{ch\zeta}{sh\zeta})sh\,\bar{\zeta} + \bar{B}\,ch\,\bar{\zeta} + B\frac{ch\,\bar{\zeta}}{sh^2\zeta} - 4Dsh\zeta - 8Ech\zeta +$$

$$+ C\frac{ch\zeta}{sh^2\zeta}+2E(1+sh^2\zeta)\frac{ch\zeta}{sh^2\zeta}+2Ech\zeta]$$

$$= \frac{1}{sh\,\bar{\zeta}}[(2A+B\frac{ch\zeta}{sh\zeta})sh\,\bar{\zeta} + \bar{B}\,ch\,\bar{\zeta} + \frac{Bch\,\bar{\zeta} + Cch\zeta+2Ech\zeta}{sh^2\zeta} - 4Dsh\zeta - 4Ech\zeta]$$

$$= \frac{1}{sh\,\bar{\zeta}}[(2A+B\frac{ch\zeta}{sh\zeta})sh\,\bar{\zeta} +(\bar{B} + \frac{B}{sh^2\zeta})ch\,\bar{\zeta} +(C+ 2E)\frac{ch\zeta}{sh^2\zeta} -4Dsh\zeta-4Ech\zeta] \quad (4.4.48)$$

At the periphery of the tunnel, $\xi = \xi_0$, $\bar{\zeta} = 2\xi_0 - \zeta$ and $\sigma_\xi - i\,\tau_{\xi\eta} = 0$. Inputting these conditions into the expression 4.4.8 yields

$$[(2A+B\frac{ch\zeta}{sh\zeta})sh(2\xi_0 - \zeta)+(\bar{B} + \frac{B}{sh^2\zeta})ch(2\xi_0- \zeta)+(C+ 2E)\frac{ch\zeta}{sh^2\zeta} -4Dsh\zeta-4Ech\zeta]$$

$$= 0 \qquad\qquad\qquad\qquad\qquad\qquad\qquad\qquad\qquad (4.4.49)$$

According to the mathematical formulae (see Kreyszig, 1979)

$$sh(2\xi_0 - \zeta) = sh2\xi_0 ch\zeta - ch2\xi_0 sh\zeta$$

$$ch(2\xi_0 - \zeta) = ch2\xi_0 ch\zeta - sh2\xi_0 sh\zeta$$

$$ch2\zeta = 1 + sh2\zeta$$

the above expression 4.4.49 can be expanded and simplified as

$$[(2A+B\frac{ch\zeta}{sh\zeta})(sh2\xi_0 ch\zeta - ch2\xi_0 sh\zeta)+(\bar{B} + \frac{B}{sh^2\zeta})(ch2\xi_0 ch\zeta - sh2\xi_0 sh\zeta)+$$

$$+(C+2E)\frac{ch\zeta}{sh^2\zeta}-4Dsh\zeta-4Ech\zeta]$$

$$=(2Ash2\xi_0-Bch2\xi_0-\overline{B}\,ch2\xi_0-4E)ch\zeta+(-2Ach2\xi_0-\overline{B}\,sh2\xi_0-4D)sh\zeta+$$

$$+(Bch2\xi_0+C+2E)\frac{ch\zeta}{sh^2\zeta}+Bsh2\xi_0\frac{1+sh^2\zeta}{sh\zeta}-Bsh2\xi_0\frac{1}{sh\zeta}$$

$$=(2Ash2\xi_0-2iB_2ch2\xi_0-4E)ch\zeta+(2iB_2sh2\xi_0-2Ach2\xi_0-4D)sh\zeta+(Bch2\xi_0+C+2E)\frac{ch\zeta}{sh^2\zeta}$$

$$= 0 \qquad\qquad\qquad\qquad (4.4.50)$$

To ensure that this identity holds, the coefficients of $ch\zeta$, $sh\zeta$ and $\dfrac{ch\zeta}{sh^2\zeta}$ must equal to zero. Consequently, these conditions together with Equations 4.4.46 and 4.4.47 constitute a system:

$$\left.\begin{array}{l} A+B_1=p \\ 2D+2E=-p\,e^{-2i\beta} \\ 2Ash2\xi_0-2iB_2ch2\xi_0-4E=0 \\ 2iB_2sh2\xi_0-2Ach2\xi_0-4D=0 \\ Bch2\xi_0+C+2E=0 \end{array}\right\} \qquad (4.4.51)$$

The conditions for these equations to hold are that both the real and the imaginary parts of each equation must be equal on both sides of the equations. Thus the equation system 4.4.51 becomes

$$\left.\begin{array}{l} A+B_1=p \\ D_1+E_1=-\dfrac{p}{2}\cos(-2\beta) \\ D_2+E_2=-\dfrac{p}{2}\sin(-2\beta) \\ 2Ash2\xi_0-4E_1=0 \\ 2B_2ch2\xi_0+4E_2=0 \\ 2Ach2\xi_0+4D_1=0 \\ 2B_2sh2\xi_0-4D_2=0 \\ B_1ch2\xi_0+C+2E_1=0 \\ B_2ch2\xi_0+2E_2=0 \end{array}\right\} \qquad (4.4.52)$$

Solution to this system is

$$A = pe^{2\xi_0}\cos2\beta$$
$$B_1 = p(1 - e^{2\xi_0}\cos2\beta) \qquad B_2 = -pe^{2\xi_0}\sin2\beta$$
$$C = -p(ch2\xi_0 - \cos2\beta)$$
$$D_1 = -\frac{p}{2}e^{2\xi_0}ch2\xi_0\cos2\beta \qquad D_2 = -\frac{p}{2}e^{2\xi_0}sh2\xi_0\sin2\beta \qquad \qquad (4.4.53)$$
$$E_1 = -\frac{p}{2}\cos2\beta(1 - e^{2\xi_0}ch2\xi_0) \qquad E_2 = \frac{p}{2}\sin2\beta(1 + e^{2\xi_0}sh2\xi_0)$$

Hence, the stress functions $\phi_1(z)$ and $\theta_1(z)$ are found and the relevant stress components can be calculated. Now the author's interest is in finding stress along the tunnel boundary. In the general case, the stress magnitude varies along the tunnel periphery, increasing at some sections but decreasing at other sections. Highly concentrated stresses are more likely to trigger off rock failures.

At the tunnel periphery, radius stress σ_ξ is zero. From Equation 4.4.36, the tangential stress σ_η can be found to be

$$\sigma_\eta = 4 \, Re \, \phi_1'(z)$$

$$= Re \left(A + B\frac{ch\zeta}{sh\zeta}\right)$$

$$= Re \left[pe^{2\xi_0}\cos2\beta + p(1 - e^{2\xi_0}\cos2\beta - i\,e^{2\xi_0}\sin2\beta)\frac{ch(\xi_0 + i\eta)}{sh(\xi_0 + i\eta)}\right]$$

Since $\dfrac{ch(\xi_0 + i\eta)}{sh(\xi_0 + i\eta)}$

$$= \frac{ch\xi_0\cos\eta + i\,sh\xi_0\sin\eta}{sh\xi_0\cos\eta - i\,ch\xi_0\sin\eta}$$

$$= \frac{ch\xi_0 sh\xi_0\cos^2\eta + i\,sh^2\xi_0\sin\eta\cos\eta - ich^2\xi_0\sin\eta\cos\eta + ch\xi_0 sh\xi_0\sin^2\eta}{sh^2\xi_0\cos^2\eta + ch^2\xi_0\sin^2\eta}$$

$$= \frac{\frac{1}{2}sh2\xi_0 - i\frac{1}{2}\sin2\eta}{\frac{ch2\xi_0 - 1}{2}\frac{1 + \cos2\eta}{2} + \frac{ch2\xi_0 + 1}{2}\frac{1 - \cos2\eta}{2}}$$

$$= \frac{sh2\xi_0 - i\,\sin2\eta}{ch2\xi_0 - \cos2\eta}$$

Therefore, at the tunnel periphery, the above expression becomes

$$\sigma_\eta = \mathrm{Re}\left[pe^{2\xi_0}\cos2\beta + p(1- e^{2\xi_0}\cos2\beta -i\, e^{2\xi_0}\sin2\beta)\frac{\mathrm{sh}2\xi_0 - i\,\sin2\eta}{\mathrm{ch}2\xi_0 - \cos2\eta}\right]$$

$$= pe^{2\xi_0}\cos2\beta + p\frac{\mathrm{sh}2\xi_0(1- e^{2\xi_0}\cos2\beta) - e^{2\xi_0}\sin2\beta\sin2\eta}{\mathrm{ch}2\xi_0 - \cos2\eta}$$

$$= p\frac{e^{2\xi_0}\cos2\beta(\mathrm{ch}2\xi_0-\mathrm{sh}2\xi_0) + \mathrm{sh}2\xi_0 - e^{2\xi_0}\cos(2\beta+2\eta)}{\mathrm{ch}2\xi_0 - \cos2\eta}$$

$$= p\frac{e^{2\xi_0}\cos2\beta\left(\dfrac{e^{2\xi_0} + e^{-2\xi_0}}{2} - \dfrac{e^{2\xi_0} - e^{-2\xi_0}}{2}\right) + \mathrm{sh}2\xi_0 - e^{2\xi_0}\cos(2\beta+2\eta)}{\mathrm{ch}2\xi_0 - \cos2\eta}$$

$$= p\frac{\cos2\beta + \mathrm{sh}2\xi_0 - e^{2\xi_0}\cos(2\beta+2\eta)}{\mathrm{ch}2\xi_0 - \cos2\eta} \qquad (4.4.54)$$

From this result, the tangential stress σ_η at the tunnel periphery, when the tunnel is bidirectionally loaded at infinity as shown in Figure 4.4.4, can be found.

Setting $\beta = 0$, the applied stress p in Equation 4.4.54 becomes p_x. Then the tangential stress σ_η induced by p_x is:

$$\sigma_{\eta1} = p_x\frac{1+ \mathrm{sh}2\xi_0 - e^{2\xi_0}\cos2\eta}{\mathrm{ch}2\xi_0 - \cos2\eta} \qquad (4.4.55)$$

Similarly, σ_η induced by the applied stress p_y can be found by setting $\beta = \frac{\pi}{2}$ in Equation 4.4.54, namely,

$$\sigma_{\eta2} = p_y\frac{-1 + \mathrm{sh}2\xi_0 + e^{2\xi_0}\cos2\eta}{\mathrm{ch}2\xi_0 - \cos2\eta} \qquad (4.4.56)$$

Thus, the stress σ_η at the tunnel periphery caused by both p_x and p_y is found according to superposition principle, which gives:

$$\sigma_\eta = \sigma_{\eta1} + \sigma_{\eta2}$$

$$= \frac{(p_x - p_y) + (p_x - p_y)\,sh2\xi_0 - (p_x - p_y)\,e^{2\xi_0}cos2\eta}{ch2\xi_0 - cos2\eta} \qquad (4.4.57)$$

It is obvious that, for a given tunnel, σ_η is a function of η which varies from 0 to 2π. From a rock mechanics point of view, the tunnel profile will fail more likely at the parts where σ_η becomes negative or tensile, alternatively, crushing may also result at highly compressed regions. If the stress σ_η can be adjusted to become constant or least variable, the tunnel profile and therefore the tunnel would tend to become most stable. Mathematically, the condition for σ_η to become constant at the tunnel periphery requires that the first order partial derivative of Equation 4.4.57 with respect to η should be equal to zero. From Equation 4.4.57, it can be operated that

$$\frac{d\sigma_\eta}{d\eta}$$

$$= \frac{2(p_x-p_y)e^{2\xi_0}sin2\eta(ch2\xi_0-cos2\eta)-[(p_x-p_y)+(p_x+p_y)sh2\xi_0-(p_x-p_y)e^{2\xi_0}cos2\eta]2sin2\eta}{(\,ch2\xi_0 - cos2\eta\,)^2}$$

$$(4.4.58)$$

Therefore, the stability condition requires the numerator of this equation to become zero, namely,

$$2(p_x-p_y)e^{2\xi_0}sin2\eta(ch2\xi_0-cos2\eta)-[(p_x-p_y)+(p_x+p_y)sh2\xi_0-(p_x-p_y)e^{2\xi_0}cos2\eta]2sin2\eta = 0$$

or $\qquad (p_x - p_y)\,e^{2\xi_0}\,ch2\xi_0 - (p_x - p_y) - (p_x + p_y)\,sh2\xi_0 = 0 \qquad (4.4.59)$

From the mapping function Equation 4.4.37, it follows that, at the tunnel periphery,

$$\xi = \xi_0, \quad x = c\,ch\,\xi_0\,cos\eta \quad, \qquad y = c\,sh\,\xi_0\,sin\eta$$

and the semiaxes of the tunnel a and b are related to focus position c and the constant ξ_0 by

$$a = c\,ch\,\xi_0 \qquad and \qquad b = c\,sh\,\xi_0 \ .$$

162

Thus, $\quad sh\ 2\xi_0 = 2sh\xi_0 ch\ \xi_0 = 2\frac{ab}{c^2}\quad,\qquad ch\ 2\xi_0 = ch^2\xi_0 + sh^2\xi_0 = \frac{a^2}{c^2} + \frac{b^2}{c^2}$

$$a^2 - b^2 = c^2\ ,\qquad \frac{a}{c} = ch\ \xi_0 = \frac{e^{\xi_0} + e^{-\xi_0}}{2}\ ,\qquad \frac{b}{c} = sh\ \xi_0 = \frac{e^{\xi_0} - e^{-\xi_0}}{2}$$

Then $\qquad e^{\xi_0} = \frac{a+b}{c}\qquad\qquad e^{-\xi_0} = \frac{a-b}{c}$

Substitution of these relations into Equation 4.4.59 gives

$$(p_x - p_y)(\frac{a+b}{c})^2 \frac{a^2+b^2}{c^2} - (p_x - p_y) - (p_x + p_y)\frac{2ab}{c^2} = 0$$

$$(p_x - p_y)[(a+b)^2(a^2+b^2) - (a^2 - b^2)^2] - (p_x + p_y)2ab(a^2 - b^2) = 0$$

Simplification of this gives

$$p_x(1 + \frac{b}{a}) = p_y(\frac{a}{b} + 1)$$

$$p_x(\frac{a+b}{a}) = p_y(\frac{a+b}{b})$$

Therefore $\qquad\qquad \dfrac{p_x}{p_y} = \dfrac{a}{b}\qquad\qquad\qquad$ (4.4.60)

This result suggests that, to achieve the most stability of the tunnel, the dimensional ratio of tunnel width (2a) to height (2b) should be equal to the ratio of the applied horizontal to vertical stress.

From Equation 4.4.60, it is recognised that, in hydrostatic stress field conditions ($p_x = p_y$) the most desirable tunnel profiles are those that have unity tunnel dimensional ratio. In this case, employment of the circular or even square profiles would give remarkable consequence in terms of tunnel stability. In other applied stress field environments ($p_x \neq p_y$) however, the circular or square profiles may not result in the desired tunnel stability, as the tangential stress does not remain constant along the tunnel periphery.

163

Engineering practice has proven this. In some underground cases, adoption of circular tunnels turned out to be an effective measure in the control of tunnel stability, whereas in others, the instability problems cannot be alleviated by the design of a circular profile and related supports.

4.5 Concluding Remarks

Fundamental equations and laws of elastic theory form the basis of analytical determination of stresses in a solid. These include the equilibrium equations, geometric equations, compatibility conditions, constitutive laws and boundary conditions. They have first been reviewed and then used for development of tunnel stability theory in this Chapter.

Tunnel stability problems have been studied by using the plane strain theory. The conventional method for plane elastic theory has been followed in order to study the stress distribution in relation to the stress field features. An emphasis of this study has been given to looking at the effect of non-hydrostatic stress conditions on tunnel stability. The concept of stress concentration factors has been proposed, which are found to be closely related to the ratio of the applied horizontal to vertical stress. This concept avoids discussions of the absolute value of the applied stress field and stress, instead, it indicates the association of the stress concentration zone with the direction of the applied major stress.

Stresses in the vicinity of a tunnel have also been studied, in relation to the depth of the tunnel below the surface, in this Chapter. It has been shown that the stresses near the tunnel increase proportionally with the thickness of the overburden.
The result explains the causes that a tunnel driven in variable geological formations tends to present more instability problems as it extends down to the deeper ground.

Upon the consideration that shear failures are often observed and reported from working sites and roof fall accident sites, a formula for the prediction of shear failure zones around a tunnel has been associated with the stress field condition.

A concept of tunnel convergence rate has been proposed. The study clearly shows that although the deformation magnitude of a tunnel is proportional to the tunnel diameter, the convergence rate, as defined by the ratio of the deformation magnitude to the tunnel diameter, is not related to the excavation size. Upon this finding, a suggestion has been made by the author on the application of the tunnel convergence rate concept from an existing tunnel to the design of a new tunnel in a similar geological environment.

To further study the effect of tunnel dimensions on tunnel stability, an elliptical tunnel model has been used. The analysis of stresses near such a tunnel has prompted the need for the complex variable method, a highly mathematical technique, to be adopted. By finding the stress function expressed in complex form for the problem, the solution has been derived and connected to the tunnel dimensions. It has been found in this Chapter, that the tangential stress on the tunnel periphery becomes invariable and equally distributed when the ratio of tunnel width to height is equal to the ratio of the applied horizontal to vertical stress.

From these result it is predicted and pointed out theoretically that circular profiles cannot always be the best choice for achieving the desired stability if the applied stress field situation is unknown at the stage of tunnel design and excavation, and in particular when the applied vertical stress is greatly different in value from the horizontal value.

CHAPTER FIVE

ANALYSIS OF TUNNEL STABILITY AND SUPPORT AFTER OCCURRENCE OF ROCK FAILURE

CHAPTER FIVE

ANALYSIS OF TUNNEL STABILITY AND SUPPORT
AFTER OCCURRENCE OF ROCK FAILURE

5.1 Rock Mechanics Problems in Association with Tunnelling in Adverse Ground Conditions

As stated in the previous chapter, upon excavation, rocks surrounding a tunnel sustain effects of stress concentration. These rocks will fail when the absolute stresses in some zones near the tunnel are so high as to be able to overcome the relevant rock strength . Alternatively, some soft and weak rocks will be destroyed under not very high ground pressures, due to the weak nature of the rocks themselves. Ground conditions, where tunnels are hardly maintained and rock failures occur extensively, are identified as adverse tunnelling conditions. They have become a major concern of the tunnel designer. In particular, tunnelling in soft ground at increasing depths is often subject to a series of rock mechanics problems in terms of tunnel deformation, support torsion and damage, rock failure and collapses. The main causes of these problems are usually attributed to:

(i) increasing ground pressure;

(ii) poor rock properties;

(iii) improper use of support with regard to support characteristics, support installation time and support structure;

(iv) lack of understanding of the interaction between support system and surrounding rock; and

(v) inadequate design of tunnel cross-section, etc..

As coal mining turns towards deeper and deeper ground below the surface, more and more tunnels require to be excavated at increasing depths in the modern

world's coal industries. Both in China and the United Kingdom tunnelling at a number of collieries has been carried out at over 800 or even 1000 metres below the surface.

Increased ground pressure due solely to an increase in overburden thickness makes the above mentioned problems become outstanding. Lack of proper understanding of the ground pressure characteristics may give no basis on which support systems are effectively designed and installed, on which tunnels are properly designed in terms of shape and cross sectional area, and on which the mechanism of interaction between the support system and the surrounding rocks may be well understood.

Rock formations within the fields of the British Coal industry mainly comprise mudstones, claystones, siltstones and sandstones. The majority of these rocks are weak or medium in strength with UCS ranging from 20 to 80 MPa. Poor rock properties result in tunnel floor heave by virtue of the effects of plastic flow and rock creep.

The complex nature of tunnelling sites and rock structures often gives rise to difficulties in finding analytical solutions to these rock mechanics problems. In the previous chapter, discussions were mainly focussed on stresses, strains and deformations of rock around tunnels prior to occurrence of rock failure. In the present chapter an attempt is made, by means of purely theoretical analysis, to investigate stresses and deformations in the surrounding rock and support of a single tunnel, after some parts of the rock structure have undergone plastic failure. Such an analysis requires some criterion to be used for identifying if the rocks have failed in some region. This indicates the need for selecting a proper failure criterion. Obviously, various rock failure theories need to be reviewed before the selection is made.

5.2 Rock Failure Theories

As a solid material, rock exhibits variations in failure style when it is subjected to various loading conditions. The failure style of rock is also affected by the structure and constitution of the rock. To estimate likely failure scope in stressed rock around a tunnel, some failure theory has to be employed, coupled with a proper stress analysis. A rock failure theory specifies the mechanical condition under which rock materials fail by fracturing or by deforming beyond some specified limit. Based on many experiments and much engineering practice, various assumptions concerning the failure mode have been put forward by notable scientists and engineers. Among those failure theories, the work by Coulomb, Navier, Mohr, Griffith, Von Mises and Tresca have played great roles in rock stability analysis and thus they are worth reviewing. Since each failure theory is built on some given failure phenomenon or on certain assumptions, no unique failure theory has been found applicable to all rocks so far.

5.2.1 Coulomb-Navier Failure Theory

Coulomb (1773) proposed that failure would occur in a material when the maximum shear stress at a point in the material reaches the shear strength, s_o. Since the maximum shear stress τ_{max} can be expressed in terms of maximum and minimum principal stresses σ_1 ams σ_3, the Coulomb's failure criterion can be stated alternatively by that failure will occur when the expression 5.2.1 holds,

$$\frac{1}{2}(\sigma_1 - \sigma_3) = s_o \qquad (5.2.1)$$

and that the failure plane will bisect the angle between the maximum and minimum principal stresses.

A shortcoming of this theory when applied to rocks is that it neglects the difference of shear strength in tension and compression cases, since rocks have higher shear strength when they are subject to compressive loading states than in tensile states. Also, numerous experiments have shown that, for most rock under the

168

uniaxial compressive loading condition, the failure plane does not show exactly 45° to the loading direction.

Navier developed this theory by assuming that the normal stress (compressive) acting on the failure plane enhances the shear resistance of the material. If σ_n and τ_n are the normal and shear stresses on the likely failure plane whose normal has an angle of θ with respect to the direction of maximum stress σ_1 (see Figure 5.2.1(a)), Equation 5.2.2 should hold true at failure.

$$\tau_n = S_o + \mu \sigma_n \qquad (5.2.2)$$

where μ is known as the coefficient of internal friction.

(a)   (b)
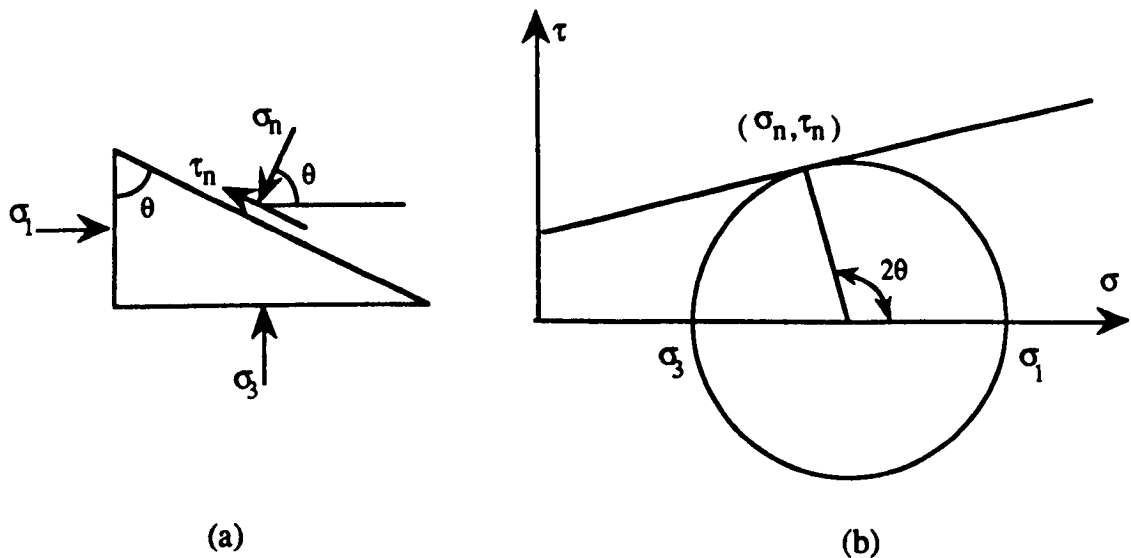
Figure 5.2.1 Illustration of the Navier's failure criterion

Referring to Figure 5.2.1 the normal and shear stresses can be expressed in terms of the maximum and minimum principal stresses, as shown in Equations 5.2.3.

$$\left. \begin{array}{c} \sigma_n = \dfrac{\sigma_1 + \sigma_3}{2} + \dfrac{\sigma_1 - \sigma_3}{2} \cos 2\theta \\[2mm] \tau_n = \dfrac{\sigma_1 - \sigma_3}{2} \sin 2\theta \end{array} \right\} \qquad (5.2.3)$$

Substitution of Equations 5.2.3 into Equation 5.2.2 yields

$$s_o = -\mu \frac{\sigma_1 + \sigma_3}{2} + \frac{\sigma_1 - \sigma_3}{2}(\sin 2\theta - \mu\cos 2\theta) \qquad (5.2.4)$$

The expression on the right hand side of formula (5.2.4) may be referred to as an equivalent shear stress, denoted by T, since the term on the left hand side, s_o, is the material shear strength. It is thus obtained that

$$T = -\mu \frac{\sigma_1 + \sigma_3}{2} + \frac{\sigma_1 - \sigma_3}{2}(\sin 2\theta - \mu\cos 2\theta) \qquad (5.2.5)$$

and the failure criterion becomes

$$T \leq s_o \qquad (5.2.6)$$

At failure, $T = s_o$. This means that failure occurs when T reaches the maximum and becomes equal to the material shear strength, s_o. By setting zero to the first order derivation of T with respect to the angle θ in Equation 5.2.5 or Equation 5.2.4., the positions where the maximum T occurs may be attained, namely,

$$\frac{\partial T}{\partial \theta} = 0 \quad \text{or} \quad \frac{\partial s_o}{\partial \theta} = 0 \qquad (5.2.7)$$

Putting Equation 5.2.5 or Equation 5.2.4 into Equation 5.2.7. yields

$$\tan 2\theta = -\frac{1}{\mu} \qquad (5.2.8)$$

This result indicates that 2θ lies between $90°$ and $180°$ and

$$\sin 2\theta = \frac{1}{\sqrt{\mu^2 + 1}} \qquad \cos 2\theta = \frac{-\mu}{\sqrt{\mu^2 + 1}} \qquad (5.2.9)$$

Substituting Equation 5.2.9 into Equation 5.2.5 yields

$$T = -\mu \frac{\sigma_1 + \sigma_3}{2} + \frac{\sigma_1 - \sigma_3}{2}\sqrt{\mu^2 + 1} \qquad (5.2.10)$$

170

Thus the failure criterion becomes

$$-\mu \frac{\sigma_1 + \sigma_3}{2} + \frac{\sigma_1 - \sigma_3}{2} \sqrt{\mu^2 + 1} \leq s_o \qquad (5.2.11)$$

The failure occurs when the identity in Equation 5.2.11 holds. This criterion is often known as Coulomb-Navier criterion.

5.2.2 Mohr's Failure Theory

Mohr's failure criterion stipulates that a material will fail when the shear stress τ_n on the failure plane has increased to a value which depends on the normal stress σ_n acting on the same plane, or when the largest tensile principal stress has reached a limiting value T_o. This criterion may be expressed mathematically as

$$\tau_n = f(\sigma_n) \quad \text{or} \quad \sigma_3 = T_o \qquad (5.2.12)$$

In fact, Equation 5.2.12 represents a curve in the $\sigma - \tau$ plane, which is called a Mohr's envelope. The physical sense of this envelope is that, for any state of stress represented by a Mohr's circle lying completely within the envelope the material will not fail, whereas if any part of the circle crosses or touches the curve the failure will take place, see Figure 5.2.2(a).

When the envelope curve is a straight line, Mohr's failure criterion is expressed as:

$$\tau_n = s_o + \sigma_n \tan\phi \qquad (5.2.13)$$

where s_o is referred to as the coherent coefficient, and ϕ is called the internal friction angle.

This line is shown in Figure 5.2.2 (b). Comparison of Equation 5.2.13 with Equation 5.2.2 shows that the Coulomb-Navier criterion is identical to a linear Mohr
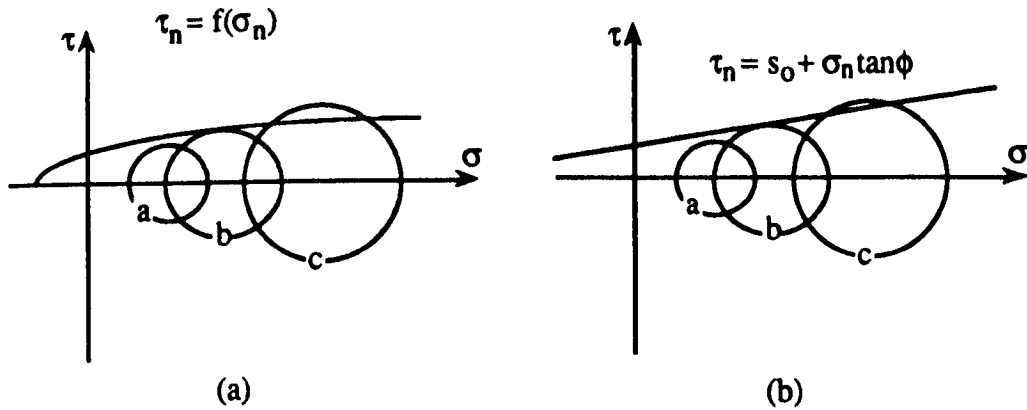
Figure 5.2.2 Illustration of the Mohr's failure criterion.

envelope. The criterion expressed by Equation 5.2.13 is thus known as the Mohr-Coulomb criterion.

5.2.3 Griffith's Brittle Fracture Theory

Using the elliptical hole theory of elasticity, Griffith studied the phenomenon of stress concentration at the tips of minute cracks that are penetrated through a plane. He put forward a fracture criterion which states that failure takes place at a point in a brittle material if the principal stresses at this point σ_1 and σ_3 satisfy the following identities,

$$
\begin{aligned}
(\sigma_1 - \sigma_3)^2 &= 8T_0(\sigma_1 + \sigma_3) \quad \text{if } \sigma_1 + 3\sigma_3 > 0 \\
\sigma_3 &= -T_0; \quad\quad\quad\quad\quad \text{if } \sigma_1 + 3\sigma_3 < 0
\end{aligned} \tag{5.2.14}
$$

Where T_0 is the uniaxial tensile strength of the material.

Murrell (1963) showed that the Griffith criterion (5.2.14) is equivalent to a parabolic Mohr's envelope, expressed by

$$
\tau_n^2 + 4T_0\sigma_n = 4\,T_0^2 \tag{5.2.15}
$$

172

5.2.4 Von Mises' Yielding Theory.

This theory (Von Mises, 1913) postulates that the yielding failure of material is caused due to the distortional energy per unit volume exceeding a critical value. The yielding failure criterion can be expressed by

$$\sqrt{(\sigma_1 - \sigma_2)^2 + (\sigma_2 - \sigma_3)^2 + (\sigma_3 - \sigma_1)^2} = \sqrt{2\sigma_0} \qquad (5.2.16)$$

where σ_0 is the yield stress in simple tension or compression.

The Von Mises' failure theory was developed from studies on metals. Since the yield stress σ_0 in simple tension for rocks is quite different from that in compression, the theory is very rarely applied in rock engineering assessments.

5.2.5 Tresca's Yielding Criterion

Tresca (1868) proposed a yielding criterion on the basis of the maximum shear stress. This criterion is shown by

$$\frac{\sigma_1 - \sigma_3}{2} = K \qquad (5.2.17)$$

where K is some constant which is determined by testing materials.

In two dimensional cases, Tresca deduced the relation between the constant K and σ_0 in Equation 5.2.16, namely $K = \sigma_0/\sqrt{3}$. Comparing the Tresca's failure theory with the Coulomb's, it is not difficult to find that both theories have the same form. Only the critical values i.e. the K in the Tresca's theory and the s_0 in the Coulomb's theory, are given different meanings.

Although these criteria were initially proposed on the basis of investigations into metal materials, some of them were later applied to rock mechanics. A review of these criteria shows that most of the failure theories assume the maximum shear stress to be the source of failure in materials. Since it incorporates both internal friction and

173

cohesive characteristics of materials and has a simpler form in expression, the Mohr-Coulomb failure criterion seems to have been popularly accepted in rock engineering assessment for the sake of mathematical convenience and ease, though Tresca's criterion Equation 5.2.17 has been used to evaluate the plastic radius around a circular excavation in a hydrostatic stress field by Fara and Wright (1963).

5.2.6 Empirical Failure Criteria

Apart from the above mentioned classical failure theories, some empirical failure criteria have also been suggested over recent decades. These empirical failure criteria are proposed essentially on the basis of the vast amount of triaxial test data which are available. They contain no hypotheses of conditions under which a rock will fail. Each criterion is so constituted that it gives the best possible fit to the data points plotted in a relevant coordinate space. Since rocks encountered in engineering sites vary in properties and have different responses to loading, the empirical failure criteria have a large number of possible expression forms. Of these, two empirical failure criteria need to be mentioned in this section. One is that by Hoek and Brown (1980) and the other by the Mining Engineering Department at the University of Nottingham.

5.2.6.1 Hoek and Brown Failure Criterion

After examining a wide range of experimental data from vast rock sample tests and considering rock discontinuity features, Hoek and Brown (1980) proposed the following rock mass failure criterion by relating together the maximum and minimum stresses at the occurrence of failure.

$$\sigma_1 = \sigma_3 + \sqrt{m_i \sigma_c \sigma_3 + s_i \sigma_c^2} \qquad (5.2.18)$$

where m_i and s_i are constants determined by the properties of rock and discontinuities pre-existing in the rock mass prior to failure; σ_c is the uniaxial compressive strength.

5.2.6.2 Frith's Failure Criterion

174

Frith (1988) modified the Hoek and Brown failure criterion. He proposed a failure criterion in the form relating the maximum and minimum stresses at failure as follows:

$$\sigma_1 = \sigma_3 + \sqrt{m_i\, \sigma_c\, \sigma_3^B + s_i\, \sigma_c^2} \qquad (5.2.19)$$

where m, si, and B are constants depending on the condition identically described by the Hoek and Brown failure criterion.

Frith's failure criterion contains one more constant than that of the Hoek and Brown's. And no further interpretation was given as to how the values of the constants were estimated.

In fact there exists an evident difference between the Hoek and Brown failure criterion and that of Frith's. The former is dimensionally homogeneous since every item in Equation 5.2.18 has a common dimension which is FL^{-2} (where F represents force and L the length), whilst the latter does not possess such features unless the constant B is identically equal to 1. An empirical equation being dimensionally homogeneous is advantageous over others, particularly when it is to be used in theoretical derivations and physical modelling.

5.2.3 Tunnel Failure Prediction Theory

One of the important applications of the rock failure theories discussed in the previous section is for prediction of rock failure zones around tunnels. An accurate prediction of tunnel stability would assist the tunnel designer in determination of tunnel cross–section in terms of dimension, shape, choice of support system and installation method. However, difficulties regarding mathematical treatments arise in the course of development of a prediction theory, which eventually blocks the advance of theoretical prediction techniques. Up to now, only one analytical prediction theory proposed by Fara and Wright (1963) has often been referred to in

the vast amount of rock mechanics literature, though, over last few years, similar work on this aspect has been attempted in the Department of Mining Engineering, particularly by Frith (1988).

5.2.3.1 Fara and Wright Theory

In the Fara and Wright (1963) tunnel failure prediction theory, elastoplastic theory is employed to evaluate stresses around a tunnel. After proper mathematical operations a predicted plastic failure radius is evaluated, by which intact and failed rock zones are distinguished. In the course of analysis, the theory of plasticity is restricted to an equilibrium condition within the stressed body. In other words, all deformation has stopped changing with time.
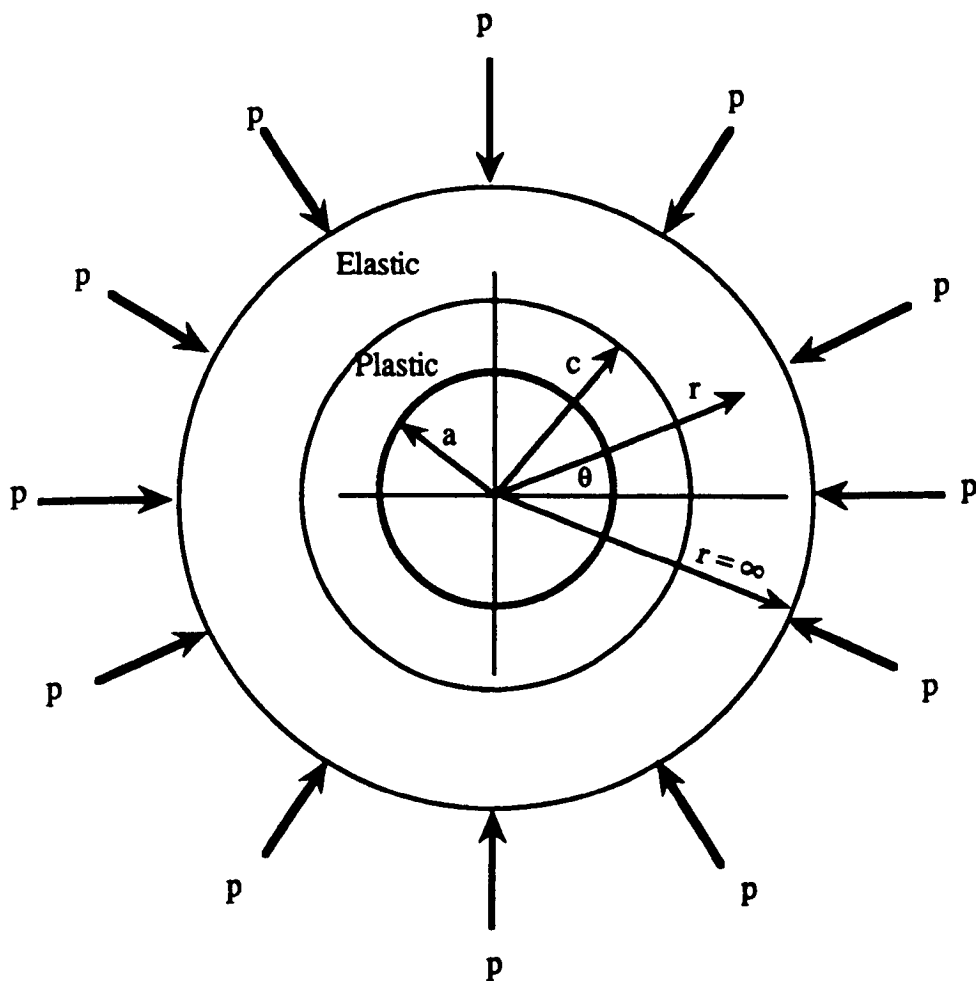
Figure 5.2.3 A tunnel failure prediction model (after Fara and Wright, 1963)

176

The theory considers a long circular tunnel excavated in an elastoplastic rock which is originally under a hydrostatic ground pressure condition, as shown in Figure 5.2.3. It is assumed that plastic failure (yielding) occurs in the rock when the Tresca's failure criterion Equation 5.2.17 is satisfied. In the polar coordinate system, the Tresca's failure criterion becomes:

$$\sigma_{\theta e} - \sigma_{re} = 2K \qquad (5.2.20)$$

where the suffix e is used to indicate that the discussion is restricted to the elastic zone, and thus $\sigma_{\theta e}$ and σ_{re} are the tangential and radial stresses in the elastic zone.

Similarly, in the plastic zone stresses still satisfy the Tresca criterion, namely

$$\sigma_{\theta p} - \sigma_{rp} = 2K \qquad (5.2.21)$$

where the suffix p indicates the discussion in the plastic zone.

The symmetric nature of the problem enables the equilibrium conditions in polar coordinates (as shown by Equation 4.2.34 but ignoring the body force) to be simplified for the plastic zone as:

$$\frac{\partial \sigma_{rp}}{\partial r} = \frac{\sigma_{\theta p} - \sigma_{rp}}{r} \qquad (5.2.22)$$

In the elastic zone, the equilibrium and the compatibility equations for polar coordinates are:

$$\frac{\partial \sigma_{re}}{\partial r} = \frac{\sigma_{\theta e} - \sigma_{re}}{r} \qquad (5.2.23)$$

$$(\frac{\partial^2}{\partial r^2} + \frac{1}{r}\frac{\partial}{\partial r})(\sigma_{\theta e} + \sigma_{re}) = 0 \qquad (5.2.24)$$

The solution to the above three equations must satisfy the following boundary conditions:

$$\sigma_{rp}|_{r=a} = 0 \qquad \sigma_{rp}|_{r=c} = \sigma_{re}|_{r=c} \Big\rangle$$
$$\sigma_{\theta e}|_{r=\infty} = \sigma_{re}|_{r=\infty} = p \qquad \sigma_{\theta p}|_{r=c} = \sigma_{\theta e}|_{r=c} \Big\rfloor \qquad (5.2.25)$$

where a is the radius of the circular tunnel, c is the radius of the boundary between the plastic and elastic zones, and p is the applied hydrostatic ground pressure.

Substitution of the Tresca's criterion of Equation 5.2.21 into Equation 5.2.22 gives

$$\frac{\partial \sigma_{rp}}{\partial r} = \frac{2K}{r}$$

Direct integration and then evaluation at the tunnel periphery (i.e. r = a), of this equation gives the solution for radial stress in the plastic zone as:

$$\sigma_{rp} = 2K \ln \frac{r}{a} \qquad (5.2.26)$$

From Equation 5.2.21, the tangential stress in the plastic zone is found as

$$\sigma_{\theta p} = 2K(1 + \ln \frac{r}{a}) \qquad (5.2.27)$$

From the discussion in the preceding chapter, stresses that satisfy Equations 5.2.23 and 5.2.24 are of the form:

$$\sigma_{re} = A + \frac{B}{r^2} \Big\rangle$$
$$\sigma_{\theta e} = A - \frac{B}{r^2} \Big\rfloor \qquad (5.2.28)$$

Evaluation of Equations 5.2.28 at r = ∞ gives A = p, and at r = c gives:

$$\sigma_{re}|_{r=c} = p + \frac{B}{c^2} = 2K \ln \frac{c}{a} = \sigma_{rp}|_{r=c} \Big\rangle$$
$$\sigma_{\theta e}|_{r=c} = p - \frac{B}{c^2} = 2K(1 + \ln \frac{r}{a}) = \sigma_{\theta p}|_{r=c} \Big\rfloor \qquad (5.2.29)$$

By solving these equations, B and c are found to be:

$$B = - Ka^2 e^{(p-k)/k}$$
$$c = a\ e^{(p-k)/2k}$$

(5.2.30)

And the stresses in the intact zone are:

$$\sigma_{rc} = p - K\frac{a^2}{r^2} e^{(p-k)/k}$$
$$\sigma_{\theta c} = p + K\frac{a^2}{r^2} e^{(p-k)/k}$$

(5.2.31)

The significance of the Fara and Wright theory lies in that it has the tunnel failure zone to be closely connected to the features of excavation diameter a, ground pressure p and the rock property K, and that the expressions of stresses in both failed and intact zones and the failure radius are simple.

In this theory, however, the Tresca failure criterion has been incorporated. Since the criterion represents a horizontal line in the $\sigma - \tau$ space, which cannot satisfactorily describe the rock strength characteristics and thus the precision of tunnel failure prediction by the Fara and Wright theory is obviously restricted.

5.2.3.2 IEM Prediction Theory

Over the last few years, a number of investigators in the Department of Mining Engineering have dedicated great efforts to the development of tunnel failure prediction theory. A theory termed Independent Element Method (IEM) has been proposed (Bonsall, 1985, Kapusniak, 1986, and Frith, 1988). This theory and corresponding computer program have received much attention from successive research students in the Department. Therefore it deserves a brief review and comment in the following part of this chapter.

In the IEM prediction theory, an attempt was made to evaluate the rock failure scope around a circular tunnel driven in stratified Coal Measures. The strata sequence around the tunnel was firstly discretised by using a mesh system defined in terms of

radial and tangential increments (dr and dθ respectively). A polar coordinate system was employed with the origin being set at the tunnel centre, as is commonly done for similar problems as shown in Chapter 4. By the assumption that the ground is subject to a hydrostatic pressure field, a corresponding equilibrium equation in the polar coordinate system was simplified as:

$$\frac{d\sigma_r}{dr} = \frac{\sigma_\theta - \sigma_r}{r} \tag{5.2.32}$$

Incorporation of various empirical failure criteria into the above equation enables the stress σ_θ to be expressed in terms of σ_r and removed from the equation, which makes a direct integration of the resultant equation possible. For instance, the following failure criterion was used (Frith, 1988):

$$\sigma_\theta = A\sigma_r^B + C \qquad \text{pre-failure strength} \tag{5.2.33}$$

$$\sigma_\theta = A'\sigma_r^{B'} + C' \qquad \text{post-failure strength} \tag{5.2.34}$$

where A, B, C, A', B', and C' are constants determined by the rock properties.

Then substitution of Equation 5.2.34 into Equation 5.2.32 produces an expression for the change in radial stress over a radial increment of the yield zone, given by

$$d\sigma_r = \frac{A'\sigma_r^{B'} + C' - \sigma_r}{r} dr \tag{5.2.35}$$

This equation can be solved by numerical methods with the initial value of σ_r being given as $\sigma_r = p_0$ at $r = r_0$. Recorded here is an incremental procedure to solve for the radial stress at all elements as stated by Frith (1988):

For the first element adjacent to the tunnel boundary, the first approximation for σ_{r1} (of the first element) is:

$$p_0 + d\sigma_{r1} = p_0 + \frac{A'p_0^{B'} + C' - p_0}{r_0} dr = p_1$$

The second approximation for σ_{r1} is

$$p_0 + \frac{1}{2} \left[\frac{A'p_1^{B'} + C' - p_1}{r_0 + dr} + \frac{A'p_0^{B'} + C' - p_0}{r_0} \right] dr = p_2$$

The third approximation for σ_{r1} is

$$p_0 + \frac{1}{2} \left[\frac{A'p_2^{B'} + C' - p_2}{r_0 + dr} + \frac{A'p_1^{B'} + C' - p_1}{r_0 + dr} \right] dr = p_3$$

Until the nth approximation for σ_{r1} is

$$p_0 + \frac{1}{2} \left[\frac{A'p_{n-1}^{B'} + C' - p_{n-1}}{r_0 + dr} + \frac{A'p_{n-2}^{B'} + C' - p_{n-2}}{r_0 + dr} \right] dr = p_n$$

The iteration is repeated until $|p_n - p_{n-1}| \leq \alpha$ where α is some predetermined small value, e.g. 1Pa, then $\sigma_{r1} = p_n$.

This procedure is performed for all of the elements along the radial line under consideration, with σ_{ri} and r_i replacing p_0 and r_0 respectively, i.e. the known values of σ_r and r for the previous element are used as the initial values for the next iteration sequence.

Obviously, such an attempt is constructive, although the theory deserves further discussion before some suspicions can be eliminated.

The IEM prediction theory was claimed to be applicable to stratified Coal Measures cases. However, when it is applied to Coal Measures, most elements defined by the IEM mesh will contain stratified structures. It can be found in such cases that the equilibrium condition for a single element can not be determined merely by Equation 5.2.32, when the element contains more than one rock type. In other words, the equilibrium of the element is also governed by the conditions of interaction between layers within the element. An interface having a high bonding strength will behave differently from that with weak or zero bonding strength. In these circumstances, a multi-layered element can hardly achieve equilibrium in both reality

and theory. This indicates that the use of Equation 5.2.32 to form the stress equilibrium condition is not sufficient and the stress components found by Equation 5.2.32 do not truly exist in the element. As a result of this, the consequence of prediction by the IEM theory becomes doubtful.

Moreover, the incremental procedure for solving the stress of each element, as stated above, was not clearly described. The physical and mathematical meanings of each step were unclear. Therefore the validity of them also remains to be verified.

The above discussion shows that the present tunnel failure prediction theories more or less have shortcomings. A common feature is that the performance of supports is simplified as either a constant resistance or non-resistance. These shortcomings indicate a need for further development of the tunnel failure prediction theory and technique. As a result, an attempt is made in the following section to seek a new model for the tunnel failure prediction technique.

5.3 Further Developments of the Tunnel Failure Prediction Theory

5.3.1 Tunnel Failure Prediction Model

In order to propose a new tunnel failure prediction model, considerations are given to the following aspects.

(1) Tunnels driven in weak and medium strength rocks at great depths need to be firstly studied at present since they are more likely to be subject to severe ground deformation that happens gradually and gently and to cause instability problems. Such instability problems are becoming matters of increasing concern to the coal industry and are drawing much attention, as coal mining activities move towards deeper resources.

(2) A very common and popular measure, taken for the alleviation of tunnels from deformation damage, is the employment of circular cross sections of tunnels and

closed form supports. To cope with this type of cross-section, a number of circular supports have been invented and employed. Concrete block ring supports, reinforced concrete linings, yielding steel ring supports, and shotcrete wire-mesh rock bolt systems are among those that are seen to be effective to various degrees in some countries. In British Coal, reinforced concrete block ring supports and yielding steel ring supports have been seen in use in a number of collieries, such as those at the Selby Complex.

Successful supports used in such cases seem to have two common features, namely sufficient strength and reasonable yieldability.

(3) Underground practice indicates that surrounding rocks in adverse tunnelling circumstances, particularly in weak and soft ground conditions at great depths, usually undergo unrestorable deformations or plastic flows in the regions where highly concentrated stresses are initially present upon the excavation of the tunnel. As a result of plastic flow, the peak stress in the surrounding rock will be reduced and moved outwards, and highly accumulated energy in the region is gradually released in the process of plastic deformation.

(4) The state of ground pressure in deep rock tunnelling conditions has a significant effect on tunnel stability. At great depths such as those towards and beyond 1000 metres, the distribution of measured values for the ratio of the vertical to horizontal ground pressures tends to narrow to a range on either side of unity (Frith, 1988). This is to say that the original ground pressure field tends to become hydrostatic. A possible explanation for this phenomenon is that geological creep over millions of years might have readjusted the various stress components in the rock. As a result, the ground stress components tend to be equalised (Wilson, 1980).

Upon these considerations, a mathematical model is proposed, see Figure 5.3.1. This model represents a circular tunnel of radius r = b driven in a homogeneous and isotropic rock mass. Under the effect of a hydrostatic stress field,
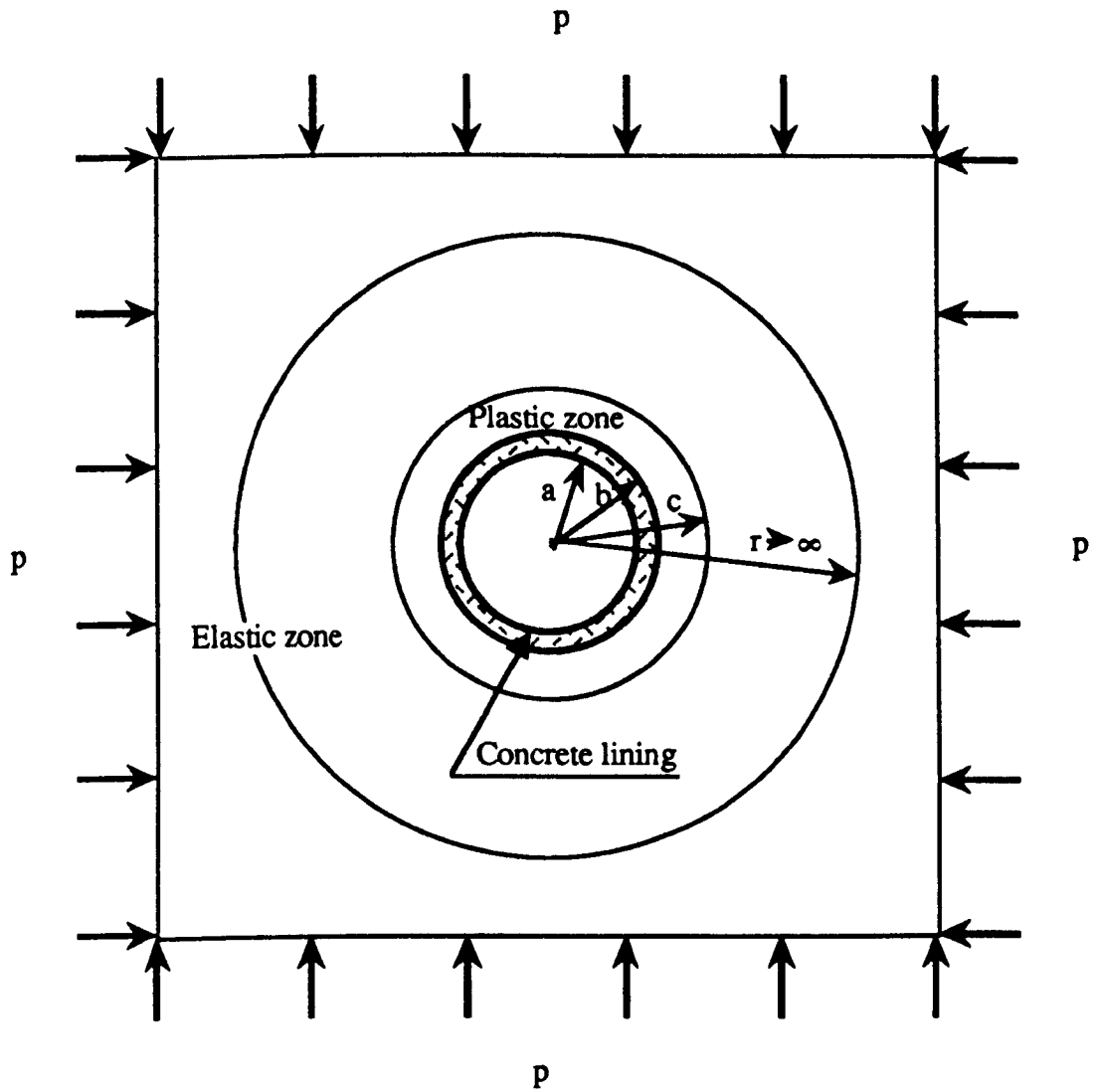
Figure 5.3.1 Model of a tunnel in a hydrostatic stress field

the immediate surrounding rock of radius $r = c$ has undergone plastic flow, whilst elsewhere the rock is intact and within the elastic limit. A circular concrete support is used. The interior and exterior radii of the support are $r=a$ and $r=b$, respectively. The support is assumed to have perfect contact with the surrounding rock.

The original ground pressure is equal to p. Compared with the ground pressure, body force of the rock mass is so small that it is neglected in this analysis. Since the tunnel is considerably long and uniformly loaded, it is assumed that tunnel deformation take place within the planes perpendicular to the tunnel axis, namely a

plane strain problem exists. Rock failure will occur when the stress state at the point under discussion satisfies the Mohr-Coulomb failure criterion:

$$\tau_n = s_0 + \sigma_n \tan\phi \qquad (5.3.1)$$

where s_0 is the coherent coefficient, and ϕ is called the internal friction angle.

Since the problem becomes an axial symmetric plane problem, the tangential and radial stress components around the tunnel become the principal stresses. Therefore, the Mohr-Coulomb failure criterion (Equation 5.3.1) can be expressed (see Figure 5.3.2) as:

$$\frac{\sigma_\theta - \sigma_r}{2} = (s_0\cot\phi + \sigma_r)\frac{\sin\phi}{1-\sin\phi} \qquad (5.3.2)$$
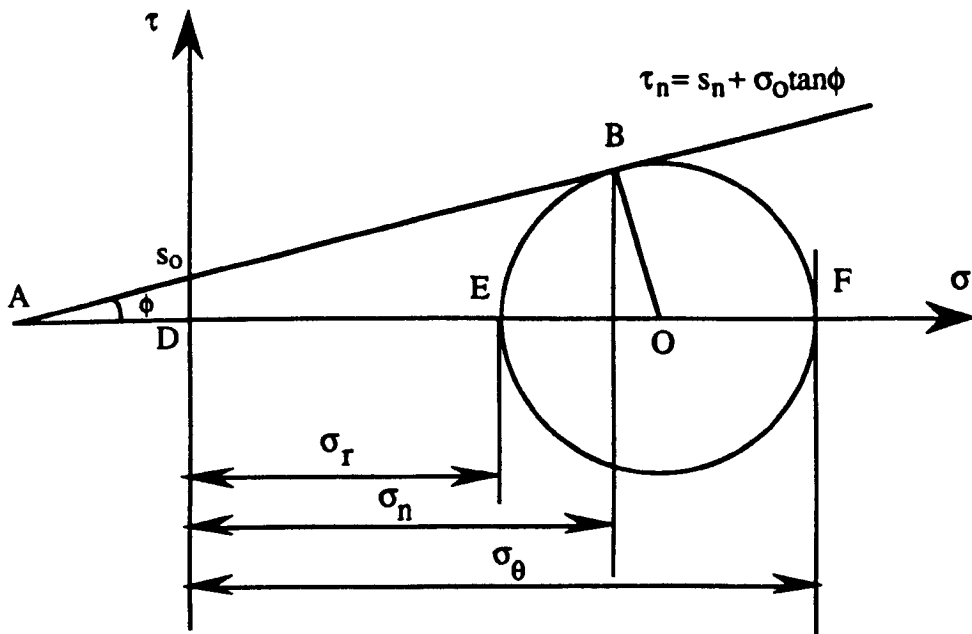
$$OB = OA \sin\phi = (AD + DE + EO)\sin\phi$$

Figure 5.3.2 The relation between the stress components and the failure criterion.

185

5.3.2 Basic Equations and Boundary Conditions

Deformation around tunnels may be elastic or plastic; if the movement is small and reversible the deformation is elastic and if the movement is large and irreversible it is plastic. No matter in the elastic or plastic state, when a rock is in equilibrium, the stress components in the rock (homogeneous and isotropic) should satisfy the equilibrium equations 5.3.3 if the body forces are negligible:

$$\left.\begin{array}{l} \dfrac{\partial \sigma_r}{\partial r} + \dfrac{\sigma_r - \sigma_\theta}{r} + \dfrac{1}{r}\dfrac{\partial \tau_{r\theta}}{\partial \theta} = 0 \\[3mm] \dfrac{1}{r}\dfrac{\partial \sigma_\theta}{\partial \theta} + \dfrac{\partial \tau_{r\theta}}{\partial r} + \dfrac{2\tau_{r\theta}}{r} = 0 \end{array}\right\} \tag{5.3.3}$$

The difference in the deformation behaviour gives rise to a need for the movements to be described separately. In the elastic range the movement of rock will satisfy the geometric equations (5.3.4) and Hooke's law (5.3.5):

$$\left.\begin{array}{l} \varepsilon_r = \dfrac{\partial u}{\partial r} \\[3mm] \varepsilon_\theta = \dfrac{u}{r} + \dfrac{1}{r}\dfrac{\partial v}{\partial \theta} \\[3mm] \gamma_{r\theta} = \dfrac{1}{r}\dfrac{\partial u}{\partial \theta} + \dfrac{\partial v}{\partial r} - \dfrac{v}{r} \end{array}\right\} \tag{5.3.4}$$

where u and v are the radial and tangential displacements, respectively; θ is the angle of orientation; and ε_r, ε_θ and $\gamma_{r\theta}$ are the radial and tangential normal strains and the shear strain, respectively.

$$\left.\begin{array}{l} \varepsilon_r = \dfrac{1-v^2}{E}\left(\sigma_r - \dfrac{v}{1-v}\sigma_\theta\right) \\[3mm] \varepsilon_\theta = \dfrac{1-v^2}{E}\left(\sigma_\theta - \dfrac{v}{1-v}\sigma_r\right) \end{array}\right\} \tag{5.3.5}$$

where E and v are the rock elastic modulus and Poisson's ratio, respectively.

186

For the plastic zone, shear stresses are considered to be predominant in causing plastic failures. Therefore, the volume of rock is popularly assumed to remain constant in the plastic zone, i.e.

$$\varepsilon_r + \varepsilon_\theta + \varepsilon_z = 0 \qquad (5.3.6)$$

where ε_r, ε_θ and ε_z are the three normal strain components at the point under discussion with the z axis being defined to be parallel with the tunnel axis.

By the assumption of a hydrostatic stress field and axial symmetric plane strain occurrence, the following identities hold :

$$\tau_{r\theta} = 0; \ \frac{\partial \sigma_\theta}{\partial \theta} = 0 \ ; \ \frac{\partial v}{\partial \theta} = 0 \ ; \ \gamma_{r\theta} = 0; \ \frac{\partial u}{\partial \theta} = 0; \text{ and } \varepsilon_z = 0 \qquad (5.3.7)$$

Equations 5.3.3, 5.3.4 and 5.3.6 are thus simplified as:

equilibrium condition
$$\frac{\partial \sigma_r}{\partial r} + \frac{\sigma_r - \sigma_\theta}{r} = 0 \qquad (5.3.8)$$

geometric equations in the elastic range
$$\left. \begin{array}{c} \varepsilon_r = \dfrac{\partial u}{\partial r} \\[2mm] \varepsilon_\theta = \dfrac{u}{r} \end{array} \right\} \qquad (5.3.9)$$

incompressible condition in the plastic zone: $\dfrac{\partial u}{\partial r} + \dfrac{u}{r} = 0$ \qquad (5.3.10)

Of the model illustrated in Figure 5.3.1, three zones are distinguished as follows:

(i) Concrete support zone.

The material in this zone is assumed to be within the elastic limit, since the support is not expected to have failed. From the elastic theory, stress components in the support must satisfy the equilibrium condition.

(ii) Plastic zone in rock

187

(iii) Elastic zone in rock

The boundary conditions for these zones are considered as:

Zone I:
$$\left.\begin{array}{ll} \text{when } r = a & \sigma_{r1} = \tau_{r\theta 1} = 0 \\ \text{when } r = b & \sigma_{r1} = \sigma_{r2} \text{ and } \tau_{r\theta 1} = \tau_{r\theta 2} = 0 \end{array}\right\} \qquad (5.3.11)$$

Here the subscriptive index numbers, 1 and 2, indicate the stress components on the boundary of the relevant zone I and II, respectively.

Zone II: Stress components on the boundaries (r = b and r = c) satisfy the Mohr-Coulomb failure criterion (5.3.2),

Zone III:
$$\left.\begin{array}{ll} \text{when } r = c & \sigma_{r2} = \sigma_{r3} \text{ and } \tau_{r\theta 2} = \tau_{r\theta 3} = 0 \\ \text{when } r = d = \infty & \sigma_{\theta 3} = \sigma_{r3} = p \end{array}\right\} \qquad (5.3.12)$$

5.3.3 Analytical Solution of Stress and Displacement in the Surrounding Rock and Support

Based on the above analysis and assumptions, the stress and strain in the three zones are deduced in this section.

5.3.3.1 Stress and Displacement in the Elastic Zone of Surrounding Rock

In the zone III the stresses and displacements are elastic. The zone can be seen as a thick wall cylinder with interior radius r = c and exterior radius r = ∞, which is subjected to the effect of a hydrostatic stress p and an interior pressure on r = c. Thus the solution to the stresses in this zone may, according to the thick wall cylinder theory, have the form:

$$\left.\begin{array}{l} \sigma_{r3} = A_3 - \dfrac{B_3}{r^2} \\ \sigma_{\theta 3} = A_3 + \dfrac{B_3}{r^2} \end{array}\right\} \qquad (5.3.13)$$

188

where A_3 and B_3 are undetermined constants depending on the boundary conditions of zone III.

Substitution of the second condition of Equation 5.3.12 into Equation 5.3.13 gives

$$A_3 = p \qquad (5.3.14)$$

From Equation 5.3.13 it is obtained that

$$\sigma_{\theta 3} - \sigma_{r 3} = 2 \frac{B_3}{r^2} \qquad (5.3.15)$$

Applying boundary conditions of Equations 5.3.2 and 5.3.12 to Equation 5.3.15 gives

$$\frac{\sigma_{\theta 3} - \sigma_{r 3}}{2}\bigg|_{r=c} = (s_0 \cot\phi + \sigma_{r 3}|_{r=c}) \frac{\sin\phi}{1-\sin\phi} = \frac{B_3}{c^2} \qquad (5.3.16)$$

Using Equations 5.3.13 and 5.3.14 in Equation 5.3.16 to eliminate $\sigma_{r 3}$ produces

$$(s_0 \cot\phi + p - \frac{B_3}{c^2}) \frac{\sin\phi}{1-\sin\phi} = \frac{B_3}{c^2} \qquad (5.3.17)$$

Thus,

$$B_3 = (s_0 \cot\phi + p)c^2 \sin\phi \qquad (5.3.18)$$

Substitution of Equations 5.3.14 and 5.3.18 into Equations 5.3.13 yields the stress distribution in the elastic zone of the rock, given by

$$\left.\begin{array}{l} \sigma_{r 3} = p - \dfrac{(s_0 \cot\phi + p)c^2 \sin\phi}{r^2} \\[2mm] \sigma_{\theta 3} = p + \dfrac{(s_0 \cot\phi + p)c^2 \sin\phi}{r^2} \end{array}\right\} \qquad (5.3.19)$$

Inputting Equations 5.3.19 into the second of Equations 5.3.5 gives

189

$$\varepsilon_{\theta 3} = \frac{1-\upsilon_3{}^2}{E_3} \left\{ p + \frac{(s_o\cot\phi + p)c^2\sin\phi}{r^2} - \frac{\upsilon_3}{1-\upsilon_3}\left[p - \frac{(s_o\cot\phi+p)c^2\sin\phi}{r^2}\right]\right\}$$

$$= \frac{1+\upsilon_3}{E_3}\left[(1-2\upsilon_3)p + \frac{(s_o\cot\phi + p)c^2\sin\phi}{r^2}\right] \qquad (5.3.20)$$

where E_3 and υ_3 are the elastic module and Poisson's ratio of the intact rock in zone III.

Substitution of Equation 5.3.20 into the second of Equations 5.3.9 yields the radial displacement u_3, given by

$$u_3 = r\varepsilon_{\theta 3} = r\frac{1+\upsilon_3}{E_3}\left[(1-2\upsilon_3)p + \frac{(s_o\cot\phi + p)c^2\sin\phi}{r^2}\right] \qquad (5.3.21)$$

5.3.3.2 Stress and Displacement in the Plastic Zone around the Tunnel

In the plastic zone, i.e. zone II, of rock in the immediate vicinity of tunnel, the stress components should satisfy the equilibrium equation 5.3.8. Since the rock in this zone has failed plastically, the Mohr-Coulomb's failure criterion should apply in the zone. Hence Equation 5.3.2 can be combined into Equation 5.3.8, which yields

$$\frac{\partial\sigma_{r2}}{\partial r} + \frac{2(s_o\cot\phi + \sigma_{r2})\dfrac{\sin\phi}{1-\sin\phi}}{r} = 0 \qquad (5.3.22)$$

This may be rearranged as:

$$\frac{\partial\sigma_{r2}}{(s_o\cot\phi + \sigma_{r2})} = -2\frac{\sin\phi}{1-\sin\phi}\frac{\partial r}{r}$$

The solution to this equation is:

$$\lg(s_o\cot\phi + \sigma_{r2}) = -2\frac{\sin\phi}{1-\sin\phi}\lg r + \lg A_2$$

or $\qquad\qquad \sigma_{r2} = A_2\, r^{-2\frac{\sin\phi}{1-\sin\phi}} - s_o\cot\phi \qquad (5.3.23)$

where A_2 is the integration constant, which is determined by the boundary conditions.

Using the boundary conditions in Equation 5.3.12, it is arrived from Equations 5.3.23 and 5.3.19 that:

when $r = c$, $\qquad A_2 c^{-2\frac{\sin\phi}{1-\sin\phi}} - s_o\cot\phi = p - (s_o\cot\phi + p)\sin\phi$

Hence $\qquad A_2 = (s_o\cot\phi + p)(1 - \sin\phi)\, c^{2\frac{\sin\phi}{1-\sin\phi}}$ $\qquad\qquad$ (5.3.24)

Substitution of Equation 5.3.24 into Equation 5.3.23 gives:

$$\sigma_{r2} = (s_o\cot\phi + p)(1 - \sin\phi)(\frac{c}{r})^{2\frac{\sin\phi}{1-\sin\phi}} - s_o\cot\phi \qquad\qquad (5.3.25)$$

Inputting Equation 5.3.25 in Equation 5.3.2 results in

$$\sigma_{\theta2} = (s_o\cot\phi + p)(1 + \sin\phi)(\frac{c}{r})^{2\frac{\sin\phi}{1-\sin\phi}} - s_o\cot\phi \qquad\qquad (5.3.26)$$

Using the incompressible condition in the plastic zone and the plane strain condition, as shown by Equation 5.3.10, the radial displacement u_2 is found, by solving Equation 5.3.10, as

$$u_2 = \frac{B_2}{r} \qquad\qquad (5.3.27)$$

where B_2 is a constant to be determined by a relevant boundary condition at $r = c$, namely:

$$u_2\, |_{r=c} = u_3\, |_{r=c} \qquad\qquad (5.3.28)$$

Combining Equations 5.3.21 and 5.3.27 into Equation 5.3.28 yields:

$$B_2 = c^2 \frac{1+v_3}{E_3} [\, (1-2v_3)p + (s_o\cot\phi + p)\sin\phi] \qquad\qquad (5.3.29)$$

191

Therefore, Equation 5.3.27 becomes:

$$u_2 = \frac{c^2}{r} \frac{1+v_3}{E_3} [\,(1-2v_3)p + (s_0 \cot\phi + p)\sin\phi]$$ (5.3.30)

5.3.3.3 Stress and Displacement in Concrete Support

Stresses in the concrete support are not expected to exceed the elastic limit of the support material, in order that the support can perform the desired functions in protecting the surrounding rock from falling. This means that the assumption of elastic zone I for the support is appropriate.

As stated earlier, stress, strain and displacement components in the elastic zone within the support should satisfy the equilibrium equation (Equation 5.3.8), the geometric equations (Equations 5.3.9) and the constitutive equations (Equations 5.3.5).

Since the problems are now confined within zone I, all arguments in the relevant equations should be denoted by the subscriptive index 1, such that, Equation 5.3.8 becomes

$$\frac{\partial \sigma_{r1}}{\partial r} + \frac{\sigma_{r1} - \sigma_{\theta 1}}{r} = 0$$ (5.3.31)

Equations 5.3.9 become

$$\left. \begin{array}{l} \varepsilon_{r1} = \dfrac{du_1}{dr} \\[2mm] \varepsilon_{\theta 1} = \dfrac{u_1}{r} \end{array} \right\}$$ (5.3.32)

And Equations 5.3.5, after proper arrangement, become:

$$\left. \begin{array}{l} \sigma_{r1} = \dfrac{E_1(1-v_1)}{(1+v_1)(1-2v_1)} \left(\varepsilon_{r1} + \dfrac{v_1}{1-v_1}\varepsilon_{\theta 1} \right) \\[4mm] \sigma_{\theta 1} = \dfrac{E_1(1-v_1)}{(1+v_1)(1-2v_1)} \left(\varepsilon_{\theta 1} + \dfrac{v_1}{1-v_1}\varepsilon_{r1} \right) \end{array} \right\}$$ (5.3.33)

192

Now substituting Equations 5.3.32 into Equations 5.3.33 gives:

$$\left. \begin{array}{l} \sigma_{r1} = \dfrac{E_1(1-v_1)}{(1+v_1)(1-2v_1)} \left(\dfrac{du_1}{dr} + \dfrac{v_1}{1-v_1} \dfrac{u_1}{r} \right) \\[4mm] \sigma_{\theta 1} = \dfrac{E_1(1-v_1)}{(1+v_1)(1-2v_1)} \left(\dfrac{u_1}{r} + \dfrac{v_1}{1-v_1} \dfrac{du_1}{dr} \right) \end{array} \right\} \qquad (5.3.34)$$

From the first one of Equations 5.3.34, it is obtained that

$$\dfrac{d\sigma_{r1}}{dr} = \dfrac{E_1(1-v_1)}{(1+v_1)(1-2v_1)} \left[\dfrac{d^2u_1}{dr^2} + \dfrac{v_1}{1-v_1} \left(\dfrac{1}{r} \dfrac{du_1}{dr} - \dfrac{u_1}{r^2} \right) \right] \qquad (5.3.35)$$

Combination of Equations 5.3.34 and 5.3.35 into Equation 5.3.31 gives

$$\dfrac{d^2u_1}{dr^2} + \dfrac{v_1}{1-v_1} \left(\dfrac{1}{r} \dfrac{du_1}{dr} - \dfrac{u_1}{r^2} \right) + \dfrac{1}{r} \left[\left(1 - \dfrac{v_1}{1-v_1} \right) \dfrac{du_1}{dr} - \left(1 - \dfrac{v_1}{1-v_1} \right) \dfrac{u_1}{r} \right] = 0$$

or

$$\dfrac{d^2u_1}{dr^2} + \dfrac{1}{r} \dfrac{du_1}{dr} - \dfrac{u_1}{r^2} = 0 \qquad (5.3.36)$$

This is a homogeneous linear second order differential equation. A general solution to it is:

$$u_1 = A_1 r + \dfrac{B_1}{r} \qquad (5.3.37)$$

Thus Equations 5.3.34 become

$$\left. \begin{array}{l} \sigma_{r1} = \dfrac{E_1(1-v_1)}{(1+v_1)(1-2v_1)} \left[A_1 - \dfrac{B_1}{r^2} + \dfrac{v_1}{1-v_1} \left(A_1 + \dfrac{B_1}{r^2} \right) \right] \\[4mm] \sigma_{\theta 1} = \dfrac{E_1(1-v_1)}{(1+v_1)(1-2v_1)} \left[A_1 + \dfrac{B_1}{r^2} + \dfrac{v_1}{1-v_1} \left(A_1 - \dfrac{B_1}{r^2} \right) \right] \end{array} \right\}$$

or

$$\left. \begin{array}{l} \sigma_{r1} = \dfrac{E_1}{(1+v_1)(1-2v_1)} \left[A_1 + (2v_1-1) \dfrac{B_1}{r^2} \right] \\[4mm] \sigma_{\theta 1} = \dfrac{E_1}{(1+v_1)(1-2v_1)} \left[A_1 + (1-2v_1) \dfrac{B_1}{r^2} \right] \end{array} \right\} \qquad (5.3.38)$$

where the integral constants, A_1 and B_1, are to be determined by the boundary conditions.

Inputting $\sigma_{r1} = 0$ at $r = a$, into Equations 5.3.38 gives:

$$A_1 + (2v_1-1)\frac{B_1}{a^2} = 0$$

Namely, $\qquad\qquad A_1 = (1 - 2v_1)\frac{B_1}{a^2}$ (5.3.39)

Another boundary condition shows that $\sigma_{r1} \mid_{r=b} = \sigma_{r2} \mid_{r=b}$ at $r_1 = b$.

Substituting the first one of Equations 5.3.38 and Equation 5.3.25 into this boundary condition gives:

$$\frac{E_1}{(1+v_1)(1-2v_1)}[A_1 + (2v_1-1)\frac{B_1}{b^2}] = (s_0\cot\phi + p)(1-\sin\phi)(\frac{c}{b})^{2\frac{\sin\phi}{1-\sin\phi}} - s_0\cot\phi$$

As a result of applying Equation 5.3.39 to the above equation, A_1 is eliminated from the equation, resulting in an expression for B_1 given by

$$\frac{E_1 B_1}{(1+v_1)}[\frac{1}{a^2} - \frac{1}{b^2}] = (s_0\cot\phi + p)(1-\sin\phi)(\frac{c}{b})^{2\frac{\sin\phi}{1-\sin\phi}} - s_0\cot\phi$$

Therefore,

$$\left.\begin{array}{l} B_1 = \dfrac{1+v_1}{E_1}\dfrac{b^2a^2}{b^2-a^2}[(s_0\cot\phi+p)(1-\sin\phi)(\frac{c}{b})^{2\frac{\sin\phi}{1-\sin\phi}} - s_0\cot\phi] \\[4mm] A_1 = \dfrac{(1+v_1)(1-2v_1)}{E_1}\dfrac{b^2}{b^2-a^2}[(s_0\cot\phi+p)(1-\sin\phi)(\frac{c}{b})^{2\frac{\sin\phi}{1-\sin\phi}} - s_0\cot\phi] \end{array}\right\} \quad (5.3.40)$$

And Equations 5.3.38 and 5.3.37 become

$$\sigma_{r1} = \frac{b^2}{b^2-a^2}\left(1-\frac{a^2}{r^2}\right)\left[(s_o\cot\phi+p)(1-\sin\phi)\left(\frac{c}{b}\right)^{2\frac{\sin\phi}{1-\sin\phi}} - s_o\cot\phi\right]$$

$$\sigma_{\theta1} = \frac{b^2}{b^2-a^2}\left(1+\frac{a^2}{r^2}\right)\left[(s_o\cot\phi+p)(1-\sin\phi)\left(\frac{c}{b}\right)^{2\frac{\sin\phi}{1-\sin\phi}} - s_o\cot\phi\right]$$

$$u_1 = \frac{1+\nu_1}{E_1}\frac{b^2}{b^2-a^2}\left[(1-2\nu_1)r + \frac{a^2}{r}\right]\left[(s_o\cot\phi+p)(1-\sin\phi)\left(\frac{c}{b}\right)^{2\frac{\sin\phi}{1-\sin\phi}} - s_o\cot\phi\right]$$

$$(5.3.41)$$

5.3.3.4 Determination of the Radius of the Plastic Zone

So far, the expressions regarding stress and displacement components in the three zones have been found to have a relation with the plastic radius, c, (see Equations 5.3.19, 5.3.21, 5.3.25, 5.3.26, 5.3.30 and 5.3.41). If the plastic radius, c, can be found, the stress and displacement in these three zones have a sole solution. In practice, the parameter, c, may be evaluated by in situ instrumentation such as the borehole multi-point extensometer. Here, a theoretical assessment method will be given.

In order to evaluate the plastic radius, c, another continuity condition on the interface between the support and the surrounding rock, namely

$$\text{when } r = b, \qquad u_{1|r=b} = u_{2|r=b} \qquad (5.3.42)$$

should be employed.

Substituting the third in Equations 5.3.41 and Equation 5.3.30 into this continuity condition, Equation 5.3.42 yields:

$$\frac{1+\nu_1}{E_1}\frac{b^2}{b^2-a^2}\left[(1-2\nu_1)b + \frac{a^2}{b}\right]\left[(s_o\cot\phi+p)(1-\sin\phi)\left(\frac{c}{b}\right)^{2\frac{\sin\phi}{1-\sin\phi}} - s_o\cot\phi\right]$$

$$= \frac{c^2}{b}\frac{1+\nu_3}{E_3}\left[(1-2\nu_3)p + (s_o\cot\phi + p)\sin\phi\right]$$

195

or $\frac{1+v_1}{E_1}\frac{b^2}{b^2-a^2}[(1-2v_1)b^2 + a^2][(s_0\cot\phi+p)(1-\sin\phi)(\frac{c}{b})^{2\frac{\sin\phi}{1-\sin\phi}} -s_0\cot\phi]$

$= c^2\frac{1+v_3}{E_3}[(1-2v_3)p + (s_0\cot\phi + p)\sin\phi]$ (5.3.43)

This equation shows that the solution to the plastic radius, c, exists mathematically, although it is implicit rather than explicit. From Equation 5.3.43 it is clearly shown that the plastic radius is closely related to the original ground stress p, rock mass mechanical properties E_3, v_3, s_0, ϕ, support parameters v_1,E_1,(b-a) and the excavation radius a.

There are a number of numerical methods available, coupled with computer aid, to determine the value of plastic radius. Such kinds of work will be described in a later part of this thesis.

5.4 Concluding Remarks

From the above discussion, it can be concluded that the original ground stress, the rock mass mechanical properties including the elastic constants and the limit strength (s_0, ϕ), support features and the tunnel size, all have various effects on the stress distribution and displacements in the surrounding rock. They also have effects on the support behaviour. Since the plastic radius can be evaluated by the expression developed in this Chapter, the range of surrounding rock requiring support becomes more clear. In particular, if a rockbolt is to be used, the desired length of the rockbolt should be so long as the anchor end of the rockbolt will be located in excess of the plastic zone. It is clear that the solutions developed in this Chapter provide the design engineer with a theoretical basis for the analysis, prediction and design of tunnel stability and support at great depths. Parameters involved in the solutions have defined meanings and can be obtained from engineering tests and experiments. A

computer programme using these formulae to predict tunnel stability problems would need far less time than the general finite element programmes. And a personal computer would be enough for carrying out such calculations.

CHAPTER SIX

INVESTIGATIONS INTO THE EFFECTS OF THE APPLIED STRESS FIELD ON TUNNEL STABILITY USING THE PHYSICAL MODELLING TECHNIQUE

CHAPTER SIX

INVESTIGATIONS INTO THE EFFECTS OF THE APPLIED STRESS FIELD ON TUNNEL STABILITY USING THE PHYSICAL MODELLING TECHNIQUE

In the previous two chapters the stress field effects on the stress distribution and deformation around a circular tunnel have been studied theoretically. It has been shown that the stress field is one of the major factors that has a great bearing on tunnel stability. However, a shortcoming in the analysis procedure is that the analytical solutions cannot show the process of the rock fracture development. Indeed, as fractures develop in the vicinity of the rock mass of the tunnel, the boundary conditions of the stability-associated problem in terms of geometry and stress are also changed. Such changes give rise to a difficulty in finding a mathematical solution to the problem as it becomes too complicated to be possibly solved by the available analytical methods. On the other hand, fracture development around tunnels is a main concern in tunnel engineering. Some fractures may result in severe collapses of tunnels and others may not. Ignorance of the effects of fractures on tunnel stability may end in failures of tunnelling design and construction.

In order that the development of various fractures around tunnels can be intensively studied, the physical modelling technique has been employed. In the present Chapter, a focus of the physical modelling investigations is directed onto the effects of the stress field on fracture initiation and development around tunnels.

6.1 Physical Modelling Theory

Physical modelling theory states the relationship between physical models and prototypes. It describes how a prediction from a physical model is made for a corresponding prototype. The theory is based on a subject known as dimensional analysis.

6.1.1 Dimensional Analysis

The need to state units when specifying a physical quantity is obvious in scientific research. Pressures and stresses are measured in Mega-Pascal (MPa), bar, and pounds per square inch, tunnel sizes and closures in metres, centimetres, feet and so on. In the physical modelling theory, the word "dimension" is a notion of units of physical quantities. The dimension of a physical quantity is usually a product of powers of dimensions of some fundamental quantities. There are three fundamental quantities in solid mechanics which may be denoted by x_a, x_b and x_c. By the dimension of these fundamental quantities the dimension of all other quantities encountered in research can be derived. The three fundamental quantities are often those of mass (M), length (L) and time (T), although force (F), length (L) and time (T) may also form the fundamental quantities. If static problems are considered, the number of fundamental quantities is reduced to two. In fact, there are many other choices of the fundamental quantities as long as any one of the selected quantities is independent in dimension of the rest and the dimensions of the selected quantities are sufficient to express the dimensions of all physical quantities involved in the problem.

Assume that the dimensions of the three fundamental quantities are A, B and C. Then the dimension of an arbitrary quantity u, D, can been expressed by

$$D = A^a B^b C^c \qquad (6.1.1)$$

where a,b,c are indeterminate constants.

Given a set of n quantities $(x_1, x_2,...,x_i,...,x_n)$, there exists an infinite number of products of powers of these quantities, as generally shown by

$$u_j = x_1^{k_1} x_2^{k_2}...x_i^{k_i}...x_n^{k_n} \qquad (6.1.2)$$

where the exponents k_i $(i = 1 \dots n)$ may have any positive or negative integral or fractional value including zero. If the dimension of the product u_j is assumed to be D_j and the dimension of the i th quantity x_i, according to Equation.6.1.1, is

$$D_i = A^{a_i} B^{b_i} C^{c_i} \qquad (i = 1,\dots,n) \qquad (6.1.3)$$

then D_j can be expressed by D_i $(i = 1,\dots,n)$ as

$$D_j = A^{a_1k_1+\dots+a_ik_i+\dots+a_nk_n} B^{b_1k_1+\dots+b_ik_i+\dots b_nk_n} C^{c_1k_1+\dots c_ik_i+\dots+c_nk_n} \qquad (6.1.4)$$

This indicates that the dimension D_j of an arbitrary quantity can be expressed by three fundamental dimensions. In other words, D_j is a product of powers of the fundamental dimensions.

The product of powers of n quantities, u_j, is called dimensionless if and only if the exponents of A, B and C in the above equation satisfy the following conditions:

$$\left.\begin{array}{l} \sum_{i=1}^{n} a_i k_i = 0 \\ \sum_{i=1}^{n} b_i k_i = 0 \\ \sum_{i=1}^{n} c_i k_i = 0 \end{array}\right\} \qquad (6.1.5)$$

A set of dimensionless products of powers of the quantities is complete if (1) any dimensionless product of powers of the given quantities that is not in the set can be expressed as a product of powers of members in the set; and (2) no member of the set can be expressed as a product of powers of the remaining members of the set.

Buckingham's theorem (Buckingham, 1914, Langhaar, 1951 and Pankhurst, 1964) states: if an equation is dimensionally homogeneous (i.e. all items in the equation have same dimension), it can be reduced to a relationship among a complete set of dimensionless products $(\pi_1, \pi_2, \dots, \pi_n)$. By the theorem, the equation can be alternatively expressed as

$$\pi_1 = f(\pi_2, \pi_3, .., \pi_n) \qquad (6.1.6)$$

If in Equations.6.1.5 at least one equation does not hold true, namely, the sum on the left hand side in at least one equation does not equal to zero, the product u_j is dimensional.

Now assume that $\sum_{i=1}^{n} a_i k_i = a_j$, $\sum_{i=1}^{n} b_i k_i = b_j$, and $\sum_{i=1}^{n} c_i k_i = c_j$. In this case the quantity

$$\pi_1 = \frac{u_j}{x_a{}^{a_j} x_b{}^{b_j} x_c{}^{c_j}}$$

is dimensionless.

For static problems, since there are only two fundamental units, the above dimensionless product becomes

$$\pi_1 = \frac{u_j}{x_a{}^{a_j} x_b{}^{b_j}} \qquad (6.1.7)$$

It has been shown (Langhaar, 1951 and Pankhurst, 1964) that there are only two members in a complete set of dimensionless products in this case. From the Buckingham's theorem (Equation.6.1.6) they can have a relationship as

$$\pi_1 = f(\pi_2) \qquad (6.1.8)$$

As this equation is entirely general, it applies to any similar system; thus it also applies to the model. In order to distinguish the equation for the prototype from that for the model, subscripts p and m are used in the following discussion to refer to the prototype and the model equations respectively, such that

$$\left. \begin{array}{l} \pi_{1p} = f(\pi_{2p}) \\ \pi_{1m} = f(\pi_{2m}) \end{array} \right\} \qquad (6.1.9)$$

If the model is designed and tested such that

$$\pi_{2p} = \pi_{2m} \qquad (6.1.10)$$

it follows that

201

$$f(\pi_{2p}) = f(\pi_{2m}) \qquad (6.1.11)$$

and therefore

$$\pi_{1p} = \pi_{1m} \qquad (6.1.12)$$

Substitution of Equation.6.1.7 into the above equation gives

$$\frac{u_{jm}}{u_{jp}} = (\frac{x_{am}}{x_{ap}})^{a_j} \ (\frac{x_{bm}}{x_{bp}})^{b_j} \qquad (6.1.13)$$

This indicates that for the similar system, the ratio of any quantity involved in the system can be found by the ratio of the fundamental quantities. These ratios are called scale factors in physical modelling. For instance, if the length and the unit weight are chosen as the fundamental quantities, the ratio of the distance (L_m) between two arbitrary points in a model to that (L_p) of the corresponding two points in a prototype must be a constant. This ratio is called the geometric scale factor and is denoted by K_l. Similarly, the unit weight scale factor, K_u, is defined as the ratio of the unit weight of the model material (U_m) to that of the corresponding prototype (U_p). Such that

$$K_l = \frac{L_m}{L_p} \qquad \text{and} \qquad K_u = \frac{U_m}{U_p} \qquad (6.1.14)$$

According to Equation.6.1.13, it is arrived at that the stress scale factor K_σ can be obtained by multiplication of K_l by K_u, i.e.

$$K_\sigma = K_l \ K_u \qquad (6.1.15)$$

The scale factors of those quantities whose dimensions are the same as that of the stress are also equal to K_σ.

6.2 Design of Physical Models of Tunnels

As stated earlier, tunnel stability is influenced by several factors, including geological setting, state of stress field environment, tunnel size and shape, and the type and degree of support employed. To examine in detail the effects of all these factors on tunnel stability will exceed the scope of this thesis due to the limited study duration. Upon the consideration that the stress field environment has a most significant effect on the tunnel stability,   attention in this Chapter is therefore focussed on the

influence of placing a tunnel of a given shape in a particular stress field environment. Additionally, the tunnel opening shape is also varied in order to examine differences which arise in the fracture patterns under the same loading condition.

6.2.1 Model Material Selection

There are a number of materials which can be employed for model construction. In the consideration of the model material selection, availability and economy are the main concerns. At the University of Nottingham , sand and fine casting plaster have served physical modelling over last few decades due to large and cheap market supply and excellence in quality and homogeneity. Therefore, they were also selected for the model making in this Chapter.

Sand and fine casting plaster are usually mixed with water to form the model material. The amount of each ingredient (i.e. sand, plaster and water) has a substantial bearing on the mechanical properties of the model material. In order to have an appropriate ratio of ingredients to constitute a desired model, the study started with investigating the properties of the model material, in relation to the proportion of sand, plaster and water. The material properties were systematically studied by means of cylindrical sample testing.

To prepare samples, plastic tubes of 50 mm diameter were sawn in 100 mm lengths for sample moulds. Each cylindrical mould was cut longitudinally in order to ease the later separation of the mould and the cast sample after setting of the model material. The cut was closed by sticking paper tape across the cut. The interior wall was greased before the mould was ready for use.

Sand and fine casting plaster were weighed by using a scale according to the given values and then put in a bucket and stirred steadily. Water of a given volume was measured with a measuring cylinder and poured into the bucket. After some one minute stirring, the liquid mix was poured into the plastic moulds. The top end of each

cast cylindrical sample was scraped with a piece of saw blade such that a cylindrical sample was formed with flat planes at both ends. Following the setting of the liquid material, the paper tape was removed from the lateral wall of the mould. The mould was expanded along the cut and the sample was taken out of the mould.

At least fifteen samples were cast for a single mix of the model material. The samples were left in an oven for 48 hours with the temperature set at 105^{0}C. After driving off the moisture, the samples were measured and weighed, and then loaded to failure. From the measurements of the sample diameter, length and failure load, the unit weight and uniaxial compressive strength (UCS) of samples were found.

Nineteen different mixes have been made and tested. The results of these mixes are shown in Table 6.2.1. Figure 6.2.1 shows the tendency of the change in both the UCS and the unit weight of the mixes.

From Table 6.2.1 and Figure 6.2.1 it can be seen that as plaster increases in proportion and sand decreases, the UCS of the mix increases and the unit weight decreases. These indicate that both sand and plaster proportions have an effect on the properties of the model material.

Upon consideration and discussion with a relevant staff member, a sand-plaster-water ratio of 450:300:250 by weight was selected for the models. From the test results, this mix gave a UCS of 1.18 MPa and a unit weight of 1.37 g/cm^3.

6.2.2 Model Preparation

The model mould was made of a square wooden plate with four wooden strips mounted by screws on it, forming a 45 cm long x 45 cm wide x 7.5 cm deep mould. After properly greasing the interior walls and base of the mould, the well-mixed liquid material at the determined ratio of 450 g sand, 300 g fine casting plaster and 250 cc water was poured into the mould. A steel bar was used to scrape along the top of the mould such that a flat top surface of the cast material was obtained. After setting, the

Sand (gram)	Plaster (gram)	Water (cc)	Unit weight (g/cm3)	UCS (MPa)
625	125	250	1.424	0.098
612.5	137.5	250	1.525	0.142
600	150	250	1.424	0.171
587.5	162.5	250	1.392	0.174
575	175	250	1.415	0.272
562.5	187.5	250	1.406	0.303
550	200	250	1.412	0.361
537.5	212.5	250	1.414	0.280
525	225	250	1.396	0.392
512.5	237.5	250	1.398	0.543
500	250	250	1.410	0.710
487.5	262.5	250	1.392	1.444
475	275	250	1.377	0.886
462.5	287.5	250	1.389	1.669
450	300	250	1.397	1.180
437.5	312.5	250	1.379	1.228
425	325	250	1.367	1.548
412.5	337.5	250	1.379	1.144
400	350	250	1.389	1.548

Table 6.2.1 The values of the unit weight and the UCS of model materials
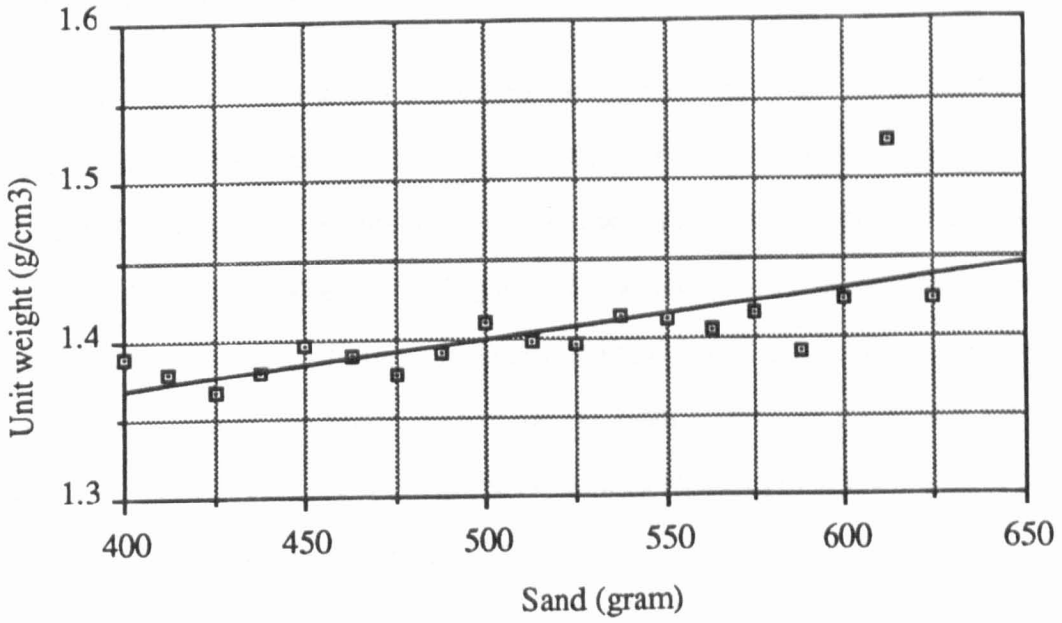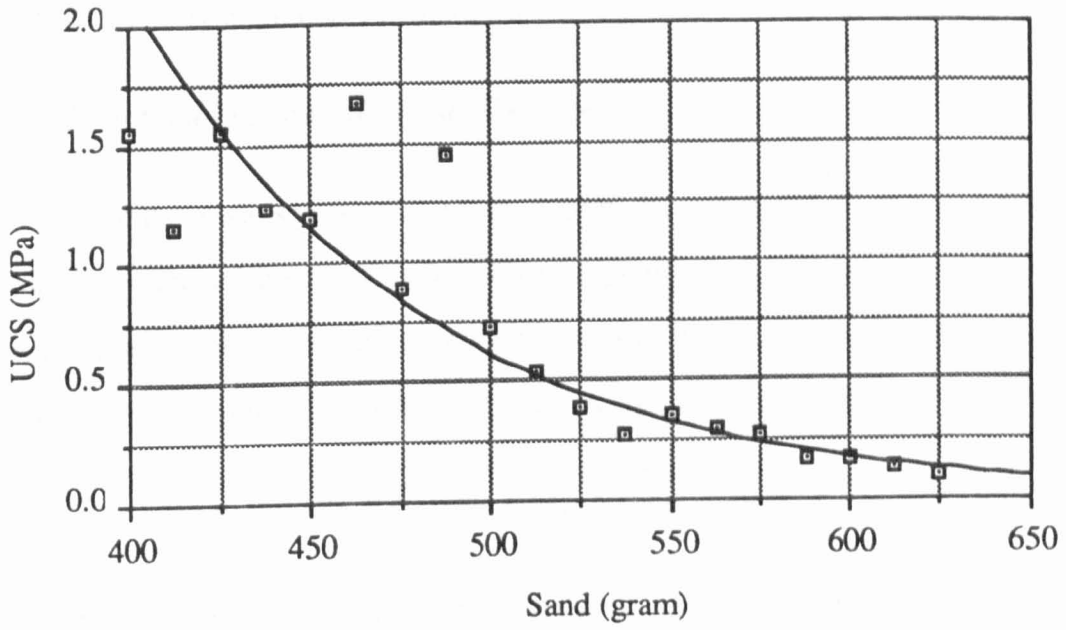
Note: Sand + Plaster = 750 grams, Water = 250 cc

Figure 6.2.1 Illustrating the tendency of the change in both the UCS and the unit weight of the mixes with the variation of sand.

mould was dismantled and removed, the block model was then left in the oven at 105°C for forty eight hours to drive off the moisture.

6.2.3 Determination of Scale Factors

For the models presented in this Chapter, the length and the unit weight of model material were selected as two fundamental quantities. The geometric scale factor K_l was chosen to be 1: 36 and the unit weight scale factor K_u was 1.37 : 2.40. Therefore, the stress and strength scale factor K_σ was calculated by Equation.6.1.15 as

$$K_\sigma = K_l \; K_u \;\; = \frac{1}{36} \times \frac{1.37}{2.40} = \frac{1}{63.1}$$

Since the uniaxial compressive strength of the mix is 1.18 MPa, the model material will represent a sandstone rock of moderate strength of 1.18 x 63.1 = 74.4 MPa.

6.3 Model Testing

A small testing rig was employed for the research. The rig can hold a model of 45 cm wide x 45 cm high x 7.5 cm thick. Figure 6.3.1 is a diagrammatic illustration of the rig. Two hydraulic pumps were used to apply separately the horizontal and vertical loads to the model. When installing a model, a steel plate was inserted between each model side and a row of rams, to obtain an equal loading condition along each side. Upon the fixing of the model in the rig, the front surface of the model was marked with a mesh of 2.5 cm x 2.5 cm grids. A tunnel was then cut at the model centre using a saw blade, screw drivers and a small scraper.

Following the completion of the tunnel excavation, the pre-loading tunnel was measured and photographed. A cover plate was then used to seal the model. Bolts were tightened so that the movement of the model could be confined within the model plane. Hydraulic pumps were then operated upon the desired horizontal to vertical stress ratio. In the process of gradual loading, the horizontal and vertical closures of the tunnel (across the tunnel centre) were monitored and measured. When the

predominant closure arrived at 1%, 2%, 5%, 7.5%, 10%, 15%, 20%, 25% and 30% of the original tunnel measurement, the loading was paused and unloaded, the front cover was unbolted and removed from the rig, and the fracture situation in the model was recorded and photographed.

Then the front cover plate was put on and bolted again in order to carry on the loading to obtain the next pre-set closure. Such a process was repeated until further loading became impractical.
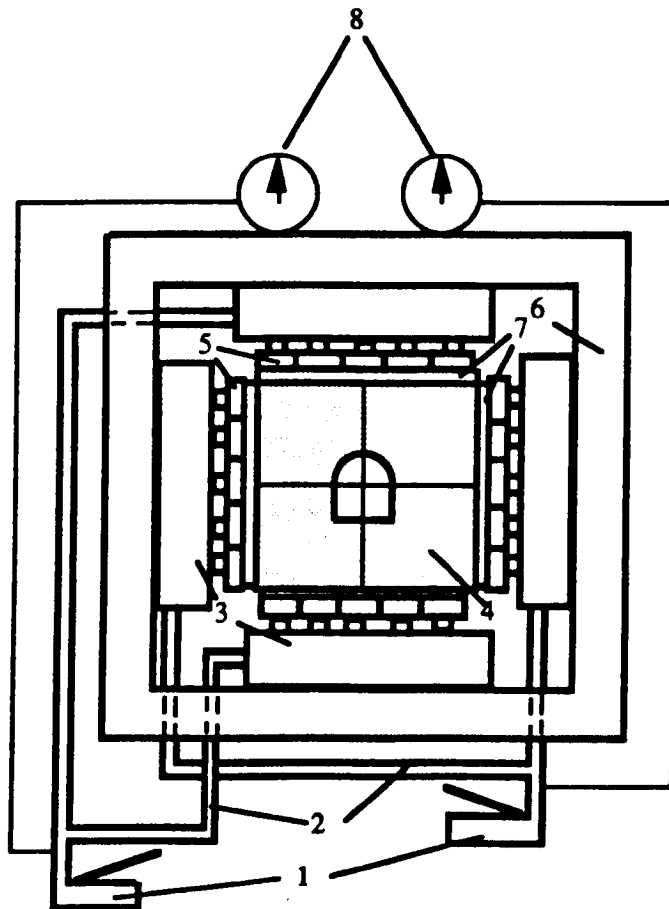
1. Hydraulic Pumps   2. Pipelines   3. Cylinders   4. Model

5. Rams   6.Rig frame   7. Steel plates   8. Pressure gauges

Figure 6.3.1 A diagram of the small testing rig.

Every model followed the same testing procedure. Four tunnel configurations were employed: circular, arch, square and rectangular (the tunnel width to height ratio for the rectangular section was equal to 2). Six different vertical to horizontal stress ratios were applied to each configuration of the models, which have been from uniaxially vertical loading with slight lateral constraint, to hydrostatic and 1:2, 1:3, 2:1, and 3:1 of the vertical to horizontal loading ratio.

6.4 Characteristics of Fracture Development around Tunnels

Model experiments were carried out, aiming at observing the development of the induced fractures with progressive increases in the intensity of the applied stress field. Particular attention was therefore drawn to looking at the effect of the stress ratio on the tunnel stability of different profiles. The results from the tests are presented in this section which will be described in the sequence of the change in the applied stress ratio.

6.4.1 Uniaxial Stress Field with Lateral Constraint

In the uniaxial vertical stress field with a constant lateral constraint of 0.18 MPa, the behaviour of the tunnels which were excavated separately in this condition were observed.

In the case of a circular tunnel of 3.6 m diameter, three nearly vertical cracks were first seen to develop in the floor and two vertical cracks in the roof at 2% tunnel closure. They were initiated at the uppermost point of the crown and the corresponding sidewalls. As the model was further loaded, the vertical cracks developed continuously from the sidewalls to both the top and bottom boundaries of the model, forming a shearing block in the tunnel roof and floor. These blocks later gave rise to an increase in the vertical closure of the tunnel. The closure due to the opposite moving of the two blocks caused a crushing at the tunnel sidewalls. All of these cracks may be seen in

Plate 6.4.1(a) when the vertical closure was 10%. Figure 6.4.1(a) illustrates the closure features of the circular tunnel against the applied vertical stress .

When a square profile tunnel was placed in this stress field, a number of nearly vertical fractures were firstly developed in both the roof and the floor after the occurrence of 2% vertical closure of the opening. As the model was further loaded, the vertical closure gradually increased and the left hand side wall buckled. As a result a few vertical fractures appeared in the left hand sidewall. Further development of the fractures led to the sidewall spalling in large pieces, when the vertical closure of the tunnel was up to 7.5% under the effect of continuously increasing the vertical stress. After this point, the nearly vertical fractures in both the roof and the floor were further developed into the deeper rock mass and the vertical fractures in the sidewalls were enlarged. However the fractures on the sidewalls all took place within an extent of 0.8 metres into the tunnel profile. Although the crossing cracks were seen in the roof, no evident roof caving occurred in the entire process of the test, in which a 25% vertical closure of the tunnel was finally recorded. Plate 6.4.1(b) illustrates the development of cracks around the tunnel when the vertical closure was up to 10%. Figure 6.4.1(b) shows the progressive increase of the tunnel closure against the vertical rock stress .

Similar fracture development was observed around an arch-profiled tunnel when it was driven and loaded in this stress field environment. The vertical fractures first appeared in the floor corners and the left shoulder of the tunnel at 2% vertical closure. Another nearly vertical crack developed in the right side shoulder of the tunnel during a continuous loading up to about 5% vertical closure. At this moment, the tunnel sidewalls were fractured by the increasing vertical load, as the cracks turned up in the sidewalls. Again, the depths within which from the sidewalls these cracks developed were as small as that of less than 0.6 m. At the 7.5% vertical closure, the failed sidewalls buckled, attempting to move into the opening. This situation is shown in Plate 6.4.1(c). With increases in the applied vertical stress, the fractures in the roof developed into the upper position and finally to the top of the model, and the fractures
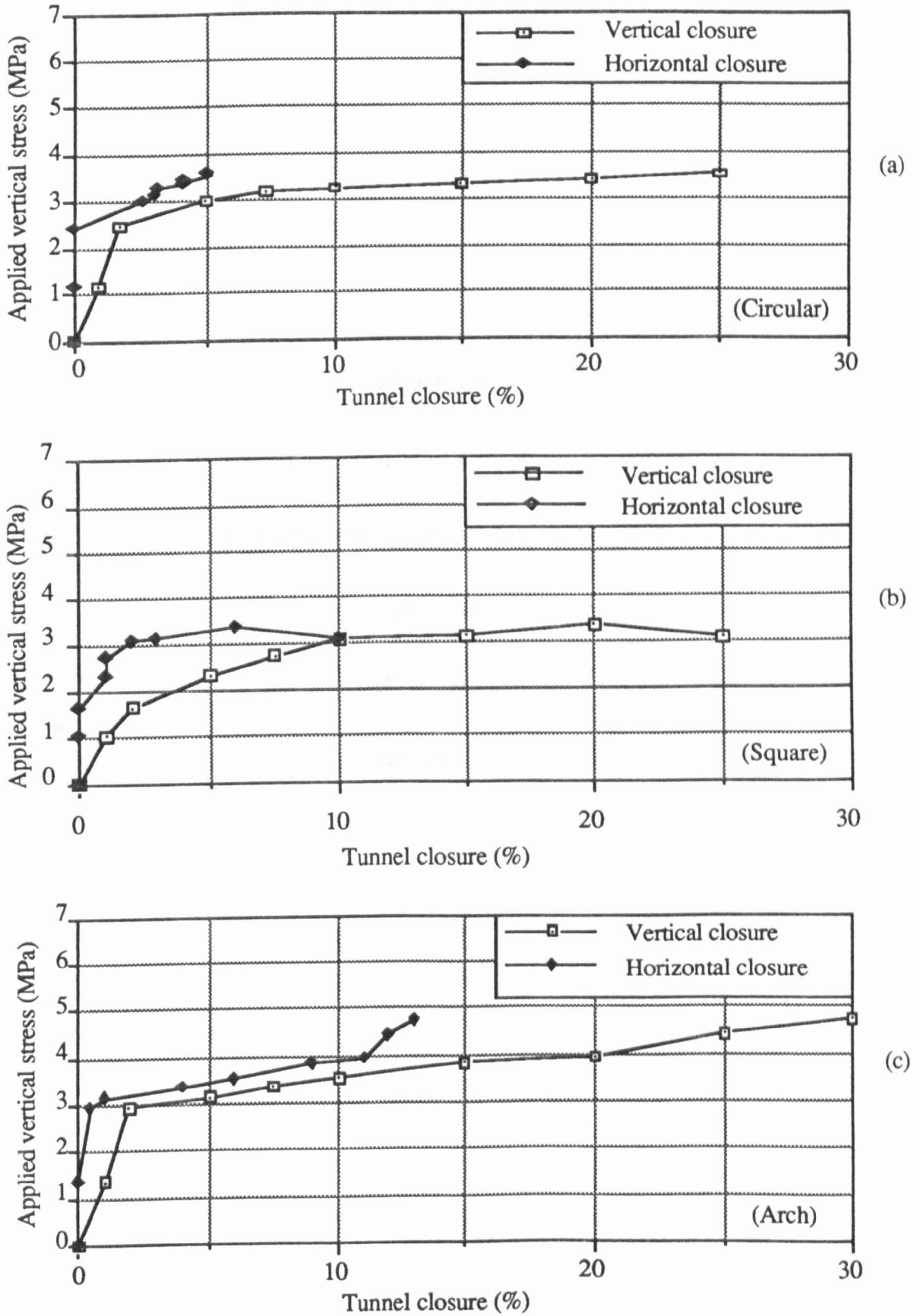
Figure 6.4.1 The tunnel closure against the applied vertical stress in the uniaxial

stress field with a lateral constraint.

Plate 6.4.1

The fracture pattern development around the unnels

in the uniaxial stress field with a lateral constraint.

(a) Circular

(b) Square

(c) Arch
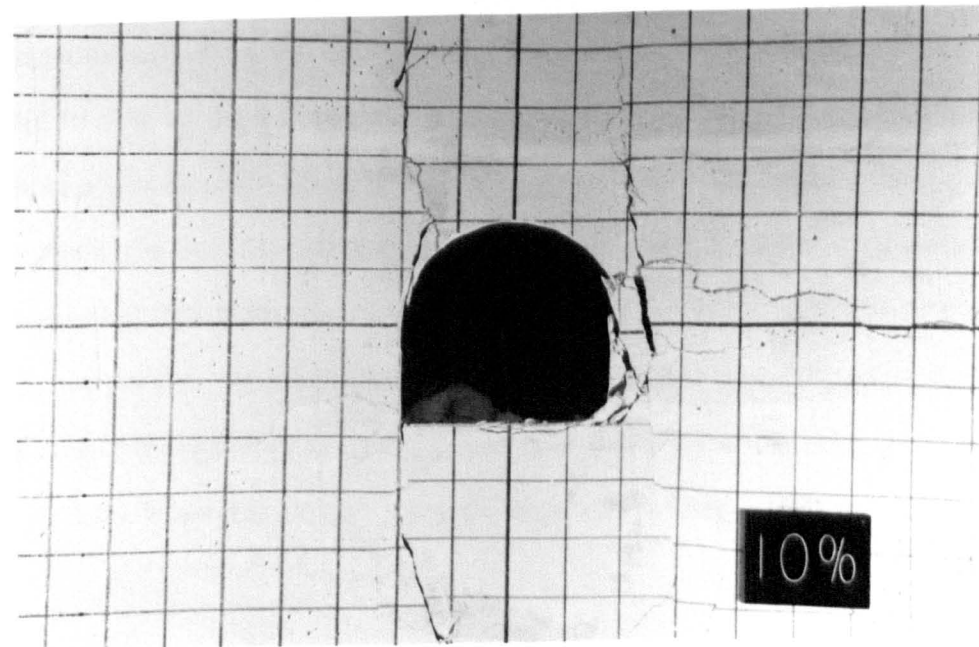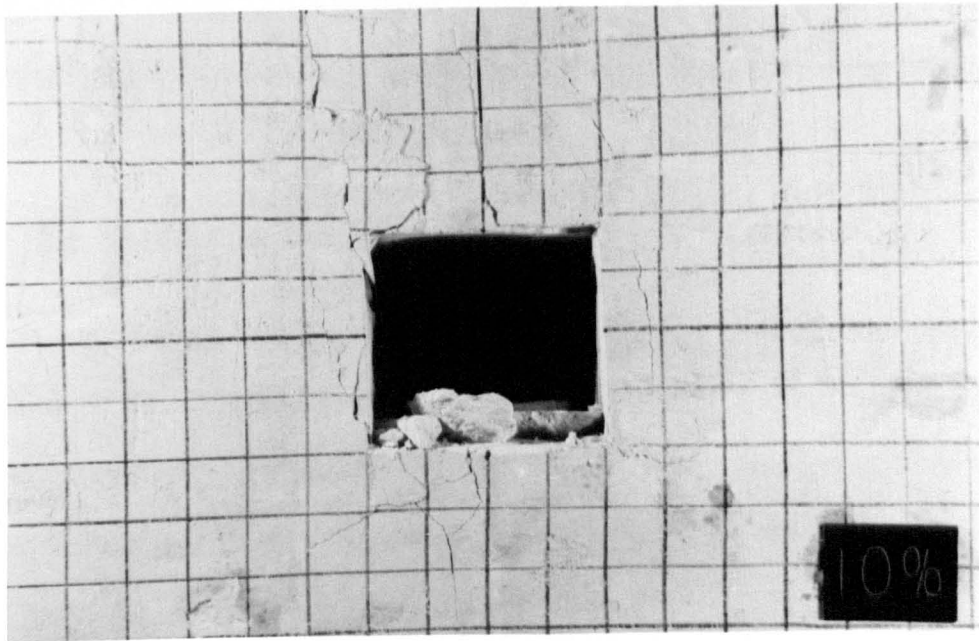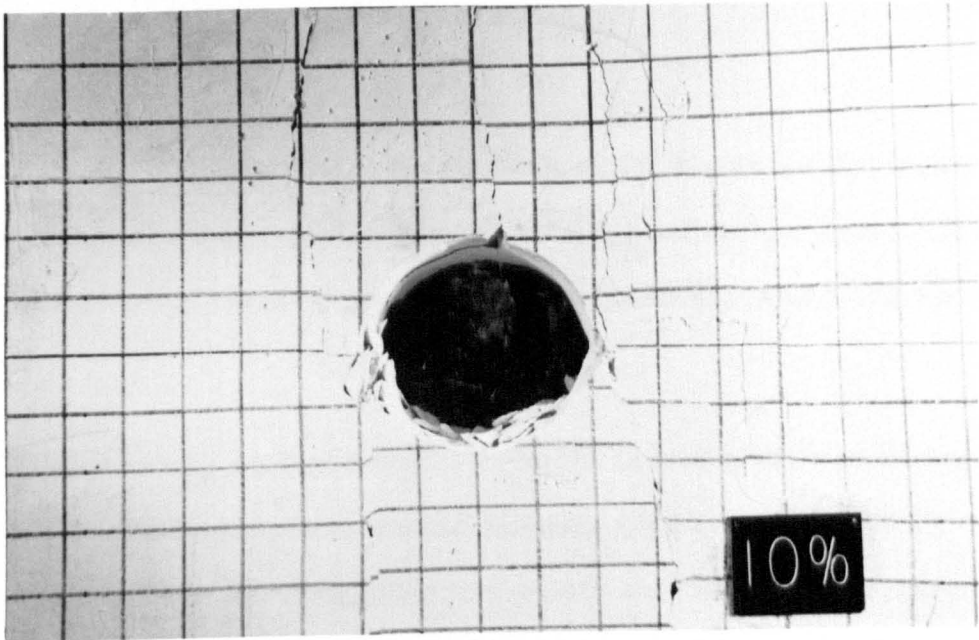
in the floor extended down to the bottom of the model. Figure 6.4.1(c) illustrates the rise in the tunnel closure with the increase in the applied vertical stress . It is clearly seen that the vertical closure of the tunnel speeds up after the value of 2% was arrived at.

When a rectangular tunnel with 2 to 1 width to height ratio was located in this stress field environment, three vertical fractures initially appeared at 2% vertical closure, one being at the centre of the roof and the rest along the floor corners down into the deeper rock mass. A further loading induced two new vertical cracks in the roof corners, forming an entire block in the roof. As a consequence of the inward movement of the two blocks in the roof and floor, sidewall slabbing and spalling occurred.

6.4.2   3:1 Vertical to Horizontal Stress Field Environment

The test results corresponding to the 3:1 vertical to horizontal stress field condition are shown in Figure 6.4.2 (a), (b) and (c) for the circular, square and arch profiles respectively. Photographs of the corresponding profiles at 10% vertical closure of the tunnel opening are shown in Plate 6.4.2 (a), (b) and (c).

Figure 6.4.2 (a), (b) and (c) illustrate progressive vertical closure up to about 5% vertical closure of the opening. After this particular point, the vertical closure increases markedly for small increases in applied vertical stress. The first cracks were observed to develop after about 2% vertical closure in all three cases with the closure increasing approximately linearly with the applied stress. In the case of the circular tunnel profile, the main fractures were seen to initiate from the horizontal apexes of the tunnel opening. The fractures then stretched nearly vertically into the roof and the floor. In comparison, the main fractures in the square tunnel opening started from the four corners of the opening. They developed almost along the vertical direction into the roof and floor. Fractures in the sidewalls occurred mainly in the vertical direction,

(a)

(Circular)

(b)

(Square)

(c)

(Arch)
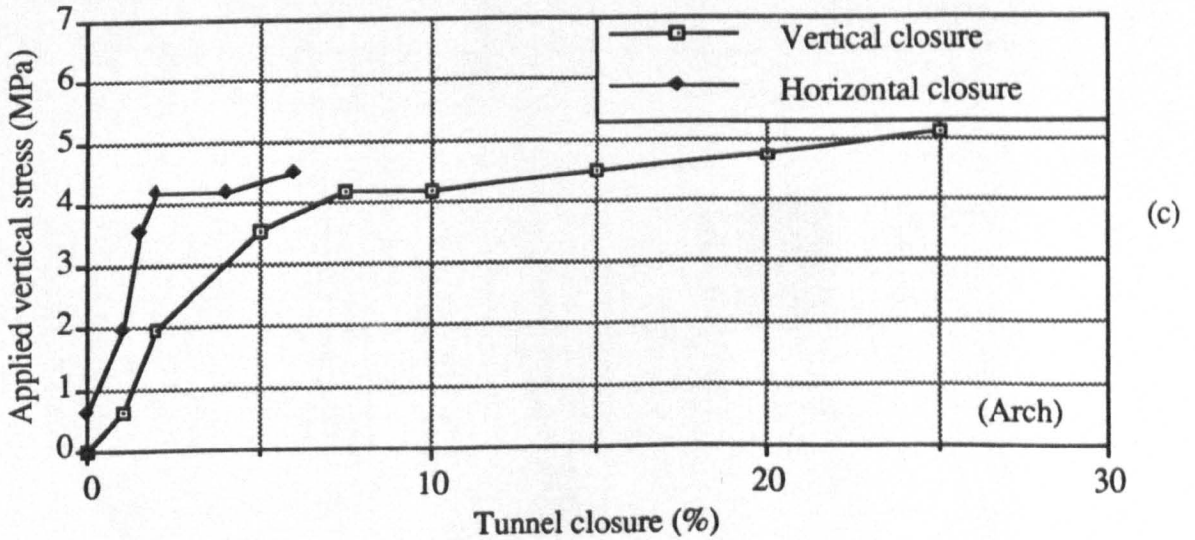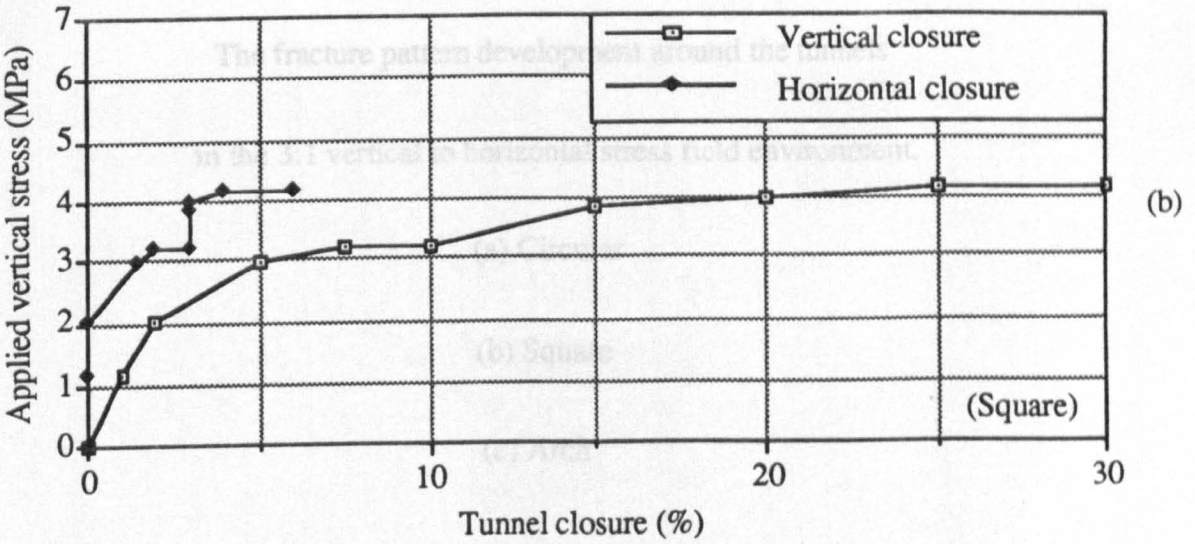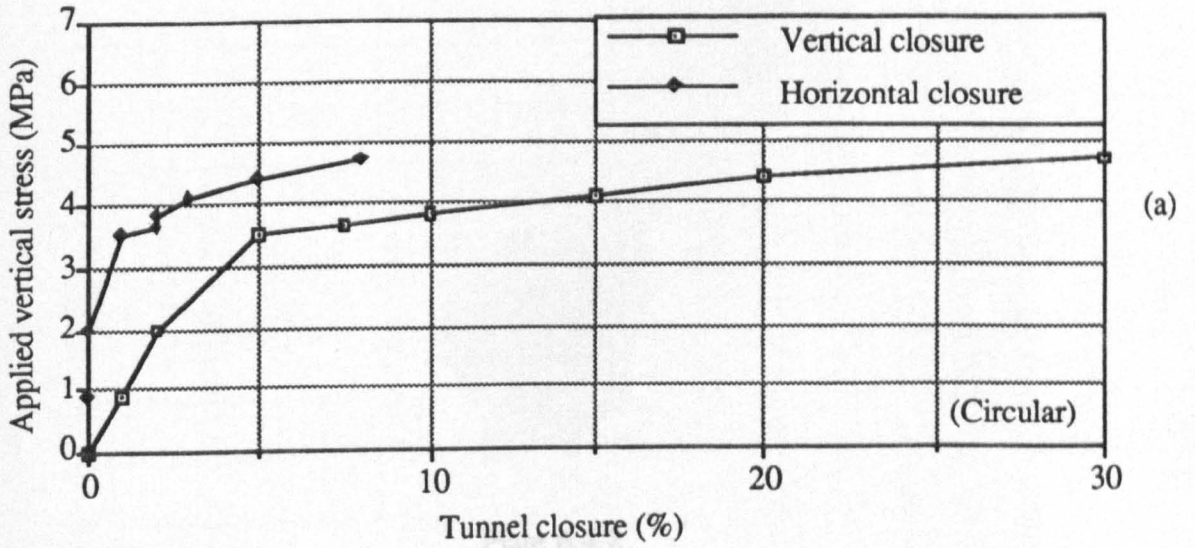
Figure 6.4.2 The tunnel closure against the applied vertical stress in the 3:1 vertical to
horizontal

214

Plate 6.4.2

The fracture pattern development around the tunnels

in the 3:1 vertical to horizontal stress field environment.

(a) Circular

(b) Square

(c) Arch
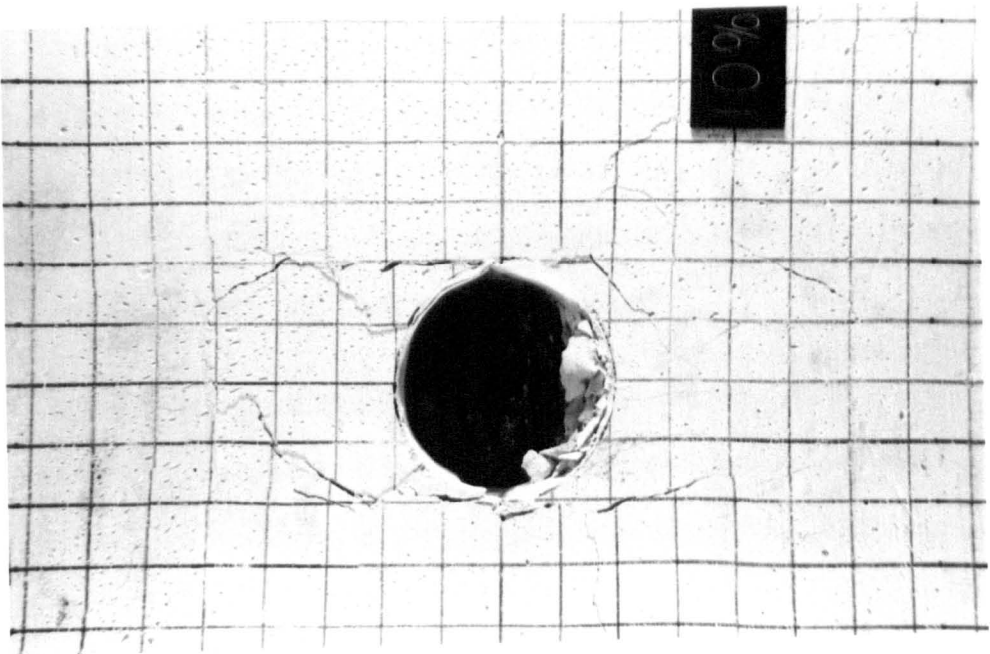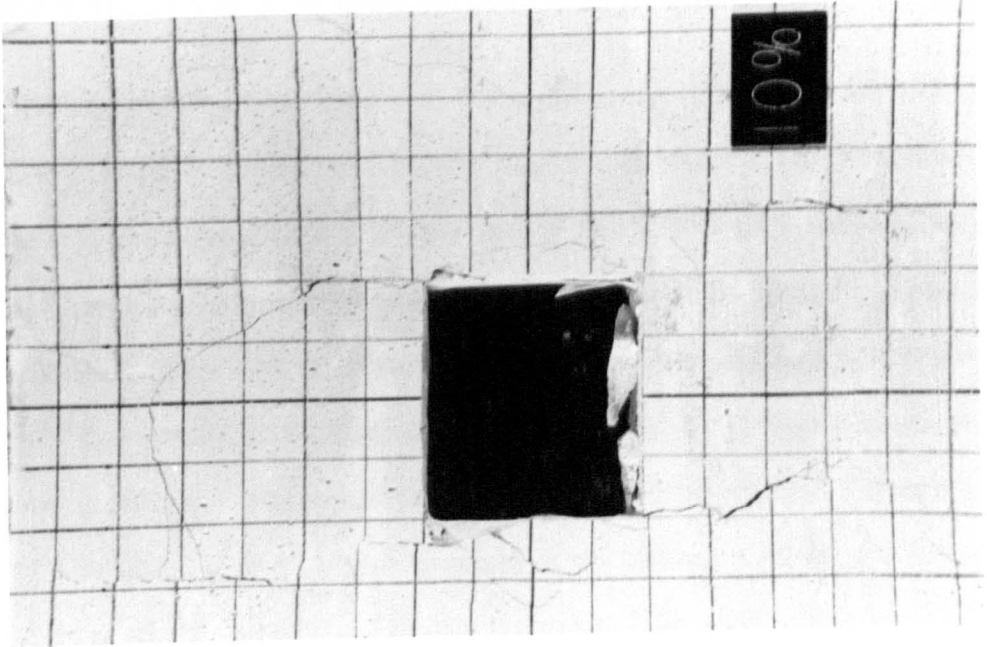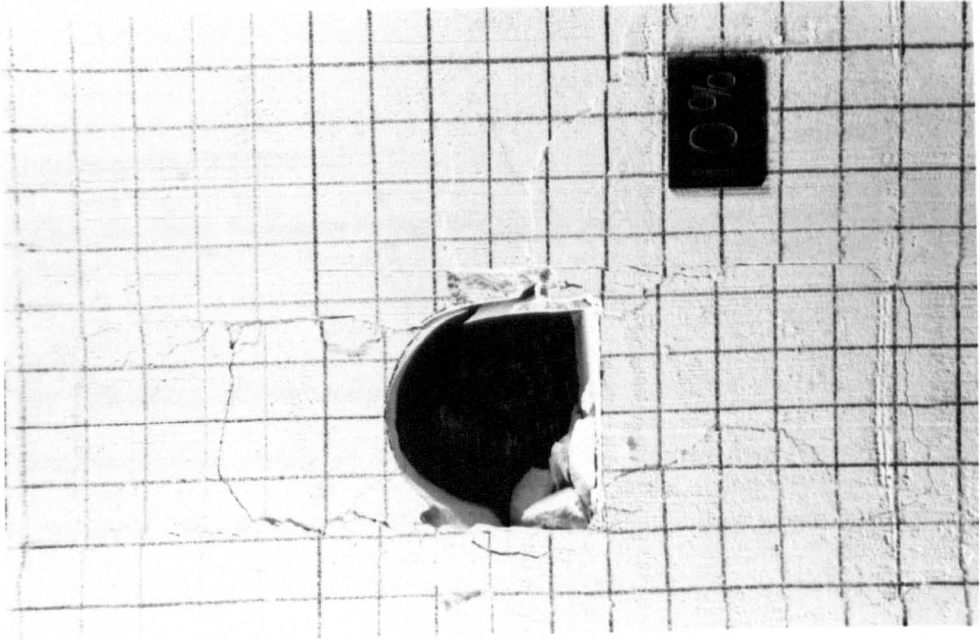
which increased the potential of side spalling in the later further test. In the case of the arch profile, the main fractures first appeared at the springline position and the floor corners.

The formation of the main fracture patterns after 5% vertical closure had a significant weakening effect on the stability of all these tunnel profiles. Horizontal closure occurred only after appreciable applied vertical stress in all cases; after 2% vertical closure, however, the horizontal closure became significant and this is undoubtedly associated with the development of the vertical closure. The side spalling appeared to be a secondary feature of the roof failure in these cases.

The fracture patterns shown in Plate 6.4.2.(a), (b) and (c) all indicate the formation of fracture zones extending to a height equal to about the excavation width. The fracture zones in the roof of each tunnel profile have allowed distinct stress relieved domes to develop by a process of shearing action immediately above the tunnel sidewalls. Due to the symmetrical loading on the model, similar fracture zones have also been formed in the floor of each tunnel profile although they are not fully illustrated in the photographs in Plate 6.4.2. The fractures in both the roof and the floor are connected by the vertical fractures in the sidewalls, forming a larger stress relieved zone which is enclosed by the fractures. This zone is termed the "tunnel failure zone" by the author. This tunnel failure zone of each tunnel profile has a long and a short axis in the vertical and the horizontal direction respectively. The ratio of the vertical dimension to the horizontal one of the zone is found to be about 3 to 1 in all cases. By referring to the features of the stress field applied, it is found that the dimensional ratio of the tunnel failure zone is approximately equal to the value of the applied vertical to horizontal stress ratio in these cases.

These results suggest that the design of the tunnel support should ensure that the support be able to sustain the dead load of the entire rock materials within the stress relieved dome, which is equal to a rock volume with a height equal to about the tunnel

width. When the rock bolt system is to be employed as the tunnel support, the rock bolt should be so long as one end of the bolt is anchored beyond the stress relieved dome, in order to secure the support quality.

From the fracture patterns shown in Plate 6.4.2 (a), (b) and (c), it is seen that the side slabbing and spalling were localised, all within 2.5 cm (equivalent to 0.9 m in the prototype) from the sidewalls. They were caused by the shear effect. It can thus be predicted that linings of tunnels under the effect of this applied stress field would experience appreciable shearing forces, especially at the springline positions for the arch and circular profiles.

6.4.3 2:1 Vertical to Horizontal Stress Field Environment

In the 2 : 1 vertical to horizontal stress field environment, the tunnels of the circular, arch and rectangular profiles exhibited slightly different fracture patterns and stability problems from that in the 3:1 vertical to horizontal stress field condition. They are shown in Plate 6.4.3 (a), (b) and (c) for the corresponding profiles at 10% vertical closure of the tunnel opening. Figure 6.4.3 (a), (b) and (c) show the diagrams of the tunnel closures against the applied vertical stress for the corresponding tunnel profiles.

From the photographs shown in Plate 6.4.3, it is visible that major fractures developed vertically in both the roof and the floor in all cases. The fractures in the roof of each tunnel profile have formed a stress relieved dome. The dome had a width about the same as the tunnel width and appeared immediately above the tunnel. The height of the dome, however, was ranging from 2/3 to 3/4 tunnel width in the cases discussed. Obviously, the values of the height are smaller, compared to those in the cases of the 3:1 vertical to horizontal stress field environment in Section 6.4.2.

The nature of the variation in the dome geometry, in particular the dome height suggests that the development of the fracture dome is not related to the tunnel profile, but to the magnitude of the applied vertical to horizontal stress ratio. As each of the

217

Plate 6.4.3

The fracture pattern development around the tunnels

in the 2:1 vertical to horizontal stress field environment.

(a) Circular

(b) Arch

(c) Rectangular

10%

10%
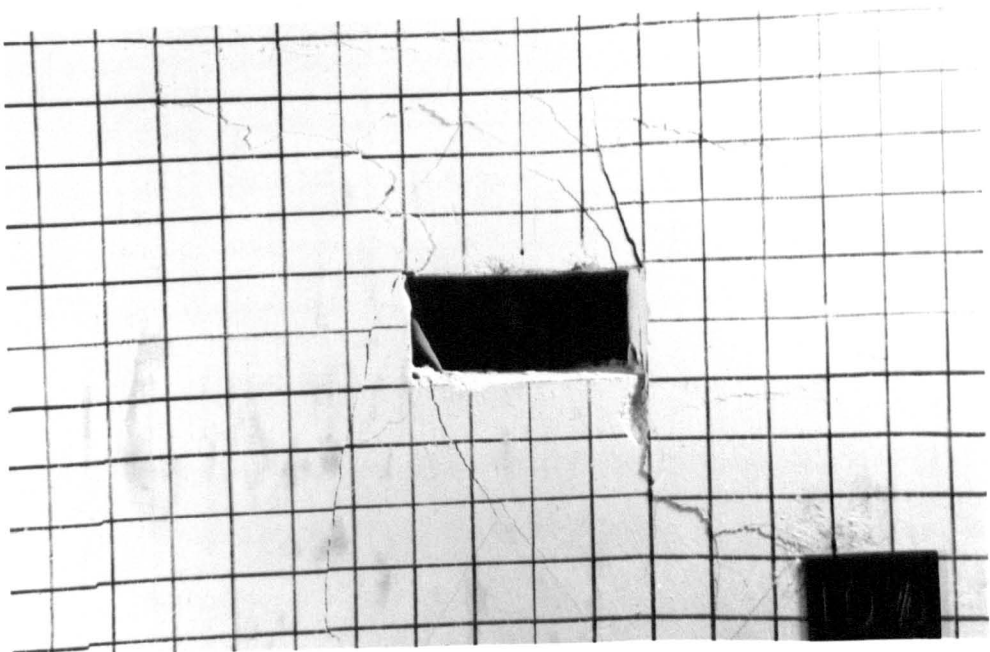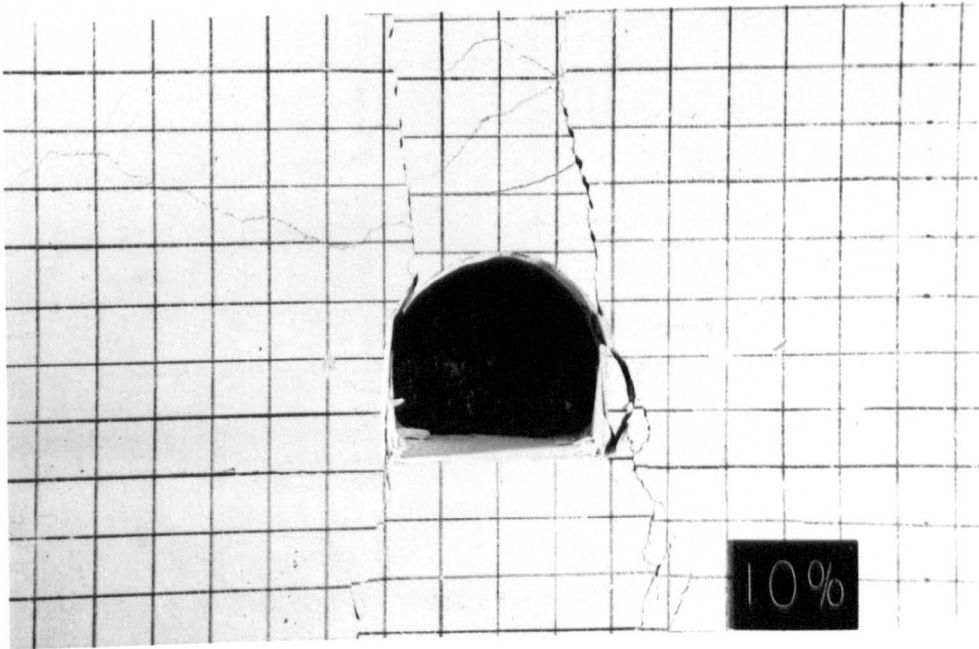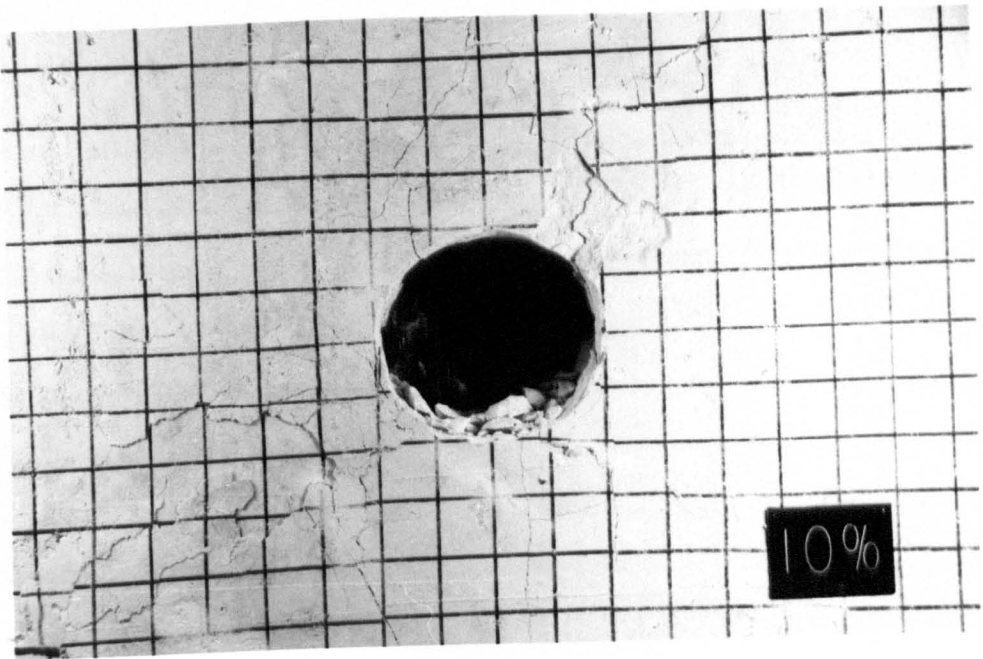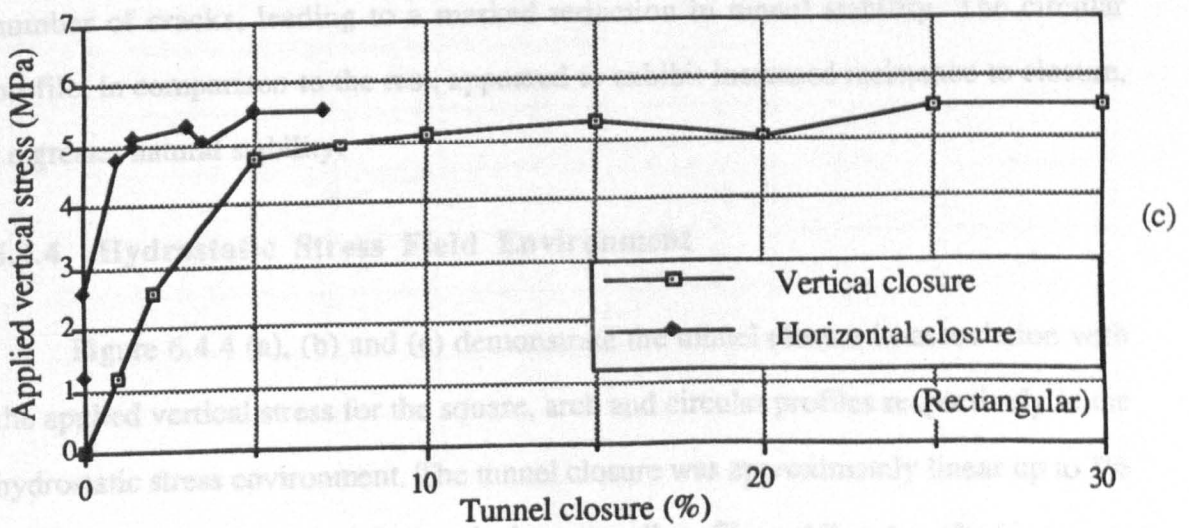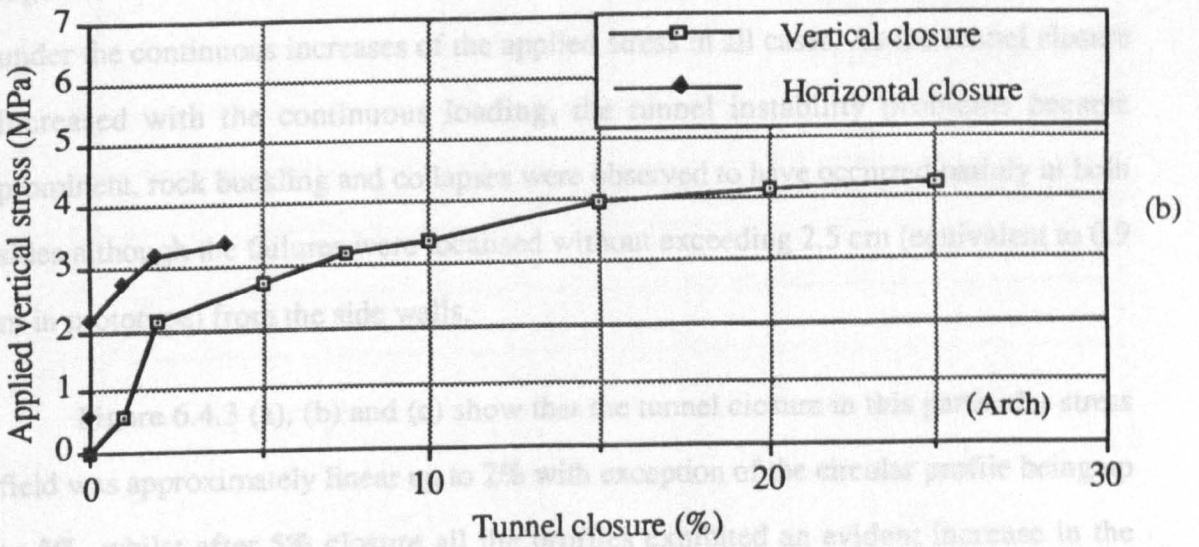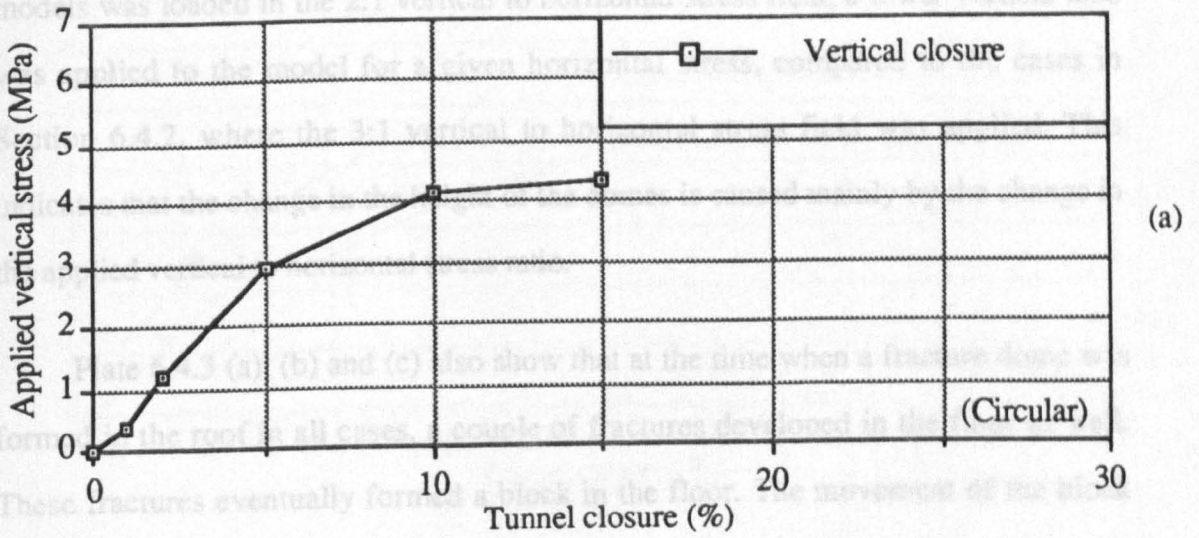
Figure 6.4.3 The tunnel closure against the applied vertical stress in the 2:1 vertical to horizontal stress field environment.

models was loaded in the 2:1 vertical to horizontal stress field, a lower vertical load was applied to the model for a given horizontal stress, compared to the cases in Section 6.4.2. where the 3:1 vertical to horizontal stress field was applied. This indicates that the change in the height of the domes is caused mainly by the change in the applied vertical to horizontal stress ratio.

Plate 6.4.3 (a), (b) and (c) also show that at the time when a fracture dome was formed in the roof in all cases, a couple of fractures developed in the floor as well. These fractures eventually formed a block in the floor. The movement of the block together with the dome in the roof contributed in the main to the tunnel vertical closure under the continuous increases of the applied stress in all cases. As the tunnel closure increased with the continuous loading, the tunnel instability problems became prominent, rock buckling and collapses were observed to have occurred mainly in both sides although the failures were localised without exceeding 2.5 cm (equivalent to 0.9 m in prototype) from the side walls.

Figure 6.4.3 (a), (b) and (c) show that the tunnel closure in this particular stress field was approximately linear up to 2% with exception of the circular profile being up to 5%, whilst after 5% closure all the profiles exhibited an evident increase in the number of cracks, leading to a marked reduction in tunnel stability. The circular profile, in comparison to the rest, appeared to exhibit increased resistance to closure, i.e.greater natural stability.

6.4.4 Hydrostatic Stress Field Environment

Figure 6.4.4 (a), (b) and (c) demonstrate the tunnel closure in association with the applied vertical stress for the square, arch and circular profiles respectively in the hydrostatic stress environment. The tunnel closure was approximately linear up to 5% vertical closure, whilst after this particular point all profiles exhibited marked increases in tunnel closure with small increases of loading, which indicated an appreciable reduction in tunnel stability. The square and arch profiles behaved similarly whilst the

220
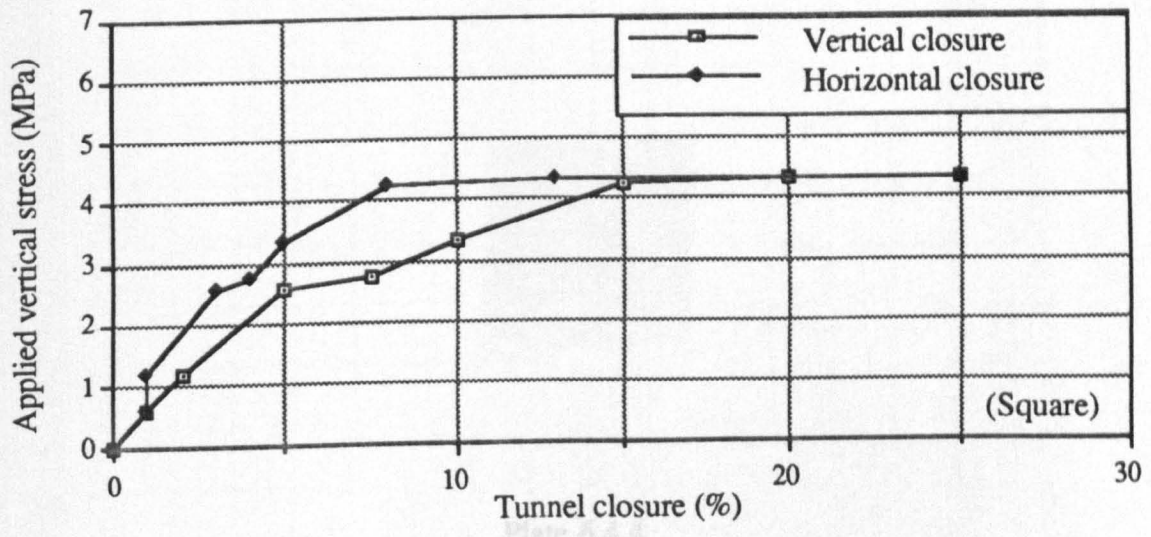
(a)
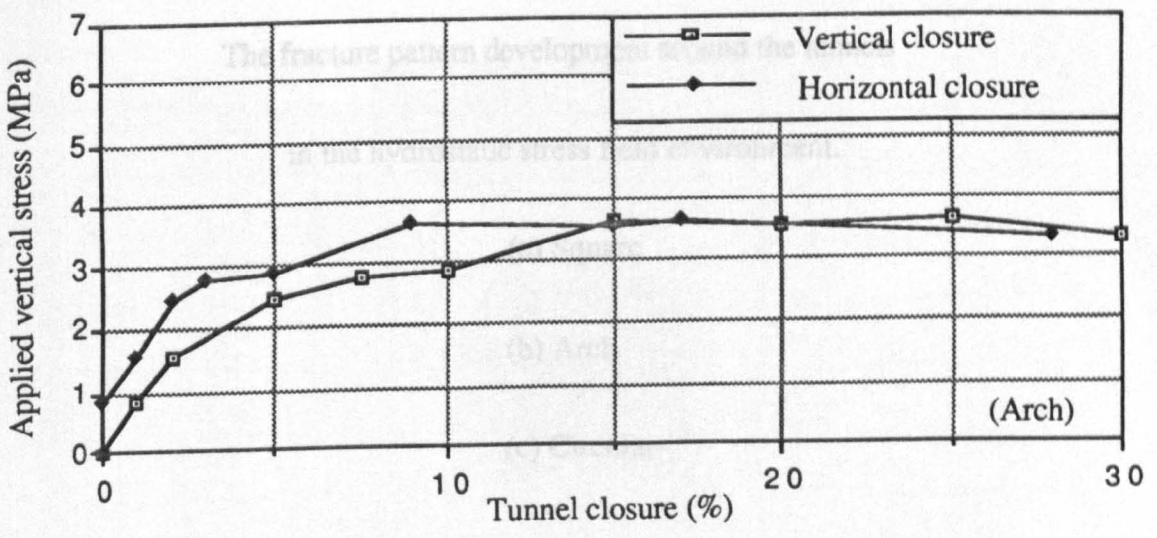
(b)
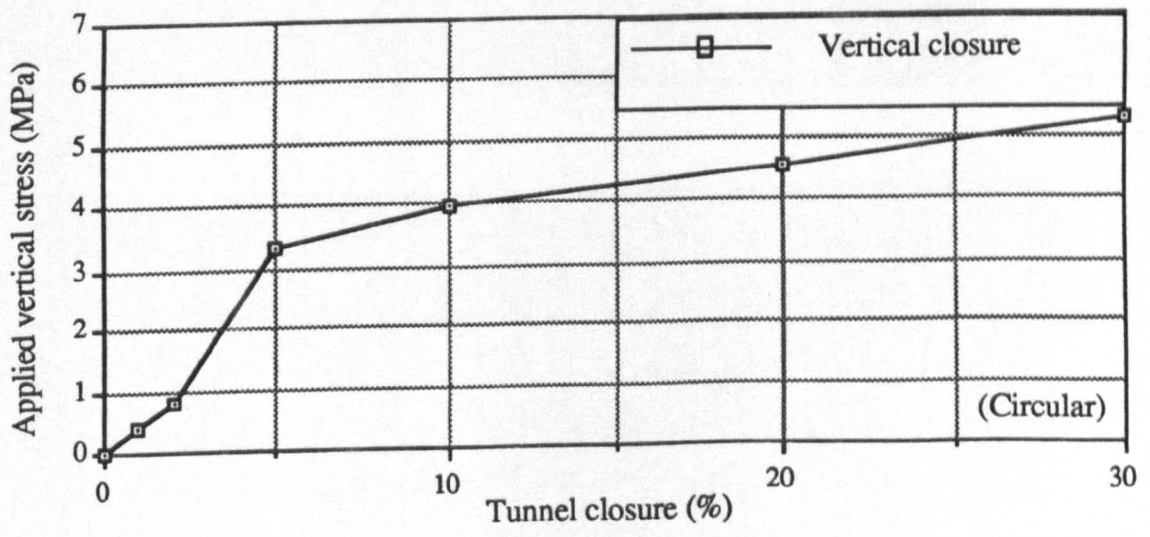
(c)

Figure 6.4.4 The tunnel closure against the applied vertical stress in the hydrostatic stress field environment.

Plate 6.4.4

The fracture pattern development around the tunnels

in the hydrostatic stress field environment.

(a) Square

(b) Arch

(c) Circular

10 %

10 %
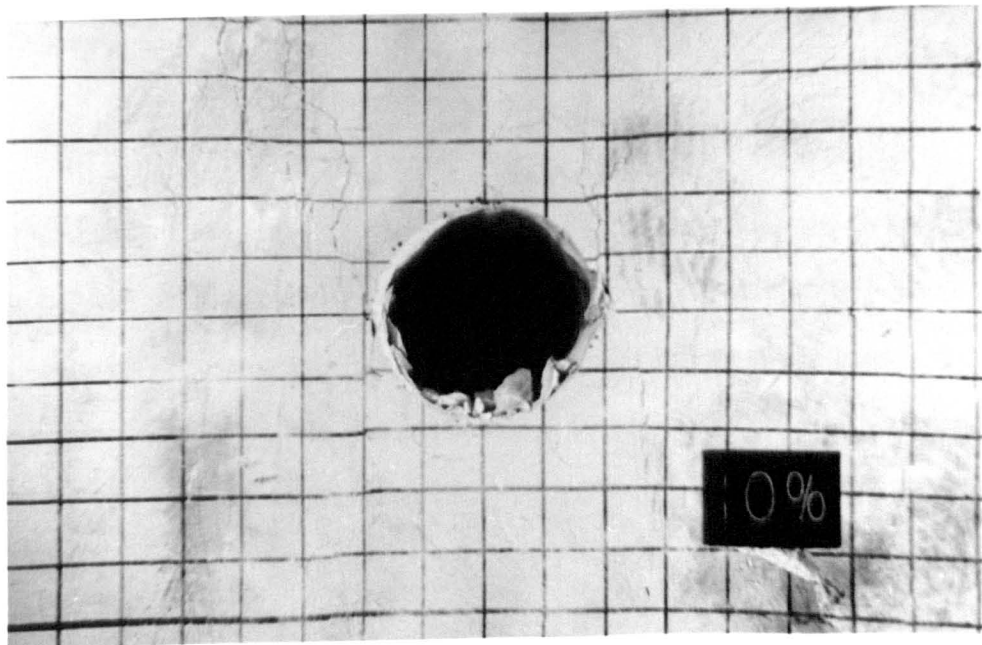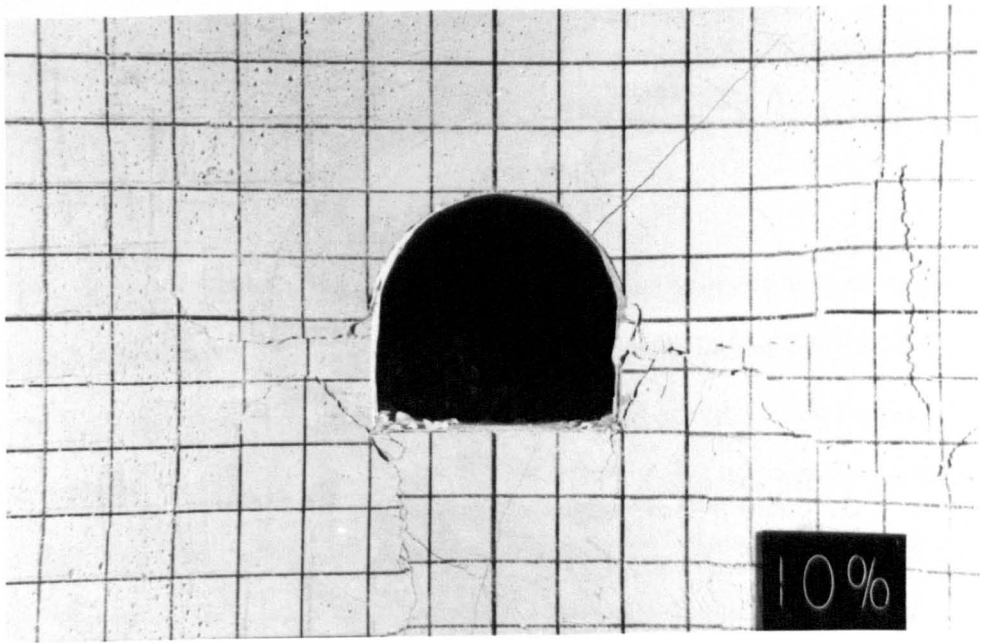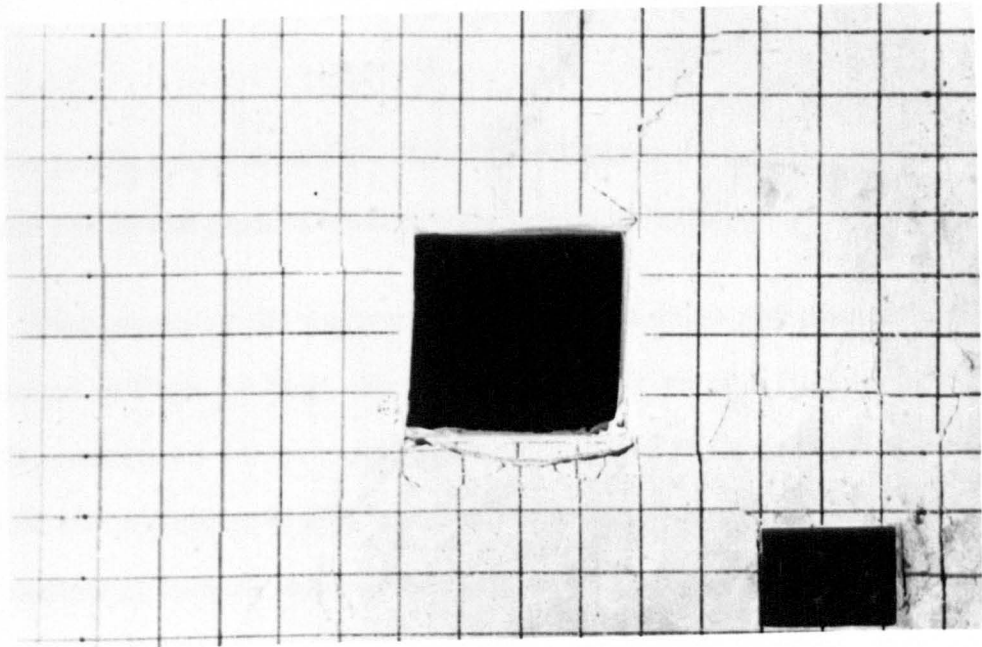
circular profile tended to exhibit enhanced resistance to the tunnel closure, namely, the circular profile had greater natural stability in this particular stress field.

Photographs of the fractures associated with these three tunnel profiles are illustrated in Plate 6.4.4 (a), (b) and (c) after 10% vertical closure. In the square profile, most cracks were produced in the most vicinity of the tunnel. The cracks in the roof did not exhibit clearly directionality. The stress relieved block produced was small and shallow in both the roof and the floor. In the arch profile, although a number of major fractures were observed developing around the opening, they exhibited uncertainty in the fracture direction. A similar result can also be found from the circular profile. All these reveal that there is a uniformity in the nature of fracture development with the considered profiles in this applied stress field, and in the feature of spalling incidents as well.

The photographs also demonstrate that all these opening shapes seem to have substantially increased natural stability in the hydrostatic stress field, as compared to those in the other stress field conditions discussed in the previous sections. The circular profile showed spalling fairly uniformly around the tunnel periphery. No appreciable roof instability features were observed to develop over the range of loading applied. Therefore the design of the support system for these three excavation shapes would become easier and require no special considerations under such stress field circumstances.

6.4.5 1:2 Vertical to Horizontal Stress Field Environment

Photographs presented in Plate 6.4.5 (a), (b) and (c) show the fracture patterns and their development around the tunnel of the circular, arch and square openings after 10% horizontal closure under the loading in the 1:2 vertical to horizontal stress field environment. It can be seen from the photographs that the fractures developed mainly in the sidewalls in all cases, although there were also a couple of nearly vertical cracks

223

Plate 6.4.5

The fracture pattern development around the tunnels

in the 1:2 vertical to horizontal stress field environment.

(a) Circular

(b) Arch

(c) Square

(a)

(b)

(c)
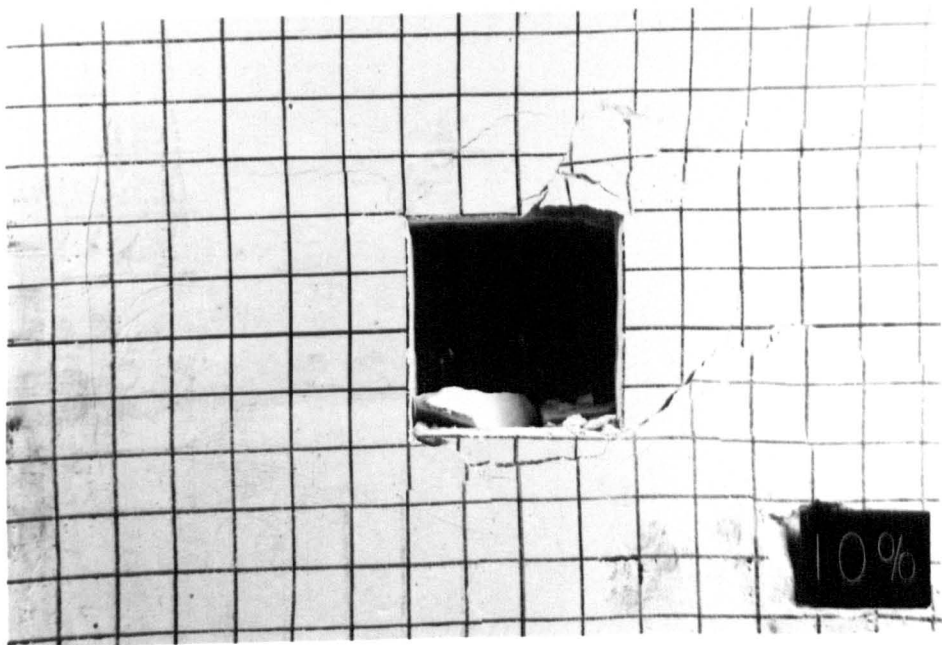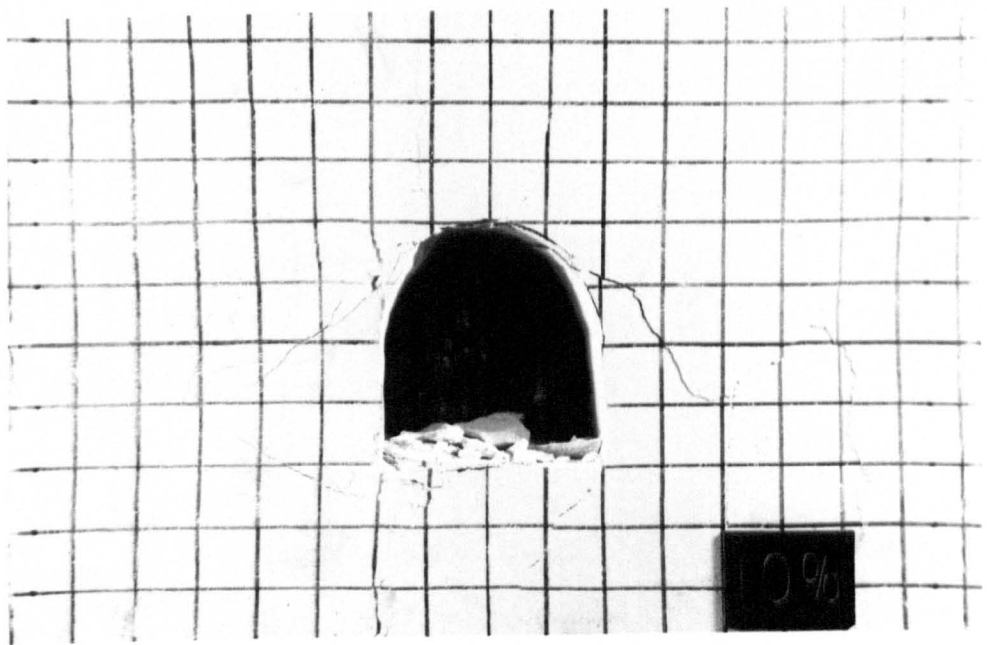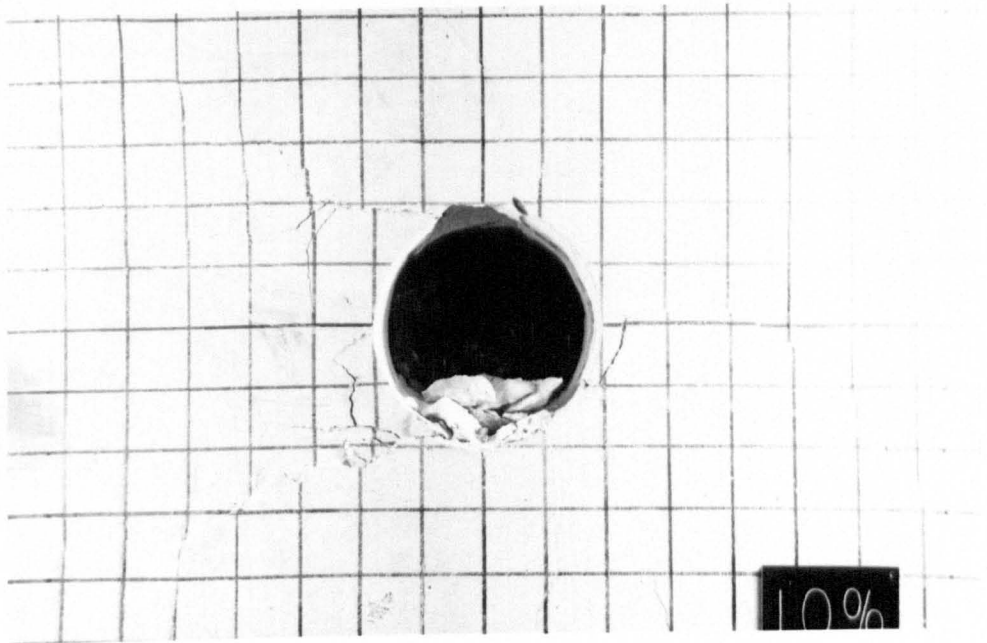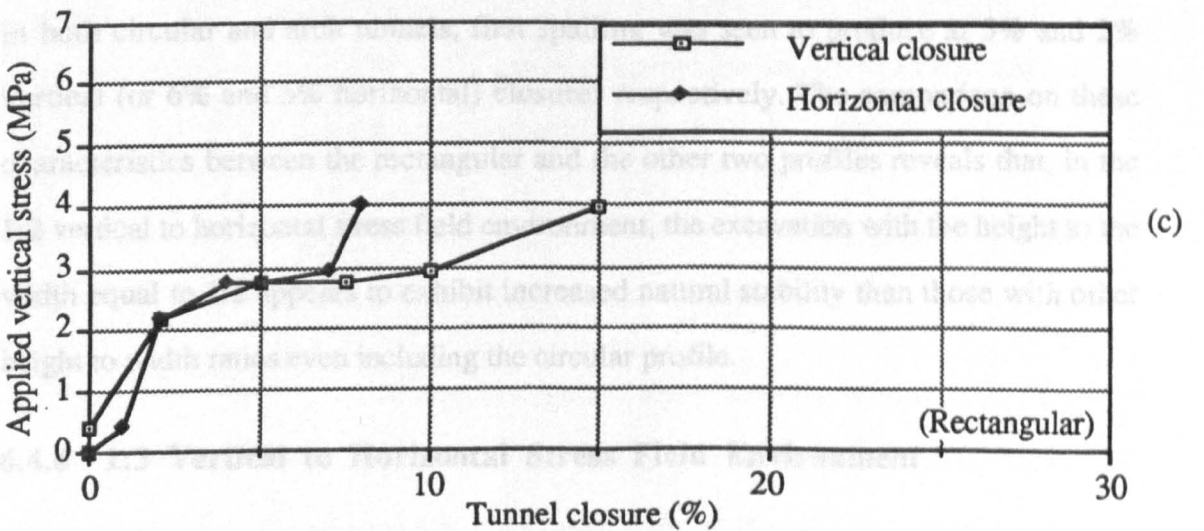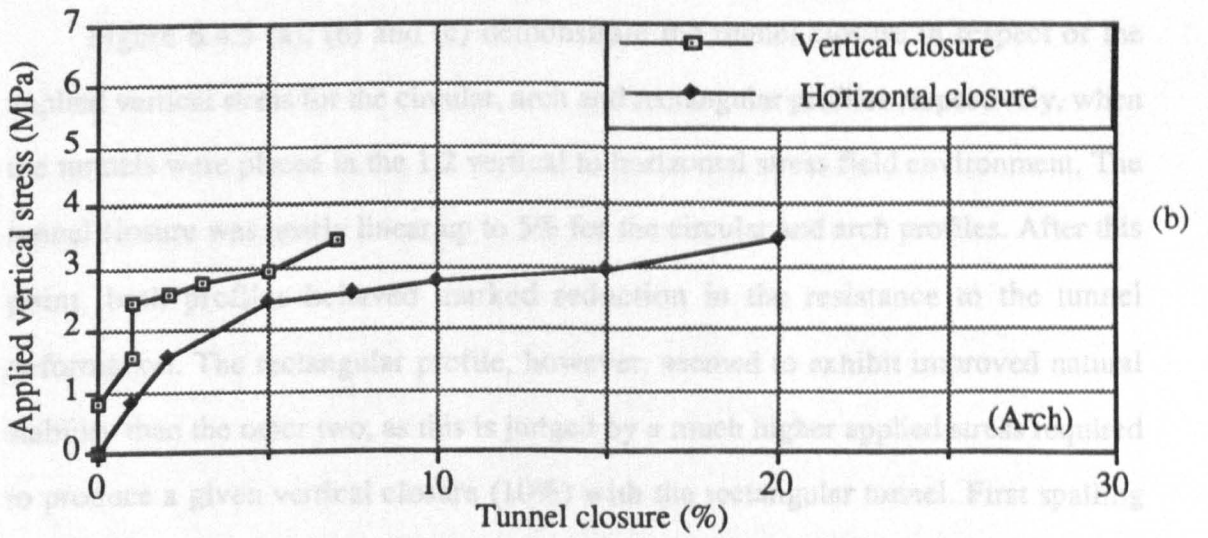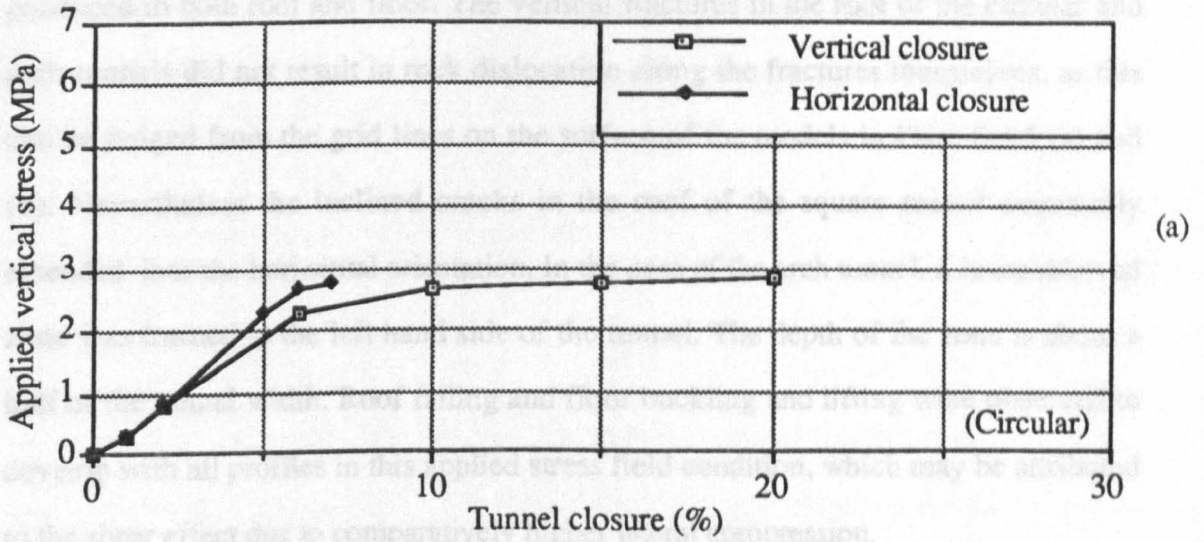
Figure 6.4.5 The tunnel closure against the applied vertical stress in the 1:2 vertical to horizontal stress field environment.

produced in both roof and floor. The vertical fractures in the roof of the circular and arch tunnels did not result in rock dislocation along the fractures themselves, as this can be judged from the grid lines on the surface of the models in Plate 6.4.5 (a) and (b). Nevertheless the inclined cracks in the roof of the square tunnel eventually extended into the horizontal orientation. In the case of the arch tunnel, a stress relieved zone was formed to the left hand side of the tunnel. The depth of the zone is about a half of the tunnel width. Roof falling and floor buckling and lifting were observed to develop with all profiles in this applied stress field condition, which may be attributed to the shear effect due to comparatively higher lateral compression.

Figure 6.4.5 (a), (b) and (c) demonstrate the tunnel closure in respect of the applied vertical stress for the circular, arch and rectangular profiles respectively, when the tunnels were placed in the 1:2 vertical to horizontal stress field environment. The tunnel closure was nearly linear up to 5% for the circular and arch profiles. After this point, both profiles behaved marked reduction in the resistance to the tunnel deformation. The rectangular profile, however, seemed to exhibit improved natural stability than the other two, as this is judged by a much higher applied stress required to produce a given vertical closure (10%) with the rectangular tunnel. First spalling was observed to occur at the 10% vertical closure of the rectangular opening, whereas in both circular and arch tunnels, first spalling was seen to produce at 5% and 2% vertical (or 6% and 5% horizontal) closures respectively. The comparison on these characteristics between the rectangular and the other two profiles reveals that, in the 1:2 vertical to horizontal stress field environment, the excavation with the height to the width equal to 1:2 appears to exhibit increased natural stability than those with other height to width ratios even including the circular profile.

6.4.6 1:3 Vertical to Horizontal Stress Field Environment

When driven in the 1:3 vertical to horizontal stress field environment, the tunnel exhibited weakened resistance to the closure and deformation. The test results showing

the applied vertical stress versus the tunnel closure for three different profiles in this stress field environment are presented in Figure 6.4.6.(a), (b) and (c) respectively. These results indicate that, in comparison with the other stress fields previously examined, this particular stress field had more markedly weakening effect on the tunnel profiles. All the tunnel profiles demonstrated sensitivity to the closure, especially after 5% vertical closure.

The fracture patterns for the circular, arch and square profiles tested are shown in Plate 6.4.6 (a), (b) and (c). It can be seen that the major fractures developed nearly horizontally in the sidewalls in all cases. They constituted a distinct stress relieved zone on each side of the tunnel. Particularly in the cases of the arch and circular profiles, the stress relieved zones around the tunnel formed a configuration with the height to width equal to about 1:3. This value of the ratio is very closely agreeable with that of the applied vertical to horizontal stress ratio.

From the photographs it can be observed that the shearing action played a significant role in the formation of the fracture patterns, as this is judged by the wedges of the failed material attempting to move laterally into the opening. The lateral movement of the wedges in the sidewalls was an important feature in all cases, which generated the floor instability, typically in the course of the arch profile test. The results from the circular opening indicate that the localise failure could also occur at the crown and the invert position under this applied stress field condition.

6.4.7 General Effects of the Applied Stress Field Environment on the Fracture Pattern and Development around Tunnels

Most test results regarding this aspect have been presented and discussed throughout Sections 6.4.1 and 6.4.6. These results reveal that the fractures developing around the tunnels are appreciably governed by the pattern of the applied stress field, particularly the direction and magnitude of the applied maximum and minimum stress components.
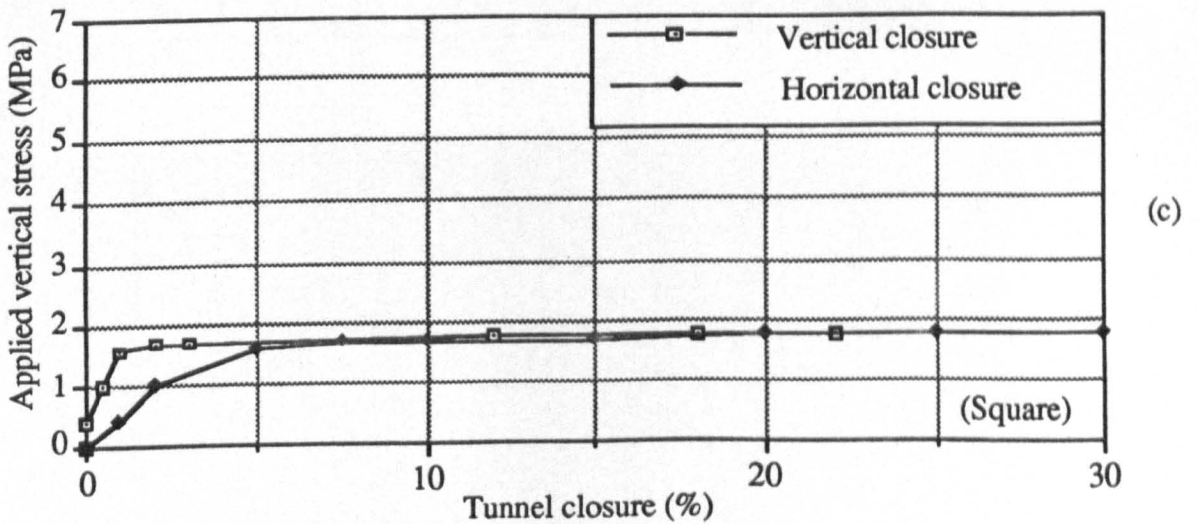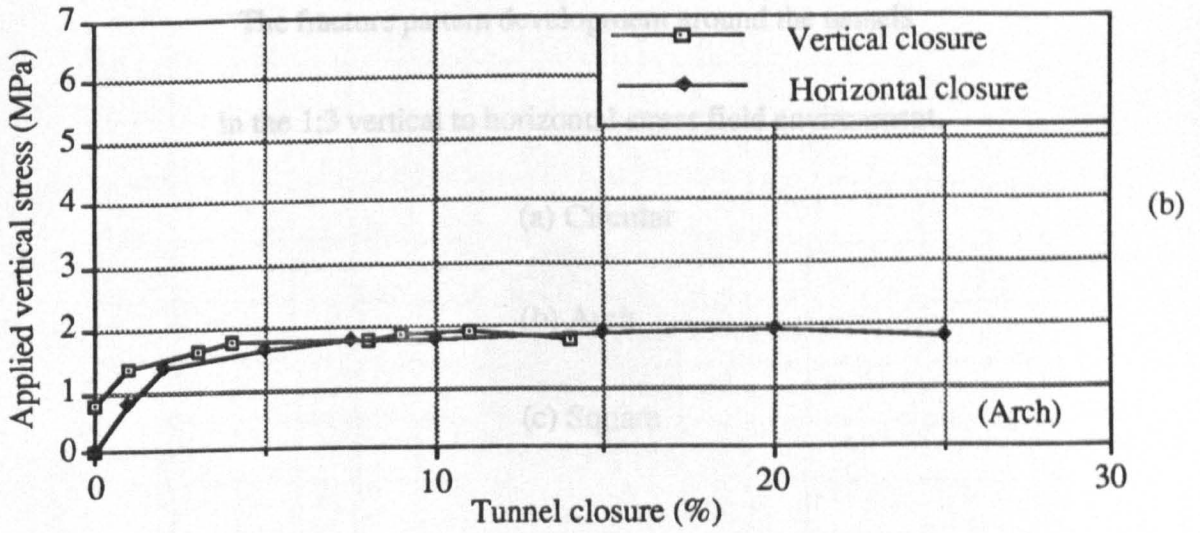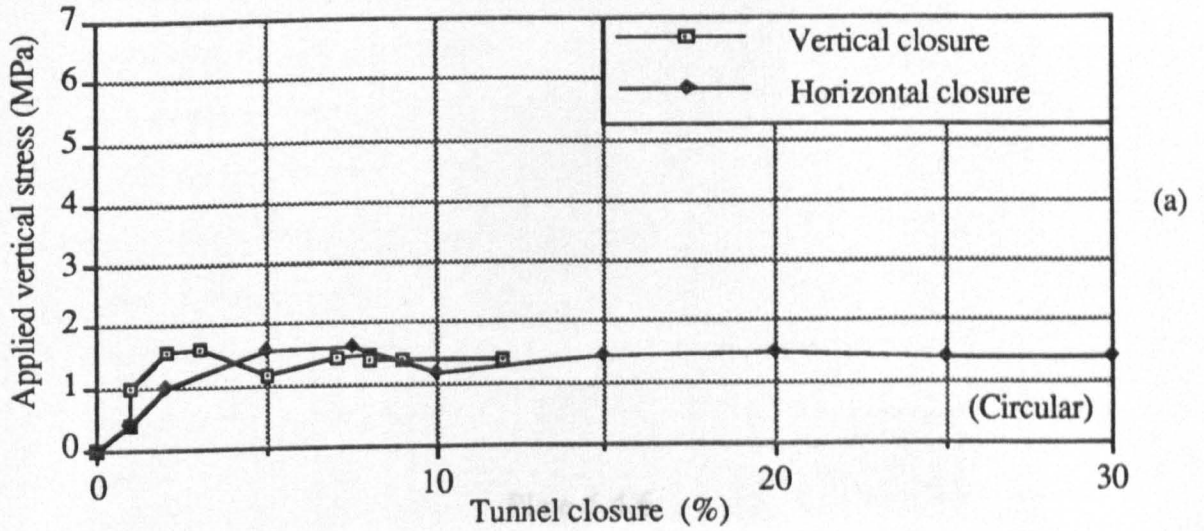
Figure 6.4.6 The tunnel closure against the applied vertical stress in the 1:3 vertical

to horizontal stress field environment.

Plate 6.4.6

The fracture pattern development around the tunnels

in the 1:3 vertical to horizontal stress field environment.

(a) Circular

(b) Arch

(c) Square
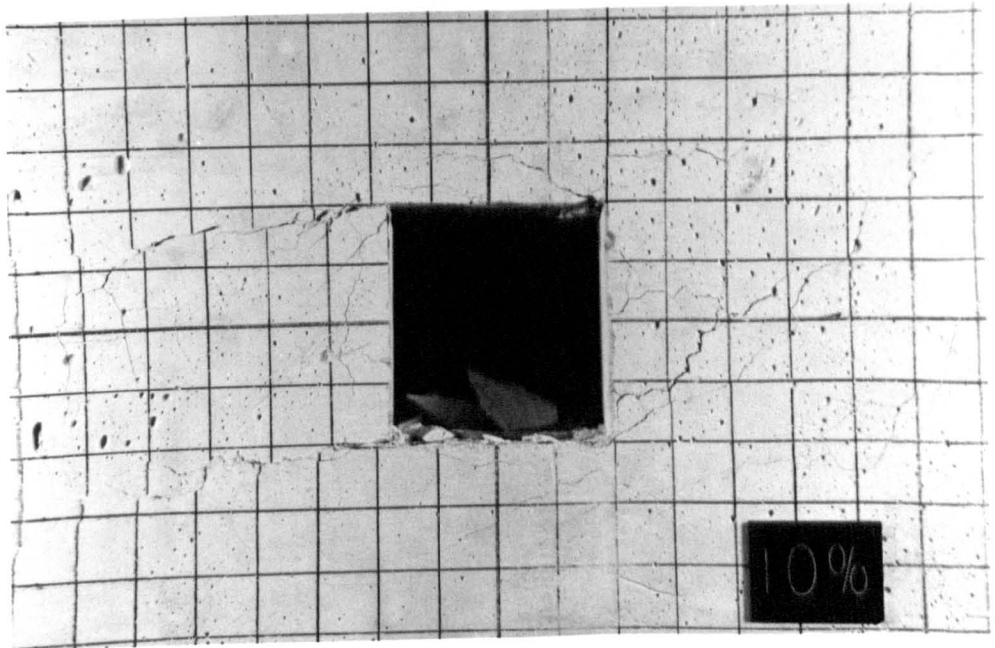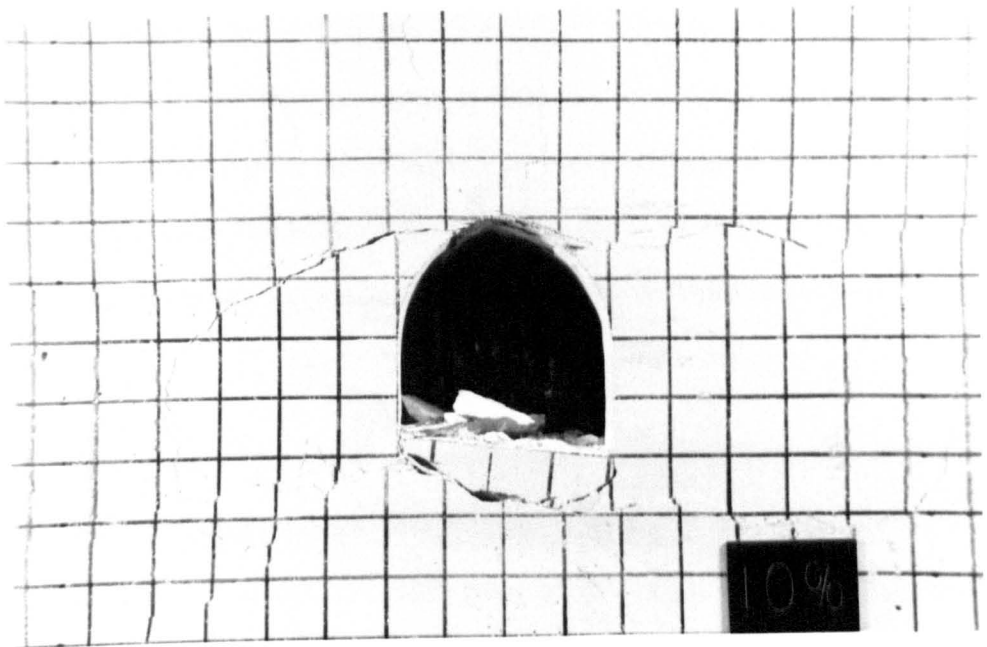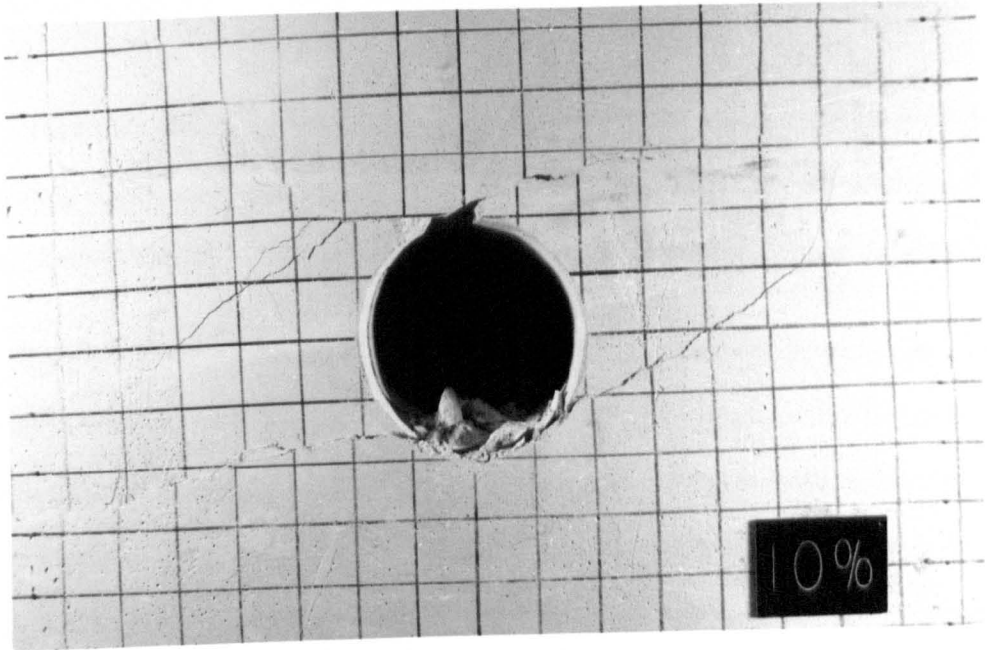
When the applied vertical stress is predominant, the major fractures will develop intensively in both the roof and the floor. However, the major fractures will develop in the sidewalls if the applied predominant stress is oriented in the horizontal direction.

The directions of the major fractures produced around the tunnels are mostly in agreement with the direction of the predominant stress applied. In the cases where the applied horizontal stress is greater than the vertical, the major fractures are mainly in the horizontal or close-to horizontal direction. These fractures are most likely to form a wedge or a stress relieved zone in both sidewalls. The depth of the wedge appears to be related to the value of the corresponding vertical to horizontal stress ratio applied, as this has been clearly shown through Plates 6.4.6 and 6.4.5. In the cases where the applied vertical stress becomes greater than the horizontal, however, the major fractures then develop mainly in the vertical or nearly vertical direction. Similarly, they will form a stress relieved dome in the roof, and many times in the floor as well. The height of the dome seems to be closely influenced by the applied vertical to horizontal stress ratio.

The occurrence of the stress relieved zone formed in either roof and floor or both sidewalls seems to have been influenced very little due to the variation in the tunnel profile, as long as the width to height ratio of the tunnel remains unchanged. The major horizontal (or closely horizontal) fractures in the tunnel roof, due to the effect of the higher horizontal stress applied, activates the roof slabbing and localised falling incidents, whereas the major vertical (or closely vertical) fractures in the sidewalls promote sidewall buckling and spalling.

6.5 Effects of the Tunnel Dimensional Ratio on the Tunnel Stability

In Chapter 4, a theory regarding the condition of the stability of an elliptical tunnel has been developed. The analysis results have indicated that the most stability of an elliptical tunnel is gained if the tunnel dimensional ratio (i.e. the long axis to the short axis) is equal to the ratio of the principal stress in the direction of the long axis to

the principal stress along the short axis. Because of the difficulty in the mathematical description for the tunnels of other than elliptical and circular profiles, the author has not extended the theory into the cases of the other tunnel profiles, such as arch, rectangular and square, etc. A question may arise as to how the results from the analysis for the elliptical profile become applicable to the design of other tunnel profiles. To answer this question, some extra model tests were carried out. The results of these models tested together with some others mentioned in Section 6.4 are employed for such study purpose. The study was confined to the rectangular profiles with the tunnel width to height ratio equal to 1:1, 2:1, and 3:1 respectively. The comparisons will be made among these tunnel profiles placed in three different stress field conditions, namely, 1:3, 1:2, and 1:1 vertical to horizontal stress fields.

6.5.1 Responses of the Tunnel Dimensional Ratio to the 1:3 Vertical to Horizontal Stress Field Environment

Three different width to height ratios of the rectangular tunnel profiles have been examined in the $3\sigma_v = \sigma_h$ stress field environment respectively. The test results regarding the applied horizontal and vertical stresses against the corresponding tunnel closures are shown in Figure 6.5.1 (a) and (b).

It is clearly shown with the graph in Figure 6.5.1(a) that, for a given stress level, the tunnel closure was appreciably smaller in the case of the tunnel with 3:1 tunnel width to height ratio than in the rest two tunnels. For example, at the 4.74 MPa horizontal stress with the 1.58 MPa vertical stress, 5% tunnel closure occurred in the tunnels having 1:1 and 2:1 tunnel width to height ratios respectively, whilst the closure of the tunnel with 3:1 width to height ratio was only 2%. This indicates that the last tunnel (W:H = 3:1) exhibited a markedly increased resistance against the tunnel deformation. Figure 6.5.1 (b) shows that the ultimate stress in the tunnel with W:H equal to 3:1 is greater than that in the square and the W:H-equal-to 2:1 tunnel cases. Plate 6.5.1 (a), (b) and (c) illustrate the variations in fracture pattern and tunnel
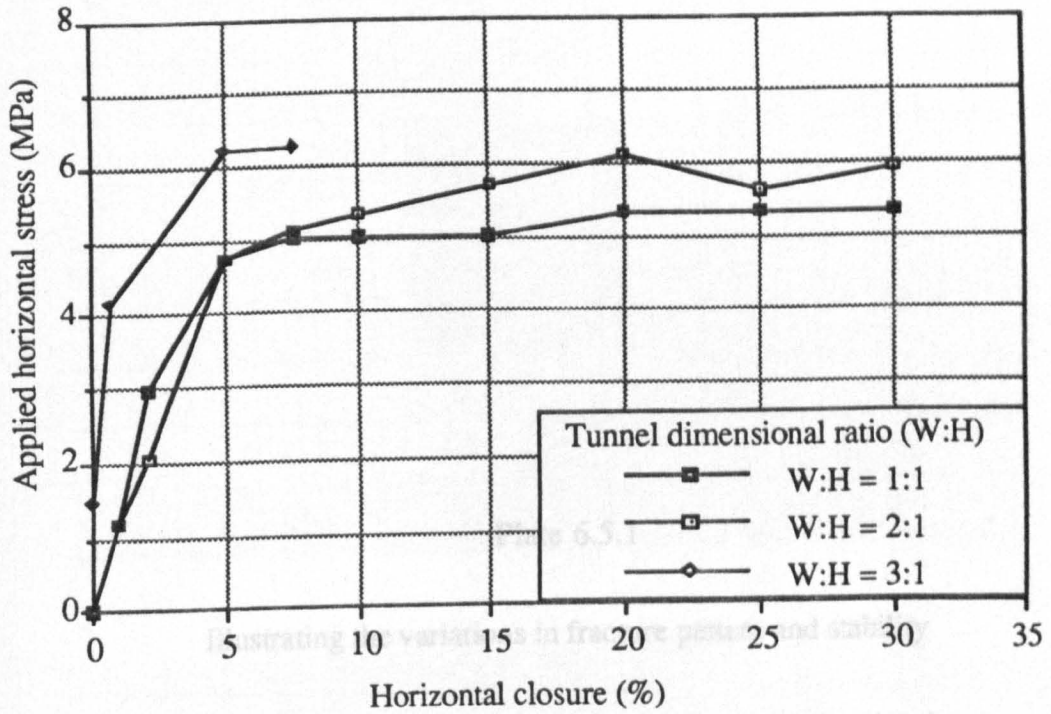
(a) A comparison on the horizontal closure for the three profiles
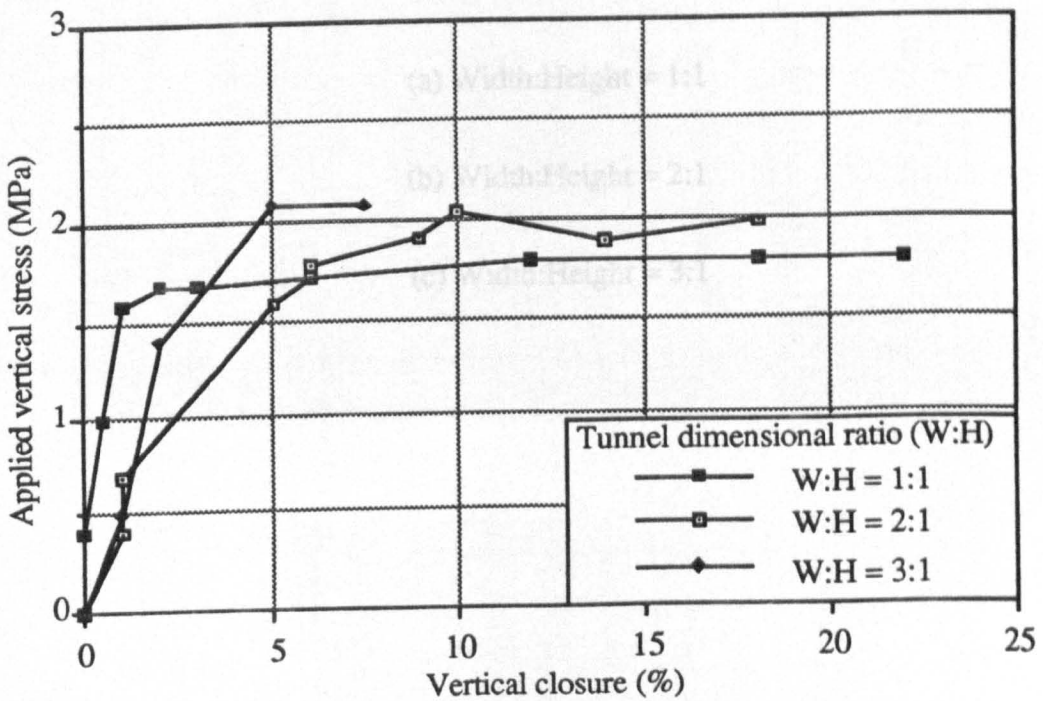
(b) A comparison on the vertical closure for the three profiles

Figure 6.5.1 The variation of the tunnel closure nature due to the difference in

the width to height ratio of the rectangular profile in the 1:3 vertical

to horizontal stress field environment.

Plate 6.5.1

Illustrating the variations in fracture pattern and stability

for the three rectangular tunnels at the same loading level

in the $3\sigma_v = \sigma_h$ stress field environment.

(a) Width:Height = 1:1

(b) Width:Height = 2:1

(c) Width:Height = 3:1
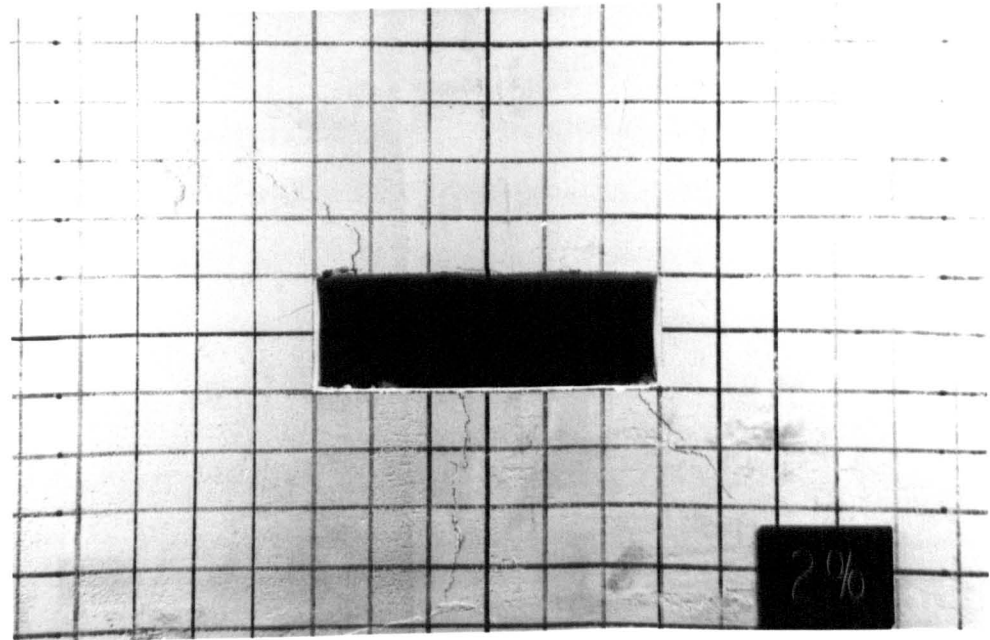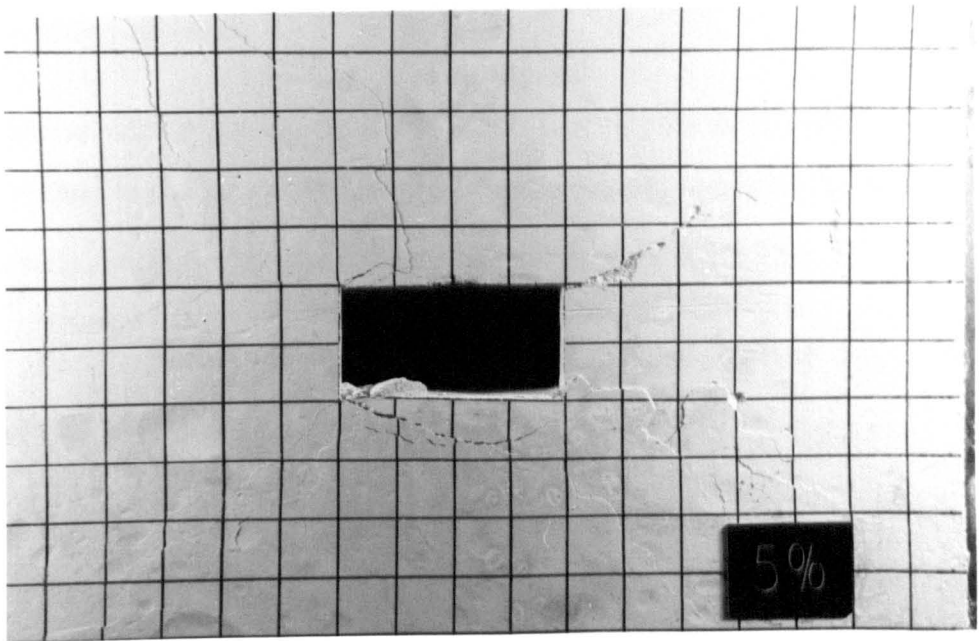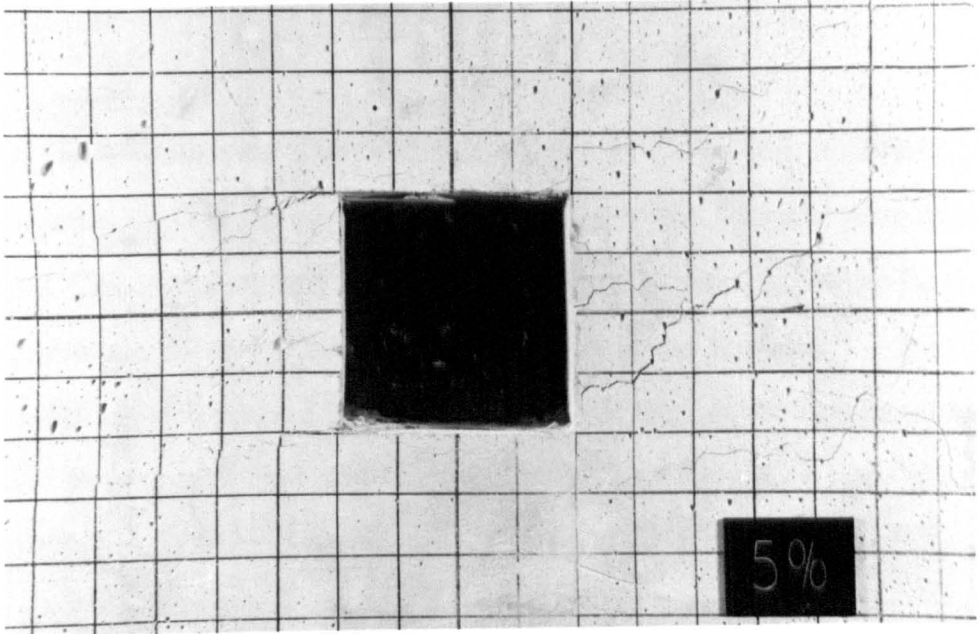
stability for these three tunnel profiles loaded at the 4.74 MPa horizontal and 1.58 MPa vertical stress level. In the side walls of the square tunnel, fractures were intensively produced. Cracks also occurred at the shallow depths of the roof and the floor, which later turned into the tunnel instability. In the rectangular tunnel of the 2:1 width to height ratio, major horizontal fractures have been produced in the right hand side wall. The floor and the roof were also fractured, which later developed into the localised roof collapse and the floor heave. Nevertheless, in the tunnel with the 3:1 width to height ratio, only three major cracks developed in the roof and floor. These cracks did not form a block in which the loosened materials tended to flush into the excavation in the later stages of the test.

The above comparison clearly shows that, among the three width to height ratios of the tunnel in the $3\sigma_v = \sigma_h$ stress field environment, the tunnel with 3:1 width to height ratio possesses the most natural markedly increased stability.

6.5.2 Responses of the Tunnel Dimensional Ratio to the 1:2 Vertical to Horizontal Stress Field Environment

Figure 6.5.2 shows the results of the comparison between two tunnels with the width to height ratio being equal to 1:1 and 2:1 respectively in the $2\sigma_v = \sigma_h$ stress field environment. The diagrams of the applied horizontal stress against the corresponding closure illustrate that the tunnel with the 2:1 width to height ratio has a noticeably higher natural stability than the square tunnel. The ultimate yielding stress for the rectangular tunnel is triple of that for the square tunnel. At the ultimate yielding stress point, only 7% closure was observed with the rectangular tunnel, whilst over 16 % closure occurred with the square tunnel. It is obvious from Figure 6.5.2 that the difference in respect of the tunnel deformation features exists between the two tunnels due to the difference in the value of the tunnel dimensional ratio.
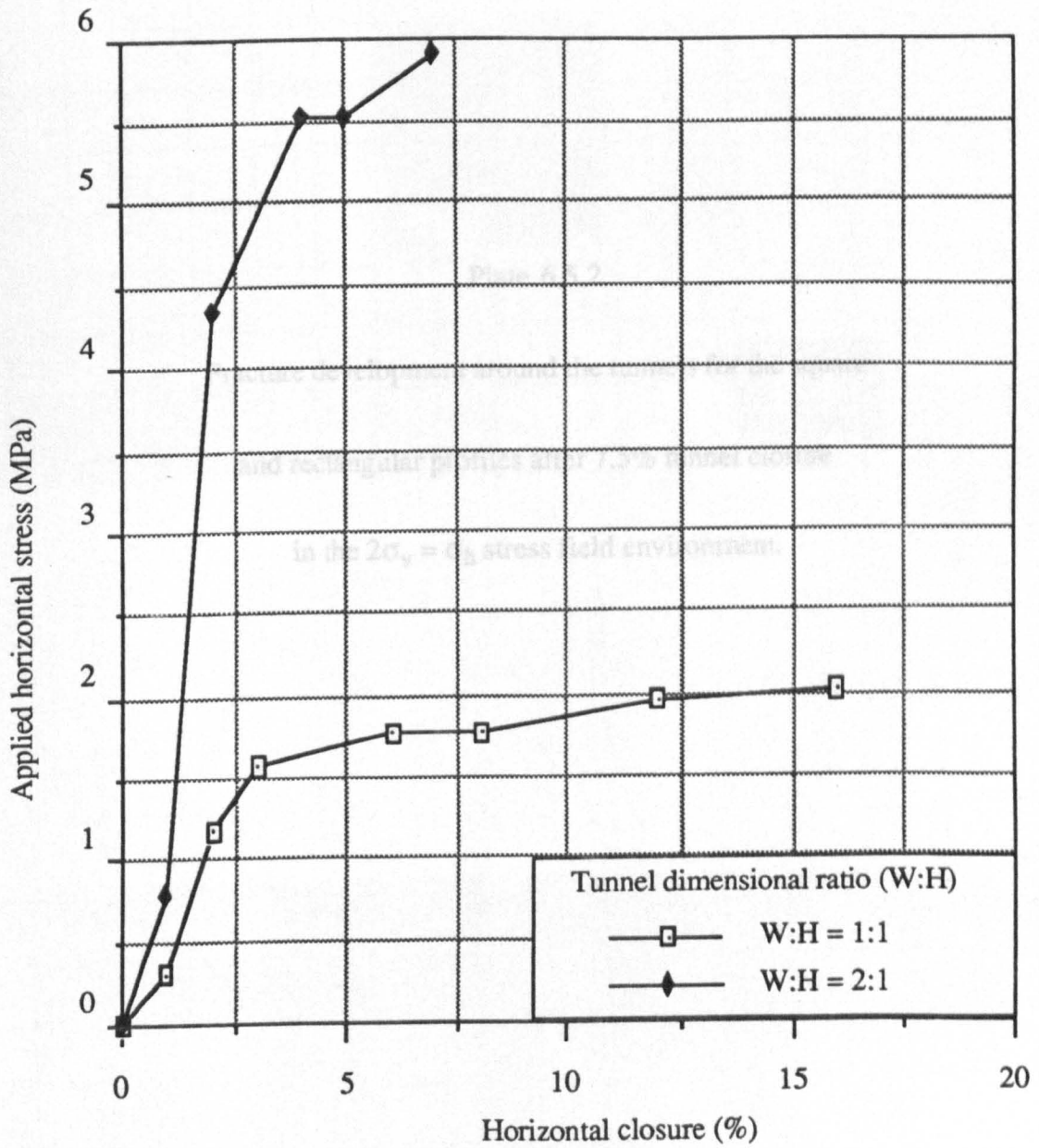
Figure 6.5.2 A comparison on the tunnel closure nature between two rectangular tunnels with 1:1 and 2:1 width to height ratio respectively, in the 2:1 horizontal to vertical stress field environment.

Plate 6.5.2

Fracture development around the tunnels for the square

and rectangular profiles after 7.5% tunnel closure

in the $2\sigma_v = \sigma_h$ stress field environment.

7.5%

7.5%
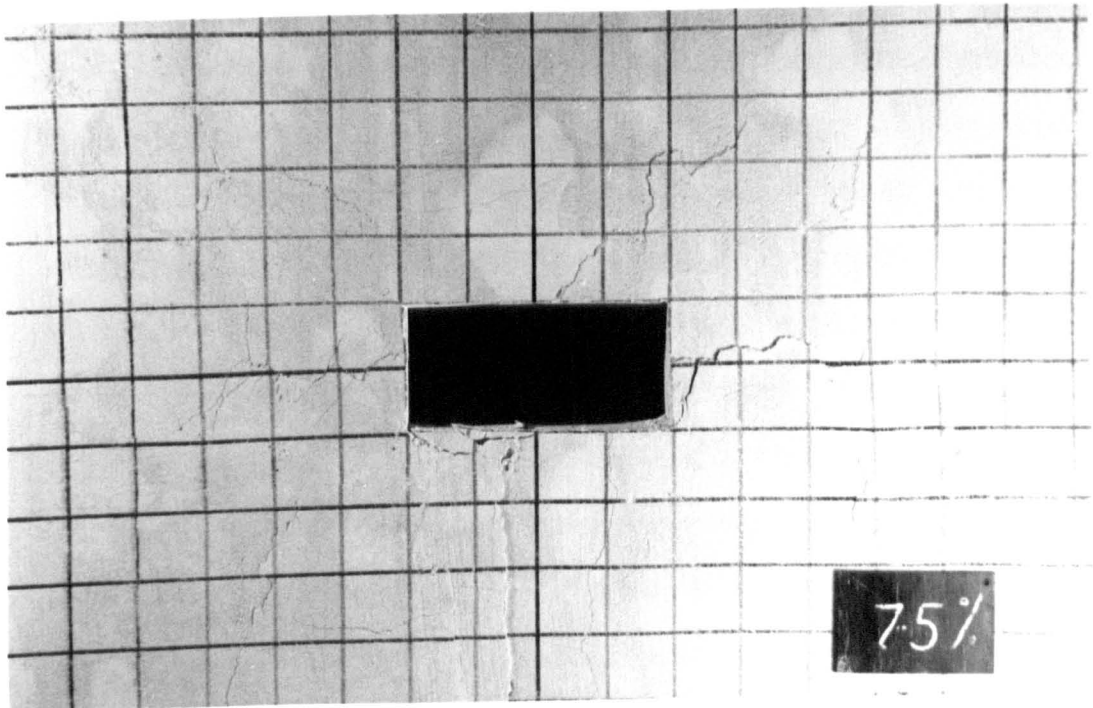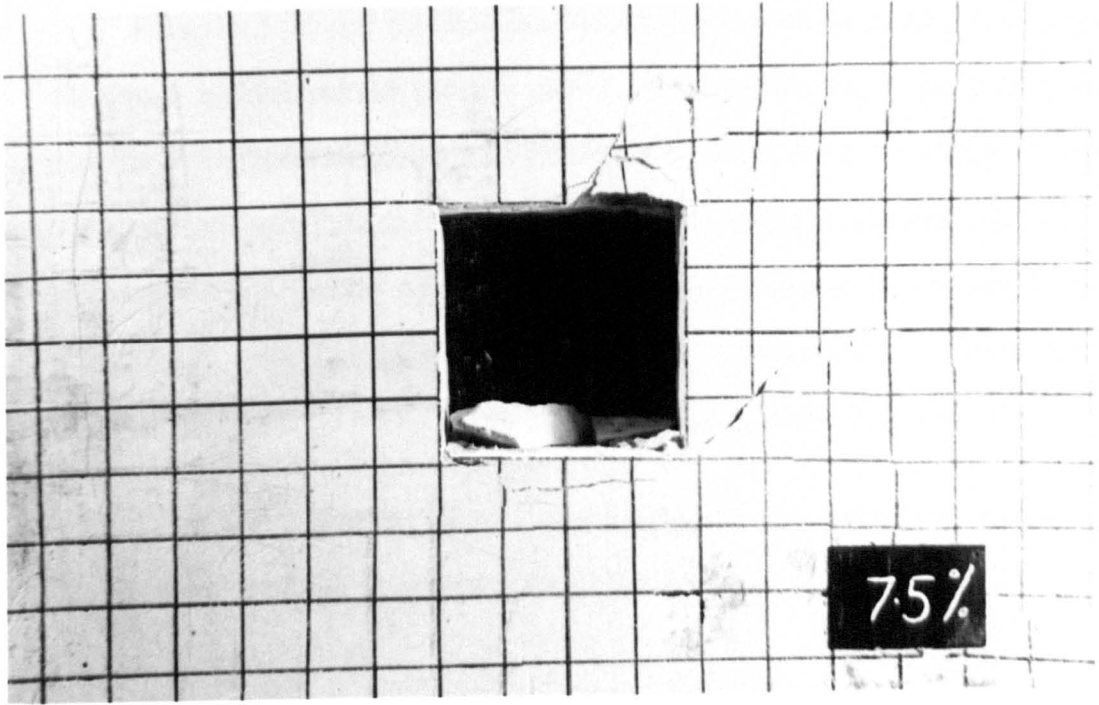
Plate 6.5.2 (a) and (b) illustrate the fractures developed around the tunnels for the square and rectangular profiles after 7.5% tunnel closure, respectively, when the tunnels were separately loaded in the $2\sigma_v = \sigma_h$ stress field environment. After this particular closure, the roof of the square tunnel failed with large pieces of debris flushing into the opening. In contrast, some fractures, though occurred and developed at the centre of the four sides of the rectangular tunnel, did not form any large stress relieved block or edge which might give rise to flushing into the excavation.

These comparisons lead to a conclusion that the rectangular tunnel is much advantageous over the square in terms of the natural tunnel stability in this particular stress field environment.

6.5.3 Responses of the Tunnel Dimensional Ratio to the Hydrostatic Stress Field Environment

A comparison has been conducted aimed at examining the differences between the square and rectangular tunnels in the hydrostatic stress field condition, in respect of the effect of the tunnel dimensional feature on the stability. Plate 6.5.3 (a) and (b) illustrate a result of this comparison after 15% tunnel closure. It can be seen from the photographs that the fractures steadily developed around the square tunnel, leaving a stress relieved dome of about 3.0 cm height (corresponding to 1.1 m in the prototype) to be formed in the roof. Contrary to this a stress relieved dome developing in the roof of the rectangular tunnel measured to be approximately 6 cm (corresponding to around 2.2 m in the prototype). When this difference is taken into account in the design of a tunnel support system, the weight of the loosened rock materials within the dome, which is referred to as the dead weight, should be fully held by the support system. In other words, in this particular stress field environment, the support capacity designed for the rectangular tunnel should be about twice of that for the square tunnel, because the dead weight from the roof of the rectangular tunnel is about twice that of the square tunnel.

Plate 6.5.3

Fracture development around the tunnels for the square and rectangular

profiles after 15% tunnel closure in the hydrostatic stress field environment.

(a) Square

(b) Rectangular (W:H = 2:1)
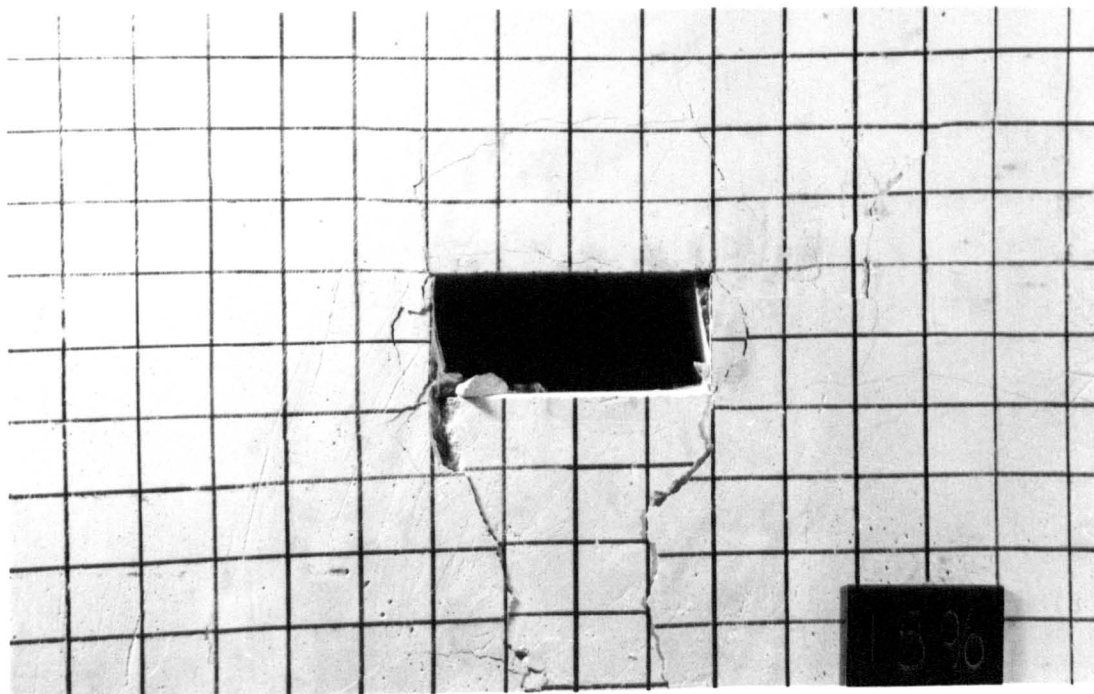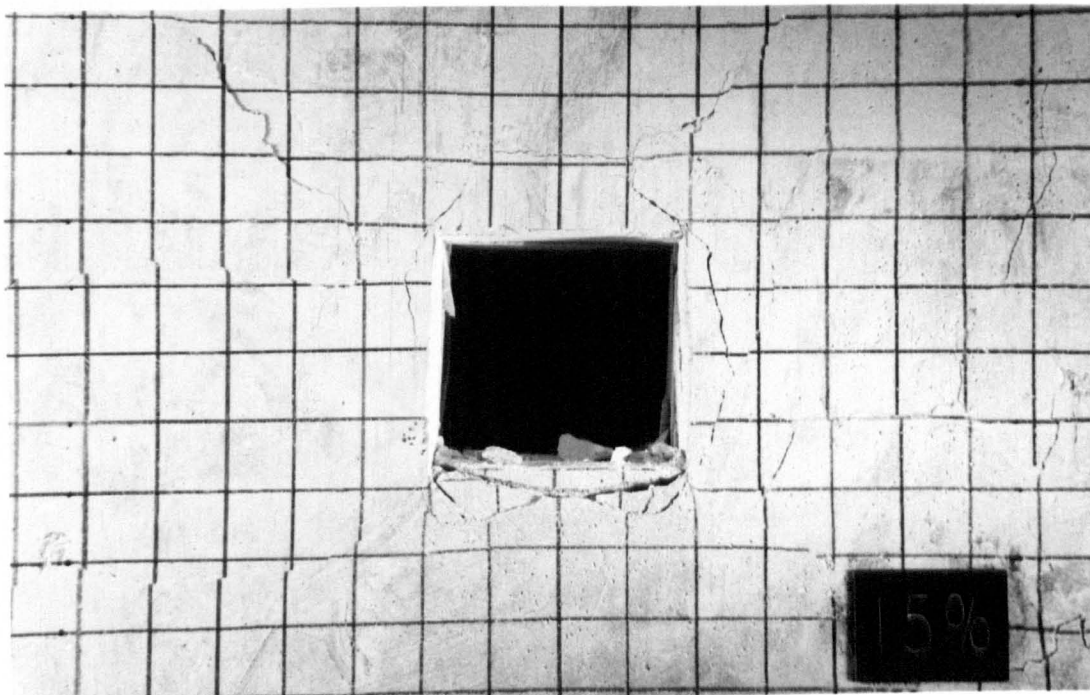
In respect of the fracture development in the floor, a difference also exists between these two profiles. For the square profile, fractures in the floor occurred at the shallow depth of around 1 to 1.6 cm (corresponding to 0.36 to 0.57 m in prototype) below the floor level, whilst in the rectangular tunnel, two major fractures initiated at the tunnel floor corners and then extended downwards into the deeper positions in the floor, forming a large stress relieved block which contributed appreciably to the floor lifting.

From these photographs it may be concluded that in the hydrostatic stress field environment, the square tunnel tends to have improved stability over the rectangular tunnel.

6.5.4 General Responses of the Tunnel Dimensional Ratio to the Applied Stress Field Environment

The above discussions reveal that the tunnel dimensional ratio has a great bearing on the fracture development in terms of the fracture pattern, intensity and direction. As the applied horizontal stress is appreciably increased (to become much greater than the vertical), a proper increase in the tunnel width from the square profile may result in a surprising improvement in the tunnel stability. However, when the applied horizontal stress is no longer greater than the vertical in magnitude, instability problems are most likely to arise in a tunnel that has a greater width than the height.

It is evident from these tests that the tunnel stability cannot be improved merely by increasing or decreasing the tunnel width without taking the stress field environment into account. The desired tunnel dimensions should have such values as the width to height ratio of the tunnel being equal to the value of the applied horizontal to vertical stress ratio.

The conclusion regarding the most suitable width to height ratio of the rectangular profile for the tunnel stability is agreeable with the theoretical analysis

results using the elliptical profile as discussed in Chapter 4. This indicates that the theoretical analysis results using the elliptical profile in Chapter 4 is applicable to the rectangular and therefore to the other profiles.

CHAPTER SEVEN

ROCK FRACTURE AND STABILITY OF TUNNELS IN STRATIFIED STRATA

CHAPTER SEVEN

ROCK FRACTURE AND STABILITY OF TUNNELS IN STRATIFIED STRATA

Coal resources are found in the sedimentary strata sequences. Extraction of the resources requires the majority of mining tunnels to be driven in these strata. A common feature of the strata is that of stratification in structure. The formation and nature of the stratified structure are governed by the historical setting, environment and the later disturbances in geology. Consequently, the mechanical behaviour of the sedimentary strata often vary from one layer to another, even in a closely related geological sequence.

Tunnels driven in the Coal Measures exhibit appreciable variations in respect of stability, as they are penetrate through different layers. As seen in practice, some tunnels are stable and require lower support capacity when they are excavated in a stratum sandwiched by competent thick strata. Others may present a number of instability problems when driven in weak and friable strata, particularly with thinly laminated structures. Obviously, the low strength of the strata is one of the major factors for instability. This factor has been well known and understood by the coal industry. The author has not repeated such work as to how tunnel stability is deteriorated by the low rock mass strengths. Instead, in the present Chapter he has attempted to investigate the following aspects:

(1) Effects of the rock stratification on the initiation and development of fractures around a tunnel;

(2) Effects of the lamination thickness on tunnel stability; and

(3) Roles that the support plays in tunnel stability control.

241

The physical modelling technique was used once again in order to carry out the investigations. A large testing rig was employed. The study started from the choice of the model materials.

7.1. Investigations into Characteristics of Model Materials Using the Orthogonal Design Method

Seeking the proper materials which possess the required physical properties for a model is a difficult task in physical modelling. When the sand, plaster and water are used as the raw materials and mixed together in building a tunnel model, a difference in ratio among these raw materials when mixed will cause a variation in the physical properties of the model material, as this may have been seen from the results presented in the previous chapter. A question arises as to what is the correct proportion of the sand, plaster and water to give the right properties of materials as required for a model. To solve this problem all applicable mixtures of sand, plaster and water are usually made and cast into cylindrical moulds to form samples. After curing in a controlled environment, these samples are tested. According to the test results the most appropriate mixtures of the raw materials will be selected for the model. This method is time consuming and costly when all possible mixtures of the materials have to be repeated because of a change in the property of one of the raw materials (i.e. when various plasters differ in properties).

7.1.1 Determination of Factors and Levels to be Examined

Experience has shown that the strength of a model material is closely related to the ratio of the sand , plaster, and water and also the curing conditions. To examine the effects of these factors on the model material strength index , varied values of each factor have been selected. A value of a factor is called a level of the factor. For instance the 48, 72, 96 and 120 hours were chosen as four levels of the factor of curing time to examine the influence of curing time on the indices of the strength and the unit weight.

Since the strength and unit weight of the model material is affected by the proportions among the raw materials instead of the weight of an individual material, what should be examined here is the ratio among the raw materials and the curing time. Therefore the weight of sand was fixed at a level of 450 grams for the investigations while the values of the other factors i.e. plaster, water and curing time were selected to vary at four levels as shown in Table 7.1.1.

Table 7.1.1   Selection of levels of factors

Level Factor	1	2	3	4
Plaster (g)	150	200	250	300
Water (cc)	250	300	350	400
Curing Time (hours)	48	72	96	120

The number of combinations of the three factors with each having four levels is calculated:

$$C = C_4^1 C_4^1 C_4^1 = 4 \times 4 \times 4 = 64 \qquad (7.1.1)$$

where C_4^1 means the number of combinations of a factor contributing one level each time from the four levels.

That is , 64 tests will be carried out if an ordinary testing procedure is followed to find the effects of these influencing factors on the examined indices. To carry out the 64 tests is time consuming, and should further levels be required in practice the number of tests to be undertaken would significantly increase. Obviously an alternative method should be sought by means of mathematics. Probably, the orthogonal design method is most applicable in this case.

7.1.2 Description of the Orthogonal Design Method and the Test Arrangement

The orthogonal design method was developed by a group of Chinese mathematicians (Beijing University, 1976). The theory is built on the basis of a statistical theory. It can be used to rank the importance of factors in influencing the magnitude of an examined index and to find a desired combination of factors in order to obtain a desired index. What is important and significant is that the application of the theory can lead to a huge saving in the number of tests. Time, labour and costs used in the tests are therefore cut to a minimum. In the situation of physical modelling where the levels of each factor are given, the orthogonal design method will identify the minimum number of tests required. It will also identify which factor is more quickly affecting the strength and unit weight of a model material , and what is the most appropriate combination among the factors for a specified strength and unit weight of the model material.

The theory of the method is based on an assumption that a level of a factor has a constant contribution to the magnitude of an index. Therefore the magnitude of the index in a test is referred to as an integration of contributions by all relevant factors with a given level of each.

To arrange a testing program a table called an orthogonal design test table is required (see Table 7.1.2). The table is designed in accordance with the number of factors and their levels to be inspected. Table 7.1.2 shows the arrangement of tests for four levels of up to five factors. The numbers 1, 2, 3 and 4 mixed and allocated in the columns underneath the headings factor 1 - factor 5 represent the levels of the corresponding factor. The table is known as a five-factor four-level orthogonal design test table, and was adopted to arrange the tests on the basis of Table 7.1.1, for which columns 2, 3, and 4 were assigned the factors of plaster, water and curing time respectively .The arrangement for the three factors of four levels listed in Table 7.1.1

is then obtained as presented in Table 7.1.3. From the table it can be seen that only sixteen tests would be carried out, which is much less than the 64 tests required by the previously stated method.

Table 7.1.2 The $L_{16}(4^5)$ orthogonal design test table

Levels\Factors Test Number	Factor 1	Factor 2	Factor3	Factor 4	Factor 5
1	1	1	1	1	1
2	1	2	2	2	2
3	1	3	3	3	3
4	1	4	4	4	4
5	2	1	2	3	4
6	2	2	1	4	3
7	2	3	4	1	2
8	2	4	3	2	1
9	3	1	3	4	2
10	3	2	4	3	1
11	3	3	1	2	4
12	3	4	2	1	3
13	4	1	4	2	3
14	4	2	3	1	4
15	4	3	2	4	1
16	4	4	1	3	2

An orthogonal design test table has the following features:

1) Homogeneity. Appearances of each level of a factor in the table are the same ; taking the factor of water in Table 7.1.3 for instance, each of the four levels (i.e. 250 cc, 300 cc, 350 cc, and 400 cc) is incorporated four and only four times.

2) Representation. The combinations of every level of a factor with every level of the other factors are the same. In Table 7.1.3, for example, level 1 of plaster (150 gram) combines once and only once with every level of the factors of water and curing

time. Each of the other levels of the plaster also combines once and only once with every level of the other factors, and vice versa.

Table 7.1.3 An arrangement of tests and the results

Levels Factors Test Number	Plaster (gram)	Water (cc)	Curing Time (hours)	Test Results	
				UCS (MPa)	Density (g/cm3)
1	150	250	48	0.2247	1.2728
2	200	300	72	0.2183	1.2018
3	250	350	96	0.2751	1.1409
4	300	400	120	0.4456	1.1023
5	150	300	96	0.0902	1.1612
6	200	250	120	0.5165	1.3177
7	250	400	48	0.3150	1.0724
8	300	350	72	0.6061	1.1775
9	150	350	120	0.0412	1.0739
10	200	400	96	0.1196	1.0425
11	250	250	72	0.8599	1.3028
12	300	300	48	1.1940	1.2778
13	150	400	72	0.0386	0.9873
14	200	350	48	0.1617	1.0891
15	250	300	120	0.3619	1.1365
16	300	250	96	1.0241	1.3772

These two features are crucial in reducing the total number of tests by the application of the method. The advantages of such design criteria become obvious in the following section.

7.1.3 Effects of the Examined Factors on the Material Unit Weight and Strength

According to Table 7.1.3 sixteen tests were carried out. In a particular test, sand, plaster and water at a pre-determined proportion were mixed together and poured into a number of cylindrical moulds. Each mould measured 51 mm diameter by 102 mm in length. When the mixture set and became solid the moulds were removed.

The cylindrical solid specimens were left in an oven at a temperature of 105^0C. Different curing times were used as required in Table 7.1.3. After curing, the specimens were weighed, measured and then tested to record their failure load. Accordingly the unit weight and uniaxial compressive strength (UCS) of each specimen was determined. An average value of the unit weight and the UCS in a group of test was taken as the value for that mixture. The values indicating the unit weight and UCS of model material of the sixteen tests are shown under Test Results in Table 7.1.3.

7.1.3.1 Strength Characteristics of the Mixtures Related to the Factors

In order to analyse the results obtained some denoted terms should be introduced. Here the values of strength and unit weight in the n th test are denoted as S_n and D_n respectively. S_{fn} is used to represent the sum of the strength of tests containing the n th level of the factor f. For example, S_{p1} refers to the sum of the strength of those tests in which the level 1 of plaster was chosen. Similarly D_{fn} refers to the sum of the unit weight of those tests (or mixtures) in which the n th level of the factor f was adopted. The following figures are subsequently obtained:

$$S_{p1} = S_1 + S_5 + S_9 + S_{13} = 0.2247 + 0.0902 + 0.0412 + 0.0386 = 0.3947$$

$$S_{p2} = S_2 + S_6 + S_{10} + S_{14} = 0.2183 + 0.5165 + 0.1196 + 0.1617 = 1.0161$$

$$S_{p3} = S_3 + S_7 + S_{11} + S_{15} = 0.2751 + 0.3150 + 0.8599 + 0.3619 = 1.8119$$

$$S_{p4} = S_4 + S_8 + S_{12} + S_{16} = 0.4456 + 0.6061 + 1.1940 + 1.0241 = 3.2698$$

By carefully examining the above four figures it can be noted that S_{p1}, S_{p2}, S_{p3} and S_{p4} are all commonly contributed once and only once by each level of the two factors, i.e. water and curing time. However S_{p1} is merely influenced by level 1 (not the other levels) of plaster. And S_{p2}, S_{p3}, and S_{p4} are correspondingly influenced by level 2, level 3, and level 4, respectively, of plaster. Obviously the difference between the four figures can only be attributed to the change in the level of plaster. Therefore the influence of plaster on the strength of the mixture material is obtained.

247

In the same way the following separate figures are obtained:

$S_{w1} = S_1 + S_6 + S_{11} + S_{16} = 0.2247 + 0.5165 + 0.8599 + 1.0241 = 2.6252$

$S_{w2} = S_2 + S_5 + S_{12} + S_{15} = 0.2183 + 0.0902 + 1.1940 + 0.3619 = 1.8644$

$S_{w3} = S_3 + S_8 + S_9 + S_{14} = 0.2751 + 0.6061 + 0.0412 + 0.1617 = 1.0841$

$S_{W4} = S_4 + S_7 + S_{10} + S_{13} = 0.4456 + 0.3150 + 0.1196 + 0.0386 = 0.9188$

$S_{C1} = S_1 + S_7 + S_{12} + S_{14} = 0.2247 + 0.3150 + 1.1940 + 0.1617 = 1.8954$

$S_{C2} = S_2 + S_8 + S_{11} + S_{13} = 0.2183 + 0.6061 + 0.8599 + 0.0386 = 1.7229$

$S_{C3} = S_3 + S_5 + S_{10} + S_{16} = 0.2751 + 0.0902 + 0.1196 + 1.0241 = 1.5090$

$S_{C4} = S_4 + S_6 + S_9 + S_{15} = 0.4456 + 0.5165 + 0.0412 + 0.3619 = 1.3652$

where S_{wi} and S_{ci} ($i=1, 2, 3$ and 4) are the sums of strength influenced by the i th level of the water and curing time respectively.

Dividing each of the above sums by four (i.e. the number of level) yields the average values of strength index, the difference of which is referred to the contribution made by the specified level of the factor. For example, $(S_{p2}/4)$ gives the contribution by the level 2 of plaster, compared with $(S_{p1}/4)$, $(S_{p3}/4)$ and $(S_{p4}/4)$. Table 7.1.4 (a), (b) and (c) are the collections of the results from the division calculation, which exhibit the tendency of strength influenced by the levels of each factor. Relations between the strength and the factors are more explicitly shown in Figure 7.1.1 (a), (b) and (c).

From Figure 7.1.1 (a) and (b) it can be found that the UCS of the mixture increases as the proportion of plaster increases and/or as the proportion of water decreases. Both plaster and water have a significant effect on the UCS of mixture material, with the former having much greater influence on the UCS. However the UCS decreases very slowly with the increase of curing time [see Figure 7.1.1 (c)]. Therefore the influence of the curing time on the UCS is not so evident and not so important in this case.

Plaster	150	200	250	300
$S_{pn}/4$	0,0987	0.2540	0.4530	0.8175
$D_{pn}/4$	1.1238	1.1628	1.1632	1.2337

(a) Influence of plaster on the UCS and unit weight

Water	250	300	350	400
$S_{wn}/4$	0.6563	0.4661	0.2710	0.2297
$D_{wn}/4$	1.3176	1.1943	1.1204	1.0511

(b) Influence of water on the UCS and unit weight

Curing time	48	72	96	120
$S_{cn}/4$	0.4739	0.4307	0.3773	0.3413
$D_{cn}/4$	1.1780	1.1674	1.1805	1.1576

(c) Influence of curing time on the UCS and unit weight

Table 7.1.4 Influence of the factors examined on the UCS and unit weight
of the model material.
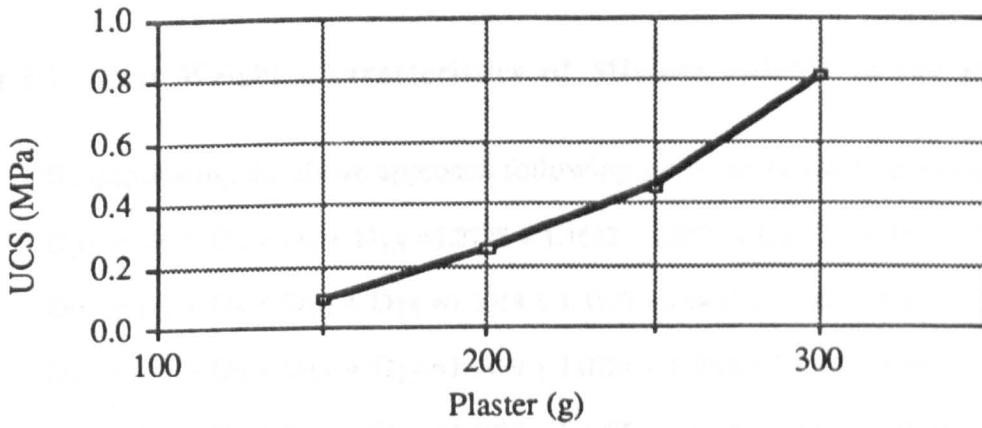
(a) UCS influenced by plaster
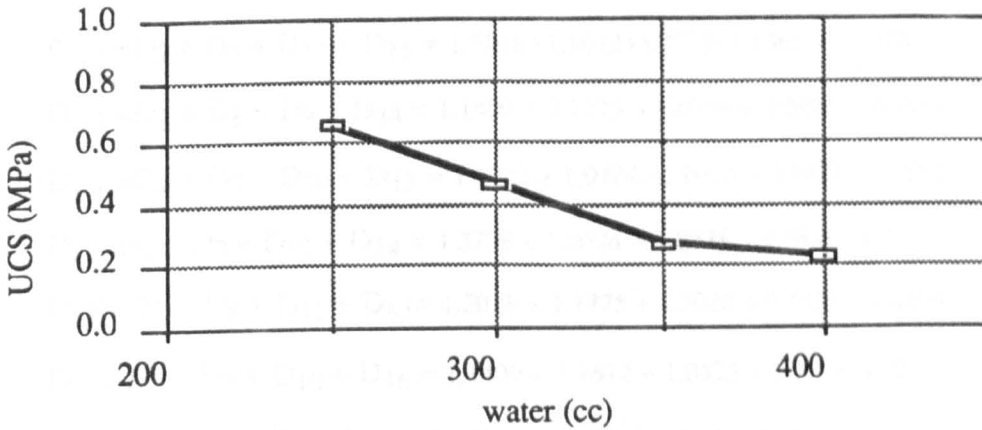
(b) UCS influenced by water
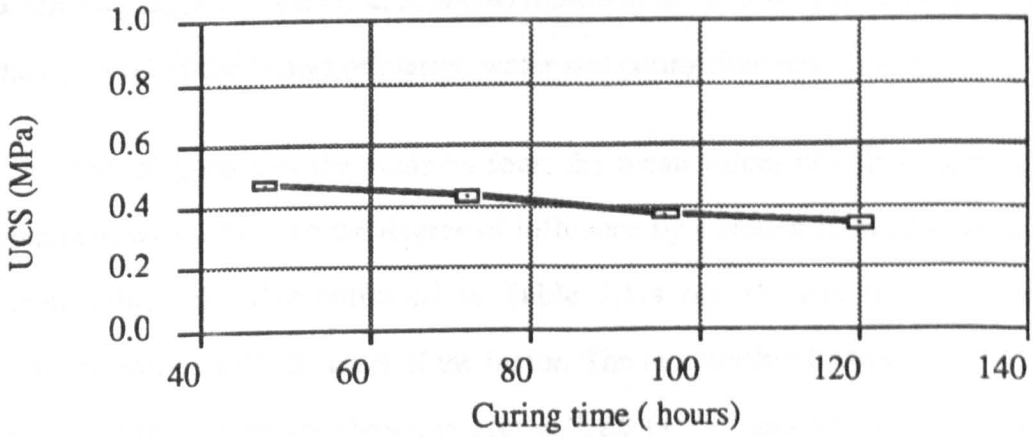
(c) UCS influenced by curing time

Figure 7.1.1 UCS influenced by the factors examined

7.1.3.2 Unit Weight Characteristics of Mixture Related to the Factors

By duplicating the above approach following sums can be easily obtained:

$$D_{P1} = D_1 + D_5 + D_9 + D_{13} = 1.2728 + 1.1612 + 1.0739 + 0.9873 = 4.4952$$

$$D_{P2} = D_2 + D_6 + D_{10} + D_{14} = 1.2018 + 1.3177 + 1.0425 + 1.0891 = 4.6511$$

$$D_{P3} = D_3 + D_7 + D_{11} + D_{15} = 1.1409 + 1.0724 + 1.3028 + 1.1365 = 4.6526$$

$$D_{P4} = D_4 + D_8 + D_{12} + D_{16} = 1.1023 + 1.1775 + 1.2778 + 1.3772 = 4.9348$$

$$D_{w1} = D_1 + D_6 + D_{11} + D_{16} = 1.2728 + 1.3177 + 1.3028 + 1.3772 = 5.2705$$

$$D_{w2} = D_2 + D_5 + D_{12} + D_{15} = 1.2018 + 1.1612 + 1.2778 + 1.1365 = 4.7773$$

$$D_{w3} = D_3 + D_8 + D_9 + D_{14} = 1.1409 + 1.1775 + 1.0739 + 1.0891 = 4.4814$$

$$D_{w4} = D_4 + D_7 + D_{10} + D_{13} = 1.1023 + 1.0724 + 1.0425 + 0.9873 = 4.2045$$

$$D_{c1} = D_1 + D_7 + D_{12} + D_{14} = 1.2728 + 1.0724 + 1.2778 + 1.0891 = 4.7121$$

$$D_{c2} = D_2 + D_8 + D_{11} + D_{13} = 1.2018 + 1.1775 + 1.3028 + 0.9873 = 4.6694$$

$$D_{c3} = D_3 + D_5 + D_{10} + D_{16} = 1.1409 + 1.1612 + 1.0425 + .3772 = 4.7218$$

$$D_{c4} = D_4 + D_6 + D_9 + D_{15} = 1.1023 + 1.3177 + 1.0739 + 1.1365 = 4.6304$$

where D_{pi}, D_{wi} and D_{ci} (i=1, 2, 3, and 4) represent the unit weight index influenced by the i th level of the factors of plaster, water and curing time respectively.

Dividing each of the sums by four, the mean values of unit weight index are obtained, which indicate the degree of influence by a certain level of a factor. These mean values are also collected in Table 7.1.4 (a), (b) and (c), each being in correspondence with the level of the factor. The relationship between the unit weight index and the factors are shown in Figure 7.1.2 (a), (b) and (c). It can be seen from Figure 7.1.2 (a) that, as the proportion of plaster increases in a mixture, the unit weight of the mixture increases gradually, However, the unit weight decreases with the increase of the proportion of water, as is shown in Figure 7.1.2 (b). This result can be attributed to the fact that the amount of water added to a mixture was not absorbed completely by the sand and plaster. Some moisture would be dried off when the mixture was left in an oven at a temperature of 105°C. Therefore some voids in the
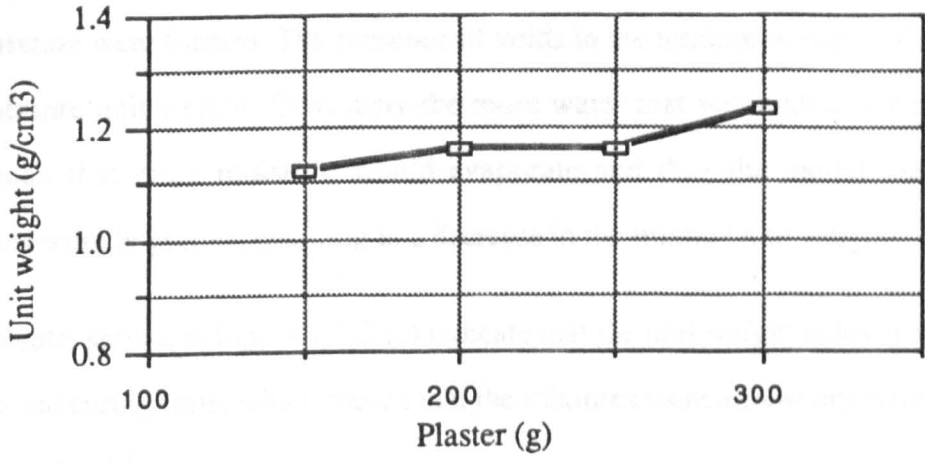
(a) Unit weight influenced by plaster
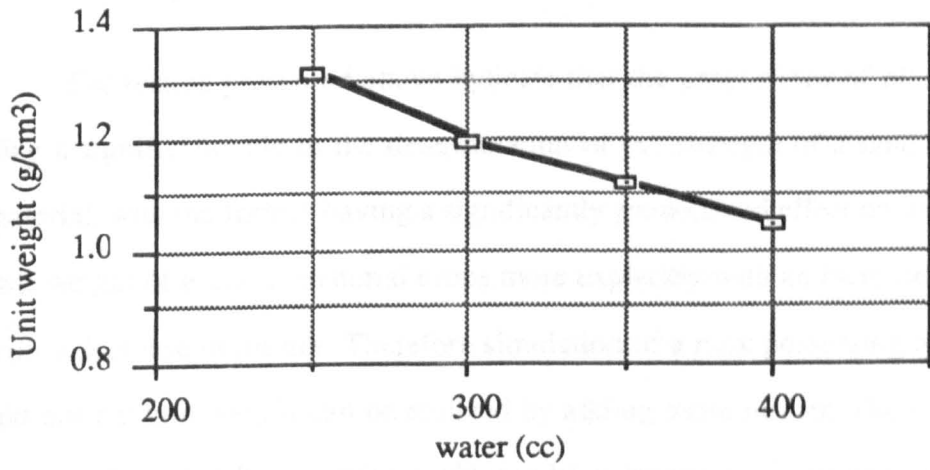
(b) Unit weight influenced by water
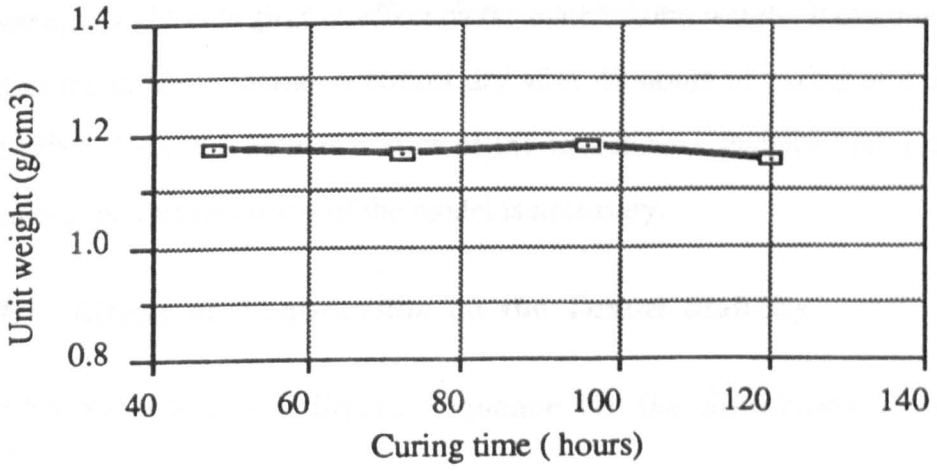
(c) Unit weight influenced by curing time

Figure 7.1.2 Unit weight influenced by the factors examined

mixture were formed. The presence of voids in the mixture would evidently affect the mixture unit weight. Obviously the more water that was added to a mixture would mean that more moisture would evaporate and thus the model material became increasingly porous, resulting in a decrease in the mixture unit weight.

Results shown in Figure 7.1.2 (c) indicate that the unit weight index is less influenced by the curing time, which means that the mixtures were almost dry after staying in the oven for 48 hours.

7.1.4. Using of the Results as a Guide-line for Modelling Materials

The results presented above indicate that the proportions of plaster and water play a significant role in the determination of the strength of a sand plaster model material, with the former having a significantly pronounced effect on its strength. The unit weight of a model material drops more explicitly with an increase in water than with a decrease in plaster. Therefore simulation of a rock possessing a high strength and normal unit weight can be realized by adding more plaster. The simulation of a weak rock with a lower unit weight can be achieved by increasing the amount of water. The curing time of the four levels examined has very little effect on the material strength and has negligible effect on the material unit weight. It can thus be concluded that the model material is almost dry after 48 hours of curing at a temperature of 105^0C. Since the characteristics of the model have become stable after 48 hours curing, no further curing of the model is necessary.

7.2 Effects of Stratification on the Tunnel Stability

7.2.1 Selection of a Strata Sequence for the Simulation Purpose

Generally speaking, the composition of strata around a tunnel is varied and complex. If the surrounding strata are divided into three parts according to their locations relative to the tunnel, namely the roof, the sides and the floor, each part may be classified into different categories in terms of strengths, strong, medium strength

and weak for instance. The three parts also consist of a number of layers with variations in the thickness and the number of laminations. Thus the number of combinations of these parts with varied layers and laminations becomes numerous, i.e. the composition of the surrounding rocks are diverse in practice. This leads to a result that the response of the surrounding rocks to a given stress field condition varies from case to case. Obviously it is impossible to examine the effect of all these strata compositions on the behaviour of a tunnel excavated in them.

However, the author has concentrated on choosing a strata sequence for the physical simulation purpose in order to study the influence of the ground stratification on the tunnel stability. The strata sequence chosen should be typical and representative in the U.K. coal industry. A search of the relevant literature reveals that, within the British Coal, the majority rock categories encountered in the sites of tunnels are mudstones,shales, fireclay stones, siltstones and sandstones with the mudstones and fireclays being most troublesome in the tunnel construction and maintenance. In the Selby Complex the mudstone seatearths have become a major source for the tunnel instability problems. The existence of these mudstones has led to the serious deformations of the tunnels, in particular, the floor lifts have caused a reduction in the tunnel height to 50 - 60 % of the originally excavated size in some collieries such as Gascoigne Wood. The behaviour of the weak mudstones in tunnel construction and maintenance have become a major concern of the mining engineer.

Upon this consideration, the physical modelling was focussed on studying the response of this kind of strata to the stress field when the excavation of a tunnel was made through it. A typical strata sequence was selected for the simulation. Figure 7.2.1 shows the strata sequence. It consists of mudstones, siltstone and sandstones. A tunnel will be located between the silty mudstone and mudstone seatearth, i.e between Numbers 4 and 6 in Figure 7.2.1, such that the tunnel instability problems related to the typical weak surrounding rocks may be simulated and studied.

NO.	Lithology	Thick-ness (m)	Unit Weight (g/cm3)	UCS (MPa)
1	Sandstone	3.00	2.42	68.1
2	Mudstone	6.94	2.24	39.5
3	Sandstone	4.13	2.42	68.1
4	Silty - Mudstone	2.06	2.16	28.0
5	Mudstone Seatearth	1.13	2.50	34.9
6	Mudstone	6.75	2.24	39.5
7	Siltstone	3.00	2.48	50.9
8	Mudstone	3.00	2.24	39.5
9	Sandstone	4.50	2.42	68.1
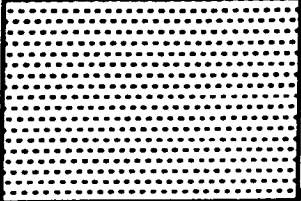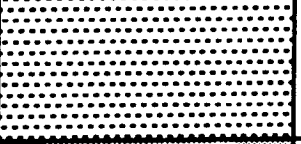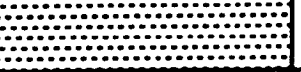
Legend :

Sandstone

Siltstone

Silty Mudstone

Mudstone

Mudstone Seatearth

Figure 7.2.1   A selection of the strata sequence for modelling.

7.2.2 Testing Rig, Scale Factors and Model Materials

A large testing rig was employed for the model tests. The rig has an interior dimension of 122 cm height, 122 cm width and 7.62 cm thickness for a model of a tunnel in the stratified condition. The model can be loaded bidirectionally by 64 rams that are equally arranged along the four sides of the model. The rams along the opposite sides are grouped together. Each ram is connected at the other end to a piston which is in turn connected to a hydraulic supply line. One end of the hydraulic supply line is connected to a hydraulic pump. Thus the 64 rams are eventually grouped into two with each group being manipulated by an individual hydraulic pump.

A dial pressure meter is connected to the outlet of each pump so that the pressures applied on the piston side of a ram are visible. The pressures on the model side of the ram (namely the pressures acting on the model edges) are found by a conversion of the meter readings incorporating the shape and dimension of the ram.

A steel plate of 2.54 cm (one inch) thickness, 110 cm length and 7.62 cm width was inserted between the model and a row of rams along each side of the model, to ensure an equal distribution of loads along each model side.

The geometric scale factor was selected to be 1:30, and the unit weight scale factor was 1:1.9. From the principles of the dimensional analysis in Section 6.1.1, the stress scale factor K_σ was calculated as:

$$K_\sigma = K_L \ K_D = \frac{1}{30} \times \frac{1}{1.9} = \frac{1}{57} \qquad (7.2.1)$$

where K_L is the geometric scale factor, and K_D the unit weight scale factor.

The results of testing of the materials in Section 7.1 were used as a guide-line while choosing proper model materials for simulating the strata sequence in Figure 7.2.1. Five different sand-plaster-water mixes were further tested and then used to represent the five different rocks shown in Figure 7.2.1. These mixes are listed in

256

Model Materials			Prototype Rocks Represented		
Sand : Plaster : Water	UCS (MPa)	Unit Weight (g/cm3)	Lithology	UCS (MPa)	Unit Weight (cm3)
450 : 300 : 300	1.1940	1.278	Sandstone	68.1	2·42
450 : 300 : 350	0.6935	1.178	Mudstone	39.5	2·24
450 : 250 : 300	0.4913	1.1382	Silty-Mudstone	28.0	2·16
450 : 200 : 250	0.6128	1.3178	Seatearth Mudstone	34.9	2·50
450 : 250 : 250	0.8936	1.3056	Siltstone	50.9	2·48

Table 7.2.1 Characteristics of the selected model materials and the corresponding rocks

Table 7.2.1. Using the scale factors calculated above, the uniaxial compressive strengths and unit weights that the mixes represent were found and are also listed in Table 7.2.1.

The mixes in Table 7.2.1 were used to construct the physical models simulating the strata sequence as shown in Figure 7.2.1. Those strata around the tunnel were considered to be laminated. The designed model structure is listed in Table 7.2.2.

7.2.3 Model Preparation and Installation

Four steel moulds were used for model casting. Each mould consisted of the front and rear steel plates, two lateral plates and one base plate. These plates were assembled via screws to form a mould with an interior dimension of 119.38 centimetres wide, 7.62 centimetres thick and 10.16 centimetres high. By raising the base plate to different positions, the height of the mould may be adjusted between 1.27 cm and 10.16 cm. This feature of the mould enables the model to be cast into the desired number of layers and to have an equal height along the whole mould horizon within an individual layer.

Upon the consideration that, in the course of the model installation, a steel plate of 2.54 cm thick had to be inserted between the model sides and the ram rows in the testing rig to ensure an equal application of loads to the model, the interior width of the moulds had to be narrowed to 116.84 cm by putting a 2.54 cm x 7.62 cm x 10.16 cm wooden plate at one interior end of the mould.

When the mould with desired interior dimensions (particularly the height) was formed, the interior faces of the mould were greased with the lubricant oil for the ease of the later separation of the cast model block from the mould. Then sand and plaster were weighed and mixed with water in the pre-determined proportions. After a well stirring for around one minute, the mixture material was poured into the mould. Before the material completely set, the over cast part of the mixture was scraped from

258

NO	Lithology Simulated	Total Thickness (cm)	Layer Thickness (cm)	Number of Layers	Material Ratio Sand : Plaster : Water	Note
1	Sandstone	10.16	10.16	1	450 : 300 : 300	
2	Mudstone	23.50	10.16 3.18	2 1	450 : 300 : 350	
3	Sandstone	13.97	3.18 2.54	1 4	450 : 300 : 300	Adding colour
4	Silty-Mudstone	6.99	1.91 2.54	1 2	450 : 250 : 300	
5	Mudstone Seatearth	3.81	3.81	1	450 : 200 :350	
6	Mudstone	22.86	2.54	9	450 : 300 : 350	
7	Siltstone	10.16	10.16	1	450 : 250 : 250	
8	Mudstone	10.16	10.16	1	450 : 300 : 350	
9	Sandstone	15.24	5.08 10.16	1 1	450 : 300 : 300	

Table 7.2.2 The model structure and sequence

the top of the mould by means of a steel plate. The desired and equal thickness of the layer was thus gained.

A few minutes later, the cast material completely set. The mould plates were unscrewed and the front plate removed off the mould. The base plate was lowered to a given position. The mould plates were then re-assembled and greased to produce a new mould volume for the casting of the next layer.

The mixture material for the next layer was directly poured on the top of the previous layer to create an interface bonding effect.

The procedure was repeated until the mould could not accept any more layer, i.e. the mould was full or could not provide a volume enough for the next layer. The Mould was then disassembled. The whole block containing a number of layers was left in an oven at a temperature of $105^{\circ}c$ for 48 hours. Twelve blocks of such moulds were needed to constitute a model.

Two hours before the model installation, the oven was switched off and the blocks were left to cool naturally.

The cooled blocks were removed out of the oven and piled up into the testing rig according to the designed strata sequence. The rig was rotated around a horizontal axis so that the vertical position of the model plane was rotated to the horizontal. Four steel plates of 2.54 cm thick were inserted between the four model sides and the four ram rows of the rig. The front of the model was marked in 2.5 cm x 2.5 cm grids with a black pen.

Two acting pumps were operated to motivate the rams stretching out slightly against the model, such that the model was held in position. The whole rig was then rotated back to the vertical position. An arch-shaped tunnel was carefully excavated at the centre of the model, using a saw blade, screwdrivers and scrapers.

Having cut the tunnel, the rig was rotated again to the horizontal position. The front cover of the rig was lifted from the floor onto the model front surface, by means of a 5 tonne crane, and fully tightened with bolts and nuts using a pneumatic wrench. At the centre of the front cover, a transparent plastic disc of 40 cm diameter was assembled for the observation of the model deformation. The rig was rotated back to the vertical position and ready for the loading test.

The dimension of the arch tunnel was 20 cm wide and 20 cm high, corresponding to 6 m x 6 m in the prototype. The crown curve was a semi-circle with a 10 cm radius corresponding to 3 m in the prototype. The tunnel location in the rock formations is shown in Figure 7.2.2.

7.2.4   Testing Procedure

The stress applied to the model were taken as a basic measurement for the later comparison purposes. At some loading levels, the model tunnel was measured for the value of closures and then unloaded for the ease of removing the front cover. When the front cover was removed off the rig, the fracture pattern and its development was observed, sketched in a notebook and photographed.

After putting and tightening the front cover to the rig, the model loading went on until the next step of the applied stress was arrived at.

This testing cycle was repeated until further loading was judged to be of no practical value.

With all of these records and photographs, the analysis of the results becomes possible and has been conducted in the following sections.

NO.	Lithology
1	Sandstone
2	Mudstone
3	Sandstone
4	Silty mudstone
5	Mudstone Seatearth
6	Mudstone
7	Siltstone
8	Mudstone
9	Sandstone

6 m

6 m
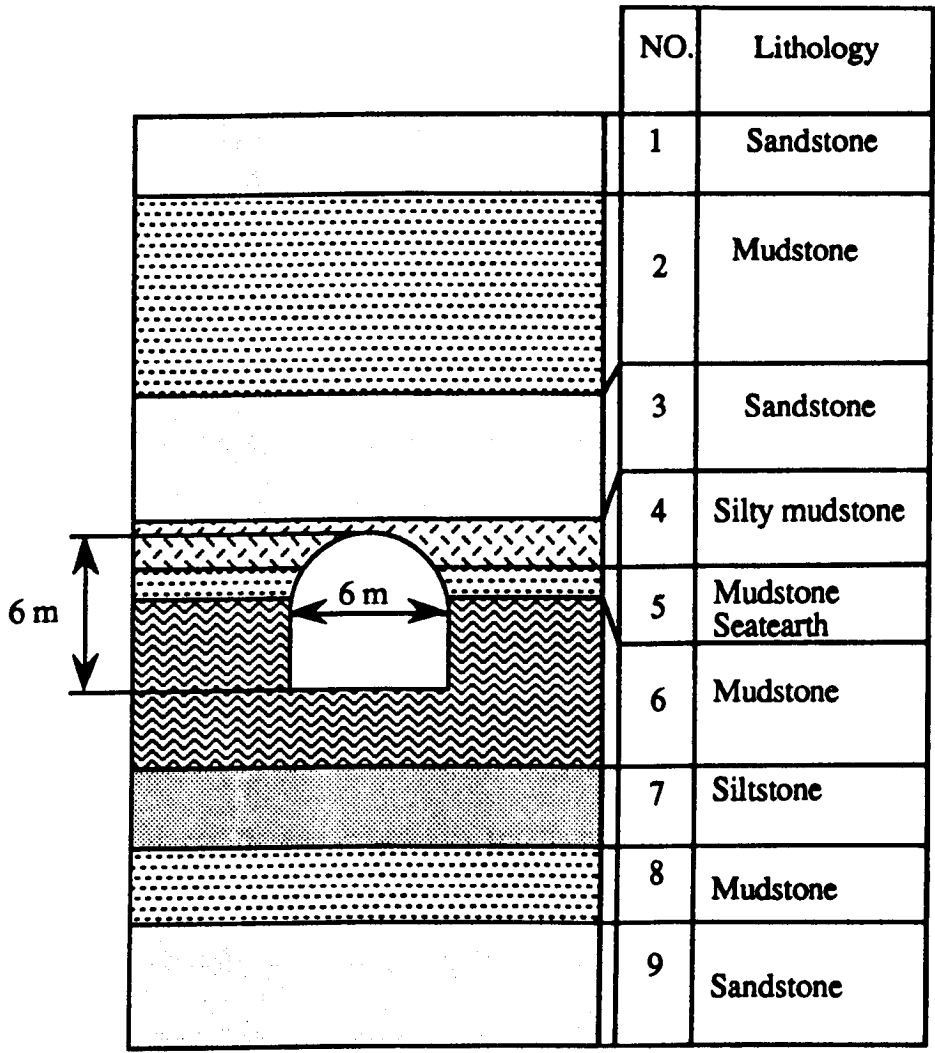
Figure 7.2.2   The location and dimension of the simulated arch tunnel.

262

7.2.5 Behaviour of Tunnel in Two Different Stress Field Environments

Two models were tested for an investigation of the tunnel behaviour. One was loaded in a 2:1 horizontal to vertical stress field. This model is denoted as L3. The other was loaded in a 1:2 horizontal to vertical stress field environment and is denoted as L5.

In the test of the L3 model where the 2:1 horizontal to vertical stress field was applied, the lateral movement was much more pronounced than the vertical. Plate 7.2.1 illustrates the tunnel deformation situation, where the pressures acting on the sides of the model were 1.019 MPa in the horizontal direction and 0.510 MPa in the vertical direction. At this moment, the horizontal closure was 7.5% and the vertical 1.5%. It can be seen from the photograph that the lateral movement took place mainly along two interface planes. One was at the crown summit level which was within the silty mudstone. The other was in the mudstone of the immediate floor. A further examination on the features of these two interface planes shows that these planes were all those between two neighbouring cast blocks. Because these pre-cast blocks were simply filled up in the model installation, the resistance against the shearing action along the interface was eventually produced by the friction on the contacting block surfaces. This resistance or the shear strength was obviously weaker than the other interfaces between two neighbouring layers within a blocks, as the later had a shear strength produced by both the friction resistance and the bonding strength. The bonding strength was formed in the course of the block casting when a next layer was directly poured onto the previous one.

The floor failure took place under the excessive lateral compression. The failure initiated from the occurrence of a detachment along a horizontal bedding plane about 2 cm (corresponding to 0.6 m in prototype) underneath the floor level. An inclined fracture then appeared near the left hand side corner, a vertical one at the centre of the floor. From the mechanics knowledge, it can be judged that the inclined fracture was

263

Plate 7.2.1

The fracture and deformation of tunnel in the stratified strata

in the $2\sigma_v = \sigma_h$ stress field environment.

STEP I
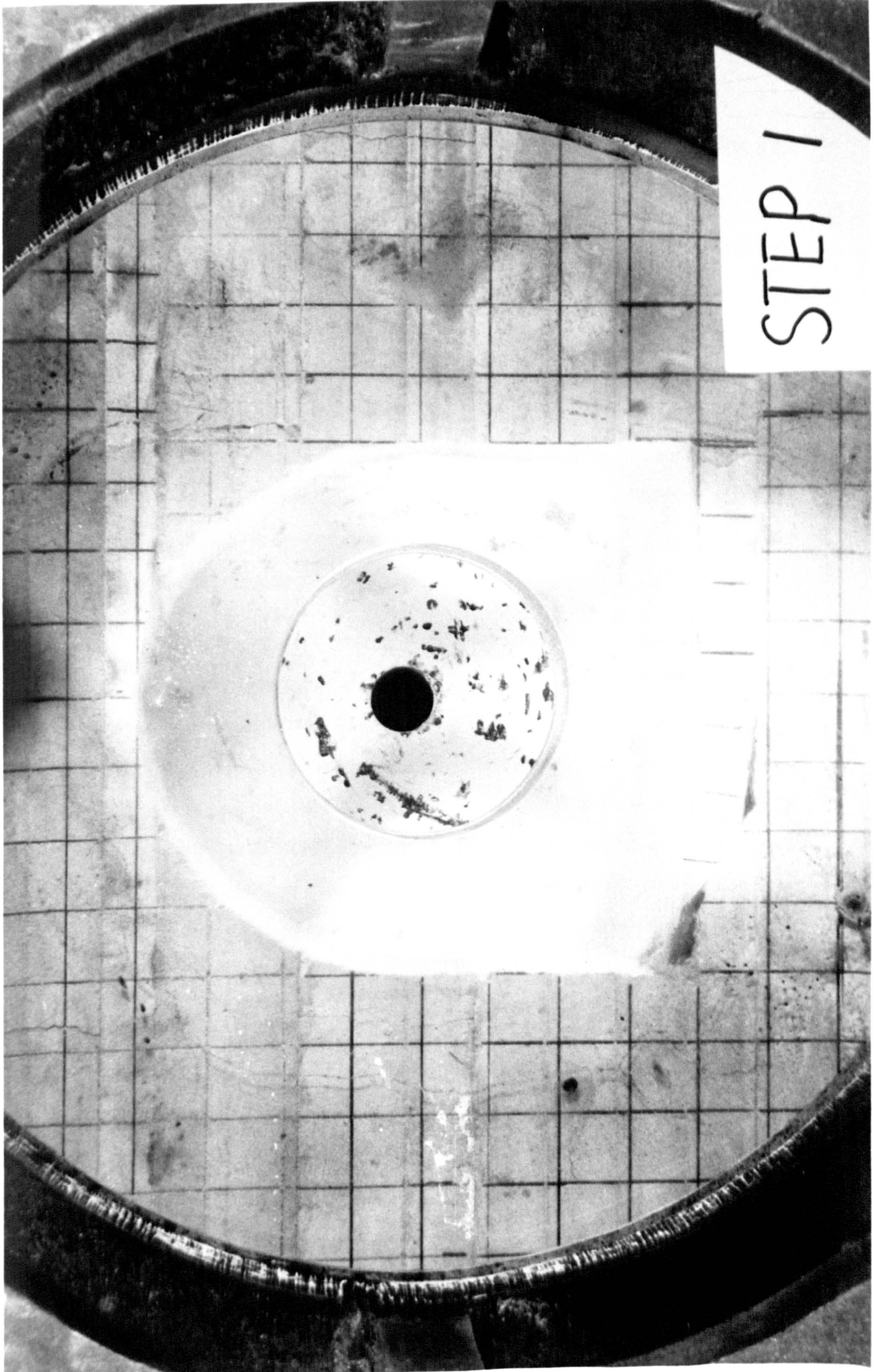
due to the shear failure and the vertical one was produced by the tensile failure via a bending deformation.

The results from this model test (L3) indicate that the rock failures are more likely to first occur along the bedding planes with low shear strengths if the predominant applied stress is in the direction of the beddings. In this stress field environment, it could be significant to enhance the strength of those bedding and / or weak planes the directions of which are in accordance with that of the maximum stress applied. The application of the rockbolts and the standing supports with high capacity may achieve a marked ending in the tunnel maintenance. A simulation of a metal support in the tunnel has been carried out by the author and will be presented in the latter part of this Chapter.

In the test of the L5 model , the 1:2 horizontal to vertical stress field was applied. A vertical fracture of about 2 cm (equivalent to 0.6 m in the prototype) long first developed in both floor corners after 1.529 MPa vertical and 0.764 horizontal stresses. At this moment, the vertical closure was 3% compared with 2% horizontal closure. As the applied stresses were increased to 2.038 MPa in the vertical direction and 1.019 MPa in horizontal, slightly peeling failures were observed at the tunnel crown and both sides, see Plate 7.2.2 (a). The floor lifted up a bit after the fractures in the floor corners developed a bit further. As a result, the vertical and horizontal closure of the tunnel were 5% and 3.5% respectively.

With continuous increases in loads up to 3.058 MPa in the vertical and 1.529 MPa in horizontal directions respectively, a number of new fractures appeared around the tunnel. In particular, the two existing fractures in the floor corners further developed into the deeper layer in the floor. They stopped the vertical development at 15.5 cm (equivalent to 4.65 m in the prototype) below the floor level, and then extended horizontally toward each other. They finally connected together and formed an envelope surface of the fracture. The zone within this envelope surface was

265

Plate 7.2.2

The fracture and deformation of tunnel in the stratified strata

in the $\sigma_v = 2\sigma_h$ stress field environment.

(a) $\sigma_v = 2.038$ MPa, $\sigma_h = 1.019$ MPa

(b) $\sigma_v = 3.058$ MPa, $\sigma_h = 1.529$ MPa

STEP 3

STE
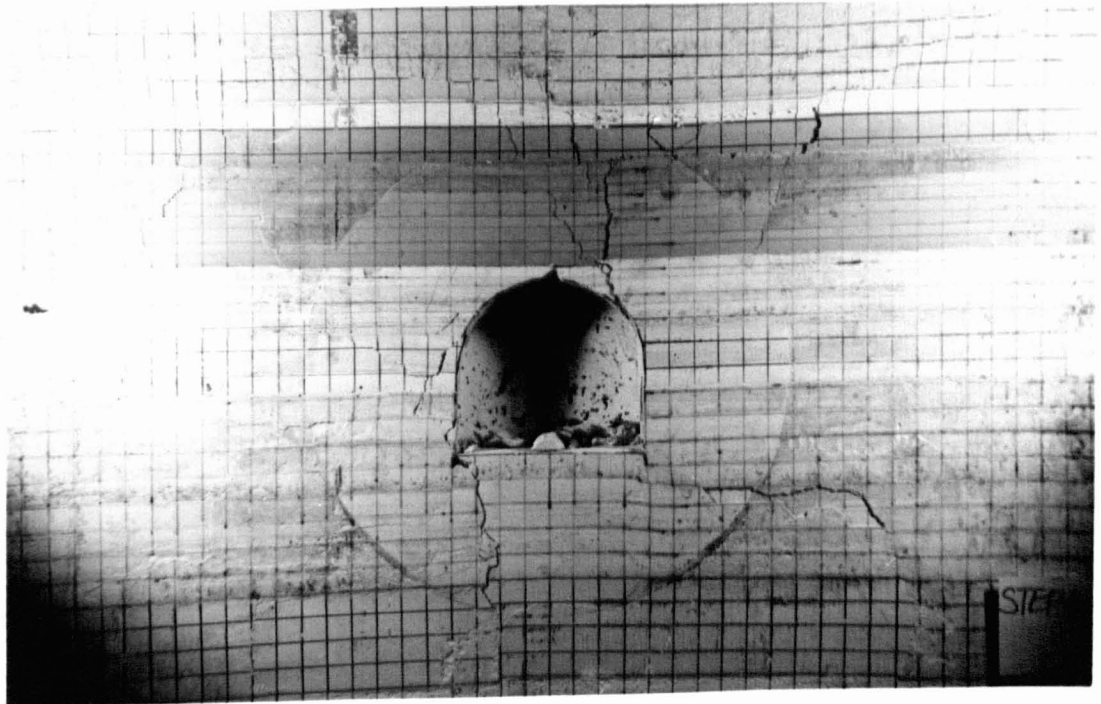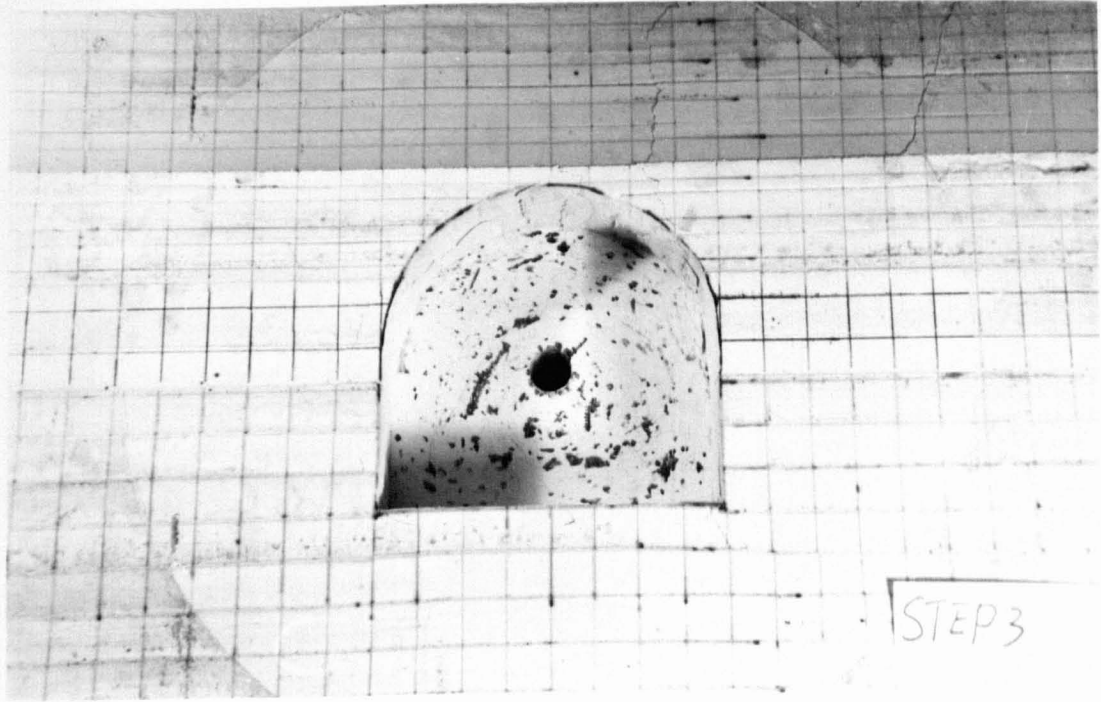
obviously relieved from the highly concentrated stresses, and it is termed the stress relieved zone. Plate 7.2.2 (b) illustrates the fracture distribution around the tunnel after this particular applied stress. The stress relieved zone is clearly shown. As a consequence of further fracturing along the tunnel periphery, a number of debris and blocks fell off the crown and shoulders to the floor.

Fractures did not join each other in the roof to form a stress relieved zone, although they also developed into the stronger sandstone (namely the number 3 stratum in Figure 7.2.1). This indicates that the stress relieved zone may also be formed around the tunnel in the stratified ground condition. However, unlike the case in the homogeneous ground condition in the previous chapter where the stress relieved zones were usually symmetrically formed in both opposite sides (namely, both sidewalls or the roof and floor), the zone is most likely to be formed in the weaker ground side in the stratified strata condition.

In engineering practice, tunnels are preferably excavated under comparatively strong roof strata, leaving the floor exposing in the weak strata, when there are no better choices for the tunnels to be sandwiched between two competent strata. Such selection aims at an effective reduction in the risk of the accidents by the roof falling. On the other hand, the floor may leave to be fractured. If a large stress relieved zone is formed in the floor, the floor lift will become substantial, as was observed in the L5 model test where the floor lift constituted an absolutely major part of the vertical closure of the tunnel.

Comparisons between the results from the L3 and L5 models show that the features in the tunnel behaviour aspect are different between the two models due to a difference in the loading pattern. Figure 7.2.3 shows the tunnel closures versus the applied vertical stress for both models. It is seen form the graphs that both vertical and horizontal closures are much greater in the L3 model than those in the L5 model. The results indicate that the bedding strength (particularly the shear strength) plays an

267
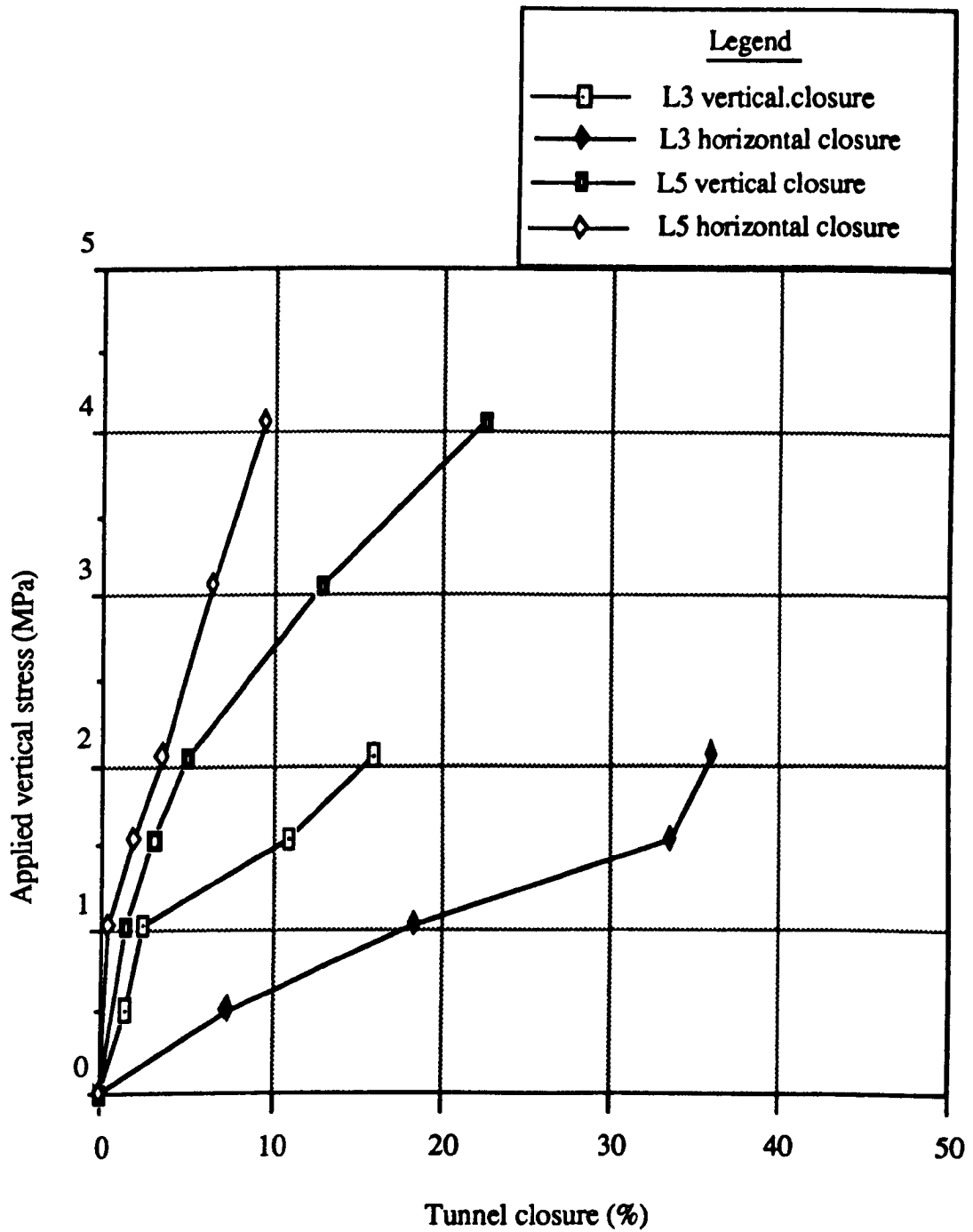
Figure 7.2.3 Tunnel closures versus the applied vertical stress for L3 and
L5 models, illustrating the effects of the stress field on the
stability of tunnel in the stratified strata condition.

important role in the formation of tunnel deformation when the applied stress in the bedding direction is greater than in the other directions. However, this role of the bedding strength becomes less significant in the case of the greater applied stress in the direction perpendicular to the bedding.

Plates 7.2.1 and 7.2.2 (b) give the comparison regarding the pattern of the floor failure. For the L3 model in the greater horizontal stress environment, the floor lift was initiated by the dislocation along a bedding, shearing across the detached layer and breaking at the centre of the layer, whilst the rise of the entire stress relieved zone formed the floor heave in the case of the greater vertical stress environment of the L5 model. The results indicates that the likely floor failure pattern and the relevant heave problems should be taken into account in the engineering design if a tunnel is to be excavated in this strata sequence and at the same location as the models tested above.

7.3 Effects of the Lamination Thickness on the Tunnel Stability

Compared with the features of the fracture development and tunnel closure in the homogeneous rocks, the lamination structure of strata around the mining tunnels have great bearing on the tunnel deformation and stability as has been demonstrated by the L3 and L5 model tests. Now the author attempts to further study the effects of the variation in the lamination thickness on the tunnel stability. For this aim, two additional models have been constructed and tested upon the basis of the results from the L3 and L5 models.

7.3.1 Strata Sequence and Lamination Conditions

The strata sequence of Figure 7.2.1 was still used for the further study. Materials used for the model construction were the same as those used for the L3 and L5 models. The only difference between the two models to be constructed and the L3 and L5 models is that of the lamination thickness. The two models to be made are noted as the L1 and L2 models and would have a minimum lamination thickness of

1.27 cm around the tunnel, in contrast with the L3 and L5 models which had a minimum thickness of 2.54 cm in the vicinity of the tunnel. The structure details of the L1 and L2 models are listed in Table 7.3.1. The total number of the laminates was increased from 26 in the L3 and L5 models to 45 in the L1 and L2 models.

The procedures of the model casting, installation and testing, all followed those for the L3 and L5 models. Therefore the results from L1 and L2 models become applicable and available for the comparisons with those from the L3 and L5 models.

7.3.2 Test Results and Discussion

In the L1 model test, where the applied stress field was 2:1 horizontal to vertical, it was observed that the crown and sidewalls fairly peeled at the initial stage of loading. As a result, the debris fell into the opening. Influenced by the predominant horizontal stress applied, the floor dislocations first occurred along two laminates within 2.6 cm (corresponding to 0.78 m in the prototype) below the floor level. The detached laminations were further deformed under the action of the compound vertical and horizontal stresses. Shear failures were seen to occur in the inclined direction across the detached bedding layers. The upper detached layer was then broken at the centre of the tunnel floor. All these movements of the floor formed an pronounced floor heave in this case, as these are illustrated in Plate 7.3.1. The photograph also shows that the lateral closure of the tunnel was produced mainly by the relative movements between the cast blocks when they were simply piled up in the course of the model installation. It proves once again that the shear strength along the bedding planes has significant bearing on the tunnel behaviour when the major stress applied is in the direction of the bedding planes or close to this direction. In this stress field environment, the shear failure along the bedding will take place on those weak interfaces that have very low shear strength due to the poor bonding condition.

Further loading on the model caused further detachment in the floor. In contrast with Plate 7.3.1, Plate 7.3.2 illustrates that the floor detachment and heave become

NO	Lithology Simulated	Total Thickness (cm)	Layer Thickness (cm)	Number of Layers	Material Ratio Sand : Plaster : Water	Note
1	Sandstone	10.16	10.16	1	450 : 300 : 300	
2	Mudstone	23.50	3.18 / 1.27	2 / 1	450 : 300 : 350	
3	Sandstone	13.97	1.91 / 1.27	11	450 : 300 : 300	Adding colour
4	Silty-Mudstone	6.99	1.27	1 / 4	450 : 250 : 300	
5	Mudstone Seatearth	3.81	1.27 / 10.16	3	450 : 200 :350	
6	Mudstone	22.86	10.16	18	450 : 300 : 350	
7	Siltstone	10.16	10.16	1	450 : 250 : 250	
8	Mudstone	10.16	5.08 / 10.16	1	450 : 300 : 350	
9	Sandstone	15.24		1 / 1	450 : 300 : 300	

Table 7.3.1 The model structure and sequence (for L1 and L2)

271

Plate 7.3.1

Illustrating the fracture and failure pattern of the tunnel floor

in the $2\sigma_v = \sigma_h$ stress field environment.

STEP 2
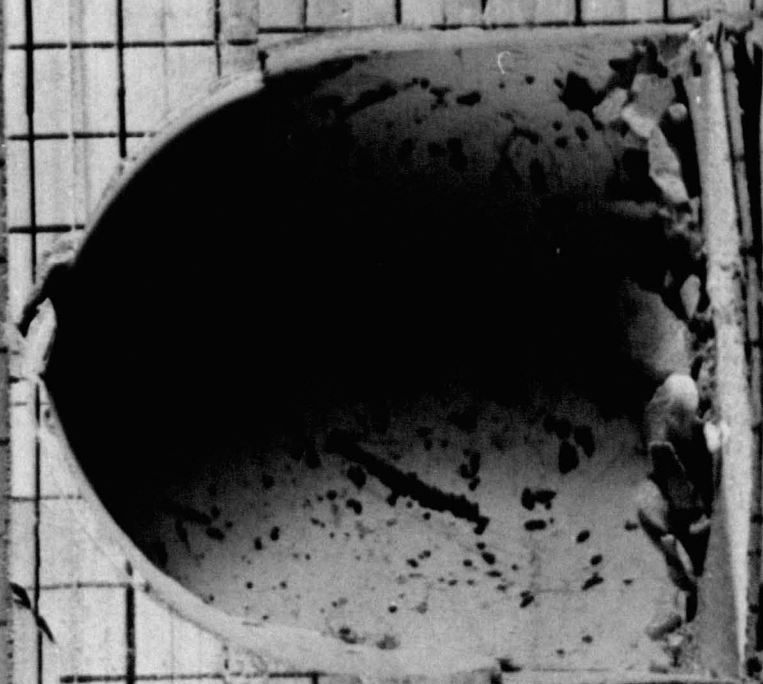
Plate 7.3.2

Floor detachment and heave become pronounced

after 11% increase in the applied load.

STEP 3
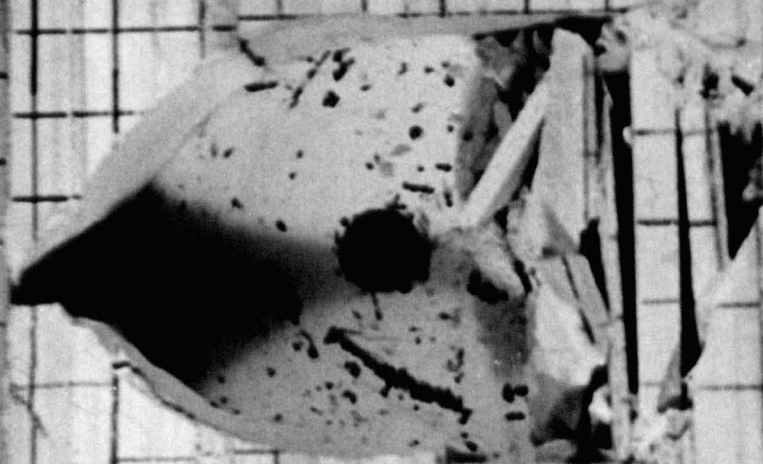
pronounced after 11% increase of loading on the model. Floor fracture developed into deeper layers below the floor level. The detached layers broke at the centre of the floor horizon, leading to more heave at the centre.

As a consequence of the lateral compression, the tunnel crown also underwent shear failure with the roof damage turning into a localised falling.

In the L2 model test, however, the patterns of fractures around the tunnel varied as the loading condition became 1:2 horizontal to vertical. Floor fracture and lifting accompanied by slight sidewall spalling was first observed at a low stress level (1.019 MPa in the vertical and 0.510 MPa in the horizontal). Upon an increase in the load by 50% to 1.529 MPa in the vertical and 0.764 MPa in the horizontal, the fractures developed intensively in the floor. The depth of fractures in the floor extended to 27.5 cm (equivalent to 8.25 m in the prototype) below the floor level. Sidewall spalling also developed whilst the roof exhibited stability and remained intact. All these phenomena are shown in Plate 7.3.3. The excessive floor heave formed the major part of the vertical closure of the tunnel.

The most marked features in the L2 model, that totally differed from those in the L1 model test, are that the floor lifting was due to the raising of the entire stress relieved zone along the fracture surfaces. This movement of the floor is of a shear style. Also the lateral closures didn't exhibit a tendency of the shear movement along the poor bonded interfaces between the cast blocks. These indicate that the bedding strength has less effect on the lateral closure in the case of the greater vertical stress.

Figure 7.3.1 illustrates the comparisons on the tunnel closure features between the L1 and L2 models. Both vertical and horizontal closures of the tunnel in the 2:1 horizontal to vertical stress field (the L1 model) were much pronounced than those in the 1:2 horizontal to vertical stress field. This indicates that the increase in the horizontal stress may lead to a significant rise in the vertical closure of the tunnel.
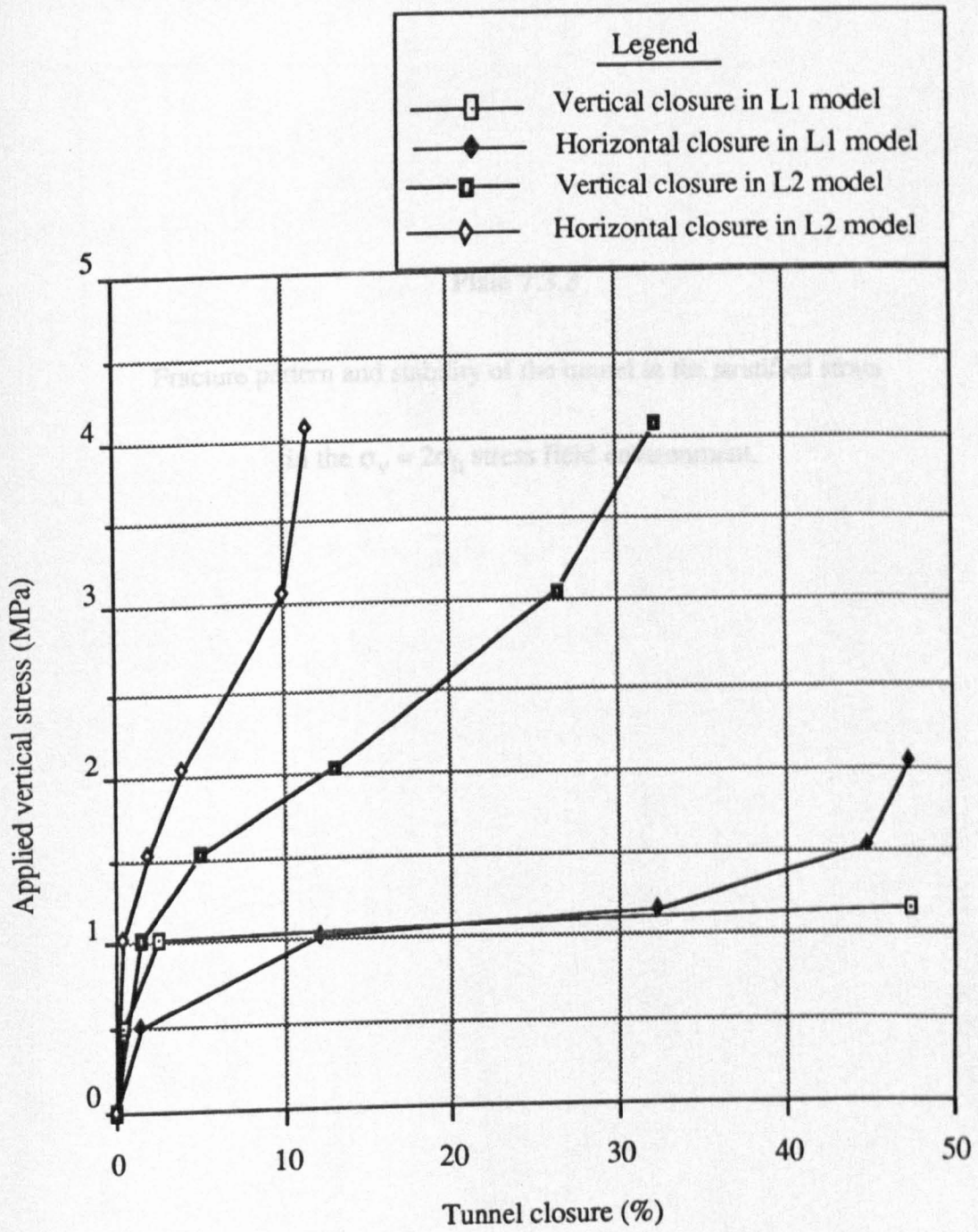
Figure 7.3.1 A comparison on the tunnel closure features for the thinner-laminated

models in the 2:1 (L1) and 1:2 (L2) horizontal to vertical stress field

conditions respectively.

Plate 7.3.3

Fracture pattern and stability of the tunnel in the stratified strata

in the $\sigma_v = 2\sigma_h$ stress field environment.

STEP 2
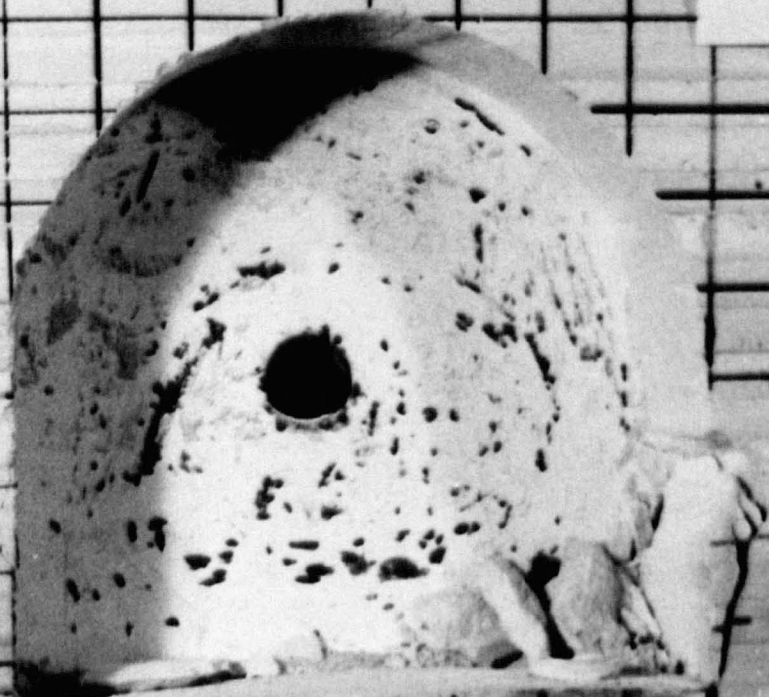
7.3.3 The Effects of the Variation in the Lamination Thickness

The L1 and L3 models were tested in the same stress environment, i.e. in the 2:1 horizontal to vertical stress field. They differ only in the aspect of the minimum lamination thickness, which was 1.27 cm (corresponding to 0.381 m in the prototype) for the L1 model and 2.54 cm (corresponding to 0.762 m in the prototype) for the L3 model. Thus the difference in terms of the tunnel closure and fracture are attributed to the variation in the lamination thickness.

Figure 7.3.2 demonstrates the closure features between the two models in the same loading environment. After 1 MPa vertical stress, both the vertical and horizontal closures of the L1 model were increased more remarkably than those of the L3 model. This reveals that the thinner laminated strata will exhibit more deformity to the tunnel in this stress field environment.

The mechanism of the increased floor lift in the thinner-laminated floor strata can be further interpreted by the theory of strut stability.

Consider a unit length of the tunnel along the tunnel axis for the analysis purpose, see Figure 7.3.3 (a). After the detachment of the first floor layer from the rest layers, the detached layer is seen as a strut with a horizontal stress P_h acting on both ends along the axis of the strut, see Figure 7.3.3 (b). As the stress P_h increases the strut (the layer) is deflected, as shown in Figure 7.3.3 (c). If the origin O is taken at one end and OX axis through the centroids of the end sections, the equation of bending of the strut (Ryder, 1969) can be written as:

$$EI\frac{d^2y}{dx^2} = M = -P_h\,y\,H\,d \qquad\qquad (7.3.1)$$

where E is the Young's modulus of the rock material; I is the moment of inertia around the horizontal neutral axis of the strut (the detached layer); P_h is the applied horizontal stress; H is the thickness of the layer (or the strut height); and d is the width of the
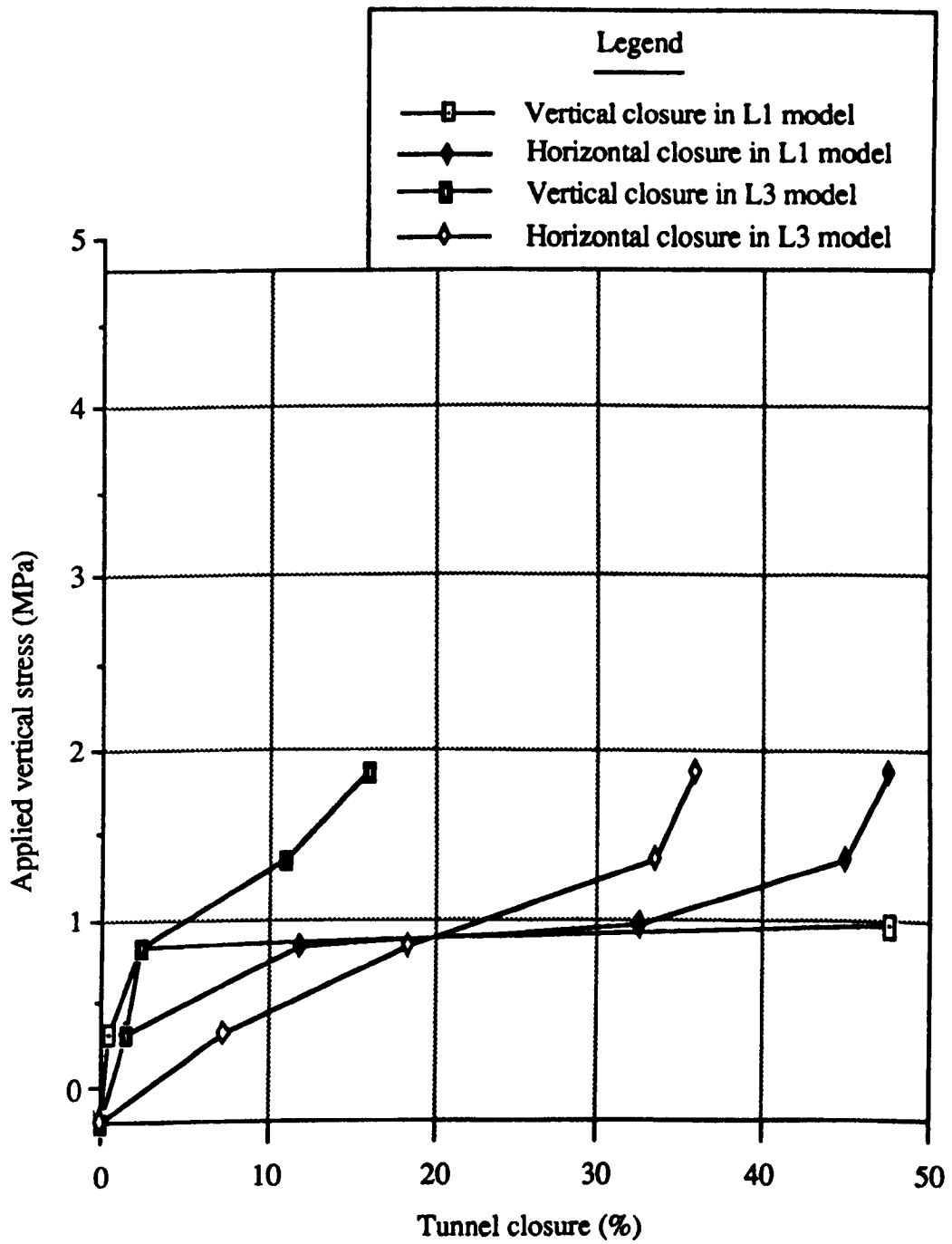
Figure 7.3.2 Illustrating the tunnel closure features of the models with

different lamination thicknesses in the 2:1 horizontal to

vertical stress field environment.

Figure 7.3.3 A mechanism of the increased floor lift due to the detachment of a thin lamination in tunnel floor in a predominantly horizontal stress field.

strut or the layer in the tunnel direction which has been assumed to be unity for this analysis.

This equation can be written as

$$\frac{d^2y}{dx^2} + \alpha^2 y = 0 \tag{7.3.2}$$

where $\alpha^2 = \frac{P_h Hd}{EI}$.

The solution is

$$y = A \sin\alpha x + B\cos\alpha x \tag{7.3.3}$$

At $x = 0$, $y = 0$, thus $B = 0$ $\hspace{3cm}$ (7.3.4)

At $x = w$, $y = 0$, $A \sin\alpha x = 0$ $\hspace{2.5cm}$ (7.3.5)

Either $A = 0$, in which case $y = 0$ for all values of x and the detached layer will not buckle, or $\sin\alpha w = 0$, which leaves A indeterminate. The least value to satisfy $\sin\alpha w = 0$ is $\alpha w = \pi$, corresponding to:

$$\alpha^2 = \frac{\pi^2}{w^2} = \frac{P_h Hd}{EI} \tag{7.3.6}$$

From this is obtained the least value of the applied horizontal stress, P_{hmin}, which will cause the detached layer to buckle. From Equation 7.3.6

$$P_{hmin} = \frac{\pi^2 EI}{w^2 Hd} \tag{7.3.7}$$

Since the moment of inertia I is related to the geometry of the cross section of the layer, and is expressed by:

$$I = \frac{H^3 d}{12} \tag{7.3.8}$$

Substitution of this into Equation 7.3.7 gives:

$$P_{hmin} = \frac{\pi^2 EH^2}{12w^2} \tag{7.3.9}$$

280

This result indicates that P_{hmin} is linearly proportional to the square of the lamination thickness H. In other words an increase in the layer thickness, H, will significantly increase the resistance of the layer against the buckling and vice versa.

In the L1 model, the layer thickness of the floor is 1.27 cm (corresponding to 0.381 m in the prototype). This value is half of that in the L3 model. According to Equation 7.3.9, the buckling resistance of the floor layers in the L1 model is only one fourth of that in the L3 model. Therefore, in response to a given stress level, the floor lift or buckling in the L1 model become more pronounced than in the L3 model.

Comparisons are also made between the L2 and L4 models for examining the effects of the lamination thickness on the stability of tunnel in the 1:2 horizontal to vertical stress field environment. Figure 7.3.4 shows that both the vertical and horizontal closures are greater in the thinner-laminated strata condition (the L2 model) than in the thicker laminated condition (the L5 model) in this loading environment. Particularly, the vertical closure consists mostly of the floor heave in both models. The mechanism of the floor failure remains the same for the L2 and L5 models, i.e. the shear fractures initiated from the floor corner and extended down into the deeper layer below the floor level. However, the maximum depth at which the fractures developed differed, with the floor in the L2 model being broken in the deeper layer below the floor level. This has led to a larger stress relieved zone to be formed in the floor, which in turn caused an increase in the volume of the expansion of the materials within the zone. Therefore the floor lift, partly as a result of the expansion of the loosened materials in the zone, became more pronounced.

7.4 Roles of Metal Support in the Improvement of Tunnel Stability

Tunnels excavated in the majority of sedimentary Coal Measures have a need for the effective support. In the UK, standing steel supports are popularly used in the tunnels. The steel supports are classified into two major categories, yielding and rigid
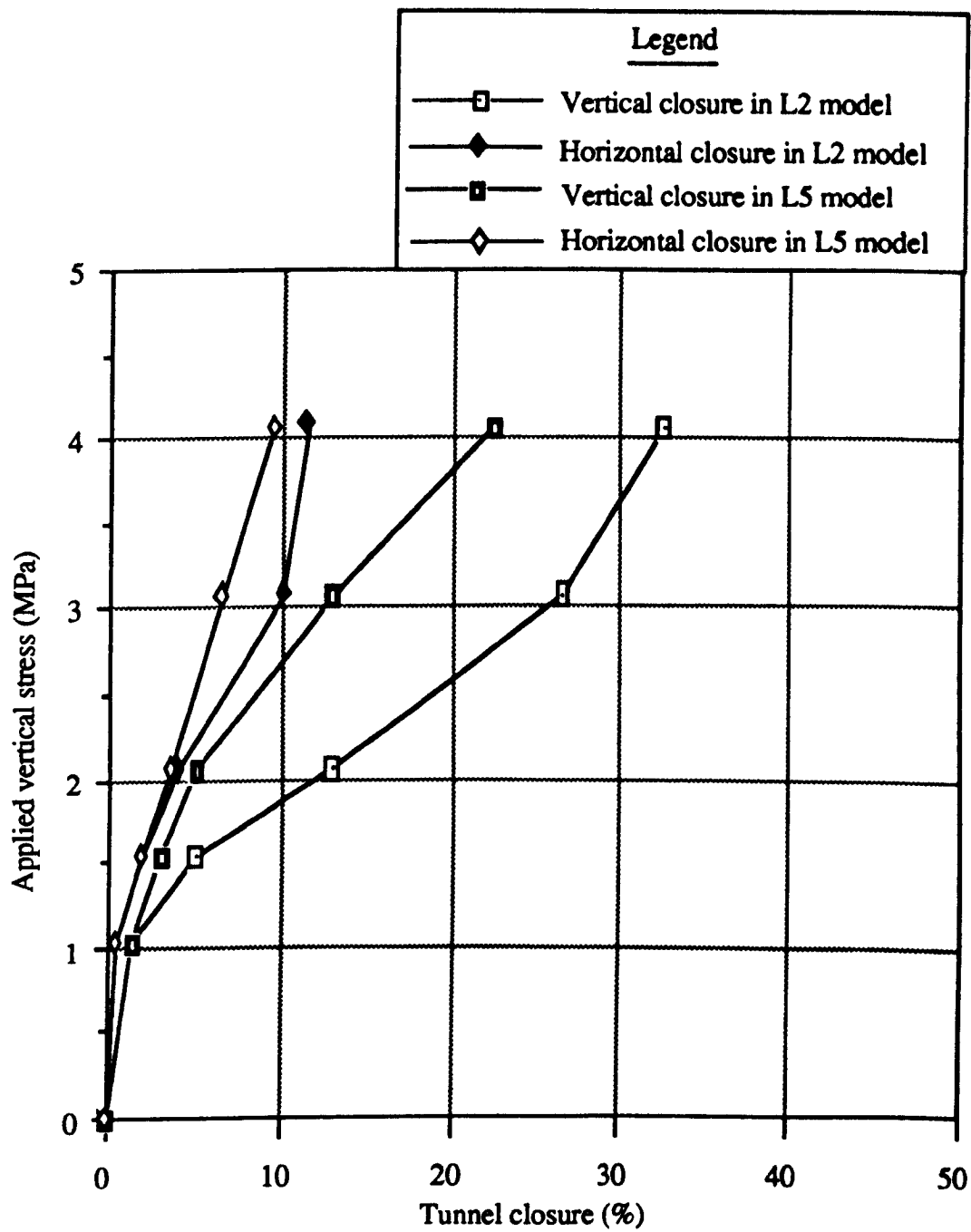
Figure 7.3.4 Illustrating the effect of the lamination thickness on tunnel closures in the 1:2 horizontal to vertical stress field environment.

supports. Information from British Steel shows that in 1990, there were 12000 tonnes of rigid steel supports supplied to British Coal, compared with 300 tons of yielding steel supports per month. This fact indicates that the rigid steel supports have been proven by years of experience in the coal industry as a very reliable system of support in heavy stress field conditions. Although the yielding support systems have been receiving increasing attention in recent years, it seems unlikely that within next few years the preference for the rigid steel supports will change to the yielding supports.

Upon this fact, the author has used a rigid metal support model in an attempt to study the roles of the system in the improvement of the tunnel stability.

7.4.1 Strata Structure Simulated and the Model Support System

The strata structure to be employed for the modelling investigations was the same as that for the L1 and L2 models. The model materials, preparation process, installation and loading condition and procedures also remained unchanged.The profile sizes of the tunnel and the scale factors followed those for the L1 and L2 models.

An aluminium bar was used for making a rigid arch support. The support consisted of three pieces, connected by 2 joint plates through bolts and nuts. Figure 7.4.1 shows the diagram of the model support. Two sets of the support were installed in each tunnel model.

7.4.2 Behaviour of the Tunnel under the Effect of the Support

Two models have been tested, with one (denoted as L6 model) loaded in the 2:1 horizontal to vertical stress field environment and the other (denoted as L7 model) in the 1:2 horizontal to vertical stress field environment. Figure 7.4.2 illustrates the closure features of the tunnel for L6 and L7 models. It can be seen from the graphs that the tunnel closures of the L6 model are remarkably pronounced over those of the L7 model, at the same applied vertical stress levels. This implies that at a given depth
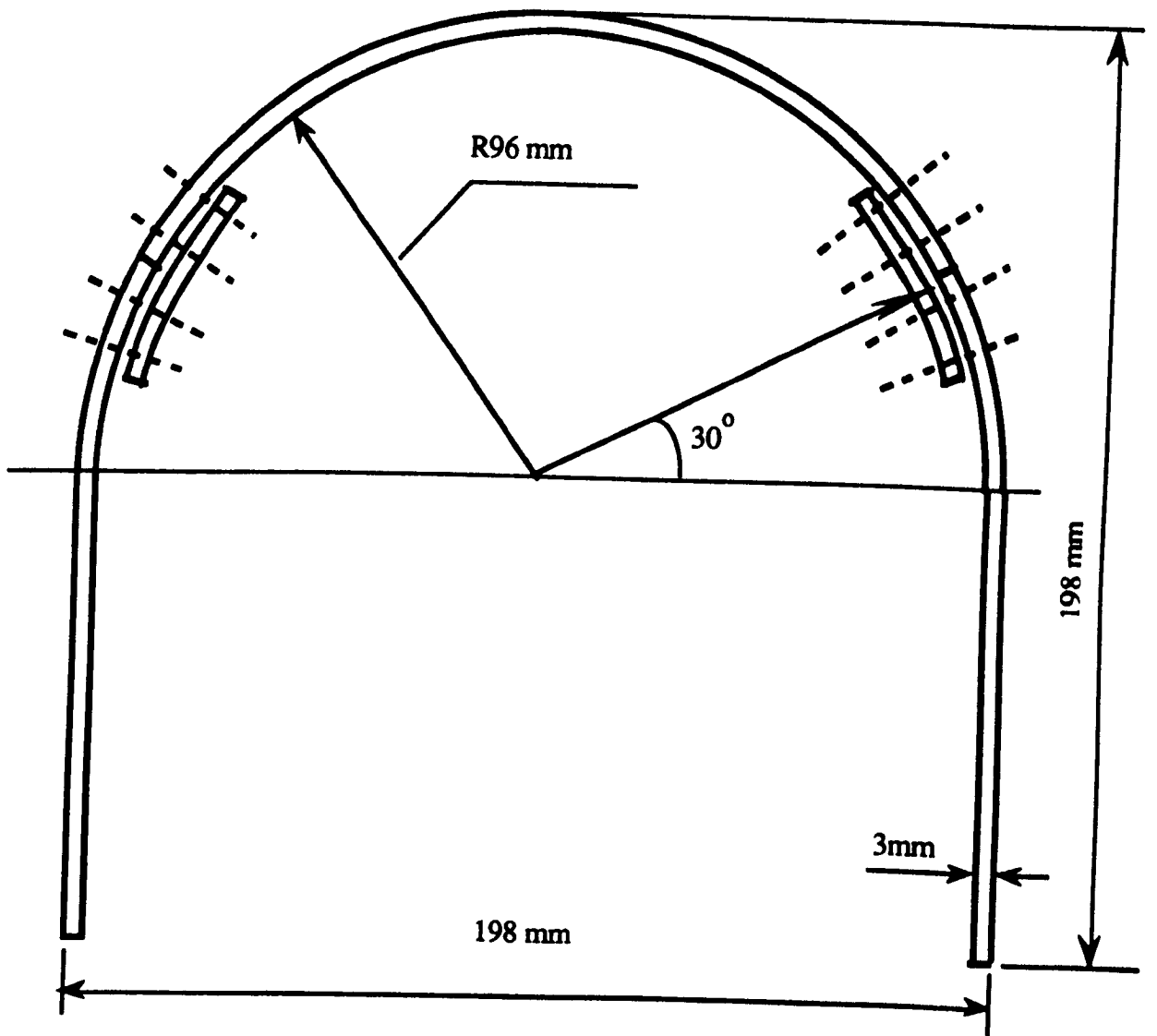
Figure 7.4.1 A diagram of a rigid metal support model (consisting of three pieces)
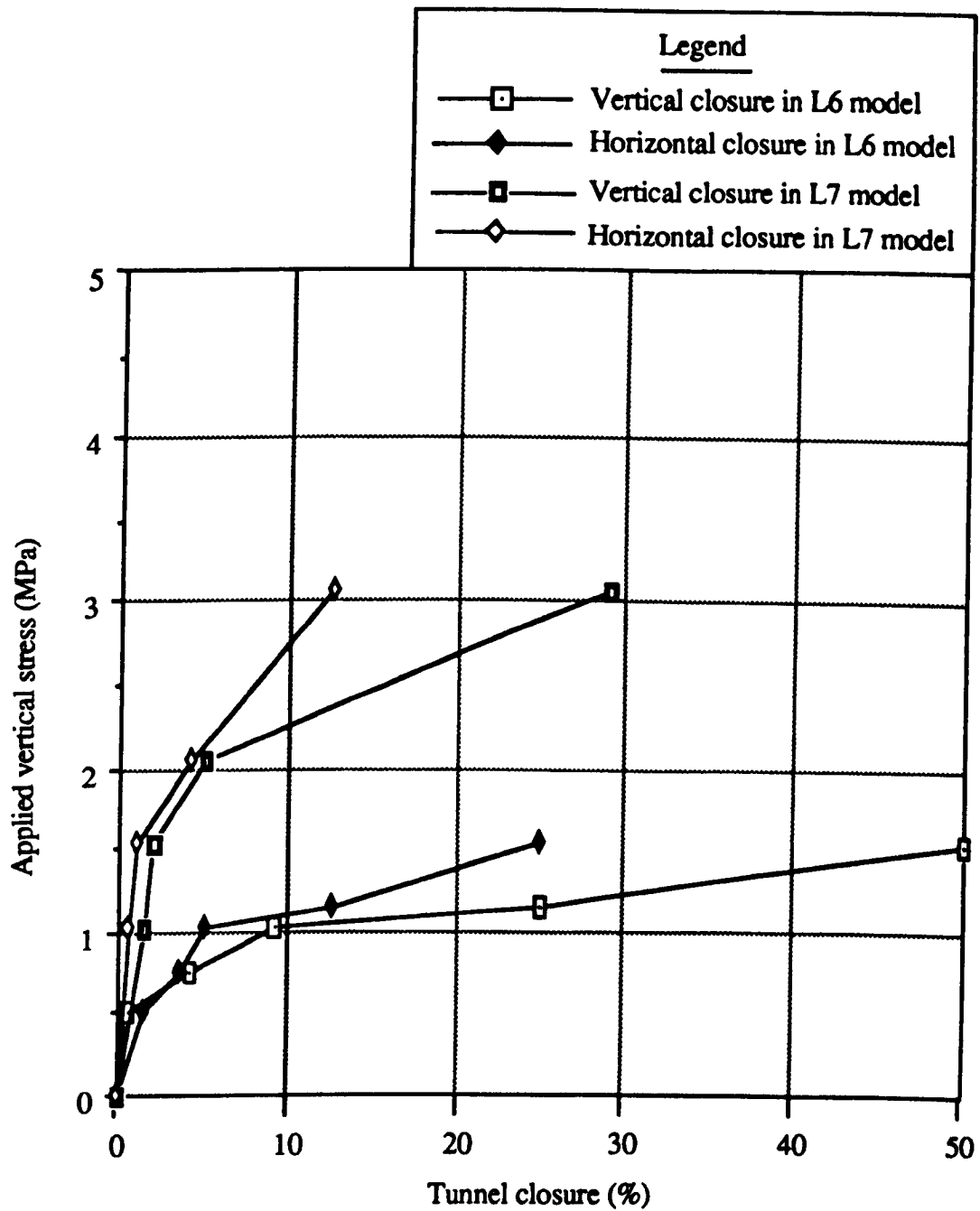
Figure 7.4.2 Closure characteristics of a tunnel with the rigid metal support in the 2:1

(L6 model) and 1:2 (L7 model) horizontal to vertical stress fields respectively

below the surface, a tunnel in a higher horizontal stress field is more likely to suffer severe tunnel deformations.

If the comparison is made between the two models for the tunnel closures at an equivalent stress level, for instance, at the 1.529 MPa vertical stress with 3.058 MPa horizontal for the L6 model and at the 3.058 MPa vertical stress with 1.529 MPa horizontal for the L7 model, the tunnel closures in the L6 model still remained greater than those in the L7 model. Obviously, this closure feature is largely due to the effect of the strata lamination. In other words, the difference in the tunnel closures between the two loading patterns does not disappear nor reverse, after the use of the metal support, as is compared with the situations of the L1 and L2 models.

The natures of the floor fracture and failure are also different between the two models. In the L6 model, the floor failure initiated from the layer separation followed by the bending and buckling of the detached layers. Thus the failure pattern tended to be gradually developing layer by layer. Plate 7.4.1 (a) clearly shows this tendency. In the L7 model test, however, the floor was first fractured by shearing across the layers. The fracture surfaces formed the boundary of a stress relieved zone in the floor strata. The materials in the zone were then raised, expanded under the action of the heavier stresses. At the same time, the tunnel crown was also cracking, and as a result localised failure and falling incidents occurred at the crown between the two supports. Plate 7.4.1 (b) clearly shows these results.

In the two models, the metal supports underwent kick-in deformation, with a more severe result observed in the L6 model. This indicates that the rigid support in the soft strata conditions and the heavily loading environments will suffer severe deformations and damage. Also, the standing rigid metal supports cannot give an effective relief of the tunnel from the floor heave in these kind of soft and weak floor conditions.

Plate 7.4.1

Fracture pattern and stability of the tunnels with the rigid

metal support in two opposite stress field conditions.

(a) In the $2\sigma_v = \sigma_h$ stress field environment.

(b) In the $\sigma_v = 2\sigma_h$ stress field environment.
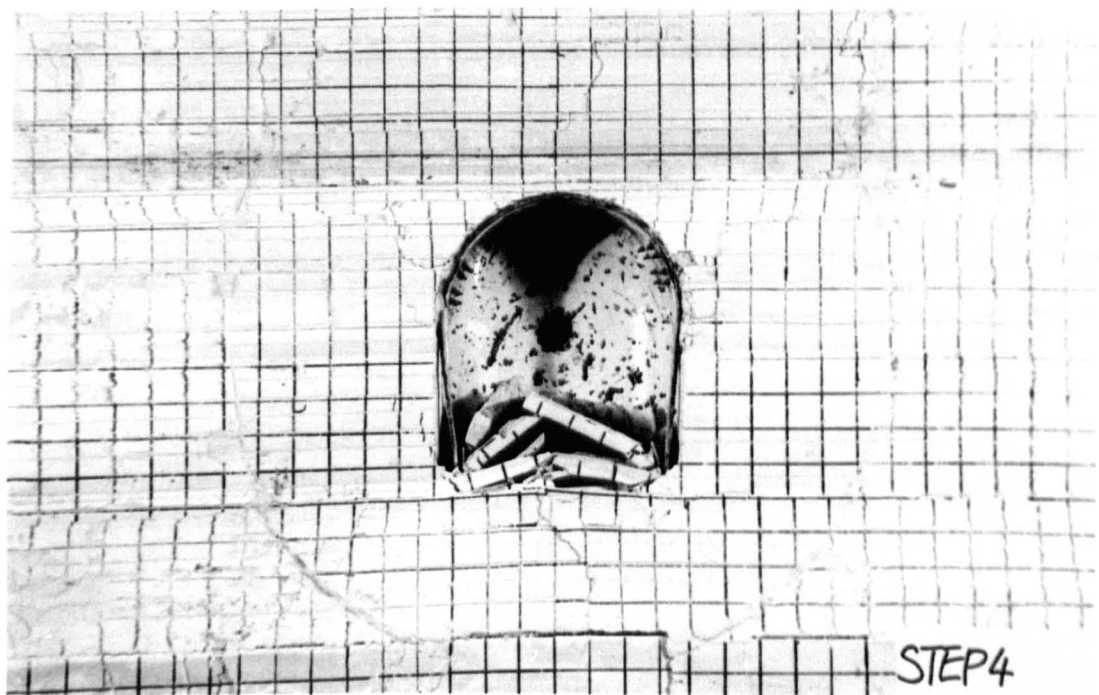
STEP 4
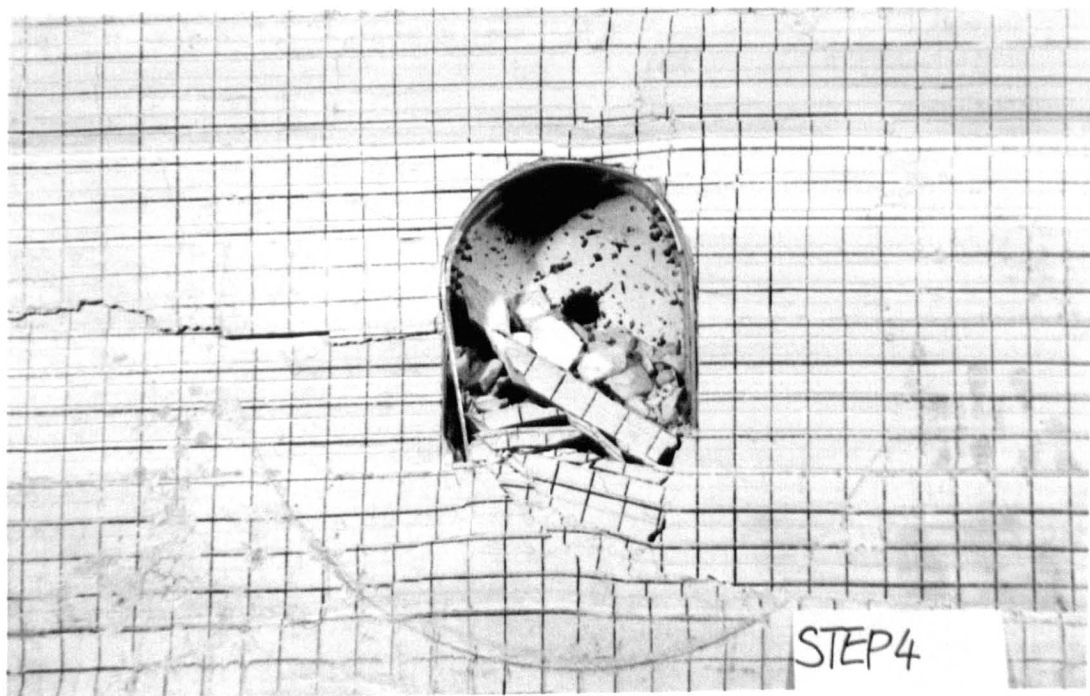
STEP 4

7.4.3 The Roles of the Support

The roles of the rigid support in the control of the tunnel deformation are studied through the comparisons of the L6 model with the L1 model and the L7 model with the L2 model.

Table 7.4.1 lists the tunnel closures for the L1 and L6 models against the applied vertical stress. It can be seen from the table that in the 2:1 horizontal to vertical stress field environment, the closure natures of both the unsupported and supported tunnels did not vary apparently at the initial loading level (i.e at 0.510 MPa applied vertical stress). The consequence seems to be due to the fact that the support had not taken the loads at this moment. After this early stage of rock movement, the support in the L6 model gradually picked up the rock pressures and thus increased its resistance against the inward movements of the surrounding rocks from the roof and both sides. Therefore the tunnel closures were reduced significantly as this can be observed from Table 7.4.1 by the comparison of the data between the two models.

Table 7.4.1 A comparison of the tunnel closure between L1 and L6 models

Applied vertical stress (MPa)	L1 model		L6 model	
	Horizontal closure (%)	Vertical closure (%)	Horizontal closure (%)	Vertical closure (%)
0.510	1.5	0.5	1.5	0.5
1.019	12.0	2.5	5.0	9.0
1.147	32.5	47.5	12.5	25.0
1.529	45.0	failure	25.0	50.0

A feature may be obvious that an increase in the horizontal resistance against the lateral movement may turn out to give a marked relief in the floor buckling and uplift. Alternatively, the relief or reduction of the appreciable horizontal stress may also result

in an effective alleviation of the floor lift trouble. This effect has already been proved by numerous cases of engineering practice. A typical example is that when two parallel tunnels are driven in the same troublesome strata environment but at different times, the first driven tunnel will experience more pronounced deformation problems than the other tunnel which is to be excavated at a period of time after the completion of the first tunnel.

Figure 7.4.3 illustrates the closure features of the L2 (without support) and L7 (with support) models in the 1:2 horizontal to vertical stress field environment. It can be seen from the graphs that , within the loading range under this particular loading circumstance, there is no evident difference between the unsupported tunnel and the supported tunnel in respect of the tunnel closures. The support showed little effect on the relief of the tunnel from the floor lifting. Rather, the tunnel tended to have an increase in the vertical closure in the L7 model, as the support legs penetrated into the floor, causing additional damage to the floor strata. This identifies the need for increasing the area of the support at floor contact, for instance, by putting on an appropriate shoe under the support foot.

A comparison on the dimensions of the stress relieved zone in the floor for the two models shows that, the adoption of the support had a significant effect in the reduction of the depth of the fractures in the floor strata, as this is illustrated in Plates 7.3.3 and 7.4.1 (b). Although the materials in the stress relieved zone will need to be cleaned and the tunnel dinted in the future as the broken floor strata buckle and heave, the volume of the materials to be cleaned and the quantity of the dinting operations will be evidently small in the case of the supported tunnel. From the long term tunnel stability point of view, the employment of the standing metal support is very beneficial in controlling the dimensions of the stress relieved zone formed in the tunnel floor, and thus is very likely to reduce the long term floor heave problem.
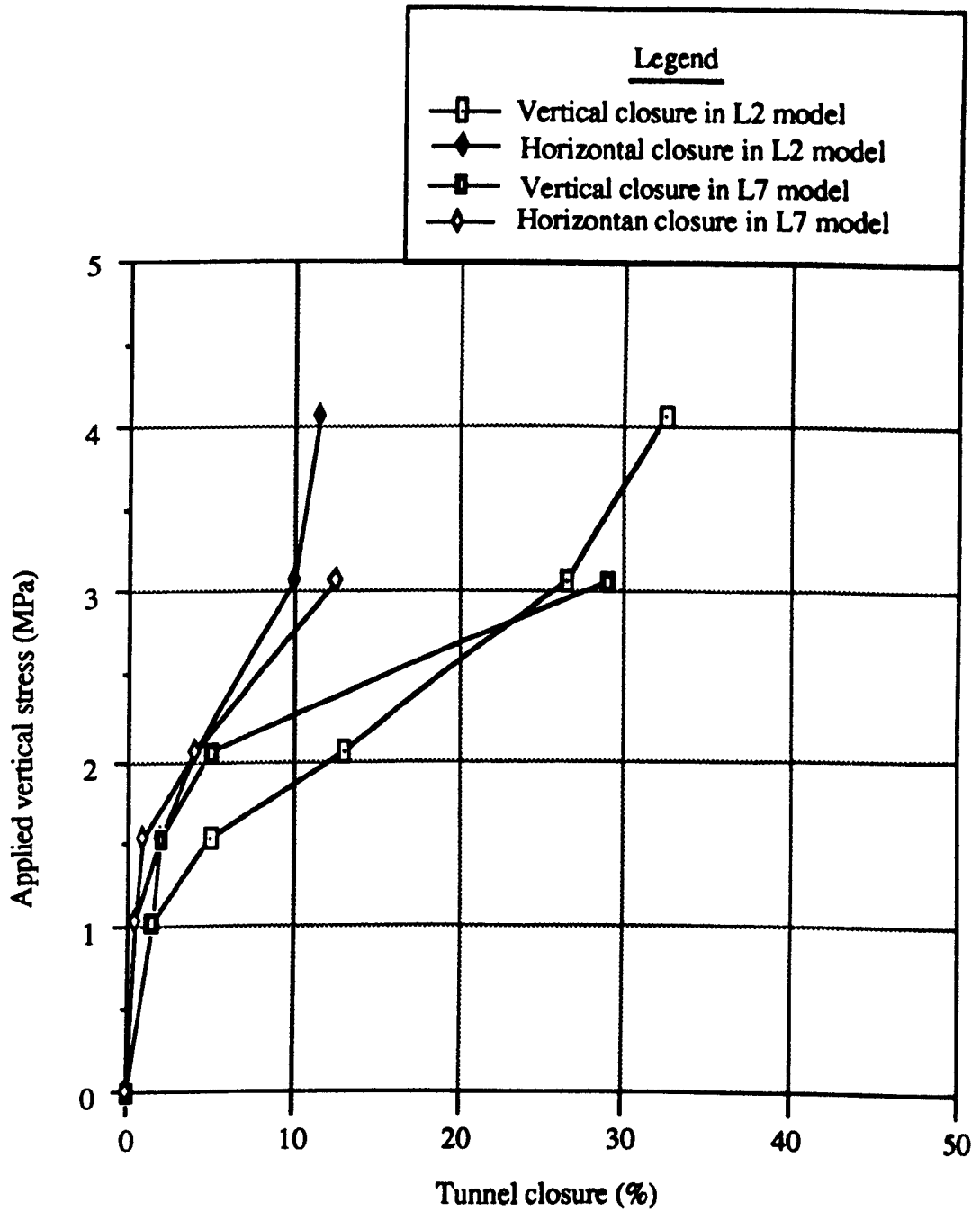
Figure 7.4.3 A comparison on the effect of the rigid support on the stability of tunnel

in the 1:2 horizontal to vertical stress field environment.

CHAPTER EIGHT

MINING INDUCED INFLUENCES ON TUNNEL STABILITY

CHAPTER EIGHT

MINING INDUCED INFLUENCES ON TUNNEL STABILITY

One of the prominent features of mining tunnels is that many of them are subjected to the influences by mining activities within their tunnel life spans. As a working face advances and approaches a tunnel, the rock stress acting on the tunnel is due to change to various degrees in terms of the direction and the magnitude. Such changes of the rock stress will unexceptionally lead to relevant changes of the rock fracture pattern, tunnel closure and support deformation. These effects are mining induced. The investigations into this particular aspect constitute an important part of the rock mechanics research and therefore have been intensively carried out over the world. In this Chapter the author attempts to focus on how the mining induced stress influences a nearby tunnel at different stages of the stress development. The work includes:

1) The instrumentation of the abutment stress ahead of a retreat longwall face;

2) Physical modelling to examine the tunnel behaviour influenced by the mining induced stress; and

3) A simulation of the mining induced effect on the stability of a rib pillar.

8.1 Instrumentation for Abutment Pressure ahead of a Retreat Longwall Face

Longwall working has a long history of successful application and has become the most common method for underground coal mining both in the United Kingdom and China. The application of the method has been extended to various complicated strata conditions. The characteristics of the mining induced stresses around the longwall face may vary with every application of the method. It is fair to say that it is impossible to discuss all the characteristics of the mining induced rock stresses in

relation to all kinds of longwall mining practice. This section has been limited to discussion of the results of the instrumentation for the front abutment stress on a retreat longwall working in a horizontal coal seam.

While working as a mining research engineer with the Central Coal Mining Research Institute in China, the author, in collaboration of his colleagues, conducted an underground instrumentation programme aimed at monitoring the change in the front abutment stresses on a longwall face at the Datong No.12 Colliery. The seam was underlying a thick sandstone main roof, which left the retreat working face under the action of the heavy periodic weighting. A special measure (softening the sandstone by water injection) was later taken to cope with the problem due to the heavy periodic weighting. As one of the methods to assess the effectiveness of this measure, a specially designed and manufactured borehole hydraulic pressure cell was used. Figure 8.1.1 shows a sketch of the structure and the installation of the pressure cell. It consists mainly of a thin-walled, hydraulic oil filled, flat metal container (A), a hydraulic pipe (P) conducted from the container to a dial pressure gauge (M) at the other end. The container is sandwiched by a steel wedge (B) on each side. Outside of the wedge on each side is an assembling wedge (C).

A borehole of 110 mm diameter and 7 m depth was drilled about 70 metres ahead of the face line for the pressure cell installation. In the course of installation, the whole set of the pressure cell was first sent to the end of the borehole by using an installation pipe. The installation pipe was then hammered at the outside end against the big end of the assembling wedge (C). The container element (A) was thus gradually tightened, kept in position and set with an initial load. Upon the completion of the installation, the initial readings of the cell pressure and the distance of the instrumentation station to the face line were recorded. Since then the readings were taken once or twice a day until the face reached the borehole position.
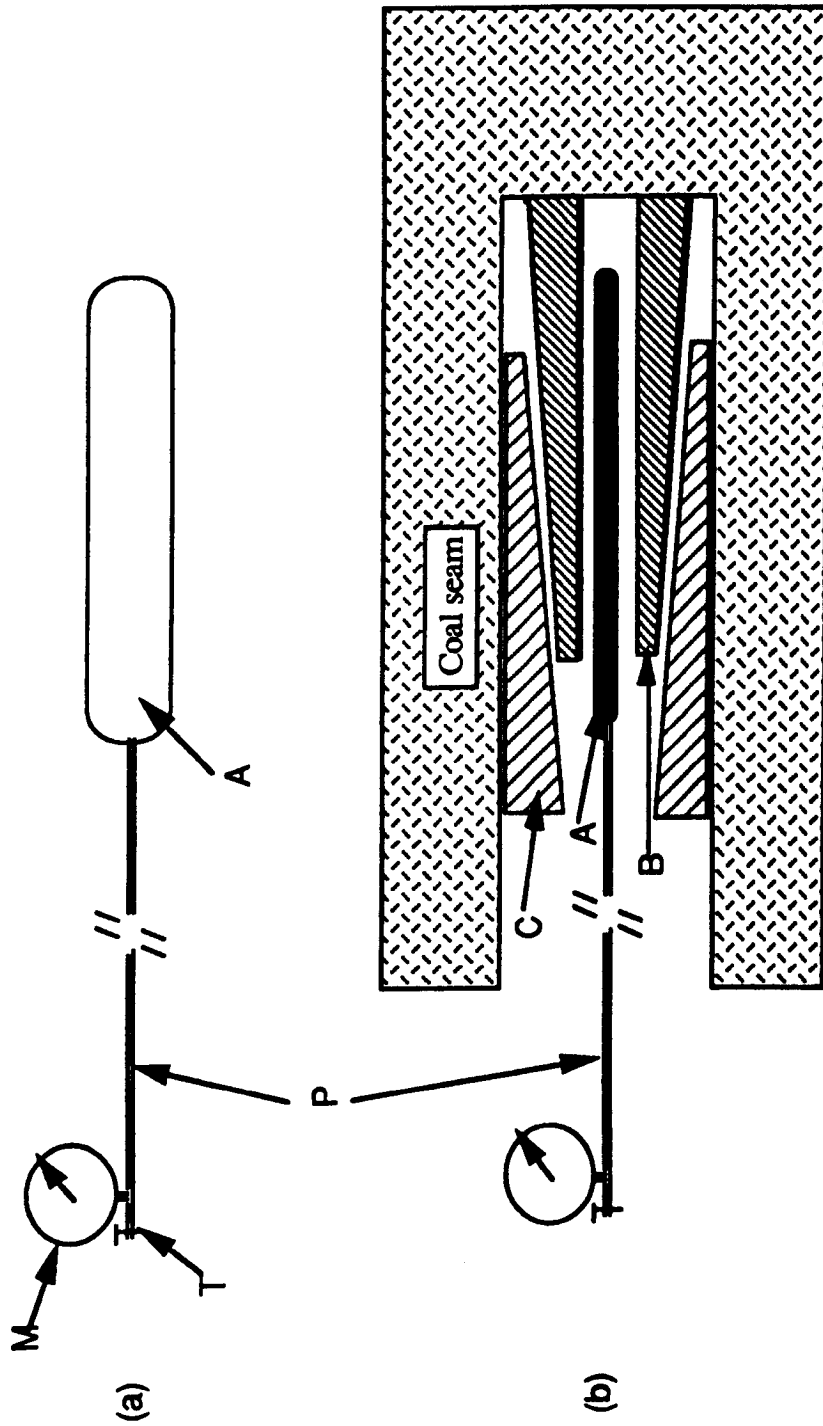
A — Thin walled flat metal container; B— Steel conducting wedge; C— Assembling wedge

P — Hydraulic pipe; T — Tap; M —Dial pressure gauge

Figure 8.1.1 A sketch of the structure and installation of a borehole hydraulic pressure cell

(a) The flat metal container.　　(b) Installation of the borehole pressure cell.

Two borehole hydraulic pressure cells have been separately used at two monitoring stations in a tailgate (a special tunnel) of the retreat working face. Figures 8.1.2 and 8.1.3 illustrate diagrams of the instrumentation results. The horizontal axis is the distance from the borehole location to the advancing faceline, whilst the vertical axis is the cell pressure taken from the dial gauge. The increments of the pressure on the basis of the initial reading are attributed to the influences of the mining induced abutment stresses. From the graphs in Figures 8.1.2 and 8.1.3 it can be seen that the affecting range of the abutment stress in these two cases is around 30 metres, with the strongly influencing range being about 12 metres. The peak abutment stress is at the faceline in both cases, although the magnitudes of the peak abutment stress are different which may be attributed to the position of the instrumentation stations in relation to the periodic weighting. Generally speaking, immediately prior to a periodic weighting of the main roof, the peak abutment stress reaches the maximum within a periodic weighting interval. This is because the hanging main roof has arrived at an extreme length at this moment. This hanging main roof is mainly supported by the solid coal around the face and thus causes the peak abutment stress to attain its highest value. On the contrary the peak abutment stress reaches the minimum immediately after a periodic weighting, as minor hanging main roof is formed above the working face.

The borehole hydraulic pressure cells were used to sense the change in the vertical abutment stress. The results so obtained identify the change in the vertical rock stress instead of the horizontal value.

The horizontal rock stress in the solid coal near the longwall boundaries are very rarely investigated, because it is commonly believed to have little influence on strata control and longwall stability (Jeremic, 1985) except at the face where the horizontal stress may affect the performance of the face supports, causing the immediate roof to move horizontally towards the goaf. The roof caving and the floor failure and lift at a longwall face will cause a relaxation of the horizontal rock stress in
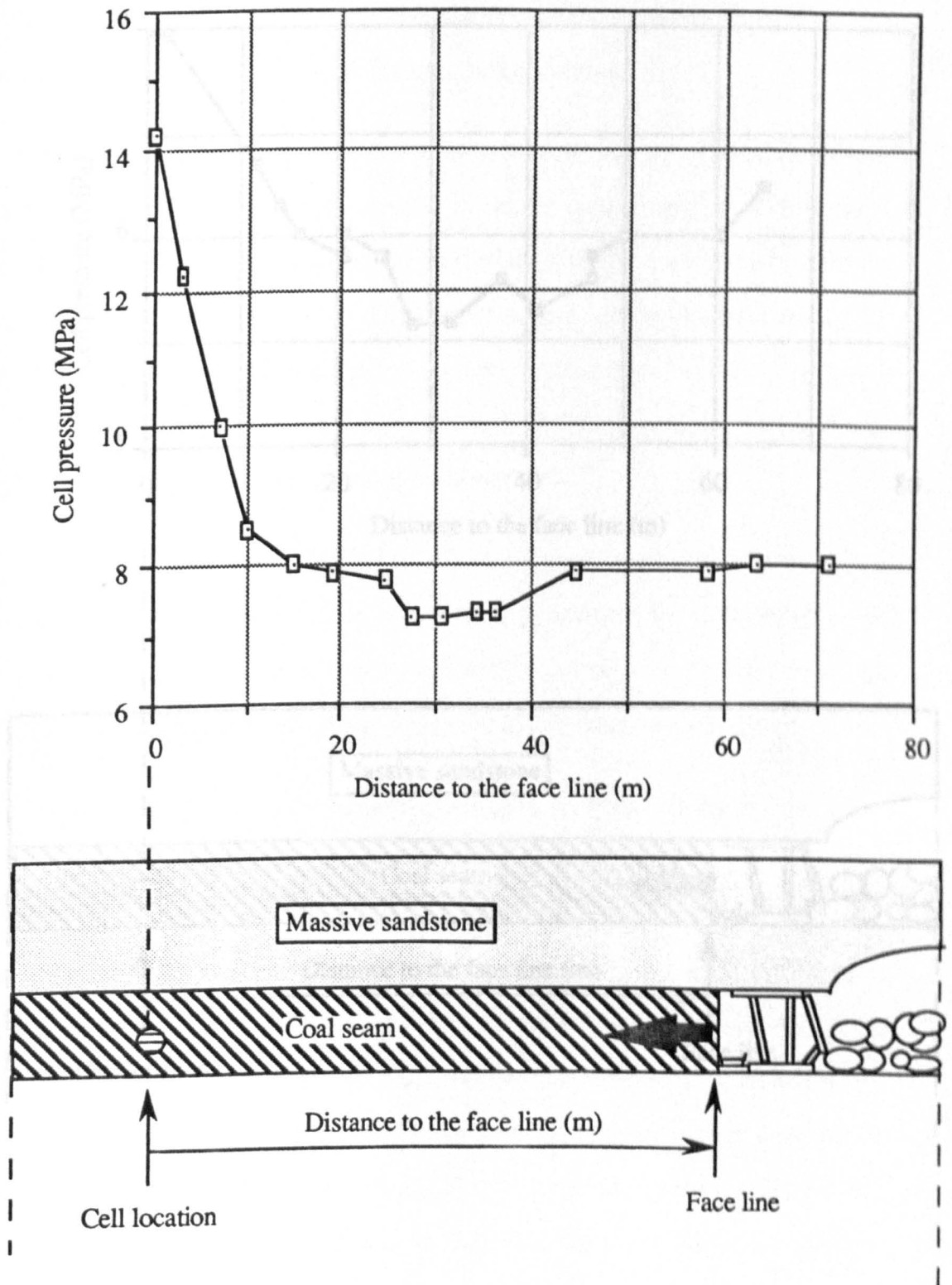
Figure 8.1.2 Instrumentation at the No.1 station using a borehole hydraulic pressure cell and the results of the front abutment stress distribution at No. 8113 face.
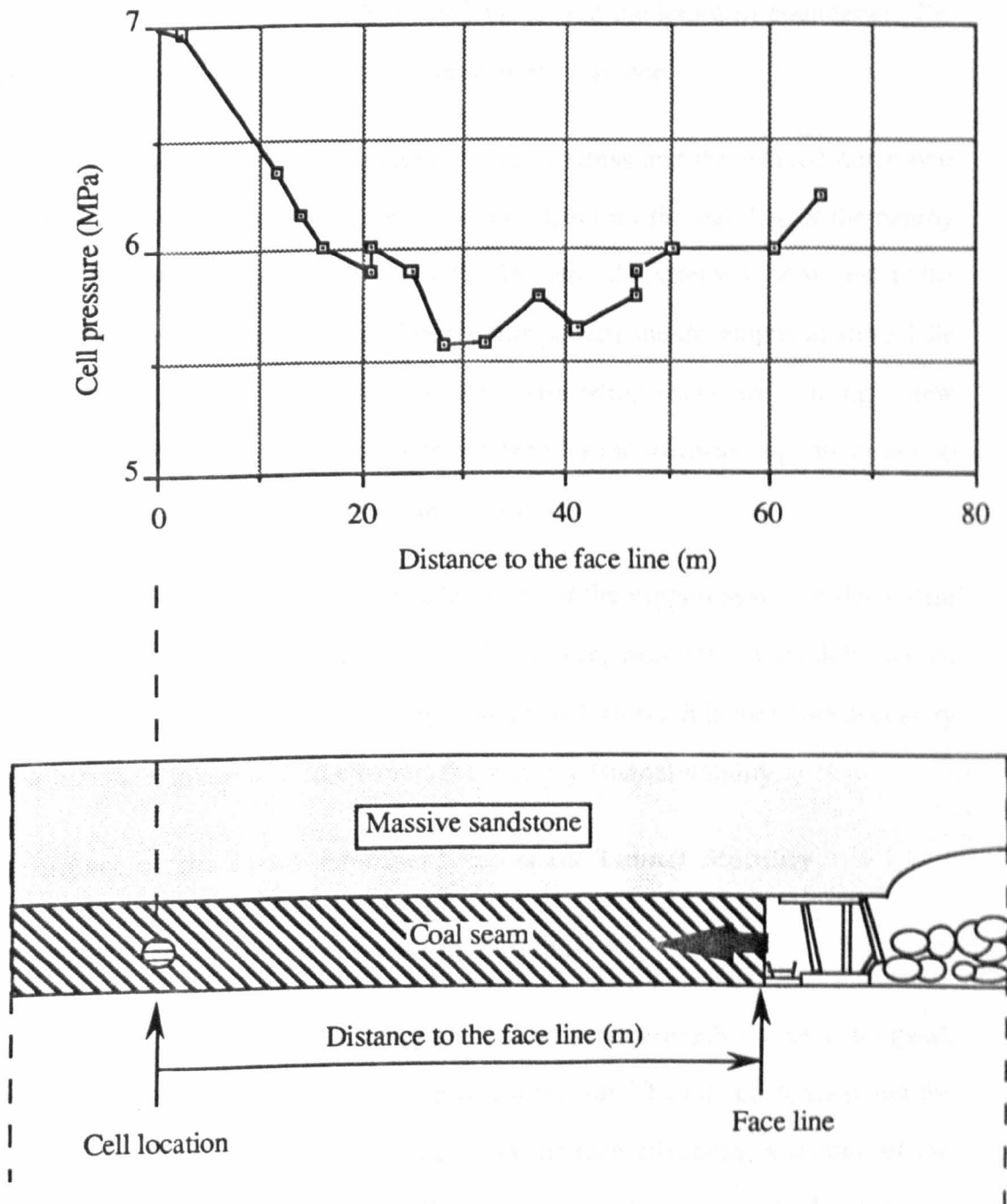
Figure 8.1.3 Instrumentation at the No.2 station using a borehole hydraulic pressure cell and the results of the front abutment stress distribution at No. 8113 face.

the vicinity of the working boundaries. The degree of the relaxation is dependent on the distance between the area under consideration and the longwall boundaries. The relaxation effect becomes weak with increase in the distance.

The combination of the increased abutment stress and the relaxed horizontal rock stress around the longwall face has an impact on the stability of the nearby roadways / tunnels. The roadways within this influenced region will be subject to the effects of the changing rock stresses. The fracture pattern and development around the roadways may change dramatically, as the surrounding rocks are gaining a new equilibrium condition. Accordingly there is a need for the roadway support system to be adjusted in order to suit the new strata condition.

It is apparent that an appropriate adjustment of the support system is dependent on the comprehensive understanding of the features regarding the strata deformation under the increasing effect of the mining induced rock stress. It is therefore necessary to look into the mining induced effect on the roadway / tunnel stability.

8.2 Impact of the Front Abutment Stress on Tunnel Stability

8.2.1 Model Structure and Loading Patterns

Considered in this section is a tunnel closely underneath a retreat longwall working panel and parallel with the retreating direction. The tunnel location and the rock structures are shown in Figure 8.2.1. As the face advances, a section of the tunnel is gradually exposed under the effect of the front abutment stress. Suppose the pattern of the front abutment stress distribution is the same as that in Section 8.1, which gives rise to an adverse impact on the tunnel stability. Then the author is concerned with the following three situations of the tunnel:

(1) The tunnel section beyond 30 metres outbye the face line. This section of the tunnel will remain in the undisturbed rock stress condition. The stress condition is assumed to be of the 2:1 horizontal to vertical stress field.

297
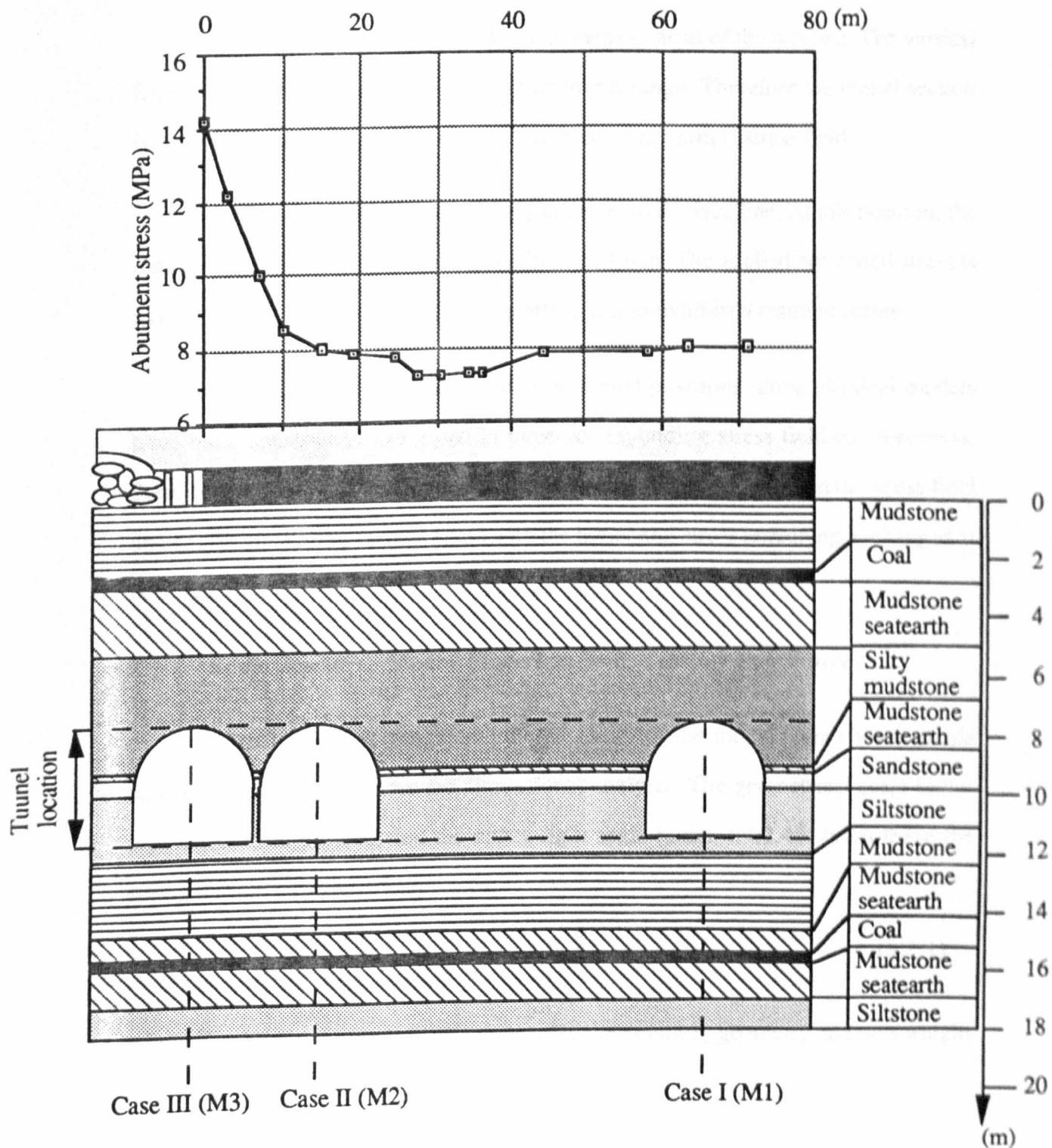
Figure 8.2.1 A tunnel closely underneath a retreat longwall panel, illustrating that the three

sections of the tunnel (M1, M2 and M3) will encounter different loading patterns

due to the mining induced effect in this geological and operational environment.

(2) The tunnel section within 12 to 30 metres ahead of the faceline. The vertical front abutment stress is gently stepping up in this range. Therefore the tunnel section is reasonably considered to be in the 1:1 horizontal to vertical stress field.

(3) The tunnel section immediately underneath the face line. At this position, the tunnel is subject to a highly vertical loading condition. The applied horizontal stress is likely to be relieved with the relaxation effect. It thus exhibits a restraint nature.

In correspondence to the above three tunnel positions, three physical models have been constructed and tested in three corresponding stress field environments, these being (1) the 2:1 horizontal to vertical stress field, (2) the hydrostatic stress field and (3) the increasing vertical stress with the horizontal stress remaining unchanged at 0.18 MPa.

8.2.2 Scale Factors, Model Materials and Testing Procedure

The materials unit weight and the geometry of the model were chosen as the fundamental dimensions for the dimensional analysis. The geometrical scale factor was selected to be 1:40, and the unit weight scale factor 1.4:2.45. From these the strength scale factor was found to be:

$$K_\sigma = K_l \, K_d = \frac{1}{40} \times \frac{1.4}{2.45} = \frac{1}{70} \qquad (8.2.1)$$

where K_σ, K_l and K_d are the scale factors for the strength, geometry and unit weight respectively.

Five different mixes of sand, plaster and water were used to simulate all rocks except the coal seams for the model of Figure 8.2.1. Coal dust with the particle size ranging from 75 μm- 1 mm (or the 200 mesh) was added to a sand-plaster-water mix in order to simulate the coal seams, since the coal seams are much small in the unit weight. Four additional mixes all added with coal dust were sampled and tested. The results are listed in Table 8.2.1.

299

Table 8.2.1 Characteristics of the model materials for the simulation of coal seams

NO	Sand (gram)	Plaster (gram)	Water (cc)	Coal dust (gram)	Unit weight gram/cm^3	UCS (MPa)
1	300	200	250	250	0.999	0.161
2	300	200	200	300	1.047	0.259
3	275	175	250	300	1.007	0.157
4	200	200	250	350	0.888	0.156

To satisfy the scale factors, the fourth group of the mixes in Table 8.2.1 was employed. Thus the model structure in terms of the thickness, the proportion among the materials, and the corresponding values of the unit weight and UCS were determined and are listed in Table 8.2.2

The model was cast according to these layers with no further lamination structure. The material mix for a layer was poured on the top of the previously cast layer after a small amount of fine sawdust was laid to weaken the strength along the interface. Other details of the casting procedure were the same as described in chapters six and seven.

After 48 hours curing in an oven at 105°C temperature, the model was installed in the small testing rig as used for the tests of the models in chapter six. An arch tunnel of 10 cm wide x 10 cm high was cut at the model centre, corresponding to a position in the strata ranging from the bottom part of the silty mudstone, through the mudstone seatearth and siltstone sandstone, to the siltstone. The model tunnel corresponds to a 4 m x 4 m arch profile in the prototype.

No	Model			Simulated reality		
	Sand:Plaster:Water(:Coaldust) (gram):(gram):(cc)(: gram)	UCS (MPa)	Unit weight (gram/cm³)	Rock	UCS (MPa)	Unit weight (gram/cm³)
1	525 : 225 : 250	0.392	1.396	Mudstone	27.44	2.44
2	575 : 175 : 250	0.272	1.415	Mudstone seatearth	19.04	2.48
3	500 : 250 : 250	0.719	1.410	Silt- mudstone	50.33	2.47
4	475 : 275 : 250	0.886	1.377	Siltstone	62.02	2.41
5	450 : 300 : 250	1.180	1.397	Sandstone	82.60	2.44
6	200 : 200 : 250 :350	0.156	0.888	Coal	10.92	1.55

Table 8.2.2 Characteristics of the model materials and the corresponding rocks

301

8.2.3 Test Results

Three models have been tested. They are noted as M1, M2 and M3 respectively.

The M1 model was first tested in the 2:1 horizontal to vertical stress field, which would correspond to the tunnel in the original stress field environment, i.e. beyond the influencing range by the frontal abutment stress. During the test, the tunnel failures mainly occurred in the floor and the crown surface after 5% tunnel closure. The failures are considered to be due to the gradual increase of the lateral compression. Plate 8.2.1 (a) shows the tunnel failure situation after 7.5% tunnel closure. It can be seen that the crown failure was localised which could be overcome by the use of tunnel supports. The floor failures were caused first by the shear along a bedding 2.5 cm (corresponding to 1 m in the prototype) below the floor level and then by breaking across the detached layer. This failure process is more or less similar to the results of the corresponding models in the previous chapter.

The M2 model was tested in a hydrostatic field condition which was intended to represent the applied stress condition at a location within the initially influencing range of the front abutment stress, namely 12 - 30 metres ahead of the face line.

The tunnel of the M2 model exhibited little difference from that of the M1 model in respect of the failure location, occurrence and pattern. As is shown in Plate 8.2.1 (b) the failure took place at a shallow depth of the floor and was localised at the crown. One exception is that the closure of a given value occurred at a much higher applied stress level in this case, compared to that in the M1 model. This indicates that the tunnel has an increased stability in the hydrostatic condition and that no marked effects of the front abutment stress will be observed if the induced rock stress is added to the original stress field to form a hydrostatic environment.

The M3 model was tested in a uniaxially vertical stress environment with a slight lateral constraint (0.18 MPa), which was approximately representing the tunnel under the effect of the peak abutment stress.

Plate 8.2.1

Illustrating the deformation and fracture pattern of the tunnel in

the originally greater horizontal stress field and the hydrostatic

stress field as a result of the superposition of the mining

induced stress at the initial stage.

(a) In the original stress field ($2\sigma_v = \sigma_h$).

(b) In the hydrostatic stress field as a result of the superposition

of the mining induced stress at the initial stage.

7·5%

7·5%
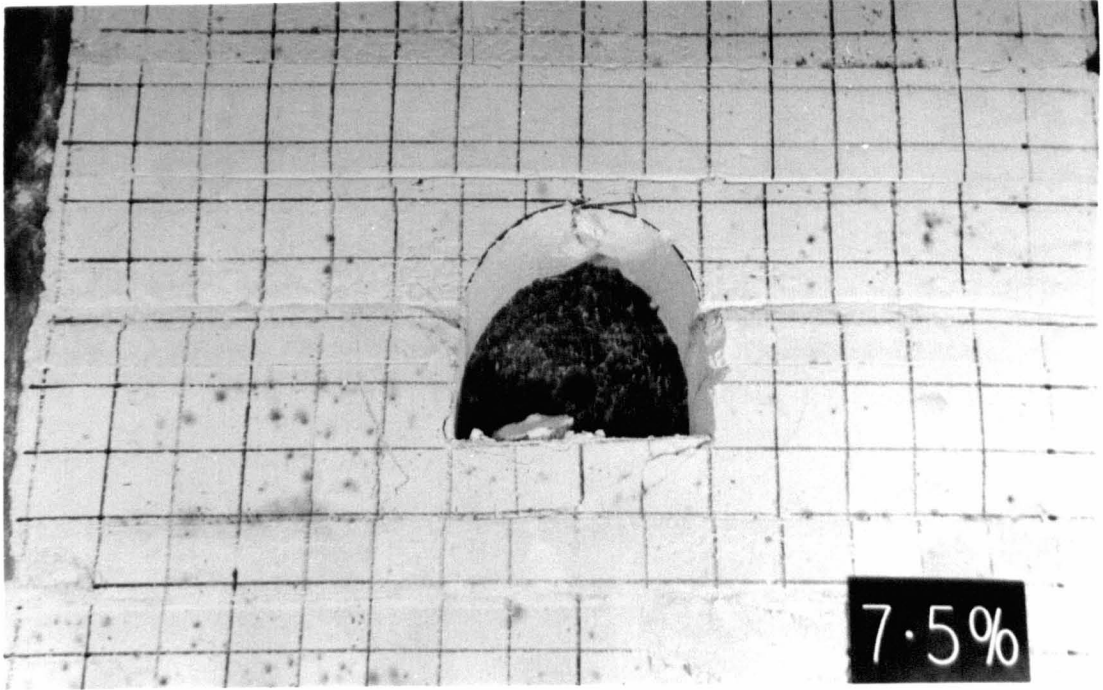
Plate 8.2.2

Illustrating the deformation and failure of the tunnel under the

violent action of the peak abutment stress.

(a) Under the action of the peak abutment stress.

(b) A result of the abutment stress effect.
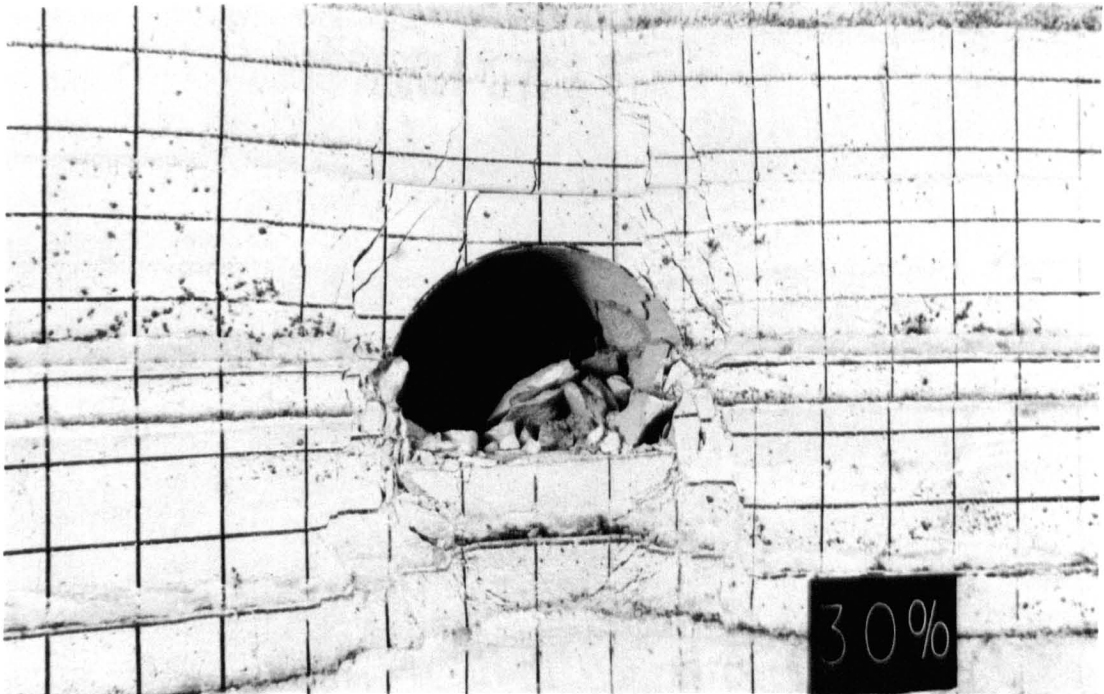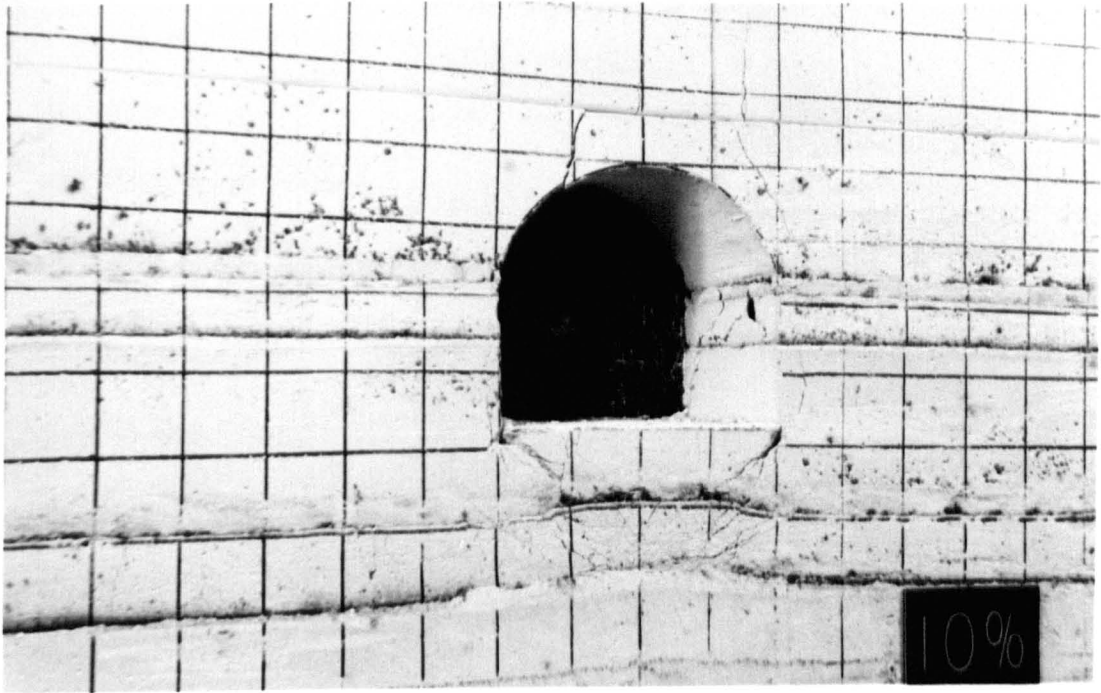
With this loading pattern, the fractures not only continued to develop toward the deeper position in the floor, but also developed in the roof. The sidewall buckling and spalling took place as well. These phenomena are clearly illustrated in Plate 8.2.2 (a). It indicates that the tunnel under the severe mining induced influence requires some additional consideration for the support system. For example, as a higher stress is expected from the roof, the sidewall buckling may occur and a lateral load may be produced and applied on the support leg, leading to a reduction in the support capacity. An increase in the designed support capacity under this circumstance should be considered, particularly the strength to withstand the vertical compression and the lateral buckling.

It can be seen from the photograph in Plate 8.2.2 that the sudden occurrence of sidewall spalling can be referred to as a result of the effect of the increasing abutment stress. The similarly adverse failure situation around a tunnel like the one shown in Plate 8.2.2 (b) has been observed by the author's practice in China. A typical example is that,while a longwall face is advancing from one side of a tunnel / raise closely underneath the seam to the other side, the tunnel will suffer heavy damages including the sidewall spalling, the roof breakage and the heave of the weakened floor. Many wooden props may be broken and require a replacement.

8.2.4 Further Discussion

The M1, M2 and M3 models can be used to further develop the concept regarding the stability of a tunnel under the effect of the mining induced stress.

Consider a given section of a tunnel which will subject to the mining induced influence as a longwall face is approaching toward it. When the working face is far away from it the tunnel is in the environment of the original stress field which is supposed to be of the 2:1 horizontal to vertical with low magnitudes. The tunnel deformation and the fracture pattern are liable to exhibit similar results with those of

the M1 model, namely, the floor failure is likely to take place at the shallow depth with a little influence on the tunnel performance. No evident instability problems occur with the roof after installation of the support.

As the working further approaches, the tunnel is gradually exposed in the initially influencing range of the frontal abutment stress. The tunnel is then subject to an increasing loading by the vertical abutment stress. The fractures around the tunnel would develop on the basis of the previously formed situation. The result can be seen as a combination of the M1 and M2 models. The sidewall cracking and spalling has not occurred yet.

When the working face continues to advance to a position very close to the tunnel, the tunnel is under the effect of the peak abutment stress. The fracture development will be intensified, the result of which should be represented by the superimposing of the M1, M2 and M3 results. The final situation may be illustrated by Plate 8.2.2 (b), where the sidewalls have be seriously damaged. The fractures in the floor extend into the deeper layers, causing more loosened materials to heave into the excavation. The fractures in the roof are worsened as well.

Since the fracture pattern and development around a tunnel changes dramatically as a working face advances toward it, the manifestations of the change have been widely used for the prediction of the periodic breaking of the massive main roof at many collieries in China. The pitmen can precisely predict the forthcoming periodic weighting by observing the intensive spalling of the coal walls of the in-seam gateways (special tunnels) near the faceline. The coal wall clapping can be heard. This prediction is based on the fact that the peak abutment stress reaches the maximum immediately prior to a periodic weighting. Under the action of the maximum peak abutment stress, the related gateways will behave like that shown in Plate 8.2.2 (b) where intensive spalling from the sidewalls occur. Additionally, the floor heave problem becomes the most serious at the entrance / exit of the face or the area of the

face ends, in comparison with the other parts of the gateways. This kind of rock stress manifestation has also been encountered by the author while working in China.

The instrumentation results regarding the abutment stress concentration is very important and useful for the design of a new panel layout in the similar environment condition. Since 1950's a design concept has been formed in the China coal industry in relation to that the mining tunnels / roadways should be allocated beyond the highly stress concentration zones. Niu (1981) reported a case study at Fenghuangshan Colliery. A tunnel allocated 20 metres underneath a coal pillar was serious damaged, resulting in a sharp increase of the annual tunnel maintenance cost. In contrast, another tunnel driven in the same strata but under a goaf area which had been destressed experienced very little deformation, with the annual maintenance cost being $\frac{1}{20}$ of the previous one. This example indicates the significance of identifying the destressed and highly stressed zones around a working panel. In a new panel layout design, the in-seam gateways are usually required to be excavated beyond the strong influencing range of the abutment stress from the neighbouring mined-out area. For instance, if the abutment stress distribution is like those given in Section 8.1, the gateways should be allocated some 12 metres apart from the boundaries of the mined-out area. This explains why in the Datong coal field, the designed widths of the rib pillars are usually 10-14 metres, in order to isolate the mined-out panel from the tailgate of the next new panel and to avoid the violent effect of the abutment stress.

Obviously the consideration on the effect of the abutment stress on the tunnel stability is appropriate and necessary. Such consideration, however, does not account the effect of the mining induced horizontal stress variations on the tunnel stability. As has been seen from the models in the present section, when a tunnel is first driven in the greater horizontal stress field (in the undisturbanced arear), the mining induced vertical abutment stress may be later added to this field, with the approaching of a working face. This may possibly form a hydrostatic stress field within the influencing range of the abutment stress concentration. A gateway in the hydrostatic loading

environment may exhibit increased tolerance to the greater stress magintude. That is why no evident differences have been observed betwwen the M1 and M2 models. This result indicates that when the influencing range of the abutment stress is some 30 metres from the panel boundaries, there is no definite need to allocate the gateways 30 metres apart from the boundaries of the neighbouring panel. The distance between the gateways and the neighbouring panel boundaries should be determined upon the consideration of the magnitude of the original horizontal stress. The most ideal location of the gateways is considered to be in the hydrostatic field, even though the absolute stress magnitude may rise in this case. Engineering practices in the Datong coal field have shown that a 10 - 20 metre distance between the roadways and the neighbouring panel boundaries will be sufficient for avoiding pronounced roadway closures, though the influencing range of the abutment stress is 30 metres by the instrumentation.

8.3   Stability Aspects of a Rib Pillar

A rib coal pillar is often left to isolate a working face system from a mined-out area, to avoid or reduce the risks of methane emission and spontaneous combustion due to the connection of a mined-out area and a working face, and to maintain a roadway for the working face. The width of the rib pillar is a very important parameter in the pillar design. A narrow pillar may not form a desired barrier to isolate the gate roadway from the mined-out area but may attract much of the abutment stress. However, an over-wide pillar will lead to a reduction in the coal recovery and become less economic.

At some collieries in China, the width of the rib pillars is ranging from 8 to 12 metres for those seams 120 - 250 metres below the surface. To cope with the increasing spontaneous combustion incidents, partly due to the remaining coal in the old mined-out areas being oxygenated by the leaking air flow through the paths of fissures and fractures in the rib pillar, the width of the rib pillars is often suggested to

increase to some 20 metres. A question arise here as to what is the minimum but reliable size of the rib pillar, which can secure the safety of the gate roadways from the above mentioned hazards? To obtain the answer, the modelling technique was again used to simulate a typical situation at a Chinese colliery taking the mining induced effect into account.

8.3.1 Strata Constitution and Model Construction

Simulated in this section is a 4 metre coal seam directly sandwiched by the massive sandstones. The roof sandstone is 20 metres thick and the floor 8 metres. The model structure is illustrated in Figure 8.3.1. A coal pillar of 12 metres is left between a 4 m x 4 m square tailgate and a mined-out area to the left of the model. Each of the strata consists of a number of layers of equally 4 metres thickness.

Four mixes of sand, plaster and water were used to simulate the corresponding layers, to one of which coal dust was added to simulate the coal seam. These mixes used are listed in Table 8.3.1.

The geometric scale factor was 1:40 and the unit weight scale factor 1:1.75. The strength scale factor was thus found to be $\frac{1}{40} \times \frac{1}{1.75} = \frac{1}{70}$.

The model casting procedure was the same as described in Section 7.2.3. After the installation of the model into the large testing rig (122 cm x 122 cm x 7.62 cm) the front surface of the model was marked with a black pen into 2.5 cm x 2.5 cm grids, so that the relative position of the fractures produced could be observed and identified. Two sets of wooden supports were used.
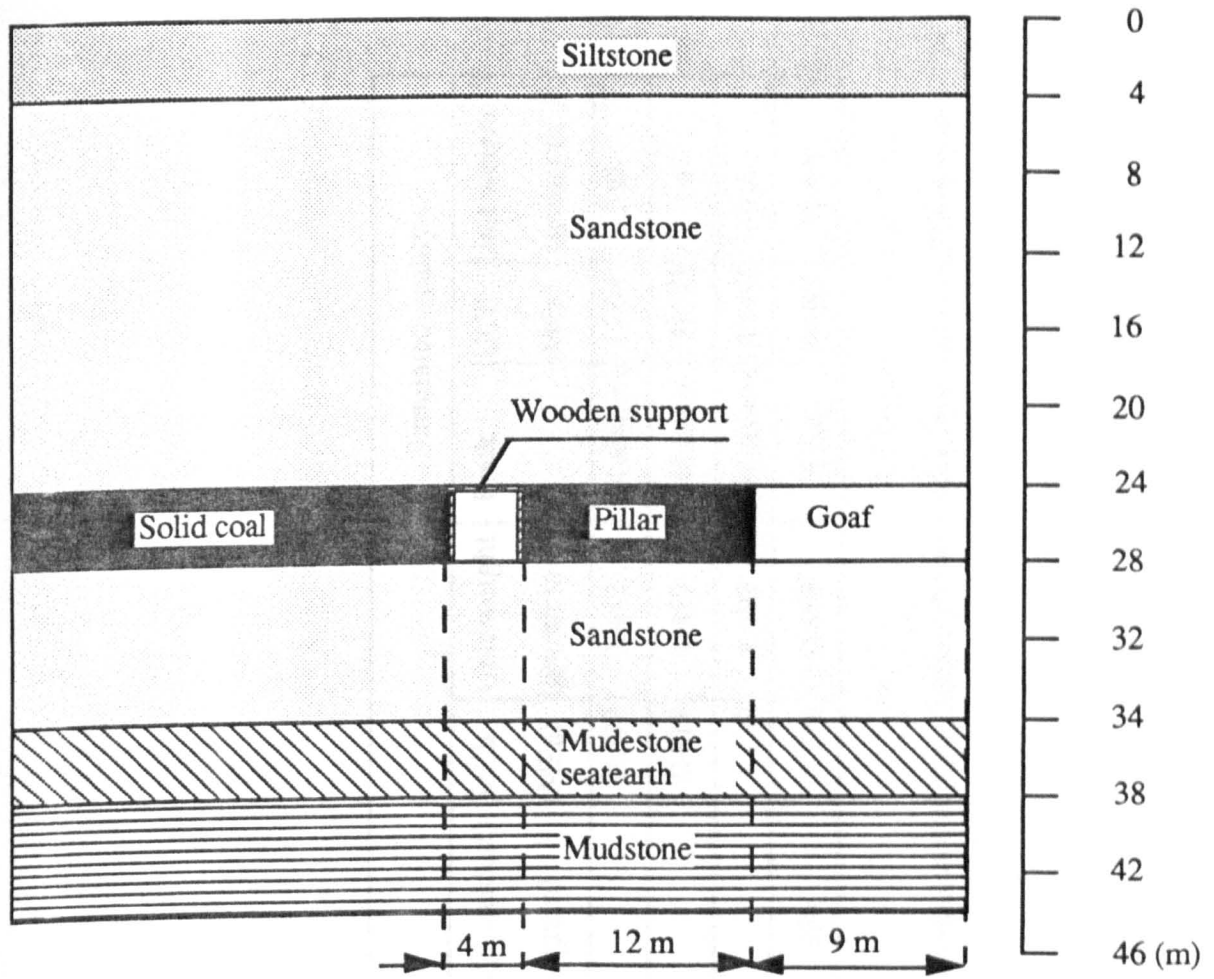
Figure 8.3.1 A model of a rib pillar and the strata sequence

No	Model			Simulated reality		
	Sand:Plaster:Water(:Coaldust) (gram):(gram):(cc)(: gram)	UCS (MPa)	Unit weight (gram/cm³)	Rock	UCS (MPa)	Unit weight (gram/cm³)
1	575 : 175 : 250	0.272	1.415	Mudstone	19.04	2.48
2	500 : 250 : 250	0.719	1.410	Siltstone	50.33	2.47
3	450 : 300 : 250	1.180	1.397	Sandstone	82.60	2.44
4	200 : 200 : 250 : 350	0.156	0.888	Coal	10.92	1.55

Table 8.3.1 Characteristics of the model materials used for a study on rib pillar stability

311

8.3.2 Model Test and Results

The model was tested in a 1:3 horizontal to vertical stress field environment, which was intended to be corresponding to a case involving the effect of the abutment stress on the rib pillar and the tailgate. At several levels of the roadway closures, the model was photographed and the closure magnitudes noted.

It has been observed in the test that, with the increase of loading the pillar was subjected to an increasing effect of the vertical compression. The right edge of the pillar was compressed more appreciably than the left edge, indicating the peak abutment stress acting at the right edge of the pillar and the sandstone roof sagging at the goaf side. Cracks, however, developed in both sides of the pillar. Some cracks are visible from the photographs and others not due to the darkness of the coal seam. Plate 8.3.1 shows the visible cracks in the pillar and around the tailgate. there are two kinds of visible cracks in the photograph. One is vertically oriented at the right hand side edge, which may have been formed by the tensile stress due to the lateral expansion of the pillar. The other is semi-rhomb shaped, which may have been produced by the shear failure owing to the predominant vertical compression. The depth of the visible fracture formation in both sides of the pillar were measured to be around 3.7 cm (equivalent to 1.5 metres in the prototype) from the sidewalls. Because of the dark colour of the seam, small and micro cracks and fissures are not seen from the photograph. By a careful observation during the test, it was seen that the core of the pillar, at least 10 to 12.5 cm (equivalent to 4 - 5 metres in the prototype), was remaining intact. This indicates that the width of the pillar is sufficient for isolating the tailgate from the connection with the goaf through the fissure and fracture paths, and that the above said risks can be efficiently reduced. Therefore there is no need to increase the width of the rib pillar in this case.

Another result which was obtained is regarding the behaviour of the wooden support system. As is seen in the Plate 8.3.1, the props and roof bar were broken

after the occurrence of the significant roadway closure. The breakage of the props are partly attributed to the buckling of coal from the sidewall., which first caused the bending of the props. The bent props thus lost their strength in the direction of the wooden fibres. The reduction in the prop strength adversely affected the performance of the support system and eventually led to the damage to the system. This result indicates that the structure of the wooden support set is less flexible and cannot stand the appreciable roadway closure. To deal with the appreciable roadway closure, it is very important that the support system has both flexibility and strength in this case.

Plate 8.3.1

Fracture pattern development in the rib pillar and rocks around a tailgate
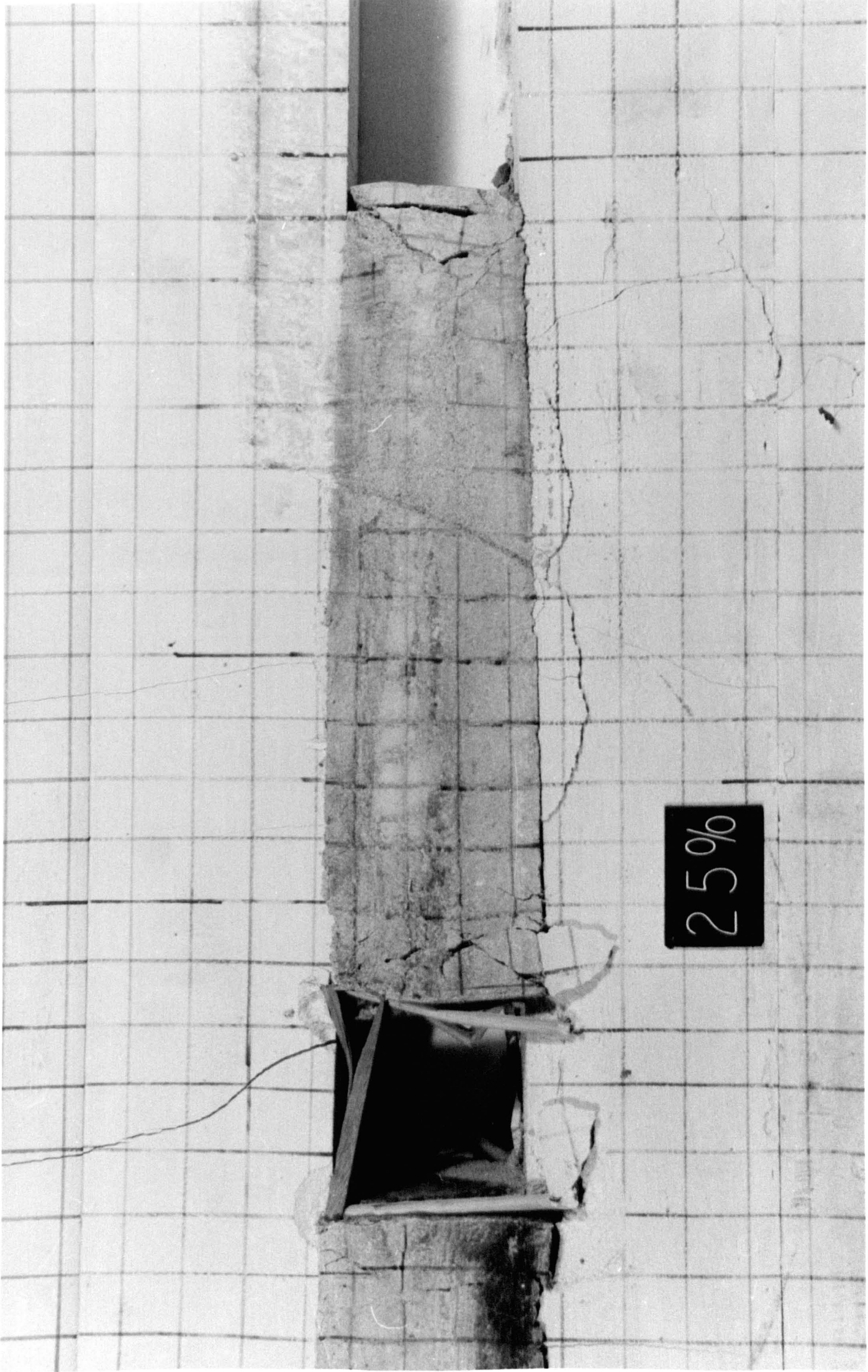
25%

CHAPTER NINE

GENERAL CONCLUSIONS AND
RECOMMENDATIONS FOR FURTHER RESEARCH

CHAPTER NINE

GENERAL CONCLUSIONS AND RECOMMENDATIONS FOR FURTHER RESEARCH

9.1 General conclusions

In the modern coal industry, production is developing towards higher concentration levels. The need for more efficient operations in order to compete in the energy market has led to some major tunnels needing to be designed and excavated for new developments at several collieries in the UK. It is apparent that these tunnels should achieve a high standard of stability during their service life.

More and more mining tunnels are being excavated at the greater depths below the surface, with the mining levels at some coal mines in the UK and other countries already at over 1000 metres below the surface. Energy resources are becoming depleted at the shallow depths. Tunnels located at such depths are more likely to encounter more rock mechanics problems due to the increased rock stress.

Aiming at solutions to these problems in relation to mine tunnel stability, a series of research programmes have been launched on a team basis at the Department of Mining Engineering, University of Nottingham in the past decades. As a part of these research programmes, the work in this thesis as performed by the author has mainly focussed on the effect of the stress field environment on tunnel stability. After three years work for this thesis, the major conclusions are drawn as follows:

The major factors that influence tunnel behaviour have been reviewed from the geological and operational points of view. Some factors such as rock formations and geological discontinuities including faults, folds and joints have already been formed as part of the rock structure. The effects of these factors, though uncontrollable, can

315

be reduced in respect of their impact on stability by careful choice of tunnel location. Other factors should be controllable in respect of design and operation.

The effects of these factors on tunnel stability are attributed to the result of performance in relation to the stress field. Many of the controllable factors influence the tunnel stability by virtue of readjusting the stress field in terms of its magnitude and orientation, under which the tunnel is loaded. Therefore the stress field characteristics become the core of the factors that influence the tunnel stability. The author's attention has been drawn to these factors which have become the focus of the work presented in this thesis.

This research started from investigation of the stress and strain distribution around a tunnel prior to the occurrence of any failure of the surrounding rock. Based on the work previously conducted by former researchers at the Department of Mining Engineering, University of Nottingham, the author continued to use a circular tunnel in a homogeneous rock as a theoretical study background. But attention has been drawn to the effect of the non-hydrostatic stress field on the stress distribution. For this aim, the elasticity theory has been employed. Upon a detailed review of the fundamental equations needed for solving the elastic problems, a more general solution regarding the stress distribution around the tunnel has been deduced, from which some special cases, in particular, in the hydrostatic condition as used by the former researchers can be obtained. According to the general solution, the author has proposed that the effect on the stress distribution around the tunnel consists of three parts: the support resistance, the hydrostatic stress field and the difference in the applied vertical and horizontal stresses. It has been found from the study of the three parts that the evident range of the active effect of the support resistance on the stress distribution around the tunnel is limited to the near vicinity of the tunnel. Beyond a distance approximately equal to the tunnel diameter from the tunnel wall, the support effect is very weak and negligible. The variation of the stress distribution along the tunnel circumference has been found to be significantly governed by the difference of

316

the applied maximum and minimum stresses under the given geological setting environment.

A further analysis reveals that the magnitude of the stresses around the tunnel is proportional to the applied vertical stress. In other words, as the mining depth increases, the mining tunnels will be subjected to the increasing stress field effect, which theoretically predicts that more rock mechanics problems will occur with tunnels excavated at the increased depth.

The stress concentration factors for the radial and tangential normal stresses and the shear stress have been discussed by the author. The factors have been related to the applied stress ratio for the discussion on the stress concentration around the tunnel. This treatment has avoided the discussion on the absolute value of the rock stresses but outlines the stress concentration zone by virtue of the values of the factors proposed.

The shear failure tendency around a tunnel has been predicted by using the concept of the maximum shear stress concentration factor K_{tmax} which is defined by the author as the ratio of the maximum shear stress at a point under discussion to the value of the applied vertical stress. The relationship between the shear failure tendency and the applied stress field feature has been discussed.

A formula for the prediction of a theoretical tunnel closure has been deduced. In the formula, the pre-excavation deformation of the rock has been taken into account. The result shows that the observable tunnel closure is proportional to the tunnel diameter. Thus the excavation size has a direct and evident effect on the deformation and stability of the tunnel. The larger the opening, the greater the tunnel closure is expected to be. The author argues that a proper reduction in the tunnel excavation size may sometimes be an effective measure for improving the tunnel stability. A further deduction shows that for a given geological setting, the tunnel closure rate, which is referred to as the ratio of the tunnel closure to the tunnel diameter, is governed by the

nature of the stress field and the support resistance. It has been indicated that the heavier stress field environment would result in a greater tunnel closure rate. An increase in the support resistance, but without exceeding the support capability, could reduce the tunnel closure rate.

From the discussion of the tunnel closure rate, a new tunnel design concept has been proposed through Equation 4.3.38. It has been indicated that the results of the tunnel closure measured at an existing tunnel can be used for the future design of new tunnels in similar geological conditions. Tunnel design in this way may avoid a need to measure the original stress field. Since the instrumentation for the tunnel closure rate is comparatively simple and easy and the new design concept (i.e. Equation 4.3.38) has a simple form of expression, the significance of the proposed concept becomes apparent when adopted.

For the convenience of an investigation into the effect of the tunnel dimensional ratio on tunnel stability, an elliptical tunnel model has been employed. For the solution of the stress distribution around the tunnel, a complex variable theory has been used with a success, this including the concepts of the analytical function, the Cauchy-Riemann equations, the Laplace equations, the conjugate functions and the conformal mapping techniques. By a conformal mapping function, the region in which the elliptical tunnel exists has been mapped onto another region where the tunnel profile becomes circular. The analysis has been carried out for the circular profile in the mapped region, from which the author draws attention to the stress distribution along the tunnel periphery and deduces the relationship between the tunnel dimensional ratio and the applied horizontal to vertical stress ratio. It has been found that when the ratio of the tunnel width to height is equal to the value of the applied horizontal to vertical stress ratio, the stress equally distributes along the tunnel periphery, which would give the optimum state of stability. Based on this finding, it has been predicted that the circular and even the square profile is most suitable to the tunnels in the hydrostatic stress field condition, whilst in other stress field environments the instability problems

cannot be effectively alleviated by the design and use of the circular or square profiles and supports.

Various tunnel failure prediction theories have been reviewed, of which a detailed comment has been given on the IEM theory as developed by former researchers at the Department of Mining Engineering. Based on this work, a prediction theory has been proposed by the author. In the theory, the Mohr-Coulumb failure criterion has been incorporated for the assessment of rock failure. The interaction between the support and the surrounding rock has been considered in the theory by the use of a closed concrete support. After a complex plasto-elastic analysis, an implicit solution has been deduced to relate the failure radius to a number of influencing factors including the stress field, the elastic constants and limit strength of the rock mass, the support features and the tunnel size. According to the plastic yielding radius evaluated by the formula developed in Chapter 5, the surrounding rock requiring support becomes more clear, which is particularly important in the design of the rock bolt length. A computer programme using these formulae to predict tunnel stability would be expected to require far less time than the general finite element programmes, and a personal computer could be employed to carry out the prediction tasks.

The characteristics of fracture development around tunnels have been intensively studied by means of the small scale physical modelling. Twenty four models have been tested for this study purpose, including four types of tunnel profiles placed separately in six different stress field environments. The results as discussed throughout Sections 6.4.1 to 6.4.6 have indicated that the fractures developing around the tunnels are appreciably governed by the pattern of the applied stress field, particularly the direction and the magnitude of the applied maximum and minimum stress components. The major fractures will develop in accordance with the predominant stress applied. They develop intensively in both the roof and the floor when the applied vertical stress is much more pronounced than in the horizontal

319

direction. But they are found to develop appreciably in the sidewalls if the applied horizontal stress is much greater than the vertical.

The directions of the major fractures produced around the tunnels are mostly in agreement with the direction of the predominant stress applied. In the cases where the applied horizontal stress is greater than the vertical, the major fractures produced are mainly in the horizontal or close-to horizontal directions. These fractures are most likely to form a wedge or a stress relieved zone in both sidewalls. The depth of the zone appears to be related to the value of the corresponding vertical to horizontal stress ratio applied. In the cases where the applied vertical stress becomes greater than the horizontal, however, the major fractures then develop mainly in the vertical or nearly vertical direction. Similarly, they will form a stress relieved dome in the roof, and many times in the floor as well. The height of the dome seems to be closely influenced by the applied vertical to horizontal stress ratio.

The occurrence of the stress relieved zone formed in either roof and floor or both sidewalls seems to have been influenced very little due to the variation of the tunnel profile, as long as the tunnel width to height ratio remains unchanged. The major horizontal (or closely horizontal) fractures in the tunnel roof, due to the effect of the higher horizontal stress applied, activates the roof slabbing and localised falling incidents, whereas the major vertical (or closely vertical) fractures in the sidewalls promote sidewall buckling and spalling.

The theory regarding the condition of the optimum state of stability for an elliptical tunnel in Section 4.4 has been extended and developed by virtue of the model tests. Comparisons between the rectangular tunnels with the different width to height ratios in three different stress field condition have been made. The conclusion drawn from the comparisons are that the tunnel dimensional ratio has a great bearing on the fracture development in terms of the fracture pattern, intensity and direction. As the applied horizontal stress is appreciably increased (to become much greater than the

vertical), a proper increase in the tunnel width from the square profile may result in a surprising improvement in the tunnel stability. However, when the applied horizontal stress is no longer greater than the vertical in magnitude, instability problems are most likely to arise in a tunnel that has a greater width than the height. Therefore the tunnel stability cannot be improved merely by increasing or decreasing the tunnel width without taking the stress field environment into account. The desired tunnel dimensions should have such values as the width to height ratio of the tunnel being equal to the value of the applied horizontal to vertical stress ratio. This conclusion also demonstrates that the result form the theoretical analysis using the elliptical profile in Chapter 4 is applicable to the rectangular and therefore to the other profiles.

A mathematical method, known as the orthogonal design method, has been employed for the investigation of the characteristics of the model materials with various proportions of the components, in order to determine the correct material for the construction of the stratified models. The use of the method has led to a saving in the test of the samples and thus the time and labour consumed. It has been shown by the tests that the proportions of plaster and water play a significant role in the determination of the strength of a sand plaster model material, with the former having significantly pronounced effect on its strength. The unit weight of a model material drops more explicitly with an increase in water than with a decrease in plaster. From the test results a guide-line has been given on the choice of the proper proportions between the sand, plaster, water and curing time for a required model material.

The effect of the stratified structure on tunnel stability has been studied by the physical modelling technique. The results indicate that the shear strength along the beddings or laminations has a great bearing on the tunnel stability when the applied stress field is predominant in the direction of the bedding / lamination plane. However, little effect of the bedding and lamination strength on the tunnel stability has been observed when the applied stress field is predominant in the direction vertical to the bedding and lamination.

The mechanism of the floor failure varies due to the influence of the stress field. When the applied horizontal stress is greater than the vertical, the floor failure initiates from the dislocation of the floor strata along the weak horizontal bedding / lamination planes, leading to a detachment of some layers. The detached layers are then bent. Both tensile and shear failures may occur to the bent layers, which eventually forms the floor lift. When the applied vertical stress becomes more pronounced than the horizontal, the vertical fractures may be produced in the weak floor strata. the fractures are more likely to form a stress relieved zone in the floor. The raising motion of the materials in the stress relieved zone forms the mechanism of the floor lift in this case.

The test results also indicates that the stress relieved zone may also be formed around the tunnel in the stratified ground condition. However, unlike the case in the homogeneous ground condition where the stress relieved zones were usually symmetrically formed in both opposite sides (namely, both sidewalls or the roof and floor), the zone is mostly likely to be formed in the weaker ground side in the stratified strata condition.

The effects of the lamination thickness on the tunnel stability have been discussed. The test results have shown that the tunnel in a thinner-laminated strata will experience more tunnel deformation problems in both 2:1 and 1:2 horizontal to vertical stress field conditions. In the 2:1 horizontal to vertical stress field condition, the increased floor lift problem in association with the lamination thickness has been explained by the use of the strut theory, whilst the problem occurred in the 1:2 horizontal to vertical stress field has been attributed to the larger stress relieved zone formed in the floor. The expanding and raising of the materials in the zone will increase the floor lift.

A standing metal support has been simulated and employed to study the effect of the support on the tunnel stability. The study shows that in the predominant horizontal stress field environment, the employment of the support will result in a reduction in

322

the tunnel closure, after the support is subjected to the rock pressure. In the case of the 1:2 horizontal to vertical stress field, however, the support function becomes less evident when the support legs penetrate the floor. This indicates the importance of preventing the support from penetration into the floor.

Another effect of the support is the reduction in the extent of the stress relieved zone in the floor, this will, from the long term tunnel stability point of view, benefit the strata control.

The mining induced effects on the tunnel stability has been considered and studied through the physical modelling technique. The abutment stress is the focus of the study. By using the underground instrumentation results that the author has previously obtained, three tunnel locations in relation to the peak abutment stress have been assumed. Corresponding to the assumption are three models tested in three different stress field environments. The results show a small effect of the front abutment stress if the induced stress is superimposed at the original stress field level to form a hydrostatic stress field environment. However, under the direct effect of the peak abutment stress, the stress field is more likely to become predominant vertical stress field. Thus the severe mining induced influences will be expected if the tunnel is directly under the effect of the peak abutment stress, as this has been confirmed by the relevant model test in the thesis. In this case, additional support density and strength are needed.

Finally, the rib pillar stability in relation to the gateway layout has been studied in order to simulate a case at a Chinese coal mine. The model test result indicates that a rib pillar with 12 metres width is enough to isolate the tailgate from the neighbouring mined-out area. This result is confirmed by the present practice at the coal mine. It has also been demonstrated by the test that it is important for the support system to have both flexibility and strength in order to deal with the appreciable roadway closure.

9.2 Recommendations for Further Studies

The work presented in this thesis has also opened some areas for further studies in the future. These are listed as follows:

(1) The effect of the stress field environment on the stability of two neighbouring tunnels, taking the relative position of the tunnels into account. The work in this aspect could be carried out by both theoretical and experimental methods. The theoretical method could involve the use of the complex variable theory and the concept of the bi-polar coordinate system. Obviously this work will require more knowledge of the mathematical elasticity. The experimental method is comparatively simple, when the small scale physical modelling technique is used.

(2) Tunnel behaviour under highly stressed strata environments needs to be further studied. One of the aims of the study should be placed on the findings of the measures to relieve the increased rock mechanics problems such as rock deformation in the soft rocks and rockbursts in the hard rock environments. A computer programme should be developed which incorporates the formulae as deduced by the author in Chapter 5 of this thesis in order to predict the tunnel failure radius in the hydrostatic stress field environment. To assess the effectiveness and correctness of the programme, the investigations should initiate at finding the rock mass properties as required by the formulae in Chapter 5.

(3) The nature and performance of various supports currently in use in the coal industry needs to be intensively studied. The study should cover the structure and strength of the supports, and the interaction between the supports and the surrounding rocks under various stress field environments. From the results of the study, a new and effective support system should be proposed for the use in adverse rock conditions.

REFERENCES

REFERENCES

Anderson, E.M. (1951) The dynamics of faulting, 2nd. ed., Oliver and Boyd, Edinburgh, pp197.

Bai, S. W.and Gu, Z.M. (1986). Deformation monitoring of galleries in fractured rockmass and research on failure mechanism of surrounding rocks. Proc. Int. Symp. Engineering in Complex Rock Formations. 3 - 7 November, Beijing, China.

Barenblatt, G.I. (1979) Similarity, self-similarity, and intermediate asymptotics. Plenum Co., New York.

Baxter, N.G. (1987). Design and stability of steel support systems with special reference to gate roadways in the Warwickshire coalfield. PhD thesis, University of Nottingham.

Bieniawski, Z.T. (1989) Engineering rock mass classifications. John Wiley & sons, New York.

Biron, C. and Arioglu, E. (1983) Design of supports in mines. John Wiley and sons. New York.

Bonsall, C.J. (1985). An investigation into the design and stability of coal mining tunnels. PhD thesis, University of Nottingham.

Bonsall, C.J., Smith, S.F., and Whittaker, B.N. (1982) Model studies of stability of mining tunnels. Proc. Symp. Strata Mechanics. Newcastle upon Tyne, April.

Borisenko, A.I. and Tarapov, I.E. (1968). Vector and tensor analysis with applications. Prentice-Hall Inc.

Bourne, D.E. and Kendall, P.C. (1977). Vector analysis and Cartesian tensors. Thomas Nelson & Sons Ltd, UK.

Brady, B.H.G. and Brown, E.T. (1985). Rock Mechanics for underground mining. George Allen & Unwin Ltd.

Branch, D.G. (1987) Study of mine tunnel stability with reference to stress conditions and deformation response of associated carboniferous rocks. PhD thesis, University of Nottingham.

Brown, E.T. and Hoek, E. (1978). Trend in relationships between measured rock in situ stresses and depth. int. J. Rock Mech. Min. Sci. 15, p211 -15.

Buckingham, E. (1914) On physical similar system, illustration of the use of dimensional equations. Phys. Rev., 4, pp345.

Budavari, S. (1983) Rock mechanics in mining practice. South African IMM, Johannesburg.

Carter, M.R. (1986) Strength behaviour of monolithic pack support structure around longwall face-ends. PhD thesis, University of Nottingham.

Cecil, O.S. (1970). Correlation of rockbolts - shotcrete support and rock quality parameters an Scandinavian Tunnels. PhD Thesis, University of Illinois, Urbana. pp 414.

Chen H. (1988) Comparison between and selection from two Effective methods for controlling massive hard conglomerate roof strata. Shanxi Mining Institute Learned Journal, Vol.6, No.4, (in Chinese).

Chen H. and Smith S.F.(1991) An investigation into characteristics of physical modelling materials using the orthogonal design method. Department of Mining Engineering Magazine, Vol.XLIII.

Chen, H. (1988) Field trials and investigations of very hard roof strata fracturing Problem during pre-injection of pressured water. Coal Science and Technology, October, (in Chinese).

Chen, H. and Niu, X.Z. (1985) A FEM study of heavy roof behaviour in longwall mining by induced fully caving with high pressure water jetting, Proc. Int. Symp. Mining Technology and Science. Sept. Xuzhou. China.

Chen, H. and Niu, X.Z. (1985) A FEM study on manifestation characteristics of rock pressure around longwall workings with very hard roof being controlled by injection of high pressure water. J. China Inst. of Min. and Tech., No.3, (in Chinese).

Chen, J. and Yuan, W.B. (1989). Analysis and design of rock-bolting system for reinforcing rockmass around roadway. Journal of China Coal Society (in Chinese). Vol.14, No.3, pp 71 - 80.

Chorlton, F. (1976). Vector and tensor methods. Ellis Horwood Ltd, England.

Coulomb, C. A. (1773). Sur une application des regles de Maximis et Minimis a quelques problemes de statique relatifs a l'Architecture, Acad. Roy. des Sciences Memoires de math. et de physique par divers savans, Vol. 7, pp343-382.

Cundall, P.A. and Strack, O.P.L. (1979). A distinct numerical model for granular assemblies. Geotechnique, Vol. 29, pp47-65.

Cutts, A. (1991). Engineering our way into the (1990)s. Mining Technology. Vol.73. February, .

Daemen, J. J. K. (1977). Problems in tunnel support mechanics. Underground Space, Vol.1 PP163-172.

Deere, D.U. et. al. (1970). Design of tunnel support system. High. Res. Rec. No.339, pp26-33.

Deere, D.U. et. al.(1967). Design of surface and near surface construction in rock. Proc. 8th U.S. Symp. Rock Mech. AIME. New York.pp237 - 302.

Dou, W. H.and Xing, N. X. (1986). Collapse of surrounding rock: analysis of mechanism and approach to prediction. Proc. Int. Symp. Engineering in Complex Rock Formations. 3 - 7 November, Beijing, China.

England A.H. (1971). Complex variable methods in elasticity, Wiley and Sons. London.

327

Evans, I. (1981). Environment Aspects . Mining Technology. October.

Fan, Q.Y. (1990). Mechanical analysis for choosing optimum orientation of underground openings. Journal of China Coal Society (in Chinese). Vol.15. No.3. pp 62 - 71.

Fan, W.X.and Zhang, T.Z. (1989). Analysis and tests of stress on split-set roof bolt. Journal of China Coal Society Vol.14, No.1.

Fara, H. D. and Wright, F. D.(1963). Plastic and elastic stresses around a circular shaft in a hydrostatic stress field. Trans. AIME, Vol.226 pp319-320.

Fathollahzaden-Aghdam, A. (1986) Rock behaviour under different states of stress and applications to stability of underground excavation. PhD thesis, University of Nottingham.

Feng, J.L. (1989). Repair of failed roadways in soft rock. Coal science and technology (in Chinese) No.4, PP 35 -36.

Flugge, S. (1958) Elasticity and plasticity. Springer-Verlag, Berlin.

Flugge, w. (1967) Viscoelasticity. Blaisdell Publ.Co. Massachusetts.

Frith, R.C. (1988). Study of prediction of closure behaviour and stability of mining tunnels. PhD thesis, University of Nottingham.

Fu, X.M.and Pan, Q.L. (1990). Rules and mechanism for swelling of weak and soft rocks. Journal of China Coal Society (in Chinese). Vol.15. No.3 pp31-38.

Gao, J.M.and Dun, Z.L. (1989). Investigation of rock bolting by photoelastic experiments. Journal of China Coal Society (in Chinese). Vol.14. No.4. pp39 - 44.

Goodman, R.E. and Shi, G.H. (1985) Block theory and its application to rock engineering. Prentice-Hall, New Jersey.

Goshtasbi, K. (1987). Model studies of mine excavation stability with special reference to gate roadways in the Warwickshire coalfield. PhD thesis, University of Nottingham.

328

Green, A.E. and Zerna, W. (1954). Theoretical elasticity. Oxford , Clarendon Press.

Greenspan, M. (1944) Effect of a small hole on the stresses in a uniformly loaded plate. Quart. Allp. Math. Vol. 2 No.1.

Griffith, A. A. (1924). Theory of rupture, Proc. 1st. Int. Congr. Applied Mechanics, Delft, pp 55 - 63.

Hai, G.W.(1990). Application of orthogonal test in selection of backfilling material for mine roadway. Coal science and technology (in Chinese) No.8 pp.

Heller, S.R., Brock, J.S. and Bart, R. (19) The stresses around a rectangular opening with rounded corners in a uniformly loaded plate.

Hoek, E & Brown, E.T. (1980) Underground excavation in rock. IMM, London.

Hou, C.J. and Ma, N.J. (1989). Stress in in-seam roadway sides and limit equilibrium zone. Journal of China Coal Society (in Chinese) Vol.14, No.4, pp21-29.

Huang, J.Y. et. al. (1989). Steel strap bolt support and its improvement Coal science and technology (in Chinese) No.8, pp26-28.

Jaeger, J.C. and Cook, N.G.W. (1979). Fundamentals of rock mechanics. Chapman and Hall, London.

Jerimic, M.L. (1985) Strata mechanics in coal mining. Balkema Publ. Ontario, Canada.

Jukes, S.G. (1983). An investigation into steel arch support characteristics of mining tunnels. PhD thesis, University of Nottingham.

Jukes, S.G., Hassani, F.P. and Whittaker, B.N. (1983) Characteristics of steel arch support systems for mining roadways. Min. Sci. & Tech. No.1 pp43-58.

Kapusniak, S.S. (1986). Long-term stability of major coal mining tunnel projects. PhD thesis, University of Nottingham.

King, H.J. and Whittaker, B.N. (1971) A review of current knowledge on roadway behaviour. Proc. Symp. Roadway Strata Control, IMinE, pp73 - 87.

Kondoh, T. and Shinji, M. (1986). Back analysis of assessing for slope stability based on displacement measurements. Proc. Int. Symp. Engineering in Complex Rock Formations. 3 - 7 November, Beijing, China.

Kreyszig, E. (1979) Advanced engneering mathematics, 4th Ed. John Wiley and sons, New York.

Kyoya, T., Kusabuka. M.and Ichikawa. Y. (1986). A damage mechanics analysis for underground excavation in jointed rock mass. Proc. Int. Symp. Engineering in Complex Rock Formations. 3 - 7 November, Beijing, China.

Langhaar, H.L.(1951) Dimensional analysis and theory of models. John Wiley, New York.

Lauffer, H. (1958). Gebirgsklassifizierung fur den Stollenbau. Geol. Bauwesen 74.pp46-51.

Lemon, R. (1991). Pumping and disposal of deep strata mine water. Mining Technology. Vol. 73. March.

Li, X.P. (1989). Effect given by pillar width on stability of roadway surrounding rock. Coal science and technology (in Chinese) No.12, pp6 - 9.

Li, X.P. and Yao, J.G. (1990). An expert system for a rational selection of the style and parameters of support in gateways. Coal science and technology (in Chinese) No.7 pp28 - 32.

Liang, J. J. (1986). A monitoring method for tunnel engineering. Proc. Int. Symp. Engineering in Complex Rock Formations. 3 - 7 November, Beijing, China.

Ling, C.B. (1948) On the stresses in a plate containing two circular holes. J. Appl. Phys., Vol.19, pp77 - 82), January.

Ling, C.B. (1948) The stresses in a plate containing an overlapped circular hole. J. Appl. Phys., Vol.19, pp 405 -411, April.

Liu, J.Y. (1990). Precautions of pressure releasing and stepped floor bolting against mine floor heave. Coal science and technology (in Chinese) No.3, pp16 - 17.

Liu, Y.T. et al. (1989). Rock stability classification of gateways in gently inclined and inclined coal seams, Journal of China Coal Society (in Chinese) Vol.14, No.3, pp21 - 36.

Liu, Z.L. (1989). Improvement of bolt shotcrete supporting in soft rock roadway. Coal science and technology (in Chinese) No.9, pp46 - 48.

Lu, Y. N. and Cai, X.H.(1986). Applying Mohr- Coulomb yield criterion to calculate elastoplastic stress in adhesive shotcrete and rockbolt lining of hydraulic pressure tunnel and its surrounding rock. Proc. Int. Symp. Engineering in Complex Rock Formations. 3 - 7 November, Beijing, China.

Ma, L.M. (1989). Pneumatic stowing trial along roadside of reusable gate,Coal science and technology (in Chinese) No.4, PP 2 - 6.

Martin, C.H. et al (1986) Australasian coal mining practice. AIMM. Sydney.

Mathematics Department Beijing University (1976) Orthogonal design (in Chinese). Publication House of the People's Education, Beijing.

Megaw,T.M. and Bartlett, J.V.(1982). Tunnels-planning,design, construction. Vol. 1 & 2. Ellis Horwood Ltd.

Merritt, A.H. (1972). Geologic prediction for underground excavations. Proc. Rapid Excav. Tunnelling Conf. AIME. New York. pp115 -132.

Miller, R.R. (1981) A study of design and structural stability aspects of mine roadway support systems. PhD thesis, University of Nottingham.

Mises, R. von. (1913). Mechanik der festen Körper im plastich deformablen Zustand, Nachr. Ges. Wiss. Gottingen, Mathematisch-Physikalisesche Klasse,pp582-592.

Mohr, O. (1914). Abhandlungen aus dem Gebiete der technische Mechanik, 2nd end., Ernst und Sohn, Berlin.

Morkovin, V. (1944) Effect of a small hole on the stresses in a uniformly loaded plate. Quart. Allp. Math. Vol. 2 No.4.

Muller, L. and Reik, G. (1986). Influence of geological conditions on excavation procedure and support of large rock caverns constructed according to NATM. Proc. Int. Symp. Engineering in Complex Rock Formations. 3 - 7 November, Beijing, China.

Murrell, S. (1963). A criterion for brittle fracture of rocks and concrete under tri-axial stress and effect of pore pressure, Proc. Fifth Rock Mech. Symp., Pergamon Press.

Muskhelishvili, N.I. (1948) Some basic problems of the mathematical theory pf elasticity. translated by Noordhoff Ltd (1953), Groningen, Holland.

Newson, S.R. (1983) Strata control - present problems, future plan. The Mining Engneer, Nov. pp229-235.

Nin, Y. and Chen, H. (1990) Finite element calculation and model testing for studying rock pressure manifestation in longwall workings during water infusion of hard roof. J. China Coal Society, Vol.15, No.1. pp 83 - 92 (in Chinese).

Niu, X.Z. (1981) Research on rock pressure and support of roadways in weak rock. Proc. Int.Symp. Weak Rock. Tokyo, Sept. 1981.

Niu, X.Z. and Chen, H.(1986) The development of rock mechanics in coal mines of china. A paper presented at Int. Conf. Engineering in Complex Rock Formations, November.

Niu, X.Z. and Gu, T.G. (1982) Control of the very hard roof by softening method using water inhection. 7th Int. Strata Control Conf. Sept. Liege,Belgium.

Niu. X.Z. and Yiao, J.G. (1983) Application of rock mechanics in coal mine design and planning. 8th Plenary Scientific Session, IBSM, Essen, June.

Obert, L. and Duvall, W.I. (1967). Rock mechanics and the design of structures in rock. John Wiley & Sons, Inc.

Omer, A.et al. (1986). Reinforcement of geotechnical engineering structures by grouted rockbolts. Proc. Int. Symp. Engineering in Complex Rock Formations. 3 - 7 November, Beijing, China.

Pankhurst, R.C. (1964) Dimensional analysis and scale factors. Chapman & Hall, New York.

Parashkevov, R. (1983) Prediction of the possibilities for the most complete utilisation of rock resistance at underground mine operations in heavy conditions. 8th Plenary Scientific Session, IBSM, Essen, June.

Patchet, S.J. (1983). Mechanical properties of rock and rock masses. Rock Mechanics in Mining Practice. edited by Budavari S., S. African Inst. Min. & Metall.

Peng, S.S. (198) Coal mine ground control, 2nd Ed. John Wiley & sons, New York.

Peng, S.S. and Chiang, H.S. (1984) Longwall Mining. John Wiley & sons, New York.

Ren, F.K. (1989). Rock stress of roadway in soft strata and roadway support. Coal science and technology (in Chinese) No.10, pp50 - 53.

Riggott, N. (1986). Rock mechanics, stability and strata loading aspects of mine roadways and support systems. PhD thesis. University of Nottingham.

Romberg, W. and Katzenbach, R. (1986). Back analysis of the shear strength of a folded rock. Proc. Int. Symp. Engineering in Complex Rock Formations. 3 - 7 November, Beijing, China.

Rukin, V.V. et al . (1986). Support of workings in complex mining and geological conditions. Proc. Int. Symp. Engineering in Complex Rock Formations. 3 - 7 November, Beijing, China.

Rutherford, H.E., Padgett, J.T. and Murphy, T.D. (1984) Coal geology: an operational application, paper presented at SME-AIME Fall meeting, Denver, CO, Oct.

Ryder, G.H. (1969) Strength of materials.Macmillan Education Ltd, London.

Savin, G.N. (1951) Stress concentration around holes. (translated, 1961), Pergamon, Oxford.

Shepherd, R. and Fisher, N.I. (1978) Faults and their effect on coal mine roof failure and mining rate: a case study in a New South Wales colliery, Mining Engineering 30, pp1325-1334

Sokolnikoff, I.S. (1956) Mathematical theory of elasticity, 2nd Ed. Mcgraw - Hill, New York.

Spruth, F. (1955) Face supports in steel and light metal. Verlag Gluckauf G.m.b.H. Essen, translated by NCB Translation Sec.

Spruth, F. (1955) Steel roadway supports, a practical handbook. Verlag Gluckauf G.m.b.H. Essen, translated by NCB Translation Sec.

Stagg, K.G. and Zienkiewicz, O.C. (1968). Rock mechanics in engineering practice. John Wiley & Sons Ltd.

Stephansson, O. (1971) Stability of single openings in horizontally bedded rock. Engineering Geology, No.5, pp5 - 71.

Stillborg, B. (1986) Professional users handbook for rock bolting. Trans Tech Publ., London.

Stout, K. (1980) Mining methods and equipment. Mcgraw Hill, New York.

Sun, G.Y. (1989). Application of orthogonal design method in mine optimum design Coal science and technology (in Chine) No.6, pp47 -50.

Sun, R.X. et. al. (1989). Mine pressure appearance along reused coalface gates with side packing. Coal science and technology (in Chinese) No.9, pp2 - 6.

Sutcliff, M. (1990) Ph.D thesis, University of Nottingham.

Sutcliffe, M.L. (1990) Stability and design aspects of mining tunnels in geologically adverse conditions. PhD thesis, University of Nottingham.

Szwilski, A.B. and Whittaker, B.N. (1975). Control of strata movement around face-ends, The Mining Engineer, July,515-525.

Takahashi, Y. et al. (1986). Application of back analysis to a tunnel with two-step bench. Proc. Int. Symp. Engineering in Complex Rock Formations. 3 - 7 November, Beijing, China.

Tan, T. K. (1986). Rockbursts, Case Records, Theory and Control. Proc. Int. Symp. Engineering in Complex Rock Formations. 3 - 7 November, Beijing, China

Terezopoulos, N. (1986). Rock mechanics design principles applied to tunnel stability in deep mining conditions. PhD thesis, University of Nottingham.

Terzaghi, K. (1946). Rock defects and loads on tunnel support. Rock Tunnelling with steel supports. ed. R.V. Proctor and T. White, Commercial Shearing Co., Youngstown, Oh. pp15-99.

Thomas, R. (1991) Ph.D thesis, University of Nottingham.

Thomson, Sir William and Tait, P.G. (1962). Principles of mechanics and dynamics. New York, Dover.

Timoshenko, S.P. and Goodier, J.N. (1951) Theory of elasticity. Mcgraw-Hill, New York.

Tresca, H. (1868). Memoire sur l'ecoulement des corps solids, Mem. Pres. div. sav. Acad. Sci., Inst. Fr., Vol.18, pp733-799.

Wang, J. H. (1989). The use of bolting in actual mining roadways at coal mines in China. Coal science and technology (in Chinese) No.8, pp 23 - 26.

Wang, X.L.(1989). Suggestions for roadway support reform in China coal mines Coal science and technology (in Chinese) No.7, pp 38 - 40.

Watson, T. (1990) Ph.D thesis, University of Nottingham.

Watson, T.P. (1990) A study of mine tunnel design with reference to support stability and behaviour. PhD thesis, University of Nottingham.

Whittaker B.N. et al. (1984) Stability aspects of major coal mining tunnel projects. Design and Performance of Underground Excavations, Cambridge.

Whittaker B.N., Smith S.F. and Chen H.(1990) Fracture development around tunnels. Proc. Int. Symp.Tunnel Construction '90', April, London.

Whittaker, B.N and Singh, R.N. (1978) Design and stability of pillars in longwall mining. Mining Engineer, July pp59 - 73.

Whittaker, B.N. (1972) Design and planning of mine layouts. Mining Department Magazine, Vol.No.XXIV.

Whittaker, B.N. (1974). An appraisal of strata control practice, The Mining Engineer, October,1302-1309.

Whittaker, B.N. (1983) Chain pillar design considerations with reference to longwall mining. Mining Department Magazine, Vol.No.XXXV.

Whittaker, B.N. and Frith, R.C. (1987) Support and stability of mining tunnels in stratified rocks. Mining Department Magazine, Vol.No.XXXIX.

Whittaker, B.N. and Frith, R.C. (1990). Tunnelling - design, stability and construction. Institute of Mining and Metallurgy.

Whittaker, B.N., Hodgkinson, D.R. and Batchlor, A.S. (1971) Roadway strata control with special reference to the South Midlands coal field. Mining Department Magazine, Vol.No.XXIII.

Whittaker, B.N., Terezopoulos, N.G and Goshtasbi-Goharizi, K. (1985) Aspects of mine tunnel stability in Carboniferous Coal Measures rock conditions. Int. Symp. Rock Mech. Excavations for Mining and Civil Works, Zacatecas, Mexico, Sept.

Whittaker, B.N.,Carter, M.R., Kapusniak, S.S. and Townley, A.J. (1985) Design and selection of support systems in mine roadways and tunnels with reference to UK coalfields. 9th Plenary Scientific Session, IBSM, Varna, June.

Whittaker, P.E. (1983). Strata loading characteristics of mining tunnels in Carboniferous rock formations. PhD thesis, University of Nottingham.

Wickham, G.E., Tiedemann, H.R. and Skinner E.H. (1972) Support determination based on geological predictions. Proc. Rapid Excav. Tunneling Conf., AIME, New York.

Williamson, I.A. (1967). Coal mining geology. Oxford University Press.

Wilson, A. H.(1980). The stability of underground workings in the soft rocks of the coal measures. PhD thesis, University of Nottingham.

Wu, S.Q. et. al. (1990). Test analysis of roadway yielding metal support and comments on its improvements. Coal science and technology (in Chinese) No. 5, pp32-33.

Xu, L.S. et.al. (1987) A collection of papers on "Studies of Hard Roof Control Techniques". Datong Mining Information Service, Datong.

Yang, S.Y. (1990). Fully mechanised mining under hard roof. Coal science and technology (in Chinese) No.2, pp49 - 52.

Yen, Z.F. (1990). Analysis of yielding metal support in gateroad. Coal science and technology (in Chinese) No.5, pp29 - 31.

Yoshinaka, R.et al. (1986). Reinforcing effect of rockbolt in rock joint model. Proc. Int. Symp. Engineering in Complex Rock Formations. 3 - 7 November, Beijing, China.

Zhang, L.B. (1990). Discussion on bolt-shotcrete-metal support system in gateroad. Coal science and technology (in Chinese) No.5 pp34-36.

Zhao, S. L. et. al. (1986). Effect and appraisal of the initial support of rock bolt and shotcrete of the Dayaoshan Tunnel. Proc. Int. Symp. Engineering in Complex Rock Formations. 3 - 7 November, Beijing, China.

Zhao, Z.R. (1986). Stress behaviour and ground pressure of tunnel with double lining. Proc. Int. Symp. Engineering in Complex Rock Formations. 3 - 7 November, Beijing, China.

Zheng, Y. T. (1986). Reform and research of tunnel support in soft rocks at Shenbei Mines. Proc. Int. Symp. Engineering in Complex Rock Formations. 3 - 7 November, Beijing, China.

Zorychta, A., Kleczek, Z. and Cyrul, T. (1986). Criteria of rock burst for longwall mining. Proc. Int. Symp. Engineering in Complex Rock Formations. 3 - 7 November, Beijing, China.